FURTHER DEVELOPMENTS IN FOURIER TRANSFORM VIBRATIONAL SPECTROSCOPY

A thesis submitted to the
University of Southampton
in support of candidature for
the degree of

Doctor of Philosophy

by

Martin Vincent Pellow-Jarman
B.Sc. (Honours), M.Sc.

Department of Chemistry
September 1994

UNIVERSITY OF SOUTHAMPTON

ABSTRACT

FACULTY OF SCIENCE
CHEMISTRY

Doctor of Philosophy

FURTHER DEVELOPMENTS IN FOURIER TRANSFORM VIBRATIONAL SPECTROSCOPY

by Martin Vincent Pellow-Jarman

The advantages of interferometers over dispersive spectrometers in the recording of infrared spectra have been known for many years. Developments in instrumentation and computation ability as well as the discovery of the fast Fourier transform have led to the present day position of interferometers predominating over dispersive instruments in the recording of infrared spectra. Since the successful demonstration of Fourier Transform (FT) Raman spectroscopy by Chase and Hirschfield in 1986 using 1.064 μm excitation, Raman spectroscopy has experienced a major revival. This revival is largely due to the fact that the problem of sample fluorescence is dramatically reduced by the use of a lower energy excitation laser.

Chapter 3 of this thesis describes the development and assessment of a Titanium: Sapphire laser based FT Raman spectrometer. This instrument was developed to allow the evaluation of excitation wavelengths for Raman spectroscopy intermediate between visible wavelengths used in conventional scanning instruments and 1.064 μm - the source of choice in commercial FT Raman spectrometers. The final prototype is described and the advantages and disadvantages of the instrument are assessed. In **Chapter 4** a study of the dependence of the emitted Raman signal intensity on particle size for inorganic powders with particle sizes in the 0.1 mm range is described.

In **Chapter 5** an assessment of a simple pyrolysis FTIR cell is outlined. A system of pure poly(butylene terephthalate) polymers and flame retardant containing formulations is used to evaluate the cell. The decomposition compounds of various test materials can be studied. In **Chapter 6** a commercially available temperature programmable high temperature high pressure FTIR gas cell is assessed by studying the transesterification process known to occur in heated blends of poly(butylene terephthalate) / polycarbonate. The cell is able to allow the monitoring of transesterification in a test system of stabilised and unstabilised blends.

Chapter 7 describes the evaluation of FT Raman spectroscopy for monitoring transesterification in poly(butylene terephthalate) / polycarbonate blends. Indirect evidence for transesterification is presented. **Chapter 8** describes the assessment of a commercially available solvent elimination interface between liquid chromatography and FTIR. Several test systems of polymers were examined, reconstructed chromatograms from time resolved FTIR spectra are presented.

ACKNOWLEDGEMENTS

I wish to express my thanks to the following people, without whom this thesis would not have been written:

to my supervisor **Dr Patrick Hendra** for his supervision, patience and guidance over the years,

to **Drs Martin Hetem** and **Gert de Wit** of General Electric Plastics Europe, for giving me the opportunity to work at General Electric Plastics in the Netherlands for six months,

to the various members of the "Hendra Group" past and present for their support and friendship, particularly **Ralph Lehnert, Heather Wilson, Bob Bennett, James Haigh, Elizabeth Llewelyn, Jonathon Agbenyega, Philip Bentley, Christopher Dyer, Andrew Brimblecombe, John Graham, Inma Campoy-Felipe** and **Morella Arruebarrena-Baez.**

to **Mrs Jill Allen,** who can always be relied upon to restore some sense of order out of the usual chaos,

to the staff of the Chemistry Department, especially **Mike Ellis,** the people in the Chemistry Stores and the tea ladies,

and finally,

to my parents **Derek** and **Bernadette** who had the good sense to have me in the first place.

CONTENTS

Part I

Chapter 3 THE CONSTRUCTION, DEVELOPMENT AND ASSESSMENT OF A TITANIUM:SAPPHIRE LASER BASED FOURIER TRANSFORM RAMAN SPECTROMETER

Part II

Chapter 1

INTRODUCTION

Chapter 1

INTRODUCTION

1.1 THE ORIGINS OF VIBRATIONAL SPECTROSCOPY

Vibrational spectroscopy has its origins in research carried out towards the end of the 19 th century[1]. The observation that particular chemical fragments gave rise to characteristic absorption frequencies led almost immediately to the well known tables of "group frequencies" and the development of one of the first non-destructive analytical procedures.

In 1928 the Raman effect was discovered by C.V. Raman[2] and almost simultaneously Mandelstam[3], after its prediction in 1923 by Smekal[4]. Early Raman spectra were recorded with a mercury lamp excitation source and the Raman light analysed with a conventional spectrograph and photographic plate. Because the equipment required to produce Raman spectra was possessed by almost every physical or analytical laboratory there was a rapid development in Raman spectroscopy[5-9]. By the late 1930's the method of choice for recording vibrational spectra was Raman spectroscopy simply because of the experimental advantages it displayed over infrared spectroscopy. After the Second World War the recording of infrared spectra became routine because of the development of sensitive infrared detectors, sophisticated electronics and servo systems. Raman spectroscopy then suffered because of the skill required to obtain Raman spectra and the restrictions of sample colour and fluorescence.

1.2 THE DEVELOPMENT OF FOURIER TRANSFORM VIBRATIONAL SPECTROSCOPY

The development of Fourier transform spectrometers can be traced back to a century ago with the invention of the two-beam interferometer by Michelson[10] in 1891. Most modern Fourier transform spectrometers used for infrared and Raman spectroscopy are

based on this two-beam interferometer. Lord Rayleigh realised it was theoretically possible to obtain a spectrum from the interference pattern generated by an interferometer by computing its Fourier transform. By comparing calculated interferograms with measured ones some simple spectra could be deduced. At the beginning of the 20 th century because of the difficulty of calculating a spectrum from an interferogram, Michelson interferometers were only used to resolve the fine structure of atomic lines. Interferometers were not used until the 1950's when the Fellgett[11] and Jacquinot[12] advantages were discovered.

Three other major advances were required to bring about the revolution in Fourier transform infrared spectroscopy and subsequently Fourier transform Raman spectroscopy. The first of these was the discovery of the fast Fourier transform (FFT) algorithm in 1964 by Cooley and Tukey[13]. The other two advances were the development and application of dedicated microprocessors to perform the Fourier transform process and small gas lasers (eg. He-Ne lasers) to Fourier transform infrared spectroscopy.

The development of Raman spectroscopy was given a boost in the 1960's by the introduction of commercial visible lasers[14]. In 1964 the first Fourier transform Raman spectrum was recorded by Chantry, Gebbie and Hilsum[15] using a Michelson interferometer. However it wasn't until 1986 when the current revolution in Fourier transform Raman spectroscopy started as a result of a more successful study performed by Chase and Hirschfield[16]. The involvement of the research group here at Southampton in Fourier transform Raman spectroscopy began shortly after this paper was published in 1987 with the successful demonstration of an Fourier transform Raman spectrometer using a commercial grade benchtop FTIR instrument[17]. The research group here at Southampton has since established itself as a centre in developing new applications for Fourier transform Raman spectroscopy.

The work reported in this thesis is described in the chronological order in which the work was carried out and can be broadly separated into two sections; i.e. applications dealing with Fourier transform Raman spectroscopy and those dealing with Fourier transform infrared spectroscopy. The experimental work described can be further

separated into six sub-sections; three dealing with Raman spectroscopy and three with infrared methods. The motivation for the Raman applications (Chapters 3, 4 and 7) was a direct consequence of research grants awarded by the then SERC and the DTI in the Fourier transform Raman spectroscopy field. The work described dealing with infrared spectroscopy (Chapters 5, 6 and 8) arose from an invitation to the candidate to join General Electric Plastics Europe for a three month stay (repeated). The candidate joined a research group which had developed a keen interest in hyphenated Fourier transform infrared spectroscopic techniques and the outcome is described in Chapters 5, 6 and 8.

The first two chapters in this thesis are intended to introduce the scope of the research described in this thesis, i.e. Fourier transform vibrational spectroscopy, but are by no means intended to be a rigorous introduction to the field. A basic knowledge of vibrational spectroscopy is assumed, the reader is referred to the many texts available in the literature for a more rigorous and detailed background[18-20].

The first, and indeed all the presently commercially available, Fourier transform Raman spectrometers use 1.064 μm laser radiation from a Nd^{3+}:YAG laser. This choice of wavelength was quite fortuitous because it apparently overcame the problem of fluorescence[21] which had long plagued Raman spectroscopists using visible lasers as excitation sources in Raman spectrometry. This leads to the question as to whether or not other laser sources of intermediate wavelength between the visible and 1.064 μm could be just as effective in avoiding fluorescence in compounds studied with Raman spectrometry. Chapter 3 reports the main body of work carried out during the course of my Ph.D. investigations. As part of a collaboration between the Department of Trade and Industry and Perkin Elmer a project was undertaken to carry out a detailed investigation into the advantages and disadvantages of using wavelengths shorter than 1.064 μm in Fourier transform spectroscopy, and indeed Raman spectroscopy in general.

Chapter 4 reports an investigation into a little understood but nevertheless important area of Raman spectroscopy, the effect on particle size on the strength of the Raman signal emitted by a powdered sample. This area of Raman spectroscopy has important implications for any quantitative work carried out with powdered samples or

inhomogeneous solids. A previously described theory is used to rationalise the results obtained in this investigation.

Chapters 5, 6 and 8 describe three discrete projects carried out during two separate three month work periods spent at General Electric Plastics Europe. The projects undertaken were: pyrolysis Fourier transform infrared spectroscopy using flame retardant-containing poly(butylene terephthalate) formulations as test materials, the evaluation of a high pressure and high temperature Fourier transform infrared gas cell using a system of poly(butylene terephthalate) / bisphenol A polycarbonate blends known to undergo a transesterification reaction at elevated temperature and the evaluation of a solvent elimination accessory designed to interface liquid chromatography and Fourier transform infrared spectroscopy.

Since the main objective of General Electric Plastics is the manufacture of high performance plastics and the maintenance of their quality and the work was carried out in a group specializing in Fourier transform infrared spectroscopy, it is not surprising that the projects undertaken during my work period at General Electric Plastics focus on developing applications of the method using systems of high performance polymers as test materials.

The work reported in Chapter 7 describes the evaluation of Fourier transform Raman spectroscopy for monitoring the transesterification reactions occurring at elevated temperatures in blends of poly(butylene terephthalate) and bisphenol A polycarbonate. This work was carried out as a result of a personal interest developed into a topic described in Chapter 6.

Chapter 9, the concluding chapter, is a brief summary of the conclusions of the experimental chapters in this thesis.

1.2 MOLECULAR VIBRATIONS

Molecules in the gas phase rotate freely about their three orthogonal axes. The angular

velocities about these three axes can only have certain values, i.e. the rotational energy of a molecule is quantized and a molecule can only change rotational energy level between two states by releasing or taking in an amount of energy equivalent to the difference in energy between two states. In addition to rotation, molecules also vibrate unceasingly. The vibrational energy levels of a molecule are also quantized and the molecule can change energy level by interacting with incident radiation either by taking in or releasing energy in the form of electromagnetic radiation. The study of this interaction between electromagnetic radiation and molecular vibrations is known as vibrational spectroscopy.

Molecules exhibit a complex series of vibrations which are linear combinations of much simpler fundamental modes of vibration. The contortions of a molecule can be described by $3N$ coordinates, where N is the number of atoms in the molecule. Three of these coordinates are required to describe the translational motion of a molecule and one is required to describe each rotation. Thus a non-linear molecule has $3N$ - 6 fundamental or normal modes of vibration whilst a linear one has $3N$ - 5 fundamental or normal modes of vibration. Such a fundamental mode of vibration can be described as a periodic motion during which the centre of mass of a molecule is not altered in position and all the atoms pass through their equilibrium position simultaneously.

One model of a diatomic molecule is the simple harmonic oscillator. Classically a simple harmonic oscillator can be viewed as two masses (m_1 and m_2) connected by a spring with force constant k (in N/m). Figure 1.1 shows a diagram of this simple harmonic oscillator. For this system, to distort the masses from their equilibrium position requires the application of a force F (in N), where $F = - kx$, x is the displacement from equilibrium in m. This system shown in Figure 1.1 will vibrate at a frequency given by:

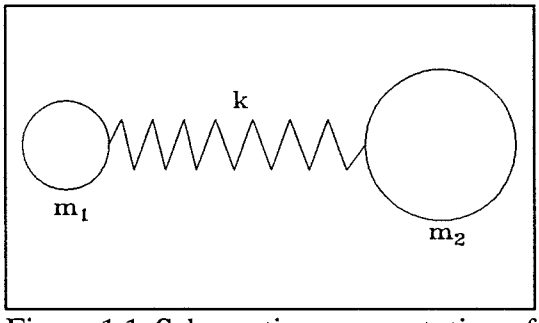

Figure 1.1: Schematic representation of a two masses (m_1 and m_2) connected by a spring of force constant k.

$$\nu_{vib} = \frac{1}{2\pi}\sqrt{\frac{k}{\mu}} \tag{1.1}$$

where μ is the reduced mass given by:

$$\mu = \frac{m_1 m_2}{m_1 + m_2} kg \tag{1.2}$$

This model predicts accurately the vibration frequencies for a diatomic molecule even though real molecules are anharmonic oscillators. The potential energy function for an anharmonic oscillator can be described by the Morse function. Figure 1.2 shows a comparison of the potential energy functions described by a typical Morse curve and an harmonic oscillator.

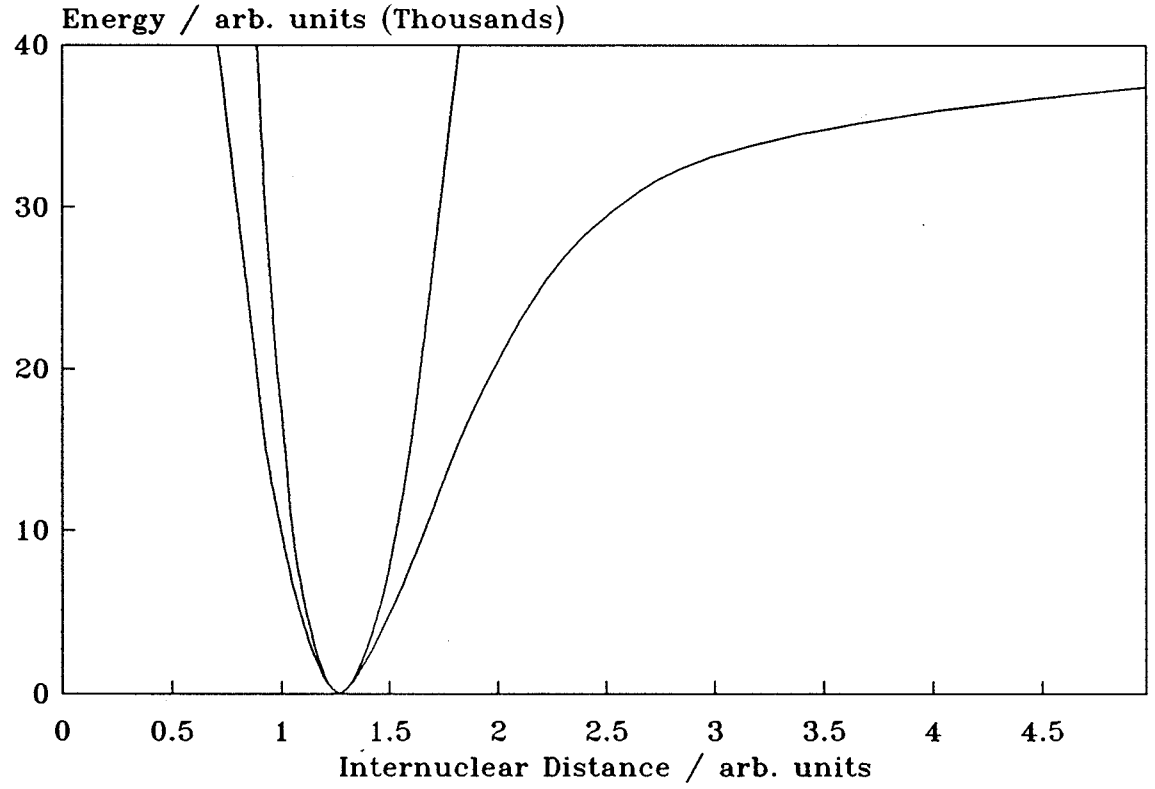

Figure 1.2: Comparison of a Morse curve with a parabolic potential energy function.

It will be seen that at small displacements the Morse and Simple Harmonic Motion (SHM) functions are almost coincidental hence under these conditions the SHM approximation is a good one.

The Morse function is:

$$E = D_{eq}[1 - \exp\{a(r_{eq} - r)\}]^2 \qquad (1.3)$$

where

D_{eq} = dissociation energy

r_{eq} = equilibrium bond length

r = internuclear distance

a = constant for molecule

Figure 1.2 shows the potential energy curves are continuous but in reality the vibrational energy of a molecule is quantized. The allowed energy levels for the anharmonic oscillator are:

$$E_{vib} = h\left[\left(V + \frac{1}{2}\right)\nu_{vib} - \left(V + \frac{1}{2}\right)^2 X_c \nu_{vib}\right] \qquad (1.4)$$

where

X_c = Anharmonicity constant

ν_{vib} = Vibrational frequency (Hz)

V = 0, +1, +2, +3 ... = Vibrational quantum number

The permitted energy levels for a molecule if drawn on the Morse curve in Figure 1.2 would consist of a series of horizontal lines which converge as V increases. Changes in the energy of a molecule thus are accompanied by the absorption or release of a quantum of energy corresponding to the difference in energy between the two states.

1.3.1 Infrared activity

For a vibration in a molecule to be infrared active, i.e. capable of interacting with incident electromagnetic radiation, the dipole (μ) of the molecule should change during

the vibration. Figure 1.3 shows the fundamental vibrational modes of carbon dioxide and plot of dipole moment (μ) and polarizability (α) versus the normal coordinate (q) of the molecule where (q) represents the progress of the vibration in units of phase angle.

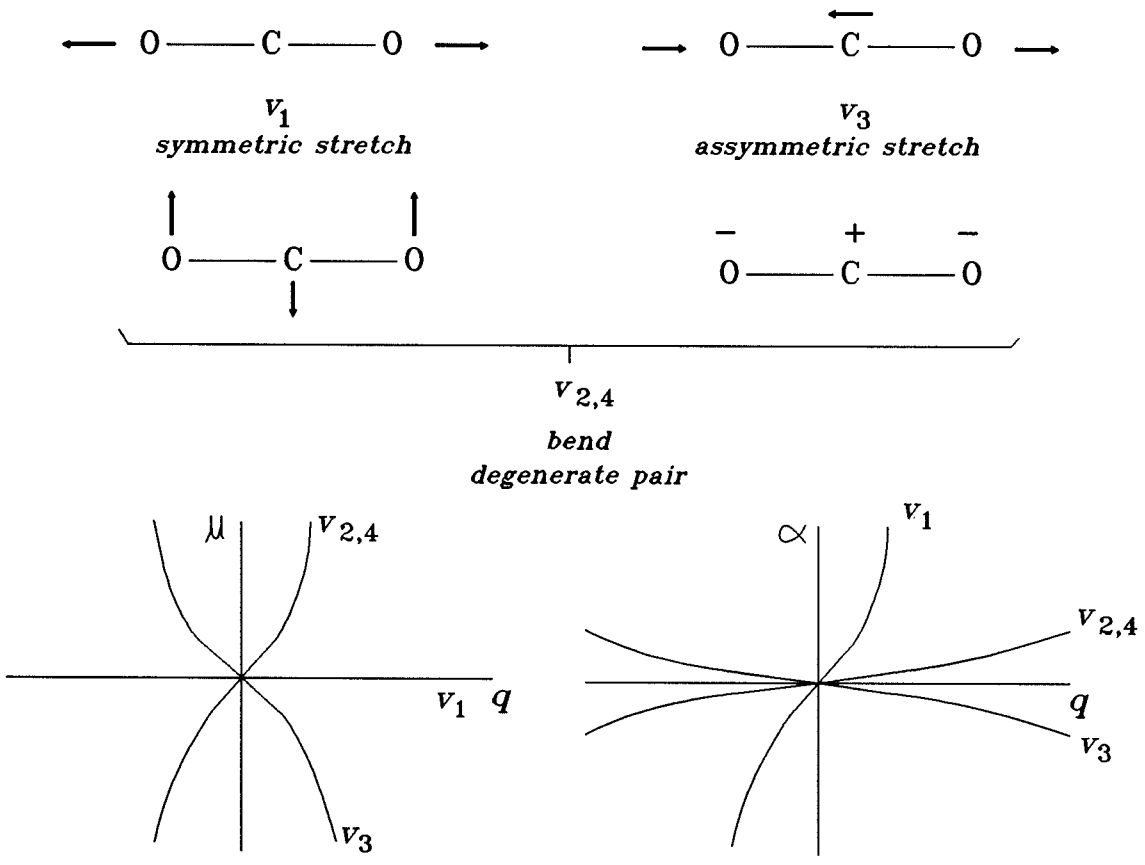

Figure 1.3: Fundamental vibrational modes of CO_2 and corresponding plots of dipole moment and polarizability versus phase angle.

The selection rule for infrared activity is given by:

$$\frac{\delta \mu}{\delta q_0} \neq 0 \tag{1.5}$$

where q_0 is the equilibrium position of the vibration. Considering the symmetric stretch of carbon dioxide, it can be seen that the dipole moment of the molecule does not change during the course of a vibration, this vibration is thus not infrared active. For the other fundamental modes the dipole moments do change and thus ν_3 and $\nu_{2,4}$ are infrared active.

1.3.2 The Raman effect

If a molecule is placed in an electric field E (V/m) then a dipole of magnitude P (V/m) is induced proportional to the electric field, with the proportionality constant given the name **polarizability** α, i.e.:

$$P = \alpha E \tag{1.6}$$

If the field is the component of an electromagnetic radiation field of frequency ν_0 (Hz) then the induced dipole will oscillate with the same frequency as the electric field.

$$P = \alpha E_0 \cos(2\pi \nu_0 t) \tag{1.7}$$

where t is time and E_0 is maximum electric field strength (V/m). If this irradiated molecule is already vibrating at a frequency ν_{vib}, its distortion from its equilibrium position is given by:

$$q = q_0 \cos(2\pi \nu_{vib} t) \tag{1.8}$$

where q_0 is the maximum distortion and ν_{vib} is the vibration frequency (Hz). If the distortion causes a change in the molecule's polarizability then the polarizability of the molecule as it vibrates in the electromagnetic field is given by:

$$\alpha = \alpha_0 + \left(\frac{\delta \alpha}{\delta q}\right)_0 q_0 \cos(2\pi \nu_{vib} t) \tag{1.9}$$

substituting α from Eq. (1.9) into Eq. (1.7):

$$P = \alpha_0 E_0 \cos(2\pi \nu_0 t) + \left(\frac{\delta \alpha}{\delta q}\right)_0 q_0 \cos(2\pi \nu_{vib} t) \cos(2\pi \nu_0 t) \tag{1.10}$$

Using the identity:

$$\cos A \cos B = \frac{1}{2}[(\cos(A+B) + \cos(A-B)] \tag{1.11}$$

Eq. (1.10) becomes:

$$P = \alpha_0 E_0 \cos(2\pi \nu_0 t) + \frac{1}{2}\left(\frac{\delta\alpha}{\delta q}\right)_0 q_0 \{\cos(2\pi [\nu_0 + \nu_{vib}] t) + \cos(2\pi [\nu_0 - \nu_{vib}] t)\} \quad (1.12)$$

Thus a molecule vibrating with frequency ν_{vib} irradiated with radiation of frequency ν_0 will have a dipole varying as ν_0 as well as $(\nu_0 + \nu_{vib})$ and $(\nu_0 - \nu_{vib})$. An oscillating dipole emits radiation corresponding to its oscillation frequency. The radiation emitted by the dipole corresponding to ν_0 is known as the Rayleigh radiation, the radiation corresponding to $(\nu_0 + \nu_{vib})$ is called the Anti-Stokes Raman radiation and the radiation corresponding to $(\nu_0 - \nu_{vib})$ is called the Stokes Raman radiation. The relative intensities of the Stokes and Anti-Stokes Raman bands are determined by the relative populations of the ground and first vibrational energy level of the states between which the vibrational transition is taking place. The relative populations of these two states can be calculated from the well known Boltzmann distribution equation.

For a molecular vibration to be Raman active the polarizability of the molecule must change during a vibration. Figure 1.3 used to illustrate the dipole moment change for carbon dioxide as a function of phase angle also shows the corresponding polarizability changes. For ν_1 the polarizability displays a large change around $q = 0$ thus this mode is Raman active but for ν_3, ν_2 and ν_4 the polarizability does not display such a change thus these modes are not Raman active.

1.4 REFERENCES

1. Jones, R.N., European Spectroscopy News, (1987), **70**, 10.
2. Raman, C.V. & Krishnan, K.S., Nature, (1928), **121**, 501.
3. Landsberg, G. & Mandelstam, L., Naturwiss, (1928), **16**, 557.
4. Smekal, A., Naturwiss, (1923), **11**, 873.
5. Raman, C.V., Nature, (1928), **121**, 619.
6. Raman, C.V., Nature, (1928), **121,** 721.
7. Landsberg, G. & Mandelstam, L., Naturwiss, (1928), **16**, 772.
8. Rocard, Y., Compt. Rend., (1928), **186**, 1107.
9. Cabannes, J., Compt. Rend., (1928), **186**, 1201.
10. Michelson, A.A., Phil. Mag. (5), (1891), **31**, 256.
11. Felgett, P., J. Phys. Radium, (1958), **19**, 187.
12. Jacquinot, P,. J. Op. Soc. Am., (1954), **44**, 761.
13. Cooley, J.W. & Tukey, J.W., Mathematics of Computation, (1965), **19**, 297.
14. Kogelnik, H., & Porto, S.P.S., J. Op. Soc. Am., (1963), **53**, 1446.
15. Chantry, G.W., Gebbie, H.A. & Hilsum, C., Nature, (1964), **40**, 133.
16. Chase, D.B. & Hirschfield, T., App. Spec., (1986), **40**, 133.
17. Parker, S.F., Williams, K.P.J., Hendra, P.J. & Turner, A., App. Spec., (1988), **42**, 796.
18. Griffiths, P.R. & De Haseth, J.A., Fourier Transform Infrared Spectrometry, (1986), Wiley, New York.
19. Banwell, C.N., Fundamentals of Molecular Spectroscopy, (1972), McGraw Hill, London.
20. Hendra, P.J., Jones, C.H. & Warnes, G.M., Fourier Transform Raman Spectroscopy Instrumentation and Applications, (1991), Ellis Horwood, London.
21. Ellis, G., Hendra, P.J., Hodges, C.M., Jawhari, T., Jones, C.H., Le Barazer, P., Passingham, C., Royaud, I.A.M., Sanchez-Blazquez & Warnes, G.M., Analyst, (1989), **114**, 1061.

Chapter 2

EXPERIMENTAL TECHNIQUES

Chapter 2

EXPERIMENTAL TECHNIQUES

2.1 VIBRATIONAL SPECTROSCOPY

2.1.1 The Michelson interferometer

The heart of any Fourier transform infrared or Raman spectrometer is the interferometer. In principle there is no difference between an interferometer used in an infrared or Raman spectrometer. Most modern interferometers are based on the two-beam Michelson device invented in 1891[1].

In a Michelson interferometer the entrant beam of radiation is divided into two beams which then are recombined after introducing a path difference. Interference occurs between the beams, the intensity variation of the beam emerging from the interferometer is measured as a function of path difference and is referred to as the interferogram.

In the classic system in Figure 2.1 one of the mirrors is fixed, the other moves on an axis perpendicular to its plane either at a constant velocity or at equally spaced points for fixed short periods. Between the two mirrors is a beamsplitter which partially reflects and transmits the incoming beam. After reflection off the mirrors the beams return to the beamsplitter which acts as a recombiner, the beams then interfere but are partially reflected and transmitted.

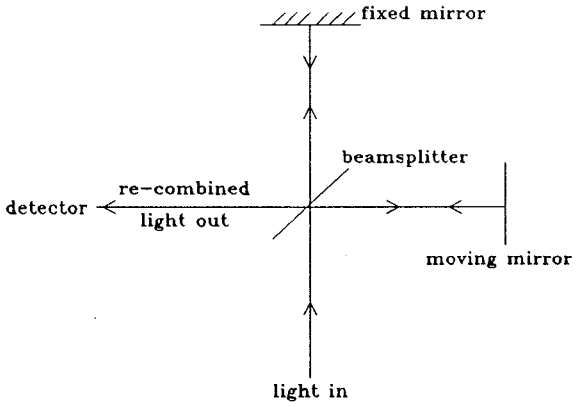

Figure 2.1: Schematic diagram of a Michelson interferometer.

The intensity of the beam reaching the detector and the source varies as a function of

path difference in the interferometer and this intensity variation ultimately yields the spectral information required.

Consider a source of monochromatic radiation in a collimated beam of wavelength λ (in cm) and wavenumber $\bar{\nu}$ (in cm^{-1}). Assume that the beamsplitter is ideal. The path difference i.e. retardation (δ) is the difference in the lengths of the paths of the two beams.

When the path difference is zero the two beams recombining at the beamsplitter are in phase and constructively interfere regardless of their wavelength. When the path difference is $\frac{1}{2}\lambda$ then the beams recombining at the beamsplitter are out of phase and destructively interfere. Displacing the moving mirror by $\frac{1}{4}\lambda$ (i.e. adding a further path difference of $\frac{1}{2}\lambda$) causes constructive interference again. With monochromatic radiation it is not possible to distinguish between zero retardation and retardation equal to an integral number of wavelengths.

If the mirror moves at a constant velocity then the signal reaching the detector varies sinusoidally, a maximum signal reaches the detector each time the retardation passes an integral multiple of λ. The intensity of the beam reaching the detector $I(\delta)$ is given by:

$$I(\delta) = 0.5I(\bar{\nu})\{1 + \cos 2\pi\,\delta/\lambda\} \tag{2.1}$$

$$= 0.5I(\bar{\nu})\{1 + \cos 2\pi\,\bar{\nu}\delta\} \tag{2.2}$$

where $I(\bar{\nu})$ is equal to the intensity of the source. Only the ac component is important in spectroscopy, the modulated component of the signal reaching the detector is the interferogram. For an ideal interferometer:

$$I(\delta) = 0.5I(\bar{\nu})\{\cos 2\pi\,\bar{\nu}\delta\} \tag{2.3}$$

The above equation can be modified to include the non-ideality of the beamsplitter and the detector by using a single wavenumber dependent factor $H(\bar{\nu})$:

$$I(\delta) = 0.5 H(\bar{\nu}) I(\bar{\nu}) \{ \cos 2\pi \bar{\nu} \delta \} \tag{2.4}$$

Combining $H(\bar{\nu})$ and $I(\bar{\nu})$ into $B(\bar{\nu})$ we get:

$$I(\delta) = B(\bar{\nu}) \{ \cos 2\pi \bar{\nu} \delta \} \tag{2.5}$$

$B(\bar{\nu})$ is the source intensity at $\bar{\nu}$ modified by the instrumental characteristics. $I(\delta)$ is mathematically the cosine Fourier transform of $B(\bar{\nu})$. The spectrum is thus calculated by computing the cosine Fourier transform of $I(\delta)$. All modern Fourier transform spectrometers use a computer algorithm based on the Fast Fourier Transform (FFT) first described by Cooley and Tukey in 1965[2].

Performing the Fourier transform of a measured interferogram of a monochromatic source is trivial, however for several spectral lines or continuous radiation a computer is usually required. For a source of continuous radiation, the measured interferogram is the resultant of all the interferograms corresponding to each wavenumber.

For a continuum source the interferogram can be represented as:

$$I(\delta) = \int_{-\infty}^{+\infty} B(\bar{\nu}) \cos 2\pi \bar{\nu} \delta \, . d\bar{\nu} \tag{2.6}$$

In principle by measuring the complete interferogram from 0 to $+\infty$ a complete spectrum at infinite resolution can be obtained. This would require moving the interferometer through a path difference (δ) of infinity and digitizing the interferogram at infinitely small intervals. The effect of limiting δ is to cause the spectrum to have finite resolution.

In Fourier transform spectroscopy, use is made of the *Nyquist Criterion* i.e. a sinusoidal waveform can be sampled unambiguously using a sampling frequency greater than or equal to twice the bandwidth of the system. In practical terms this means that the interferogram must be sampled at a minimum of twice the frequency of the shortest wavelength of interest in the required spectrum. In practice, the sampling frequency used in recording an interferogram is sufficiently in excess of the minimum Nyquist frequency to avoid complications from any signals which may fold back into the spectral domain

of interest because they have not been sampled at a high enough frequency in the recorded interferogram. The sinusoidal interferogram produced by a small helium-neon (He-Ne) laser beam shone into the interferometer is usually used to generate a reference scale to allow the interferogram to be sampled at precisely known intervals of distance.

2.1.2 Advantages of Fourier transform over conventional spectrometers

2.1.2.1 The Jacquinot advantage[3]

The Jacquinot advantage is related to the relative optical throughputs of an interferometer and a grating spectrometer. The collection optics of a grating spectrometer and an interferometer have similar f-numbers. Light entering a grating instrument must pass through a narrow slit typically 100 μm wide and 5 mm high. The entrance to an interferometer with a similar performance resolution is a circular hole about 8 mm in diameter. Thus, the optical throughput of an interferometer is far superior to that of a conventional grating spectrometer.

2.1.2.2 The Felgett advantage[4]

In a grating instrument only a small fraction of light entering the instrument falls on the detector, the rest is wasted. In a spectrograph the entire spectrum, or a large section of it, is recorded continuously. This is known as the multiplex advantage. An interferometer possesses a similar advantage called the Felgett advantage. In an interferometer all wavelengths entering the instrument fall on the detector simultaneously. Thus each data point in the interferogram contains information about every wavelength. However a complete interferogram must be collected to recorded a spectrum thus the Felgett advantage is not as great as the multiplex advantage.

2.1.2.3 The Connes advantage[5]

All spectra show improvements in signal to noise if averaged. In practice this relies on the fact that the spectra should be exactly superimposed. For a grating instrument

because of mechanical wear errors are introduced. For an interferometer the wavelength of the reference laser does not change hence spectra can be exactly superimposed.

2.1.3 Fourier transform infrared spectroscopy

In addition to an interferometer a Fourier transform infrared spectrometer requires a source and a detector. The sources vary from instrument to instrument but are usually one of the following: Globar, Nernst glower, nichrome coil or tungsten filament lamp. Various detectors may also be used in a Fourier transform spectrometer. They are either thermal detectors or quantum detectors, the most common examples of each type being the deuterated triglycine sulphate (DTGS) and mercury cadmium telluride detectors (MCT) respectively.

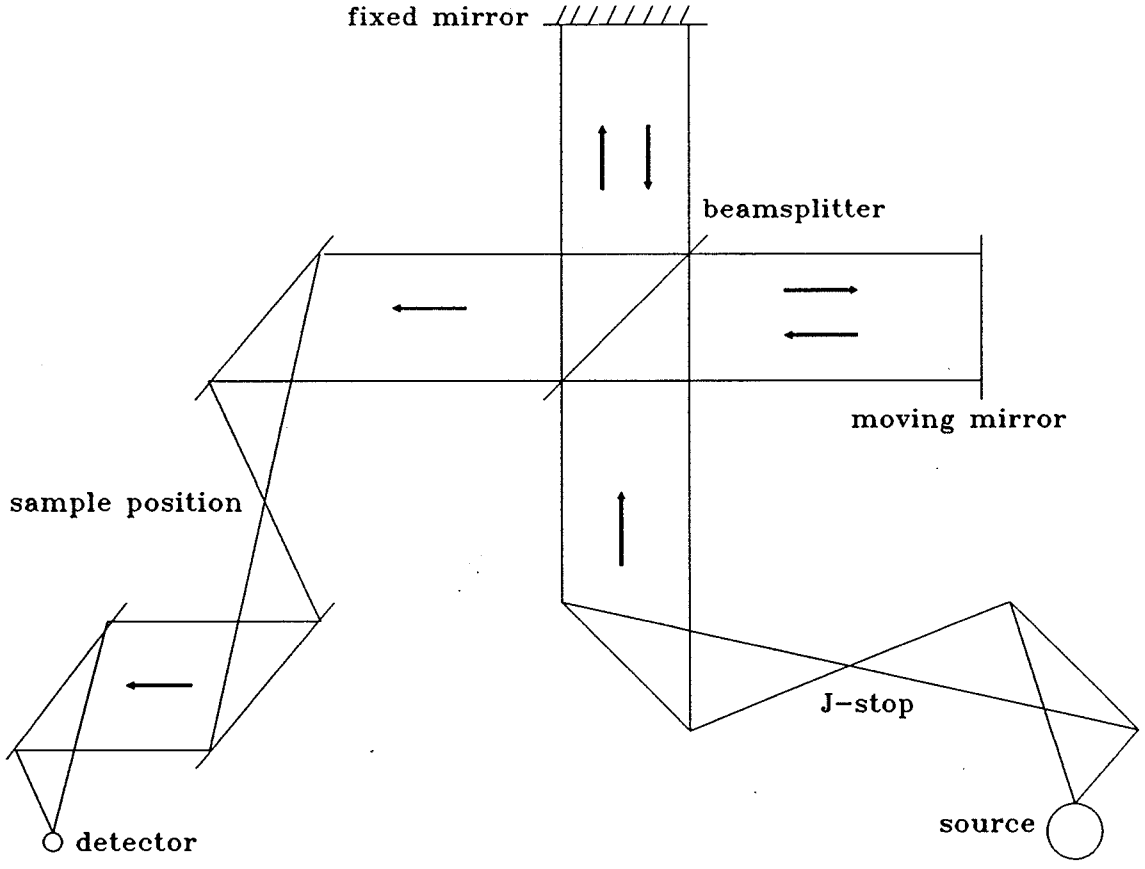

Figure 2.2: Simple schematic diagram of a Fourier transform infrared spectrometer.

Figure 2.2 shows a simple schematic diagram of a typical Fourier transform infrared spectrometer.

2.1.4 Fourier transform Raman spectroscopy

Most commercial Fourier transform Raman spectrometers consist of some type of Fourier transform infrared spectrometer modified for the Raman experiment. This modification is made by fitting a system of collection optics before the interferometer to collect the scattered Raman radiation. The collection optics are matched to the interferometer in such a way that the image of the sample formed by the collection optics occurs at the J-stop. Figure 2.3 shows a schematic diagram of such a Raman spectrometer.

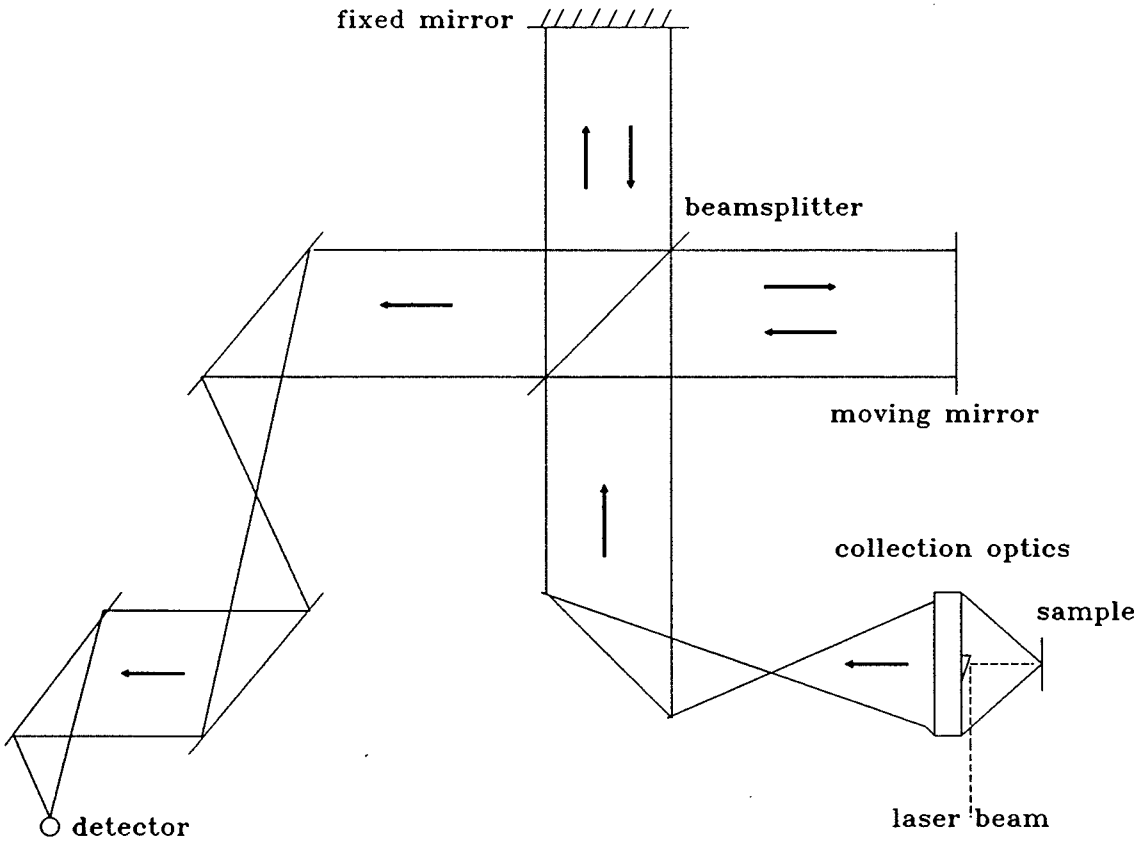

Figure 2.3: Simple schematic diagram of a Fourier transform Raman spectrometer.

Further modifications to the infrared instrument are necessary to optimise the performance of the Raman spectrometer. The potassium bromide beam splitter for an infrared spectrometer performs optimally in the mid-infrared region of the electromagnetic spectrum (i.e. 4000 to 400 cm^{-1}). The Raman spectrum when excited with the usual wavelength of 1.064 μm falls in the region 9400 to 5400 cm^{-1}, a quartz beamsplitter outperforms potassium bromide in this region of the electromagnetic spectrum. Similarly, the aluminium mirrors found in a Fourier transform infrared spectrometer can be replaced with gold coated mirrors to improve the performance of the Fourier transform Raman spectrometer.

All commercially available Fourier transform Raman spectrometers use a 1064 nm Nd^{3+}:YAG laser as the excitation source for the Raman experiment. In principle there is no reason why another laser cannot be used. Chapter 3 in this thesis describes the development of a Titanium-Sapphire laser based Fourier transform Raman spectrometer. This laser source is continuously tunable between 700 and 950 nm and is ideal to investigate the advantages of using lasers operating in this region of the infrared as sources for Fourier transform Raman spectroscopy.

In a typical Raman experiment the intensity of the Rayleigh radiation scattered by the sample is 10^{10} times greater than the intensity of the Raman signal. To allow the Raman radiation to be observed the Rayleigh radiation must be attenuated to at least the intensity of the Raman radiation. This is achieved with the use of Rayleigh rejection filters which have a large optical density at the laser line and allow the Raman radiation to pass through them with a minimum of energy loss. These Rayleigh rejection filters can be placed anywhere in the collected beam path before the detector.

Detectors in most commercial Fourier transform Raman spectrometers are a high impedance Indium Gallium Arsenide semiconductor device or a Germanium photodiode. A typical detector of 1 mm^2 will have a noise equivalent power of the order of 10^{-15} WHz^{-1} but the Germanium photodiode needs cooling to about 77 K.

2.2 LIQUID CHROMATOGRAPHY

Chapter 8 of this thesis describes the evaluation of a solvent elimination interface between liquid chromatography and Fourier transform infrared spectroscopy. Briefly outlined in this section are the principles of the two chromatographic techniques interfaced with Fourier transform infrared spectroscopy in the experiments which are described in Chapter 8.

2.2.1 Reverse phase high performance liquid chromatography

Liquid chromatographic (LC) techniques using small column particle packing diameters (typically 10 μm) to achieve a high column efficiency require pumping pressures of several hundred atmospheres to achieve reasonable flow rates. High performance liquid chromatography is the name given to these LC techniques.

The use of an isocratic elution, i.e. single solvent to carry the analytes through the column, is the simplest way to perform a chromatographic separation. Often a gradient elution is needed to perform a desired chromatographic separation. With gradient elution, the ratio between two or more solvents that usually differ significantly in polarity is varied in a preprogrammed manner either continuously or in a series of steps during a chromatographic separation. Columns are usually constructed from stainless steel tubing and have typical dimensions of 10 to 30 cm in length and 4 to 10 mm inside diameter. Typical particle sizes of the packings are between 5 and 10 μm.

High performance liquid chromatography is a type of chromatography where partition takes place either by physical absorption or the formation of covalent bonds. Partition chromatography can also be divided into normal and reverse phase chromatography. In normal phase chromatography, the stationary phase is highly polar and a non-polar solvent is involved as the mobile phase. Hence, less polar components are eluted first. In reverse phase chromatography the mobile phase is polar while the stationary phase is non-polar, thus the most polar component elutes first and increasing the mobile phase polarity increases the elution time.

2.2.2 Size exclusion chromatography

Size exclusion or gel permeation chromatography relies on the selective retention of the components of a mixture by a column packing material due to of the components' ability or otherwise to penetrate the pores of the packing. Starting with a packing material in equilibrium with a solvent, the introduction of a solute will result in the solute diffusing into the pores of the packing material assuming the physical size of their molecules permits them to enter the pores. Replacing the liquid phase with pure solvent will cause the solute to diffuse back out of the pores of the packing material. Therefore a solute will move along a bed of packing material if no other mechanism of absorption other than pore diffusion takes place.

The pore sizes of a typical packing are not uniform but have a range of values depending on the type of packing material used. Solute molecules too large to penetrate any of the pores of the packing material will be eluted from a packed column when a volume of solvent corresponding to the interstitial void volume has passed through the column after a sample injection has taken place. For a range of molecular sizes, the pore diameters will be sufficient to allow selective penetration of some of the pores. The elution volume and therefore elution time for these molecules will thus be a function of molecular diameter. For molecules smaller than the minimum pore size the elution volume will simply be a function of the total solvent volume in the column. Gel permeation thus requires control of the pore sizes of the packing material to achieve the required separation. By varying the pore size of the packing material the average molecular weight range over which separation occurs can be altered.

A packing gel can only be used with a solvent that wets the gel and hence can be absorbed by the gel. For organic solvents typical gel materials are made from polystyrene, polyvinyl acetate, and polymethyl methacrylate. Starch, polyacrylamide, polydextran and sulphonated polystyrene can be used to make gels suitable for aqueous solvent systems.

2.3 REFERENCES

1. Michelson, A.A., Phil. Mag. (5), (1891), **31**, 256.
2. Cooley, J.W. & Tukey, J.W., Mathematics of Computation, (1966), **19**, 297.
3. Jacquinot, P,. J. Op. Soc. Am., (1954), **44**, 761.
4. Connes, J. & Connes, P., J. Op. Soc. Am., (1966), **56**, 896.
5. Felgett, P., J. Phys. Radium, (1958), **19**, 187.

Chapter 3

THE CONSTRUCTION, DEVELOPMENT AND ASSESSMENT OF A TITANIUM:SAPPHIRE LASER BASED FOURIER TRANSFORM RAMAN SPECTROMETER

Chapter 3

THE CONSTRUCTION, DEVELOPMENT AND ASSESSMENT OF A TITANIUM:SAPPHIRE LASER BASED FOURIER TRANSFORM RAMAN SPECTROMETER

3.1 INTRODUCTION

Since Chase and Hirschfield[1] first successfully demonstrated an FT Raman spectrometer, almost without exception, the source of choice has been the continuous Neodymium: YAG solid state laser operating at 1.064 μm. In many respects, this selection has turned out to be highly fortuitous because the range of wavelengths required for analytical scattering (1.064 to 1.7 μm) is just covered by both the extended germanium and InGaAs detectors, both of which are of high performance. The wavelength is long enough to ensure that the fluorescence normally caused by visible excitation is minimised. The Nd^{3+}:YAG laser is also relatively cheap and requires little expensive service maintenance. In these respects it enjoys enormous advantages over the Kr^+ and Ar^+ lasers used in conventional scanning spectrometers.

The use of 1.064 μm radiation does show some disadvantages and these disadvantages raise the question of whether other lasers and / or wavelengths might be as useful as 1.064 μm.

3.1.1 Disadvantages of 1.064 μm excitation in Raman spectroscopy

The intensity of the Raman bands in a Raman spectrum is directly proportional to ν^4 (where ν = absolute frequency of the Raman band). This represents a loss in intensity of the Raman scattered radiation of a factor of 18 when comparing 1064 nm to 488 nm, a typical Argon laser wavelength. For bands of higher Raman shift from the laser line this intensity reduction is even more marked.

Water based samples suffer from self-absorption of Raman radiation[2] because of overtones and combinations of the normal infrared absorptions, i.e. if a sample is dissolved in water prior to examination using 1.064 μm excitation the water will absorb some of the radiation emitted by the sample. This is especially a problem because samples dissolved in water are usually dilute and hence weak Raman emitters. Effectively the study of biological samples using FT Raman is severely limited by this phenomenon. Reducing the excitation wavelength in the Raman experiment will move the Raman radiation away from the absorption region of water and hence offer improved sensitivity for these specimens.

As samples are heated the "blackbody" background emitted by the heated surface limits the temperature at which a Raman spectrum can be obtained. In practice with 1064 nm excitation this temperature is around 180 to 200 ^{o}C[3]. Again the reduction of the excitation wavelength would allow samples to be studied at higher temperatures than with 1.064 μm excitation.

It has recently been highlighted by Schrader et. al.[2,4], Petty[5] and Everall[6] that organic liquids may show self absorption of the Raman spectrum excited with 1064 nm excitation due to overtones and combinations of mid-infrared vibrations, i.e. in a similar manner to the absorption phenomenon seen with aqueous samples. Obviously, a move to a shorter excitation wavelength will reduce this effect if the Raman radiation is moved into a region where the organic liquid concerned absorbs less radiation.

3.1.2 Cost advantages of shorter wavelength excitation

The majority of commercially available FT Raman spectrometers are based on modified standard FTIR instruments. The main costs involved in the modification of an FTIR instrument for the Raman experiment are the detection system (approximately £3K for an InGaAs device) and the laser (approximately £15K for a Nd^{3+}:YAG laser).

A laser for FT Raman spectroscopy should have a linewidth of less than 1 cm^{-1}, be capable of being focused to a spot size of at least 250 μm at the sample and generate a

stable power output, ie. 0.5 W with less than 0.1 % power fluctuation, to be competitive in performance to a Nd^{3+}:YAG laser. Diode lasers are becoming increasingly attractive as an alternative excitation source for Raman spectroscopy as they offer higher stable outputs, for example GaAlAs diode lasers (750 - 860 nm) and InGaAs diode lasers (960 - 980 nm). Suitable diode lasers producing 0.5 W and operating at 800 nm are steadily becoming cheaper and will be available shortly for ~ £2.5K.

The Raman spectrum produced by a laser device operating at 800 nm can be detected using a Silicon semiconductor. These devices are mass produced for a little as a few pounds each. Thus, the motivation to experiment with shorter excitation wavelengths for FT Raman spectroscopy is extremely strong from a purely financial point of view.

3.1.3 The use of charge coupled devices as detectors for Raman spectroscopy

Recently, attempts have been made to move away from the 1.064 μm near infrared source, but for completely different reasons to those given in Section 3.1.2. Perhaps the "best practice" in current Raman techniques is to use a suitable laser illuminating a specimen as would be done in a conventional Raman spectrometer, to collect the scattered light and then examine it with a spectrograph and a charge coupled device detector (CCD).

Normally (if not always), the spectrograph is fronted with a transmission filter to eliminate the elastically scattered and reflected light at the source wavelength. Reports describing the use of deep red laser sources rather than visible ones for Raman spectroscopy have proliferated recently[7-20] and it is now clear from many of these reports that a spectrograph and CCD can offer very high sensitivity indeed due to the multiplex advantage. They are also ideal for use with microscopes and other "difficult" sampling systems.[14,18] It is likely that the recent attraction of shorter wavelength excitation is due to the restriction imposed by the use of CCD detection. The sensitivity range of CCD's is restricted to the close near infrared (or very deep red) and hence source wavelengths beyond 700 - 750 nm are not frequently used.

Regardless of whether the spectrograph / CCD or the modified FTIR approaches become the instruments of the future in routine analytical usage, there remains one question - should analysts "stick" to 1.064 μm or look to shorter wavelength sources?

Shortening the wavelength below one micron as we said here could have advantages - increasing sensitivity, opening of aqueous systems and high temperatures but there will be a consequent price to pay - an inevitable increase in the incidence of fluorescence and this chapter describes an attempt to assess the problem.

In order to be able to invoke sources from the visible to 1 μm, an FT instrument is essential. This chapter therefore describes the development and assessment of a Ti:Sapphire laser based FT Raman spectrometer to fully explore the advantages offered using excitation wavelengths in the range between the typical diffraction instrumental excitation wavelengths (i.e. Ar^+, He-Ne & Kr^+ laser wavelengths) and the wavelength used in most FT instruments (i.e. 1.064 μm).

The project involved the development of two prototype instruments. The first prototype was constructed to demonstrate the feasibility of the experiment, once this was achieved a more elegant prototype was constructed. The development of both of these prototypes is described in this chapter, however the first prototype is only given limited attention because the second was superior in performance and all the experiments carried out with the first instrument were repeated with the second one and indeed the bulk of the project was focused on the development and assessment of this machine.

3.2 THE FIRST PROTOTYPE

Figure 3.1 shows a schematic layout of the first prototype instrument. A typical FT Raman system consists of an excitation source; a set of Rayleigh rejection filters (marked as F in Figure 3.1); an interferometer and a sensitive detector.

3.2.1 The excitation source

The same excitation source i.e. a Titanium:Sapphire laser was used throughout this investigation and both prototypes used the same source. Figure 3.2 shows a schematic layout of the Titanium:Sapphire laser. The laser used was a model 479

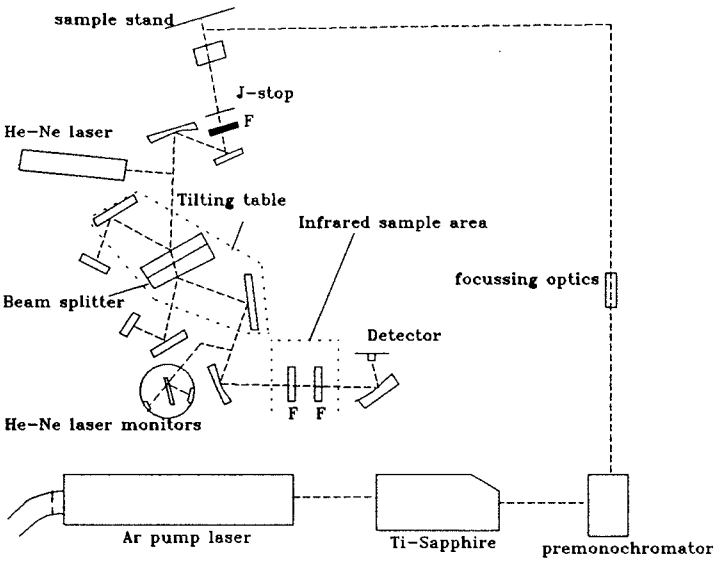

Figure 3.1 - Ti-Sapphire 1720 FT Raman prototype.

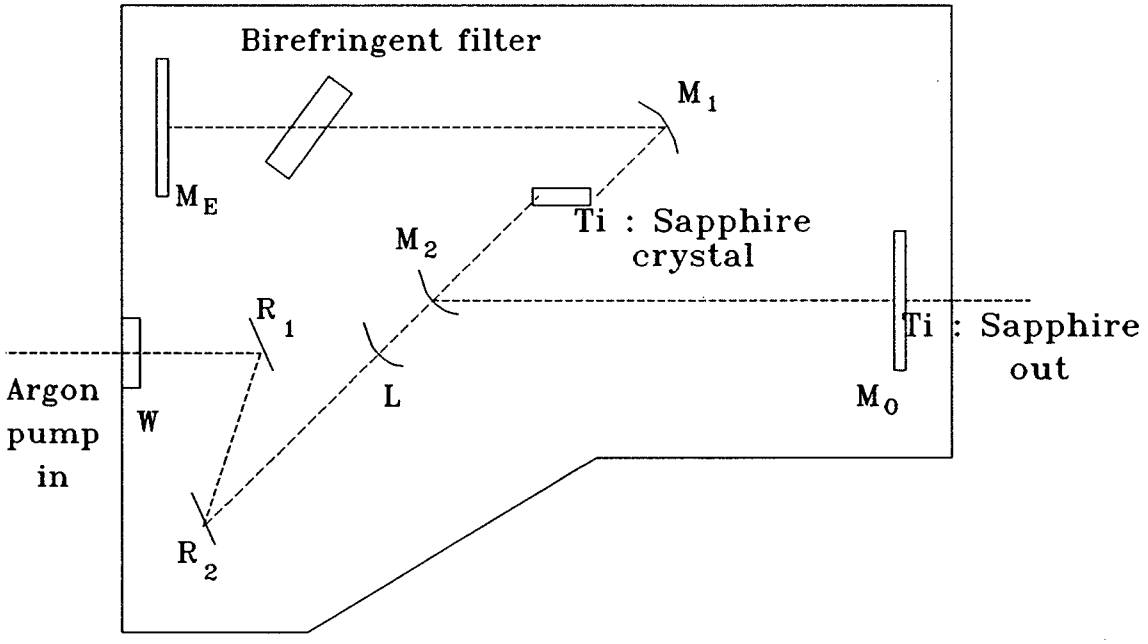

Figure 3.2: Schematic layout of Ti:Sapphire laser.

Lexel Ti:Sapphire laser pumped by a 5 W (all lines) argon ion laser. The output of the laser can be tuned to the appropriate wavelength using a 3-plate birefringent quartz filter and one of the three mirror sets optimised for the wavelength range required. Figure 3.3 shows the typical tuning curves of the Ti:Sapphire laser using each of the mirror sets. The effective range of the laser is thus from 700 to 950 nm.

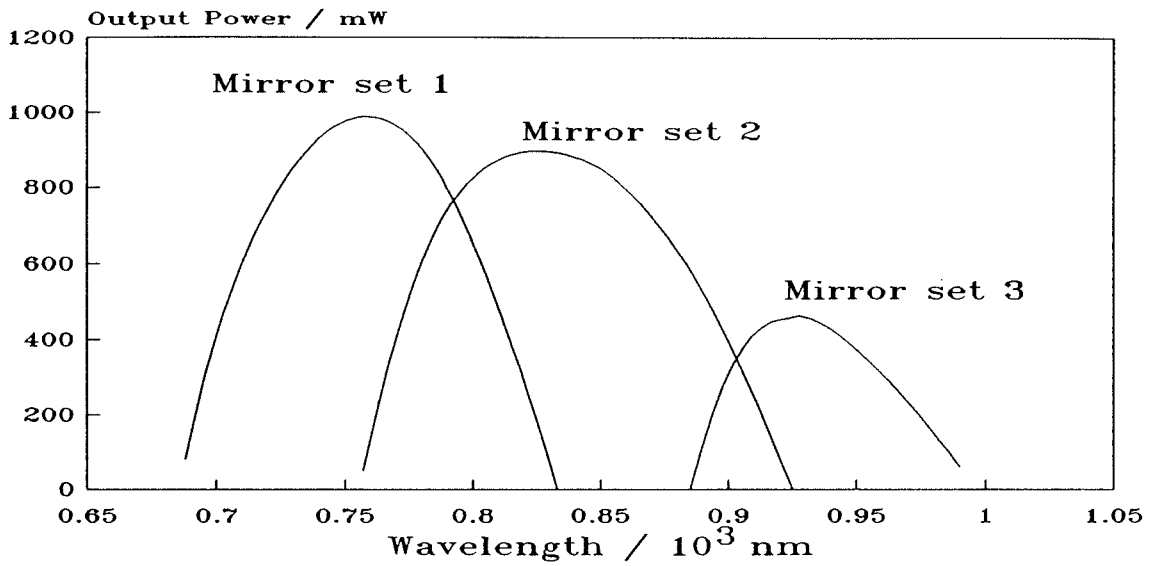

Figure 3.3: Typical Ti:Sapphire tuning curves.

The intensity of the Rayleigh radiation emitted by the sample that enters the interferometer in FT Raman spectroscopy must be attenuated by a factor $\sim 10^{10}$ to prevent the detector being saturated. Any background radiation emitted from the laser even if it is of extremely weak intensity may be noticed in an FT Raman spectrum if it is not removed before the sample is irradiated because of reflection off the sample into the interferometer. It was found that the Ti:Sapphire laser emitted a relatively strong background which completely obscured the collected Raman radiation and thus had to be removed. Initially this was accomplished using an Anaspec premonochromator but this device was judged to be inadequate because 40 percent of the power entering the premonochromator was lost and the undesirable background was not completely eliminated. To solve the problem a Barr Associates 780 nm line filter was used to filter the laser radiation. The transmission curve of this filter is shown in Figure 3.4. The motivation for the choice of 780 nm as the excitation wavelength is described in the next section.

3.2.2 The Rayleigh rejection filters

The initial excitation wavelength chosen for the first prototype was controlled primarily by the availability of Rayleigh rejection filters.

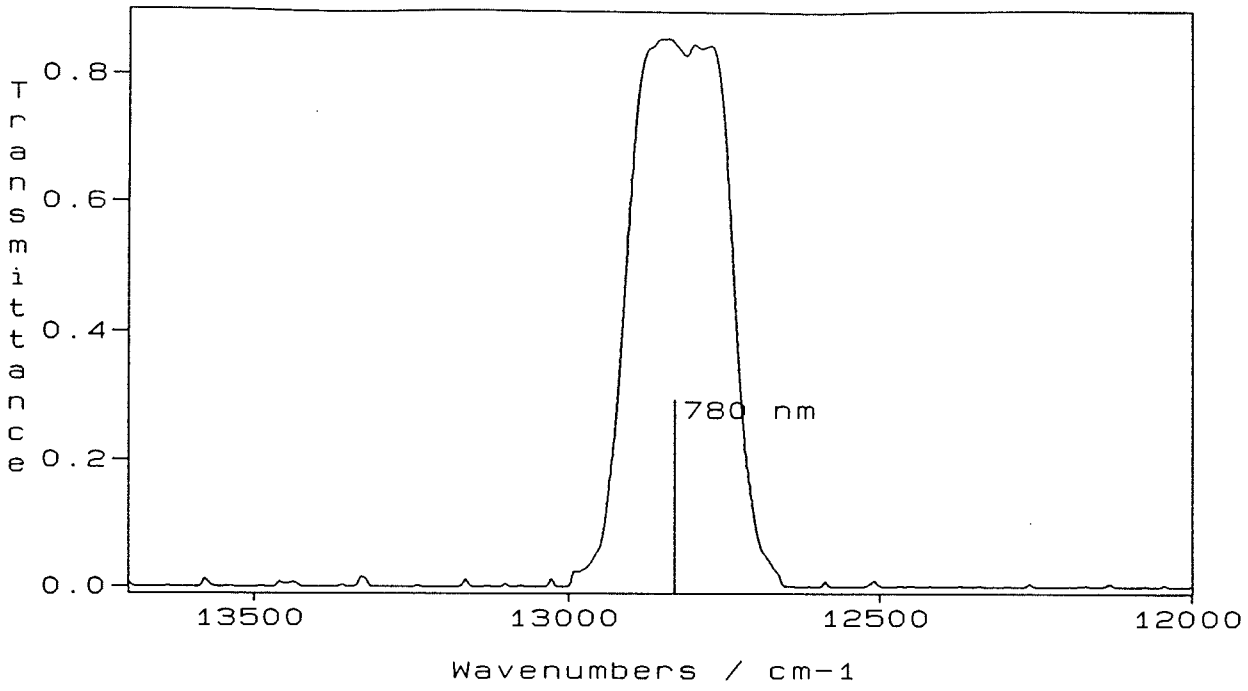

Figure 3.4: Transmission curve of 780 nm Barr Associates line filter.

As stated above the Rayleigh rejection filters required for FT Raman spectroscopy must provide an attenuation of 10^{10} at the wavelength of the laser line. The filters for the first prototype were two holographic notch filters loaned from Kaiser Optics (Miami, Florida) allowing us to record Stokes and Anti-Stokes radiation under the appropriate conditions. The filters were designed for optimum rejection at 780 nm and have a cutoff of 150 cm^{-1} for the Stokes Raman radiation. Thus all the spectra recorded with the first prototype used 780 nm excitation.

The choice of excitation wavelength was somewhat fortuitous because it corresponded to the peak power output of the laser as can be seen from Figure 3.3. Although laser power was not a problem using relatively low laser wavelengths (i.e. 750 to 800 nm) the reduction in laser power caused by changing to Mirror sets 2 and 3 meant that a primary consideration in the choice of wavelength when moving to higher wavelengths (i.e. above 800 and 900 nm) in further investigations was the available laser power. The curves in Figure 3.3 show that in principle with a 5 W Argon ion pump laser there should be adequate power at all wavelength ranges between 710 and 950 nm, in practice the inability of the pump laser to maintain TEM_{00} (i.e. Gaussian intensity beam profile)

meant that the maximum designed power output of the Ti:Sapphire laser was rarely attained.

No other excitation wavelength was used with the first prototype because of the unavailability of suitable Rayleigh rejection filters. Once these filters were available the second prototype was operational, thus investigations using excitation wavelengths other than 780 nm were carried out exclusively with the second prototype.

3.2.3 The interferometer

The first prototype used a modified Perkin Elmer 1720 FTIR instrument as the interferometer. A commercial FTIR instrument has aluminium mirrors, which are adequate for the mid-infrared wavelength range and the wavelength range of the Raman scattered radiation produced by 1.064 μm. However these instruments exhibit poor transmission at wavelengths shorter than 800 nm due to reflection losses at the mirrors. Figure 3.5 shows the relative reflectivity of gold and aluminium in the near infrared region.

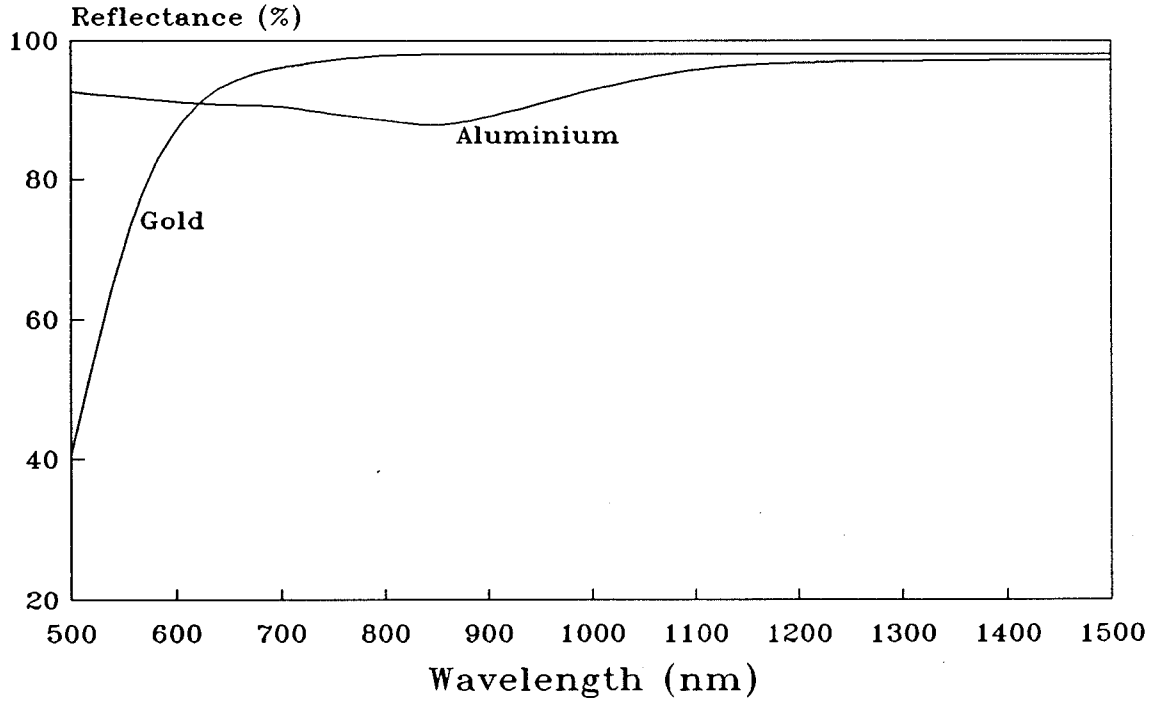

Figure 3.5: The relative reflectance of Gold and Aluminium as a function of wavelength.

In the 1720 interferometer some of the mirror were gold coated mirrors but four of the mirrors in the interferometer were still aluminium. For one mirror the reflection losses are not serious but for a number of mirrors (n) the reflection loss at a specific wavelength is proportional to R^n where R is the percentage reflectance. The consequence of this is that the performance of the instrument is somewhat poorer than it should have been. Since the main goal of the work here was simply to demonstrate the feasibility of FT Raman at shorter wavelengths this reduction in performance was tolerated. In the next prototype all of the mirrors were gold coated to give maximum possible performance.

The 1720 instrument used also had a quartz beamsplitter as opposed to a wide range KBr one usually used in the combined commercial FTIR/Raman instrument.

3.2.4 The detector

The detector used in this prototype was a Silicon detector with preamplifier constructed by Mr Bob Bennett of Perkin Elmer. Figure 3.6 shows a typical response curve for a Silicon detector.

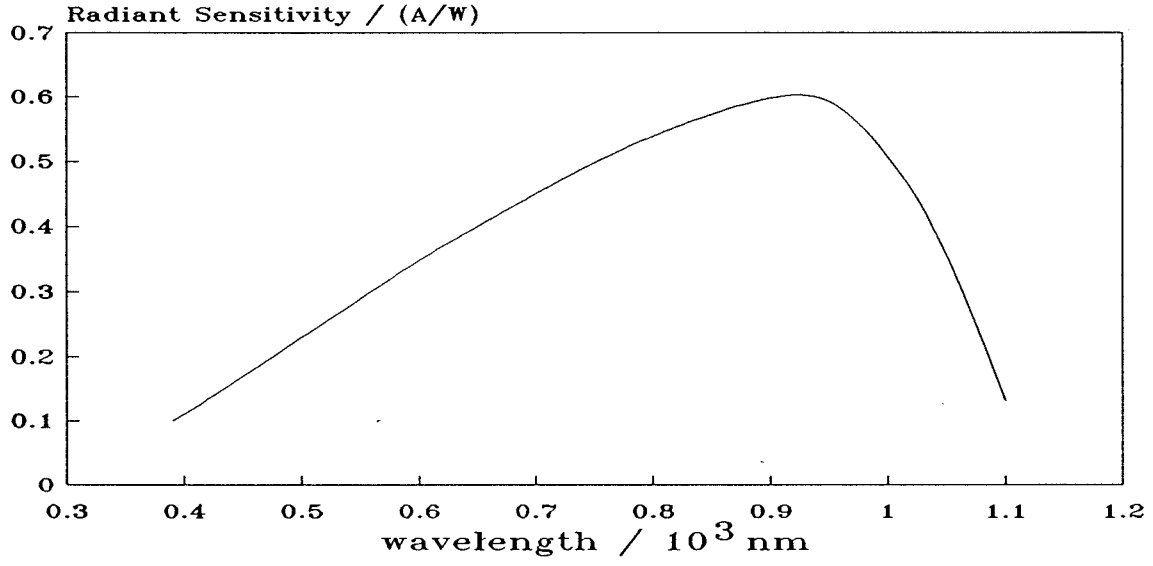

Figure 3.6 : Typical Silicon detector response as a function of wavelength.

From the figure it can be deduced that with 780 nm excitation the long wavelength cutoff

of the Raman radiation should be 3700 cm^{-1}.

3.2.5 Selected results

The initial performance of this instrument was poor thus the samples chosen for study were relatively strong Raman scatterers, therefore only two spectra recorded with the first prototype are shown here. Figure 3.7 shows the Raman spectrum of Sulphur.

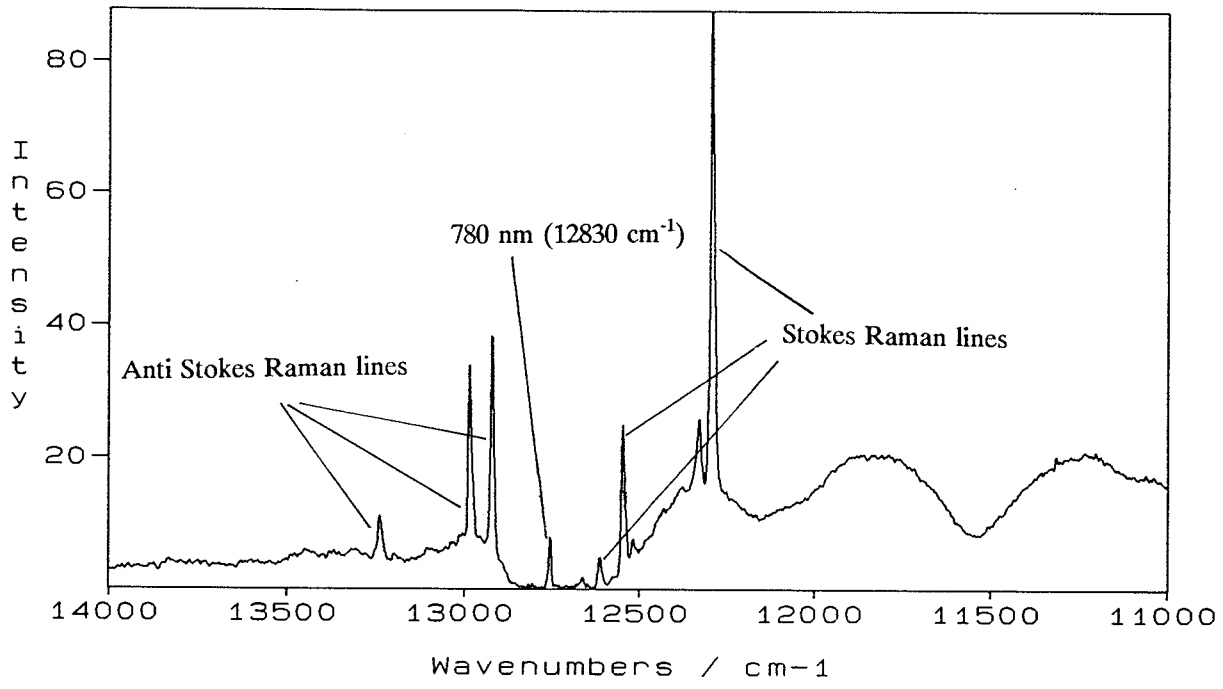

Figure 3.7: The Raman spectrum of Sulphur (780 nm excitation).

The ordinate scale in Figure 3.7 is in absolute wavenumbers, the spectrum has not been corrected for the instrumental response[21]. Both the Stokes and Anti Stokes radiation can be seen and the position of the laser line is also evident, i.e. the filters did not eliminate the elastically scattered component. The broad background is the result of background radiation emitted by the laser (Section 3.2.1) which has not been adequately filtered with the pre-monochromator. Subsequent spectra do not show this background because the problem was remedied by using a laser line filter. Figures 3.8 and 3.9 show the Raman spectrum of anthracene recorded with 1064 and 780 nm excitation. Again both spectra have not been corrected for the instrumental response.

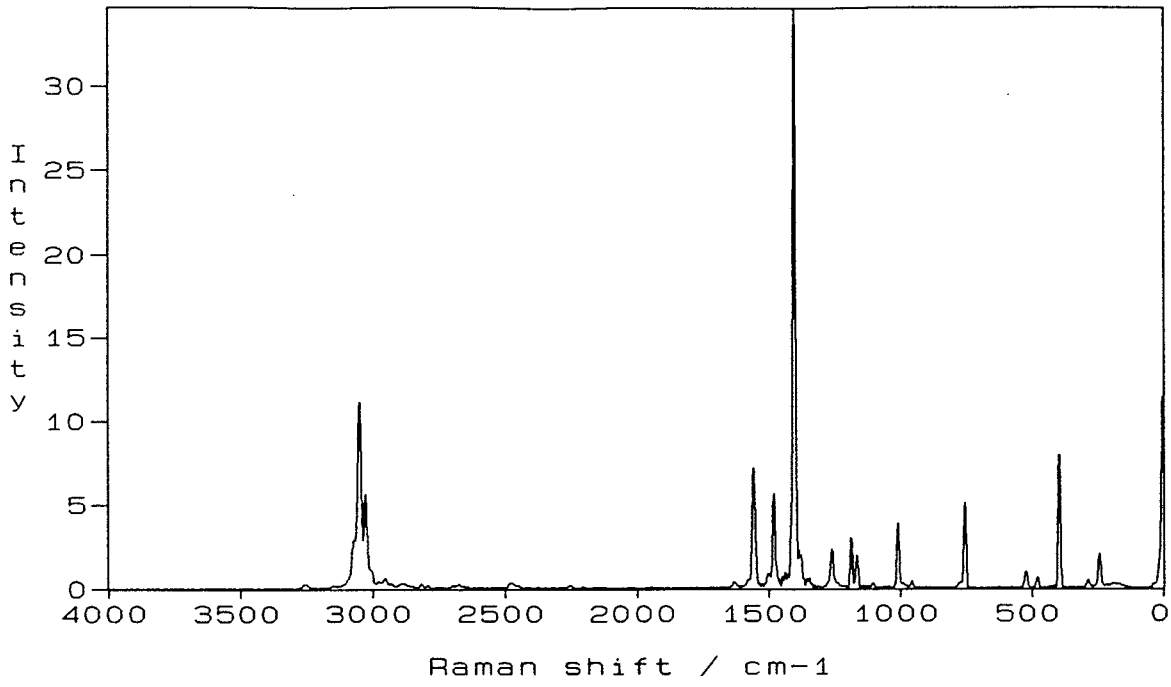

Figure 3.8: Raman spectrum of Anthracene (1064 nm excitation).

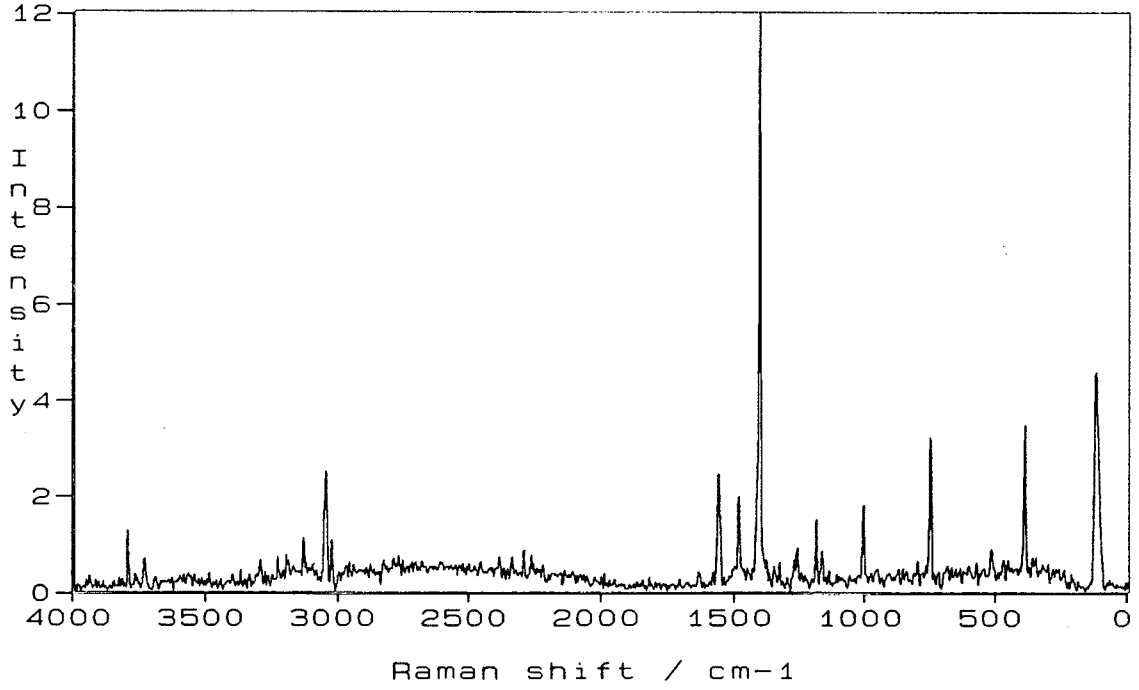

Figure 3.9: Raman spectrum of Anthracene (780 nm excitation).

3.3 THE SECOND PROTOTYPE

Figure 3.10 shows a schematic layout of the second prototype instrument. The same excitation source and Silicon detector with preamplifier as before were used in this instrument but in all other respects the machines are very different.

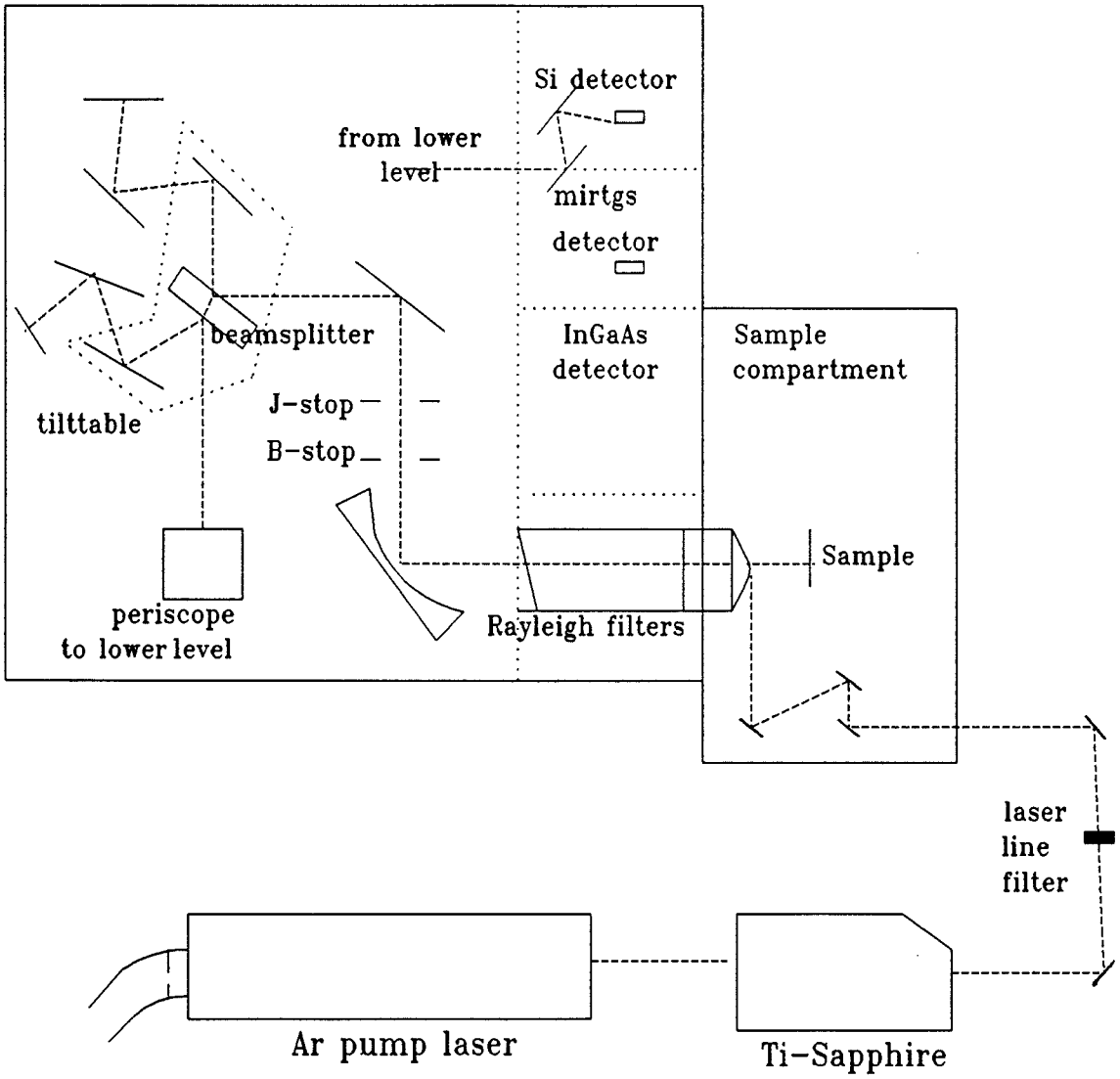

Figure 3.10 - Schematic layout of second prototype Ti:Sapphire based FT Raman spectrometer.

The main differences between this instrument and the one described in Section 3.2 was that this instrument was designed for longer term usage (the other instrument was only operational for approximately two weeks), a more sophisticated interferometer was used

and excitation wavelengths other than 780 nm were available.

3.3.1 The excitation source

For each discrete excitation wavelength chosen, a matching set of Rayleigh rejection filters and laser line filters had to be constructed. The range of excitation wavelengths that could be used was thus limited financially because of the expense of producing the filters required for each new wavelength. In addition problems with the laser power output meant that it was more desirable to chose a wavelength close to a peak in the tuning curve (given in Figure 3.3) rather than any other wavelength, thus 835 and 920 nm (in addition to 780 nm) were chosen as the "best" laser wavelengths to use to fully explore the potential of the wavelength range 700 to 950 nm in view of the circumstances. Figure 3.11 shows the transmission curves of the line filters used at 835 and 920 nm.

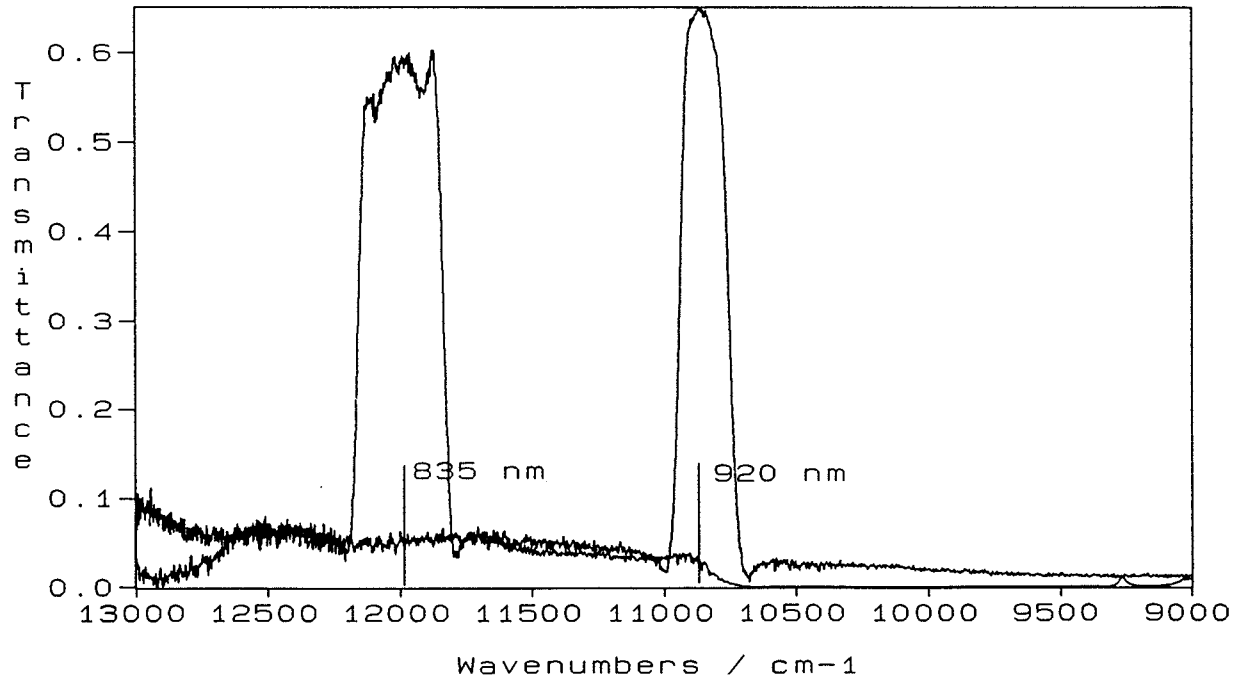

Figure 3.11: Transmission curves of 835 and 920 nm laser line filters.

3.3.2 The Rayleigh rejection filters

For each wavelength chosen, a matching set of Rayleigh rejection filters were made. Unfortunately the 1" filters loaned from Kaiser Optics for the first prototype had to be returned. PL Coatings (Belfast, Northern Ireland) were chosen as suppliers of the required filters for each wavelength as part of the project proposal*. The design of the interferometer used required that the rejection filters were placed in a tube immediately following the collection optics and thus the filters had to be in the form of two 65 mm diameter units with one placed at 0^{o} and the other at 10^{o} with respect to the incident collected Raman radiation before it entered the interferometer. Figures 3.12, 3,13 and 3.14 show the combined transmission profiles of each of the sets of Rayleigh rejection filters made by PL Coatings, one filter has been placed at 10^{o} and the other at 0^{o} as in the instrument. In each figure the position of the laser line is marked.

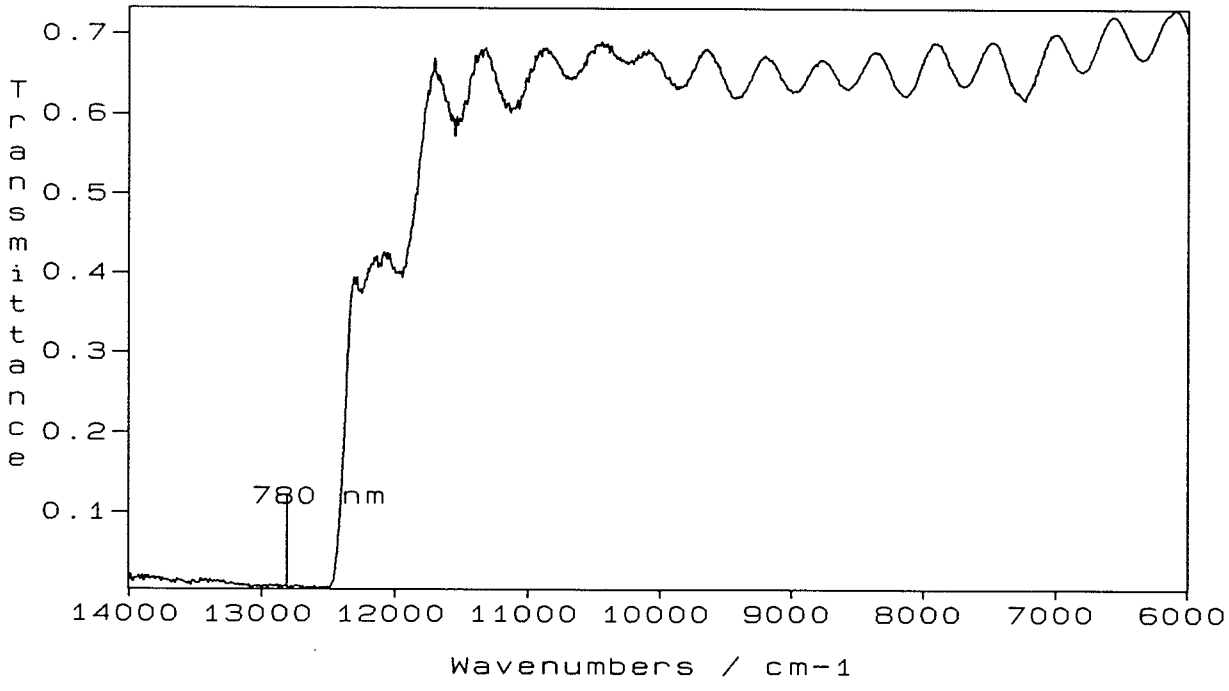

Figure 3.12: Combined transmission curves of 780 nm Rayleigh rejection filters.

*The project was funded under a joint LINK scheme involving the University, Perkin Elmer and P.L. Coatings.

The filters provided by P.L. Coatings were disappointing in that they permitted us to approach to only 450 cm^{-1} of the exciting line. State-of-the-art Nd^{3+}:YAG filters will permit operation for 100 cm^{-1}. Further, the filters show distinct "rippling" in their transmission characteristics, a feature largely eliminated in contemporary Nd^{3+}:YAG rejection filters. Unfortunately failings were unavoidable as no other source of Rayleigh rejection filters was available.

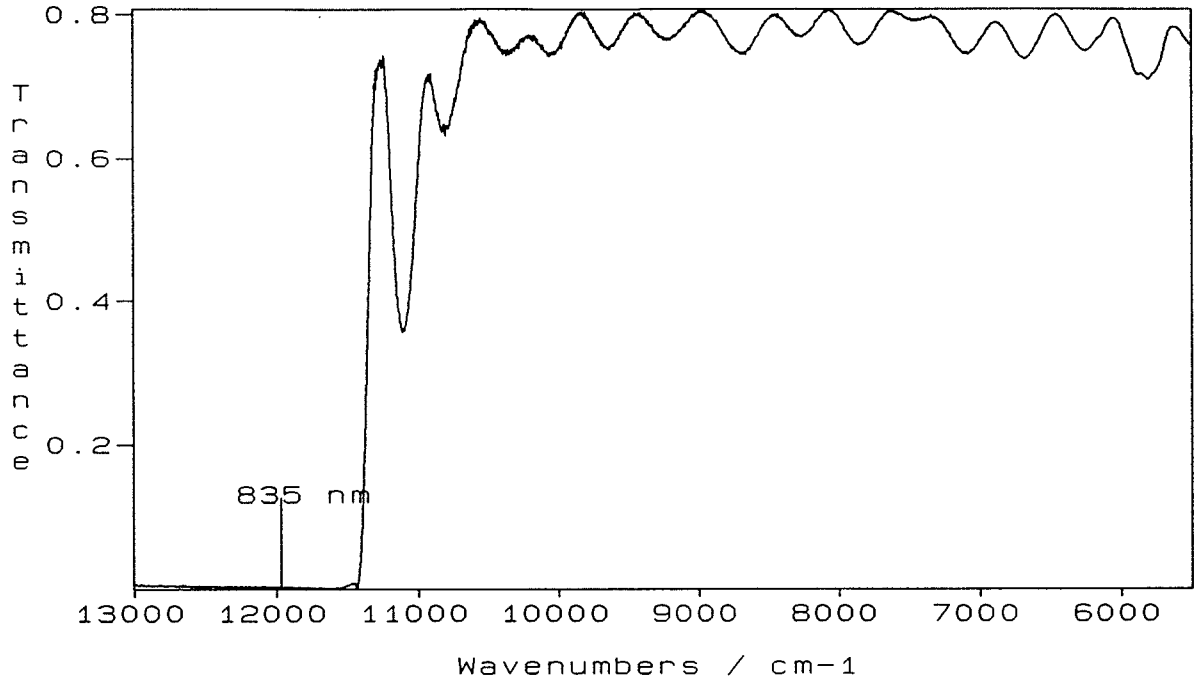

Figure 3.13: Combined transmission curves of 835 nm Rayleigh rejection filters.

3.3.4 The interferometer

For this instrument a Perkin Elmer System 2000 interferometer was used. As mentioned in Section 3.2.3 the interferometer had gold optics and the beamsplitter was quartz.

3.3.5 The detector

The same Silicon detector was used in the instrument when either 780 or 835 nm were used as excitation sources. With 835 nm as an excitation source the long wavelength

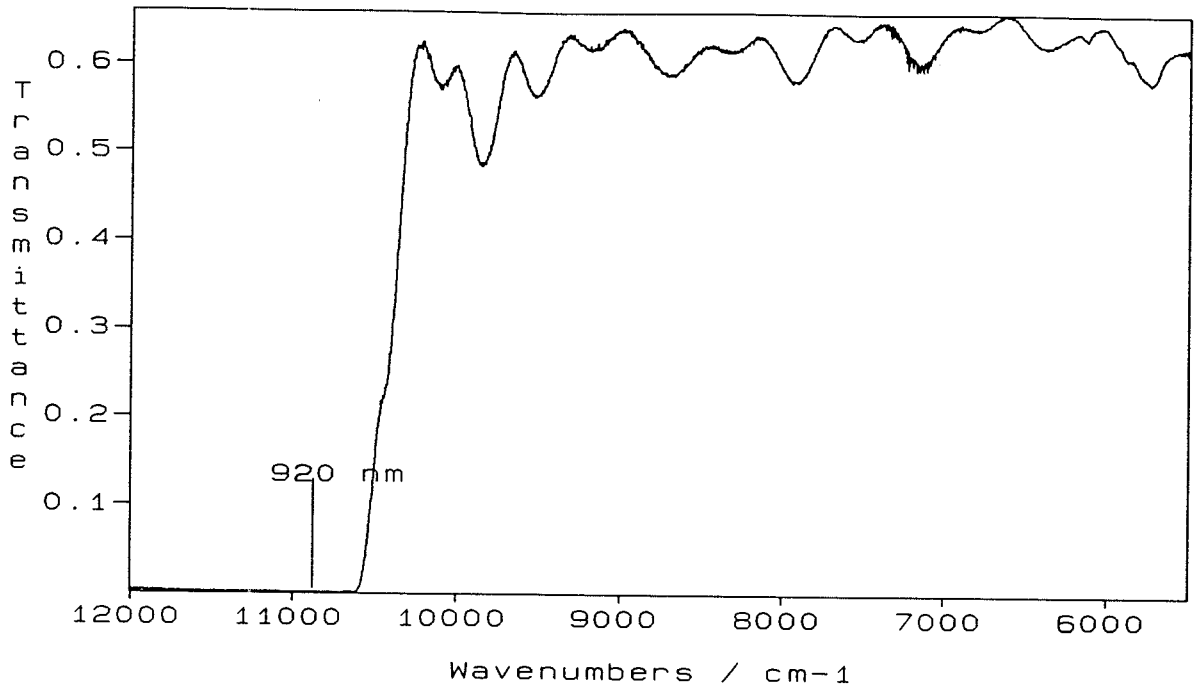

Figure 3.14: Combined transmission curves of 920 nm Rayleigh rejection filters.

cutoff of the Raman spectrum was hence 3300 cm^{-1}. When 920 nm was used as an excitation source, the usual InGaAs detector used for 1.064 μm excitation was activated, this offering a long wavelength cutoff of 4500 cm^{-1}.

3.3.6 Instrument response profiles of the second prototype

Figures 3.15 and 3.16 show the instrument response profiles for the second prototype (shown in Raman shift) with 780 and 835 nm respectively. In both figures the Silicon detector was used.

The response curves have been generated by dividing the recorded spectrum of a tungsten light bulb that has been suitably attenuated to prevent detector saturation by the calculated spectrum of a tungsten light bulb (i.e. from Planck's equation corrected for the emissivity of tungsten).

Figures 3.17 and 3.18 show the instrument response functions for 920 nm excitation using the Silicon and the InGaAs detectors respectively.

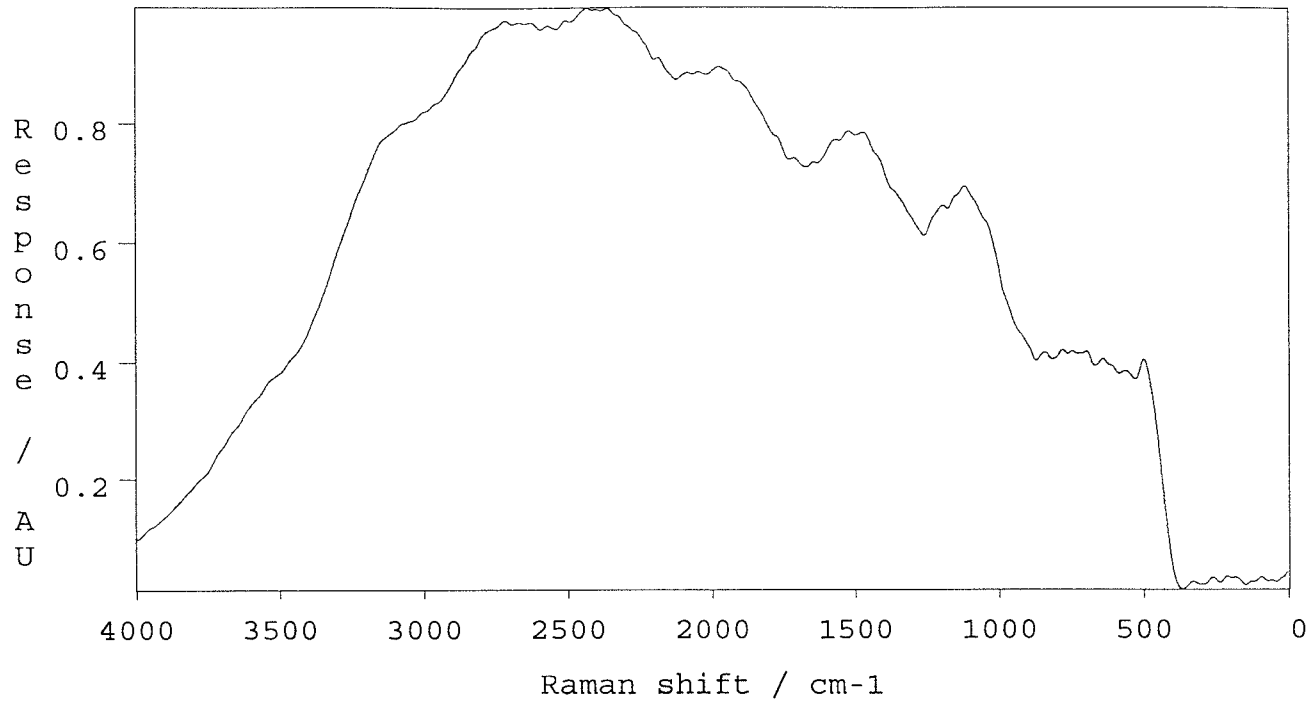

Figure 3.15: Instrument response profile of second prototype using 780 nm excitation.

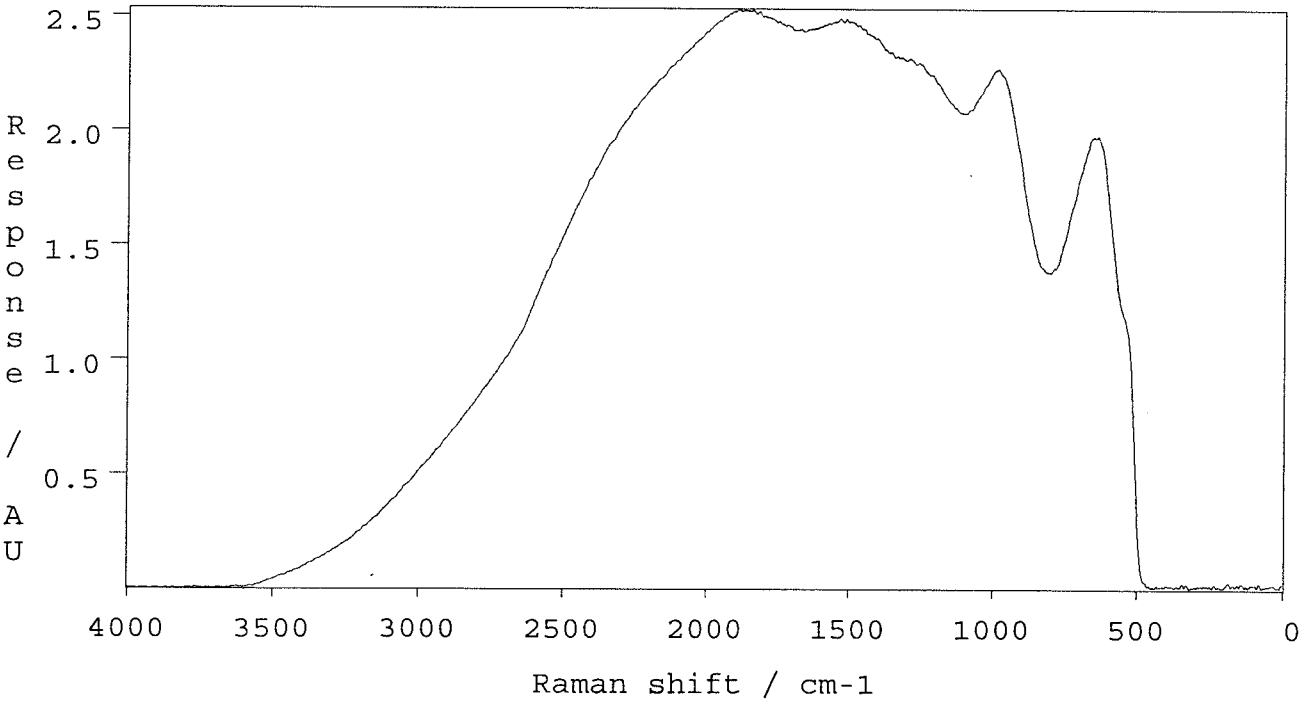

Figure 3.16: Instrument response profile of second prototype using 835 nm excitation.

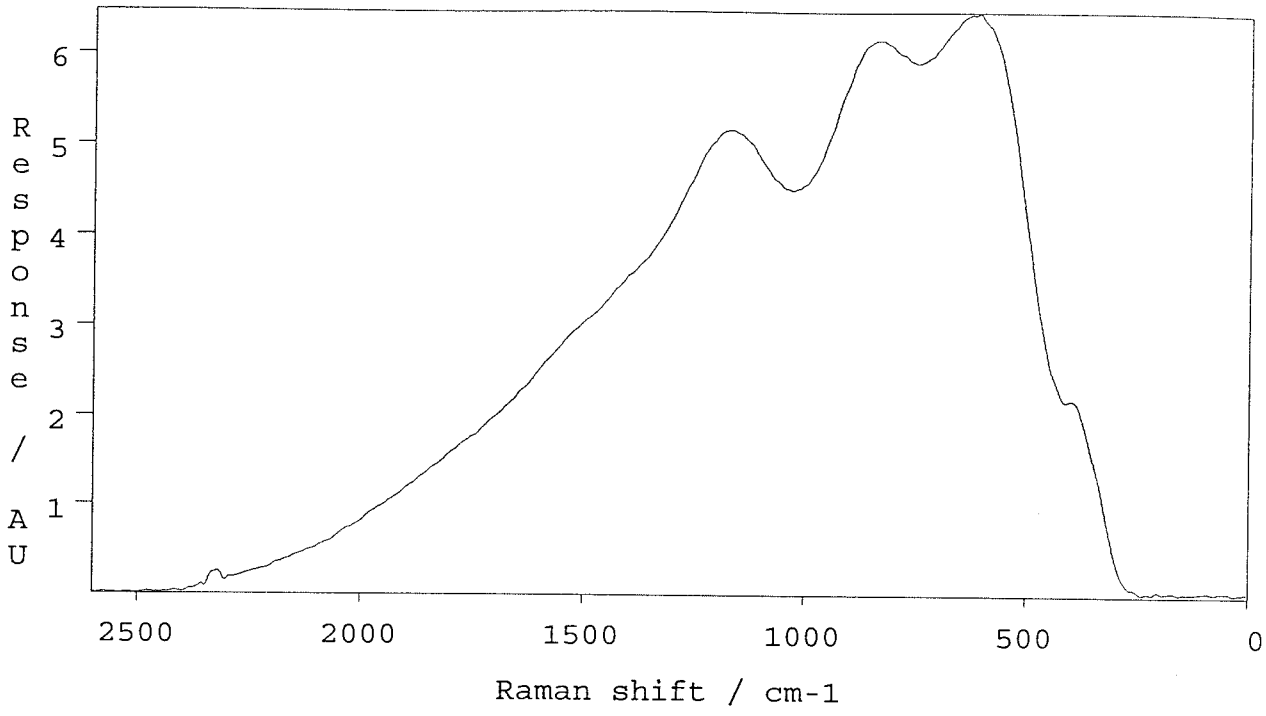

Figure 3.17: Instrument response function for 920 nm excitation using Silicon detector.

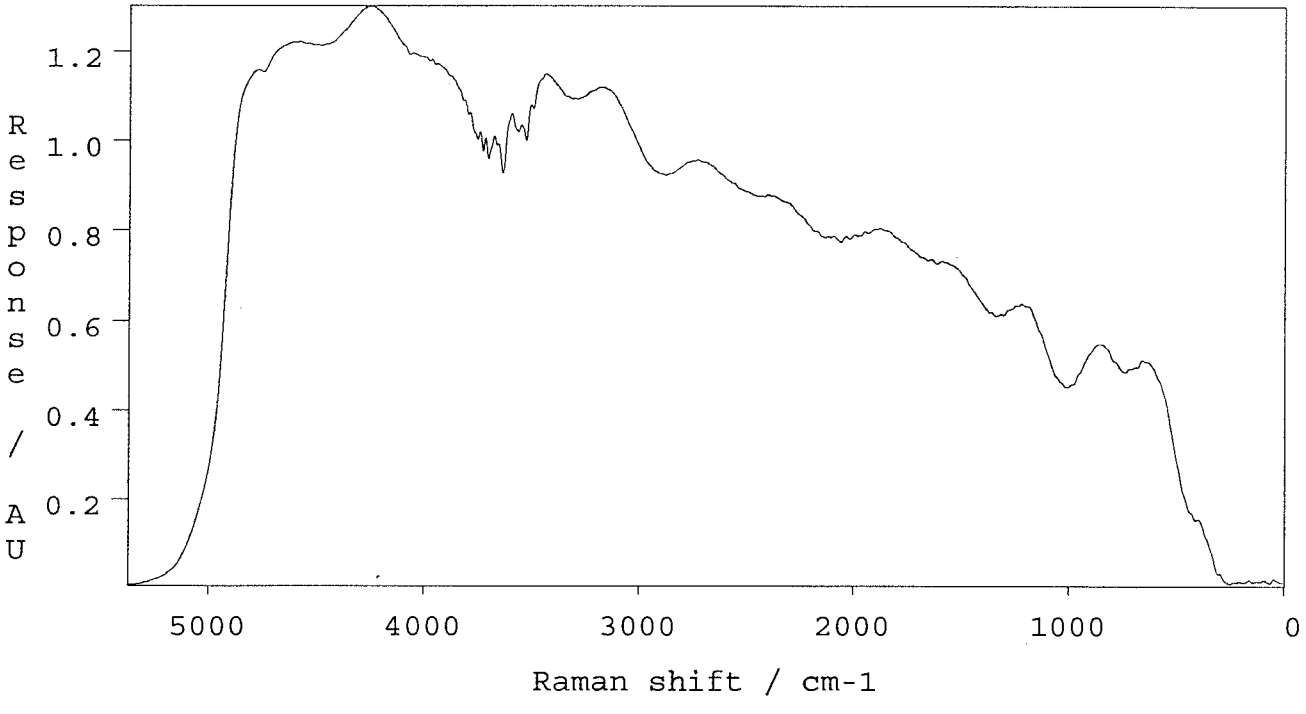

Figure 3.18: Instrument response function for 920 nm excitation using InGaAs detector.

All of the subsequent spectra reported in this chapter have been recorded using the instrument described here (Section 3.4) with one of the three excitation wavelengths (i.e. 780, 835 or 920 nm).

3.4 COMPARISON OF 780, 835 AND 920 NM AS EXCITATION WAVELENGTHS FOR RAMAN SPECTROSCOPY

A complete comparison of deep red laser sources in FT Raman spectroscopy must include a wide range of examples showing the quality of Raman spectra that are to be expected using these wavelengths. Possibly the best way to achieve this is to chose a "basket" of samples representative of the materials usually examined with FT Raman spectroscopy and display the spectra obtained using these identical samples at the wavelengths evaluated. Fifteen samples were chosen and these could be broadly divided into inorganic, organic and polymer samples.

3.4.1 Inorganic samples

Four inorganic compounds were chosen, they were barium sulphate, potassium ferrocyanide, potassium ferricyanide, and potassium chromate. Figures 3.19 to 3.22 show a comparison of spectra obtained of each compound at 780, 835, 920 and 1064 nm.
In each figure the spectra recorded at 780, 835 and 920 nm were recorded on the Titanium:Sapphire laser based instrument described in Section 3.3. The spectra shown using 1064 nm excitation were recorded using a Perkin Elmer 1720 FT Raman spectrometer with a Neodymium:YAG laser and InGaAs detector. In each spectrum no account has been made of the instrumental response function. Thus it is noticeable that the relative peak heights in each spectrum differ in intensity.

The short wavelength cutoff of the Ti:Sapphire based instrument at each excitation wavelength used was dependent on the Rayleigh rejection filters used. In each case the Raman spectrum could be recorded to within approximately 450 cm^{-1} of the laser line. On the FT Raman instrument used to record the spectra shown at 1064 nm the cutoff was approximately 200 cm^{-1}. The implication of this is that some of the Raman spectrum

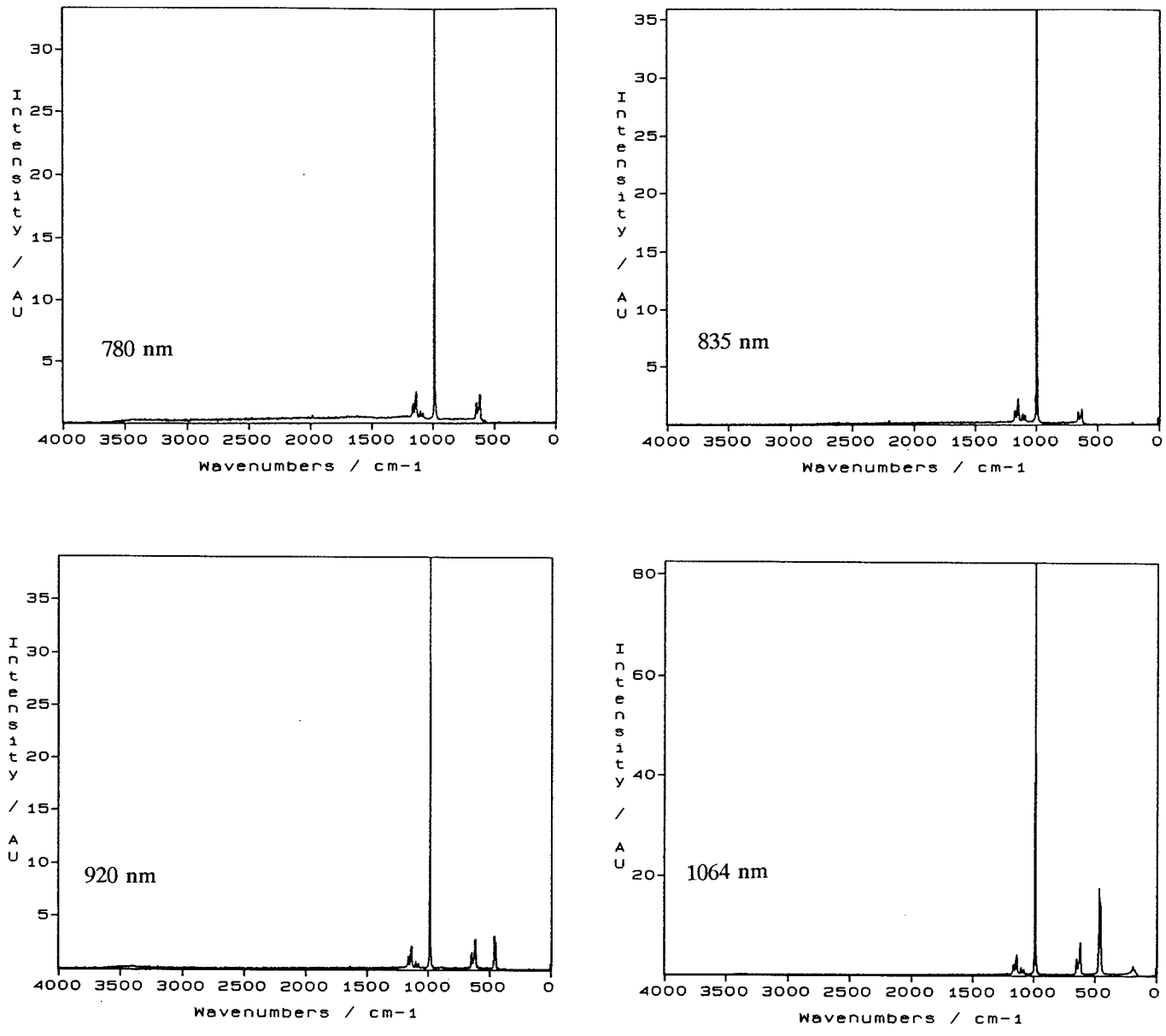

Figure 3.19 - Raman spectra of barium sulphate.

is lost using the Titanium:Sapphire laser based instrument. This is not a weakness of the excitation wavelength however because there is no reason why the Rayleigh rejection filters at these wavelengths cannot match the performance of the Rayleigh rejection filters used at 1064 nm.

Although the inorganic samples chosen were by no means representative of inorganic samples as a whole it was found that in general inorganic samples gave good spectra at

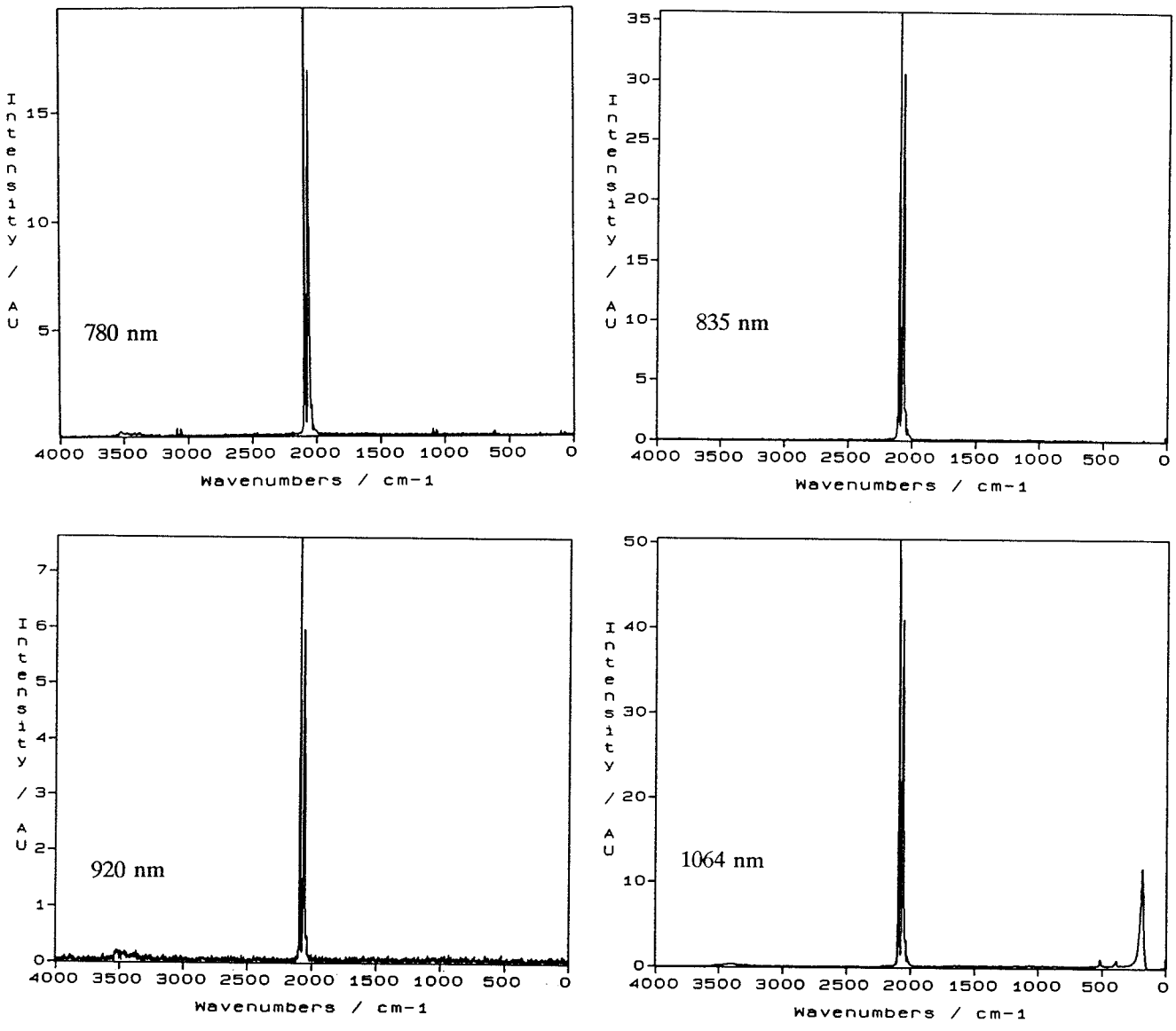

Figure 3.20 - Raman spectra of potassium ferrocyanide.

all the wavelengths examined with very little fluorescence. In some cases the samples burned because of absorption at the laser wavelength, when this occurred e.g. copper sulphate, nickel sulphate it was found that the problem occurred at all wavelengths and often reducing the laser power and scanning for a longer time allowed a spectrum to be collected.

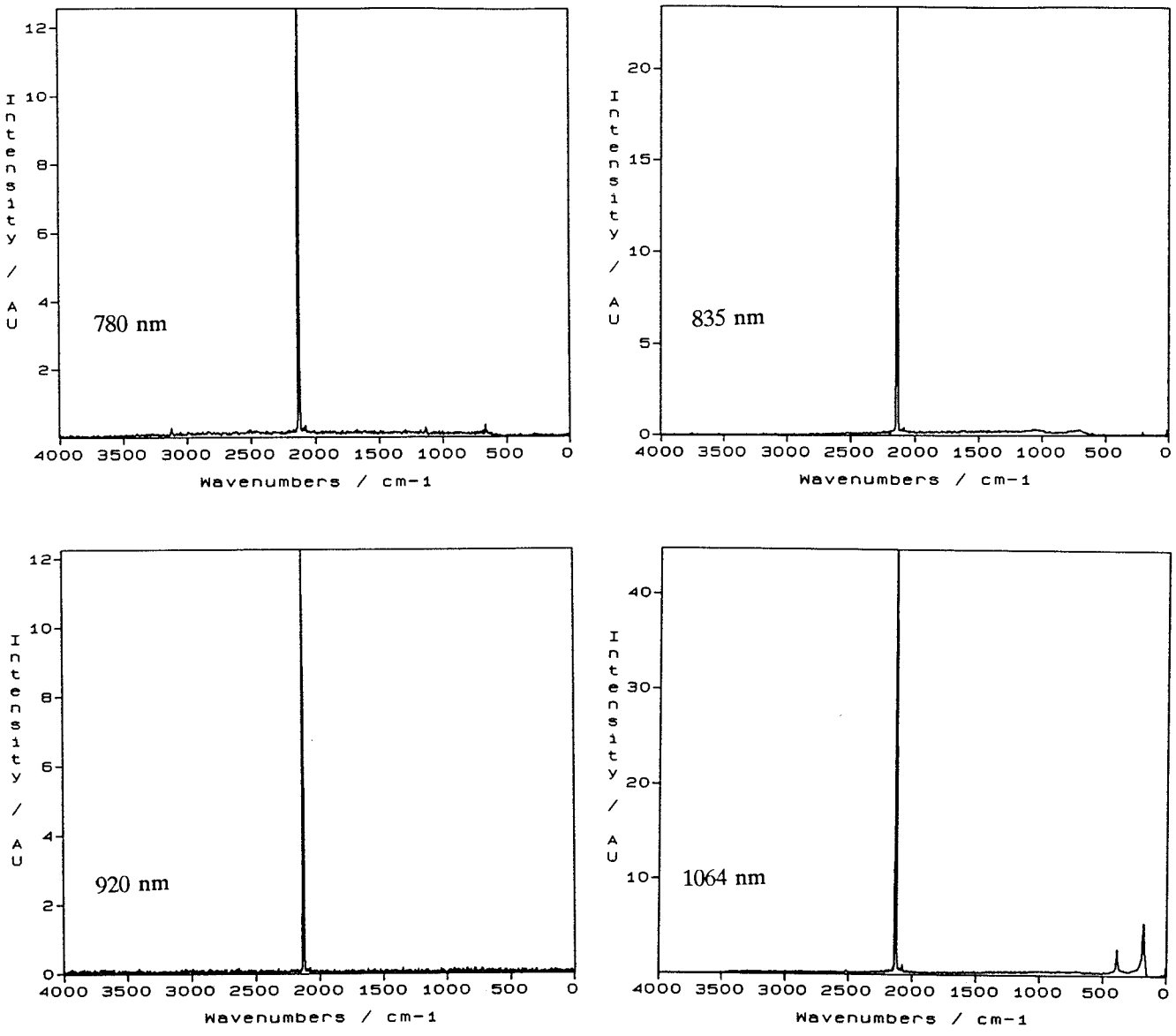

Figure 3.21 - Raman spectra of potassium ferricyanide.

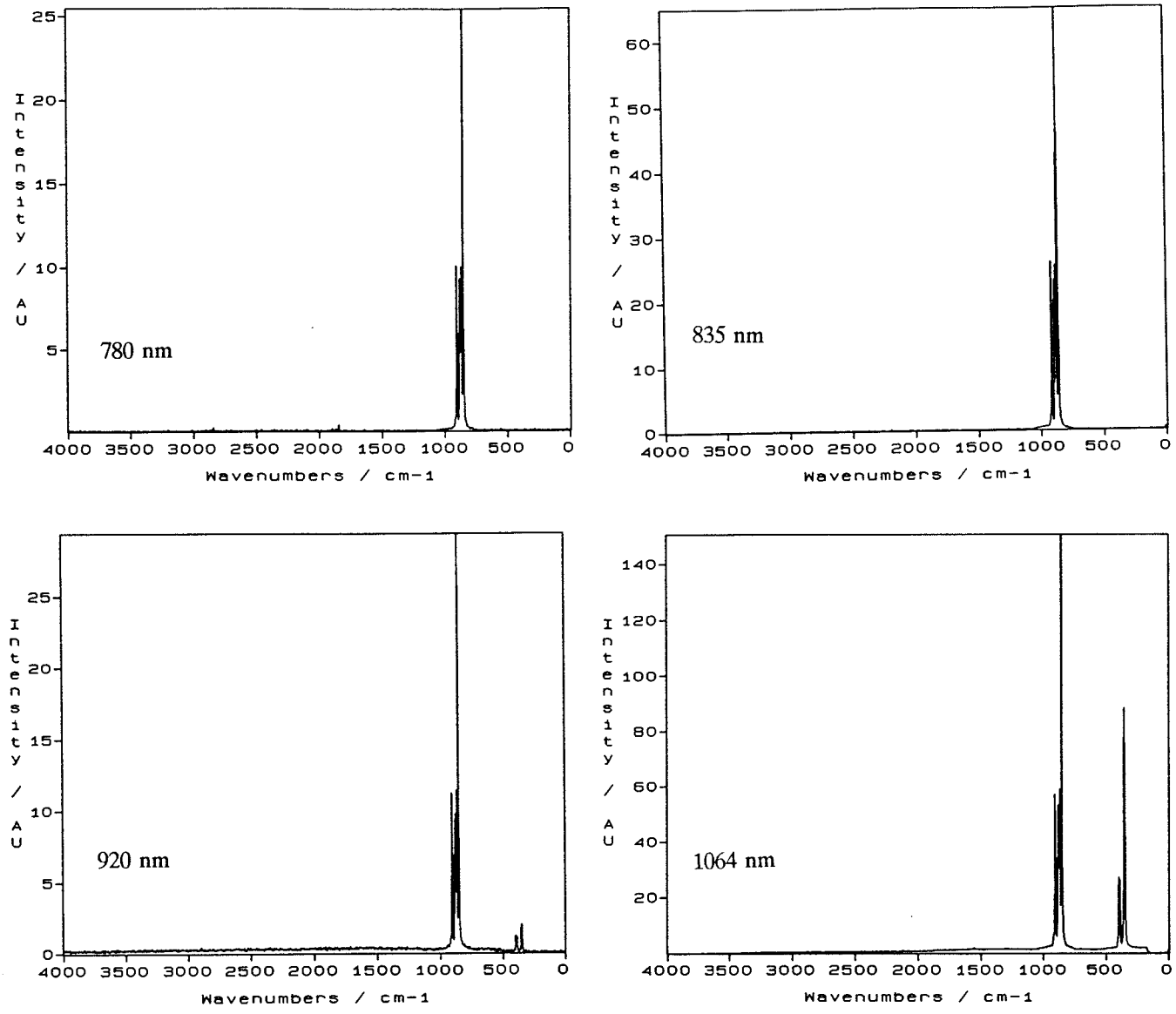

Figure 3.22 - Raman spectra of potassium chromate.

3.4.2 Organic samples

Six samples were chosen to be representative of organic samples for the four wavelengths as a whole. Sample were chosen that were likely to show relatively significant changes in levels of fluorescence over the excitation wavelength range studied.

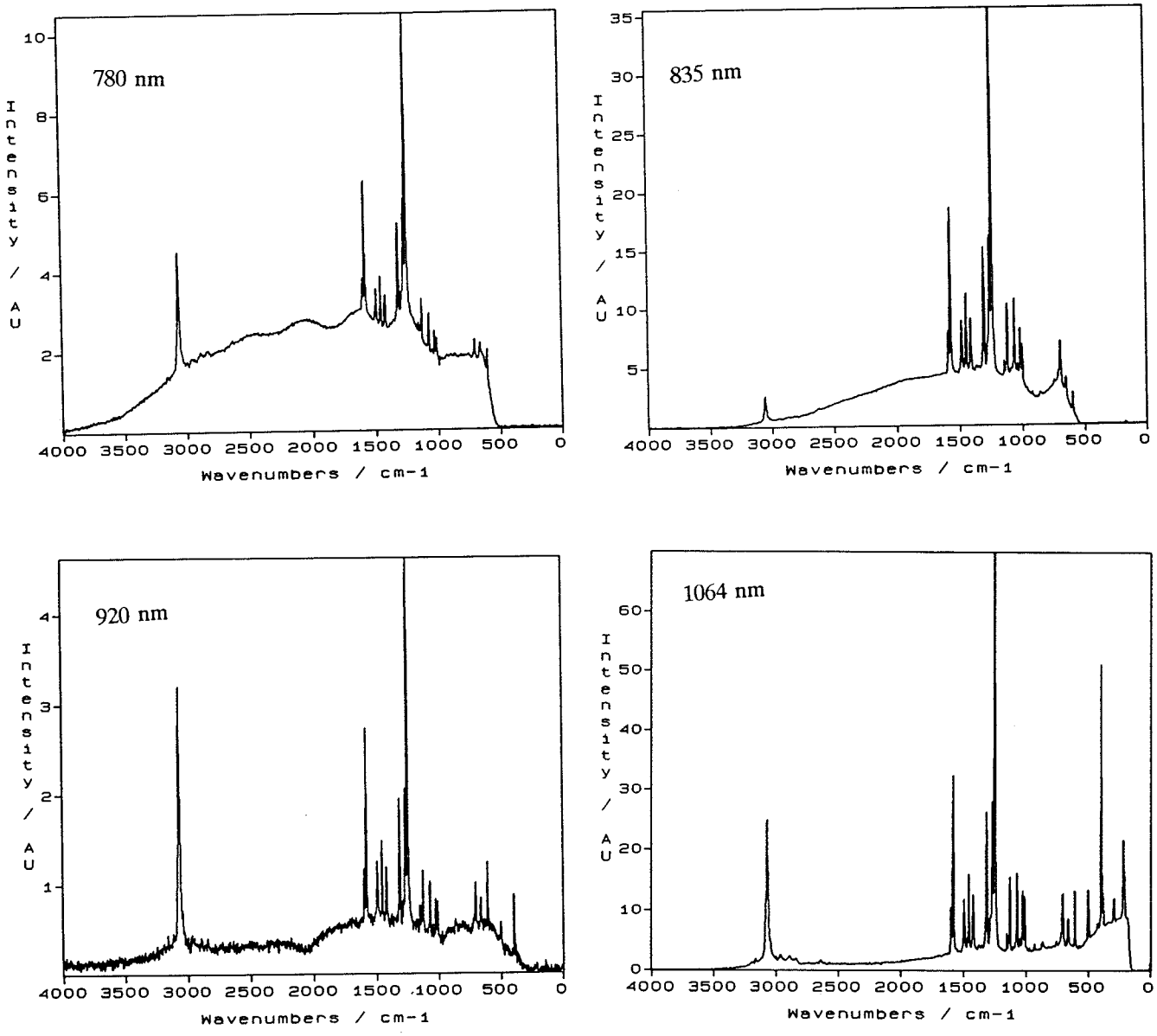

Figure 3.23 - Raman spectra of 2-mercaptobenzothiazole.

Again the spectra recorded with 780, 835 and 920 nm were recorded with the instrument

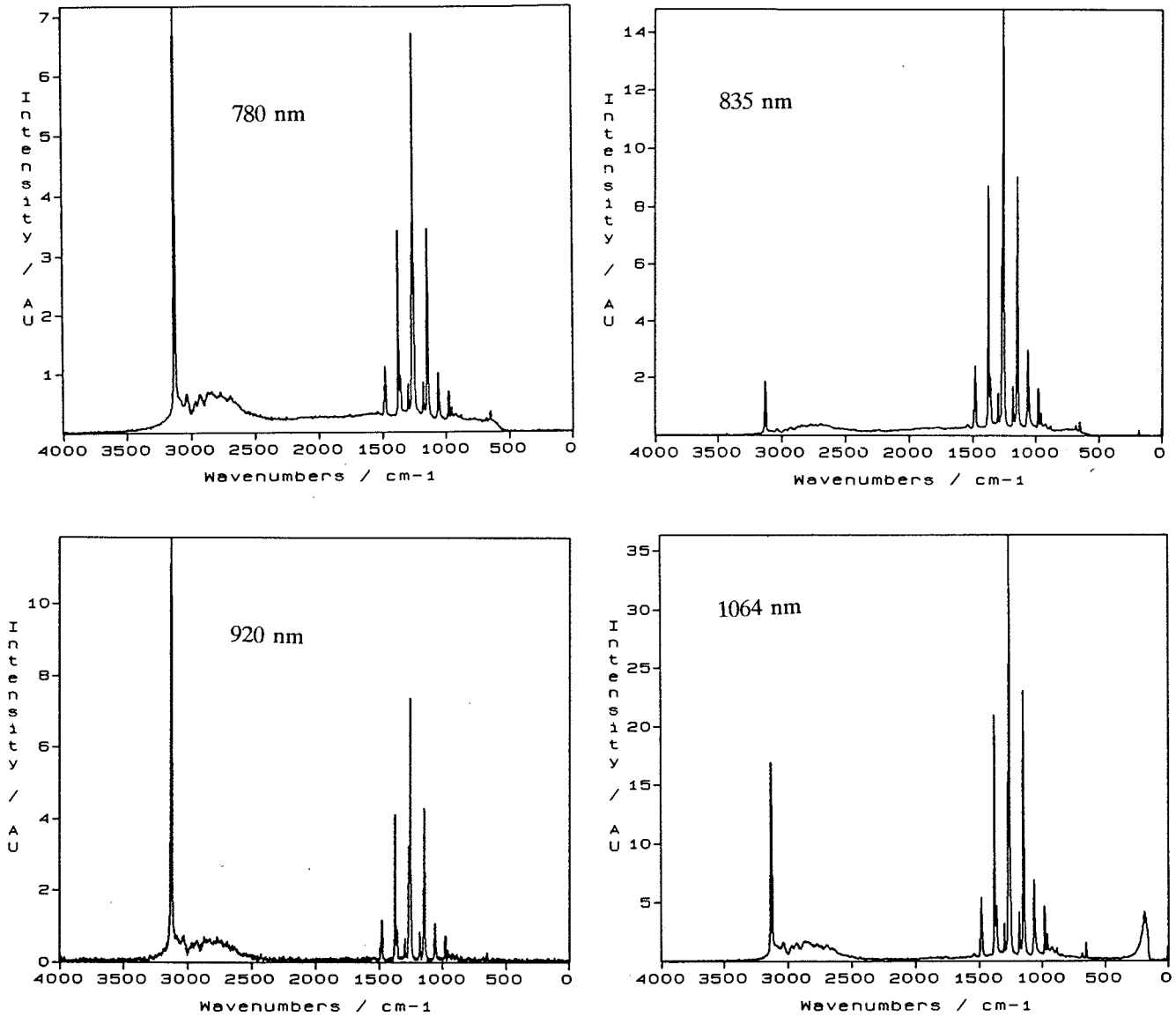

Figure 3.24 - Raman spectra of triazole.

described in Section 3.3. The spectra shown recorded with 1064 nm were obtained using the same instrument referred to above. The spectra shown have not been corrected for the instrumental response.

With organic samples the difference in the quality of spectra obtainable is far more noticeable than with the inorganic ones. The problem of sample fluorescence is much more significant with shorter wavelengths than with the examples shown in Section 3.4.1.

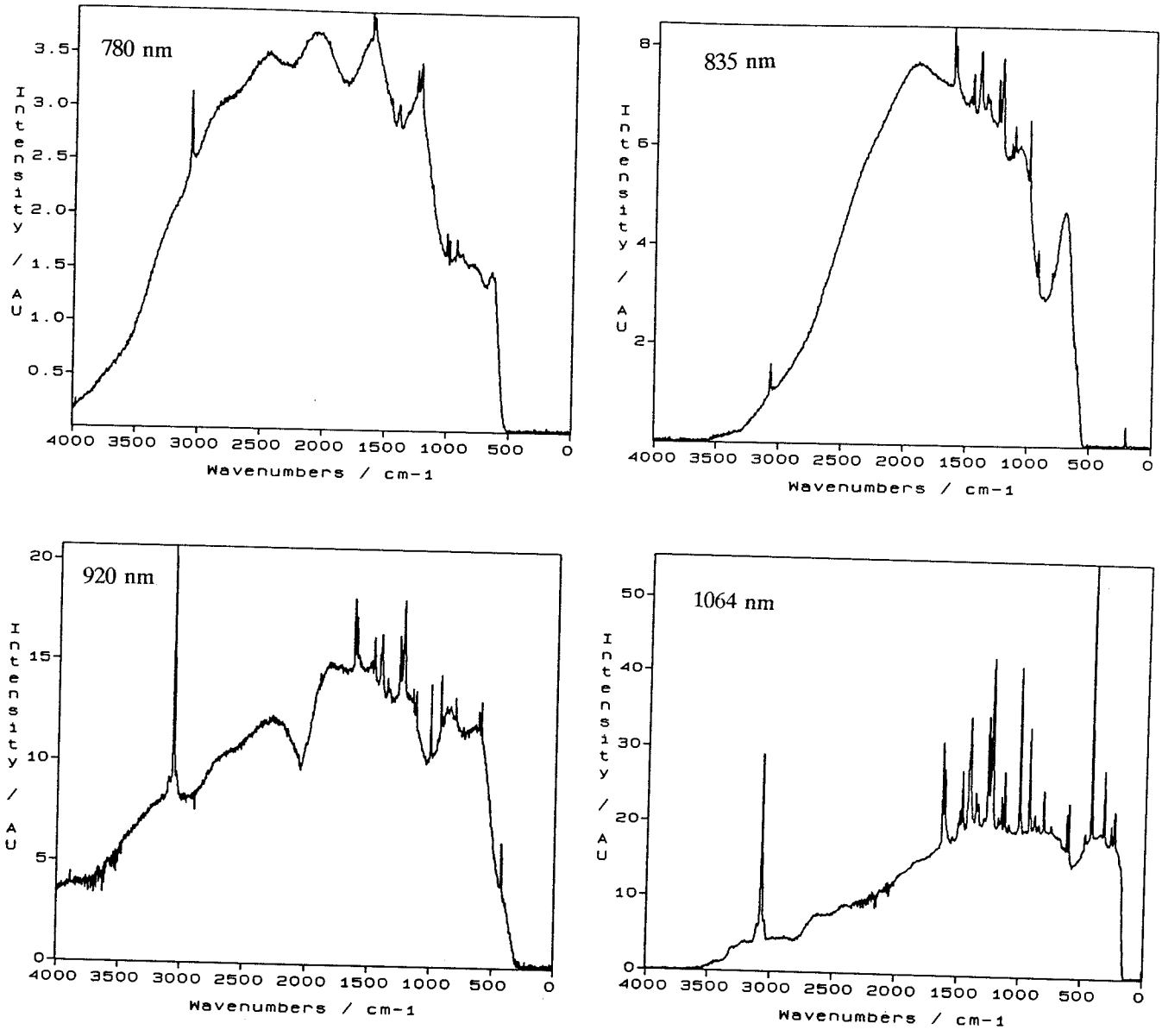

Figure 3.25 - Raman spectra of 2-mercaptobenzoxazole.

2-Mercaptobenzothiazole (Figure 3.23) shows significant fluorescence at 780 nm however the important peaks in the spectrum are still visible. The level of fluorescence decreases markedly at 835 nm and by 920 nm the quality of the Raman spectrum is similar to that obtained using 1064 nm. The signal to noise ratio (SNR) is somewhat less in the spectrum shown at 920 nm than that shown at 1064 nm, this is not a intrinsic feature of the excitation wavelength but rather a reflection on instrumental limitations. The spectrum at 920 nm was recorded with a lower laser power, hence the lower SNR.

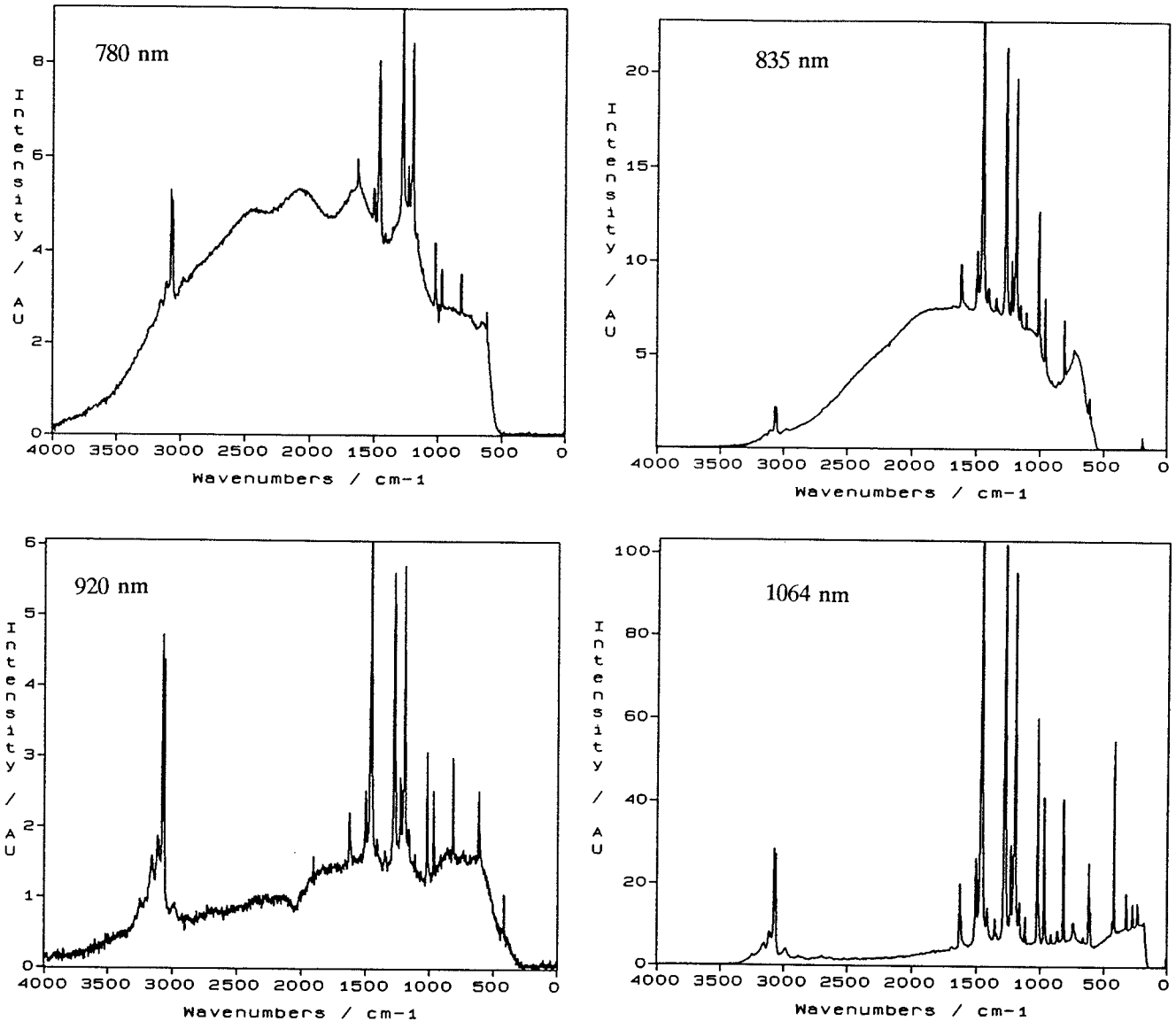

Figure 3.26 - Raman spectra of 2-mercaptobenzimidazole.

Figure 3.24 shows the spectrum of triazole recorded at the four different wavelengths. Some reduction in fluorescence occurs as the excitation wavelength increases but nonetheless the quality of the spectra is good in all cases.

Figures 3.25 and 3.26 show the Raman spectra of 2-mercaptobenzoxazole and 2-mercaptobenzimidazole at the four wavelengths. In both cases the level of fluorescence is high in the 780 and 835 nm spectra. The fluorescence level in the 920 nm spectra is

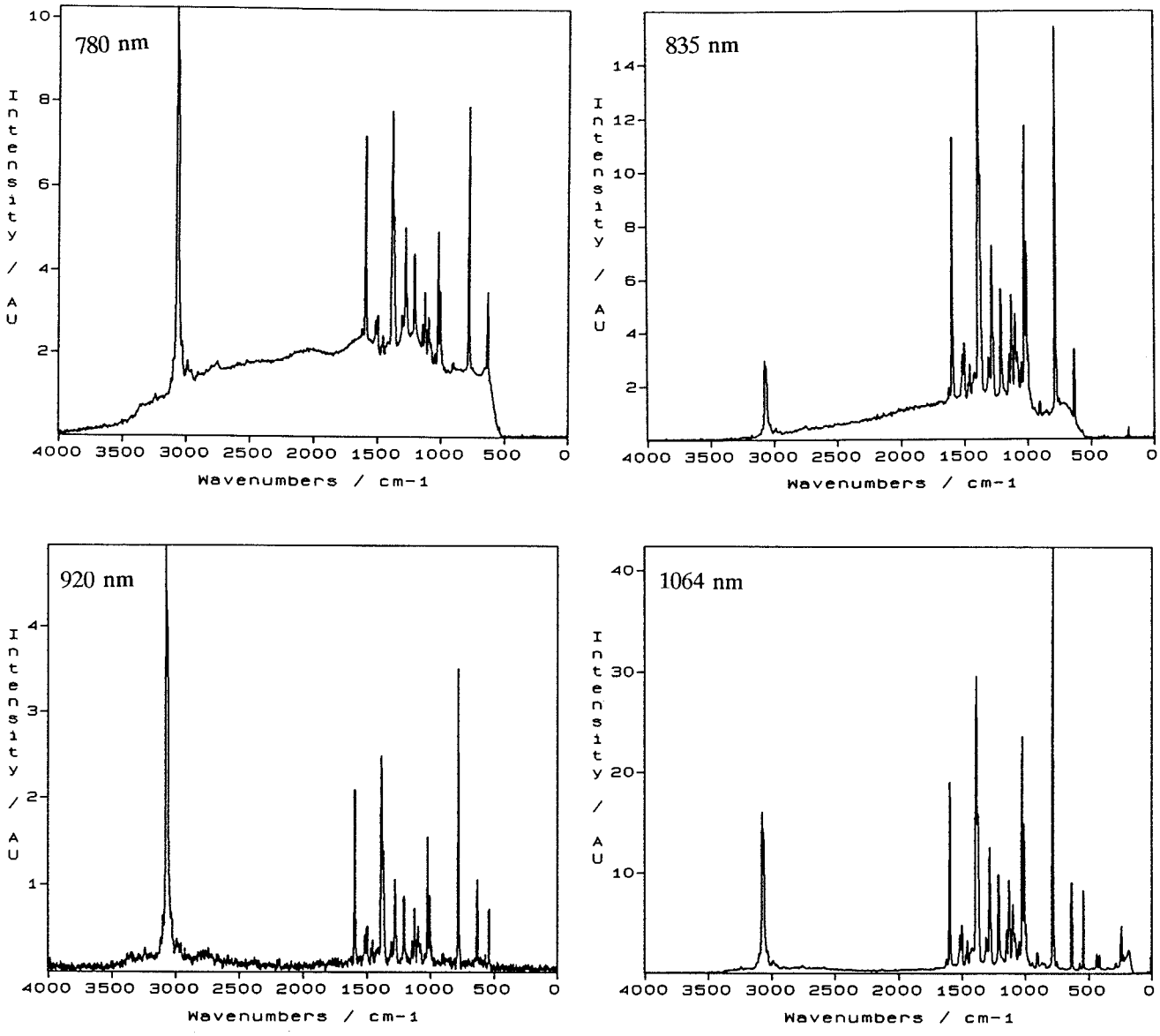

Figure 3.27 - Raman spectra of benzotriazole.

slightly greater than in that sourced at 1064 nm indicating a small advantage of adopting Nd^{3+}:YAG in using these two samples.

Figure 3.27 shows the spectra of benzotriazole. The 780 nm spectrum has some fluorescence which is slightly reduced at 835 nm. By 920 nm the level of fluorescence has disappeared.

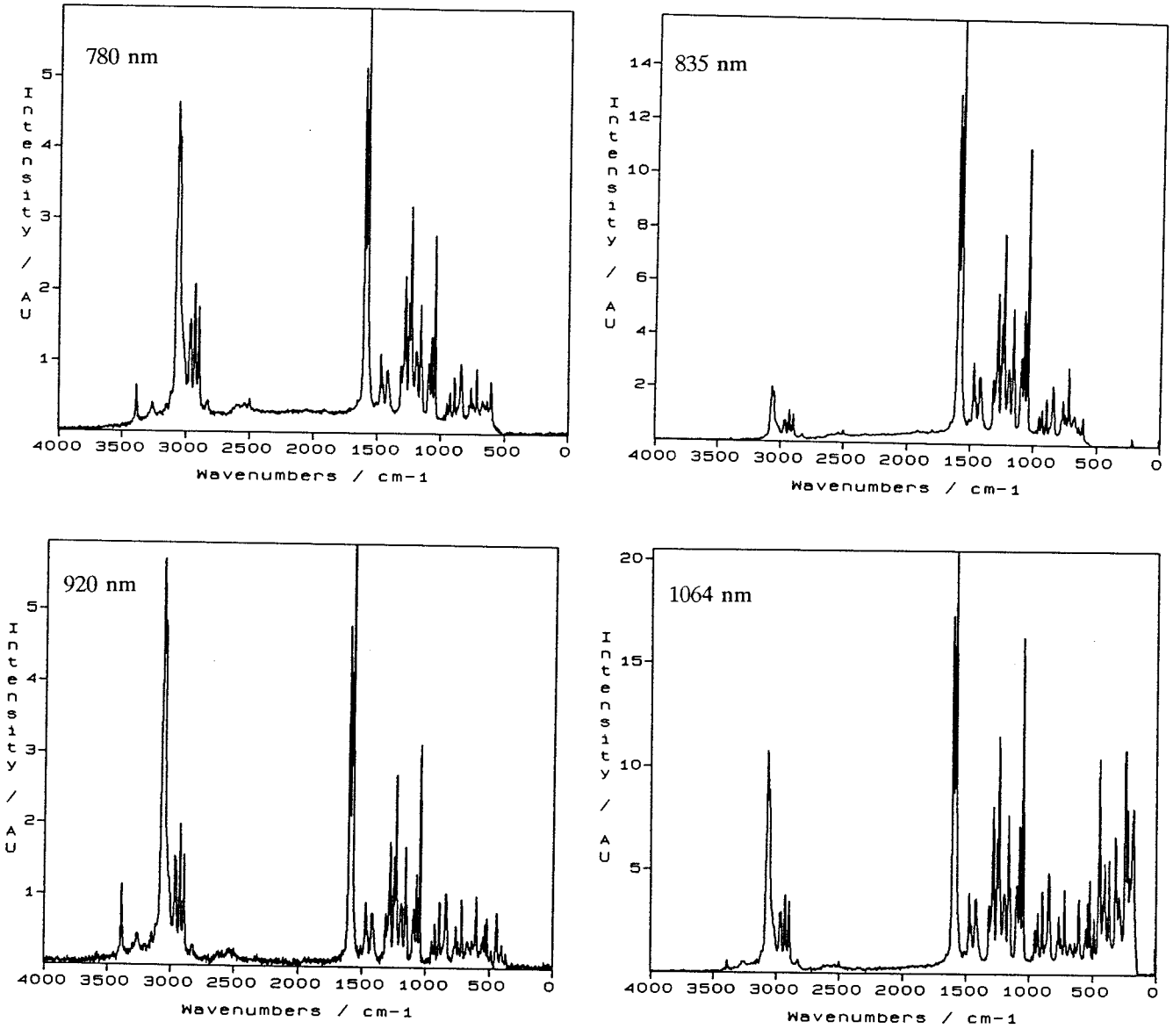

Figure 3.28 - Raman spectra of diclofenac.

Figure 3.28 shows the spectrum of the sodium salt of diclofenac. Here the quality of the spectra is good at all the wavelengths tried.

Large differences in the level of fluorescence are observed in general with organic samples. Some give perfect spectra and others display unacceptable levels of fluorescence. In general the high success rate of 1064 nm excitation means that there is little advantage in using shorter excitation wavelengths certainly in the region of 780 or

835 nm. However in the majority of cases 920 nm excitation yields similar quality spectra to 1064 nm. Unfortunately when using 920 nm excitation the long wavelength response of the Silicon detector is not adequate.

3.4.3 Polymer samples

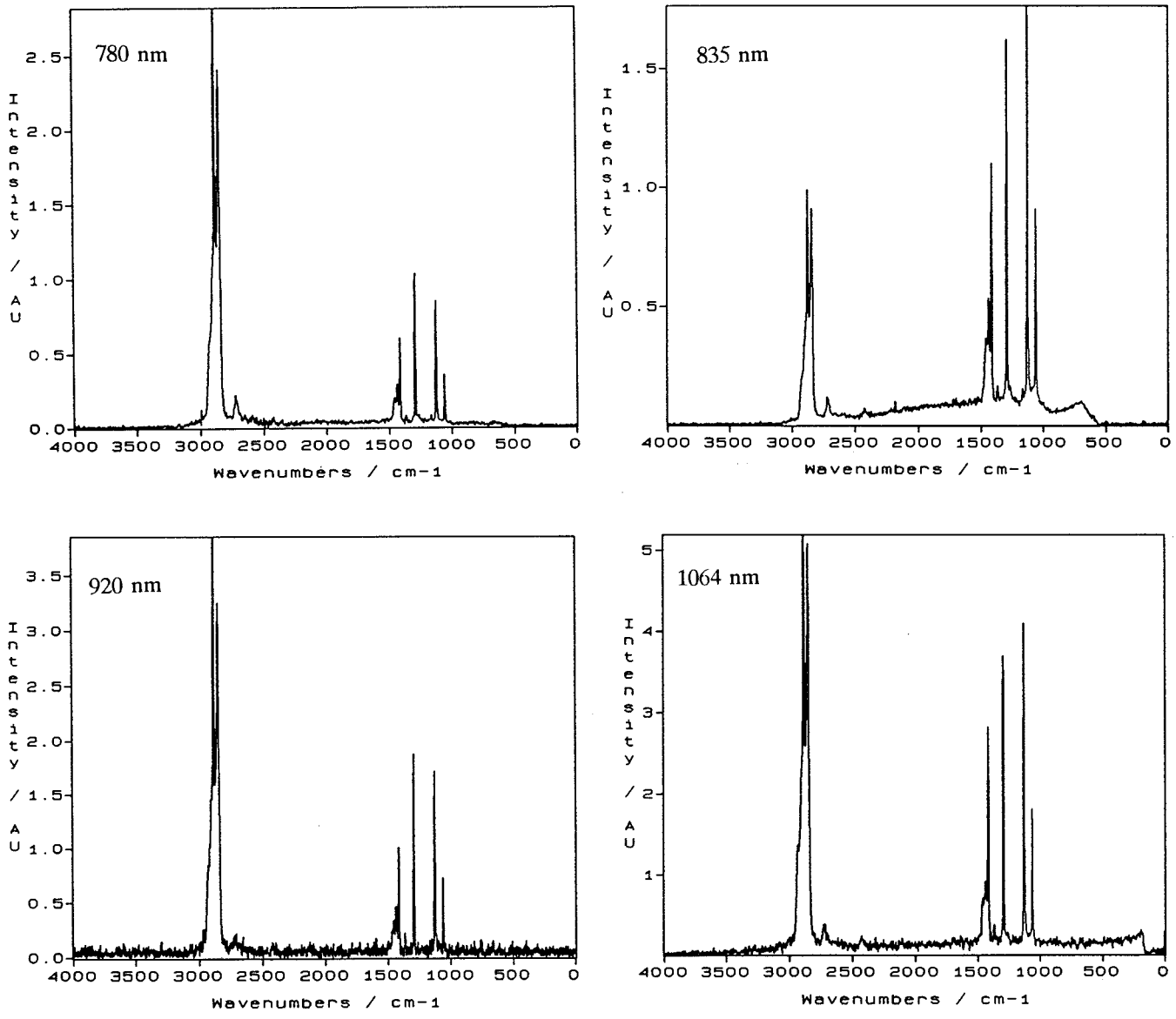

Figure 3.29 - Raman spectra of polyethylene.

Five polymer samples were chosen as representative samples to show the variation in spectral quality obtainable using the four excitation wavelengths. They were polyethylene,

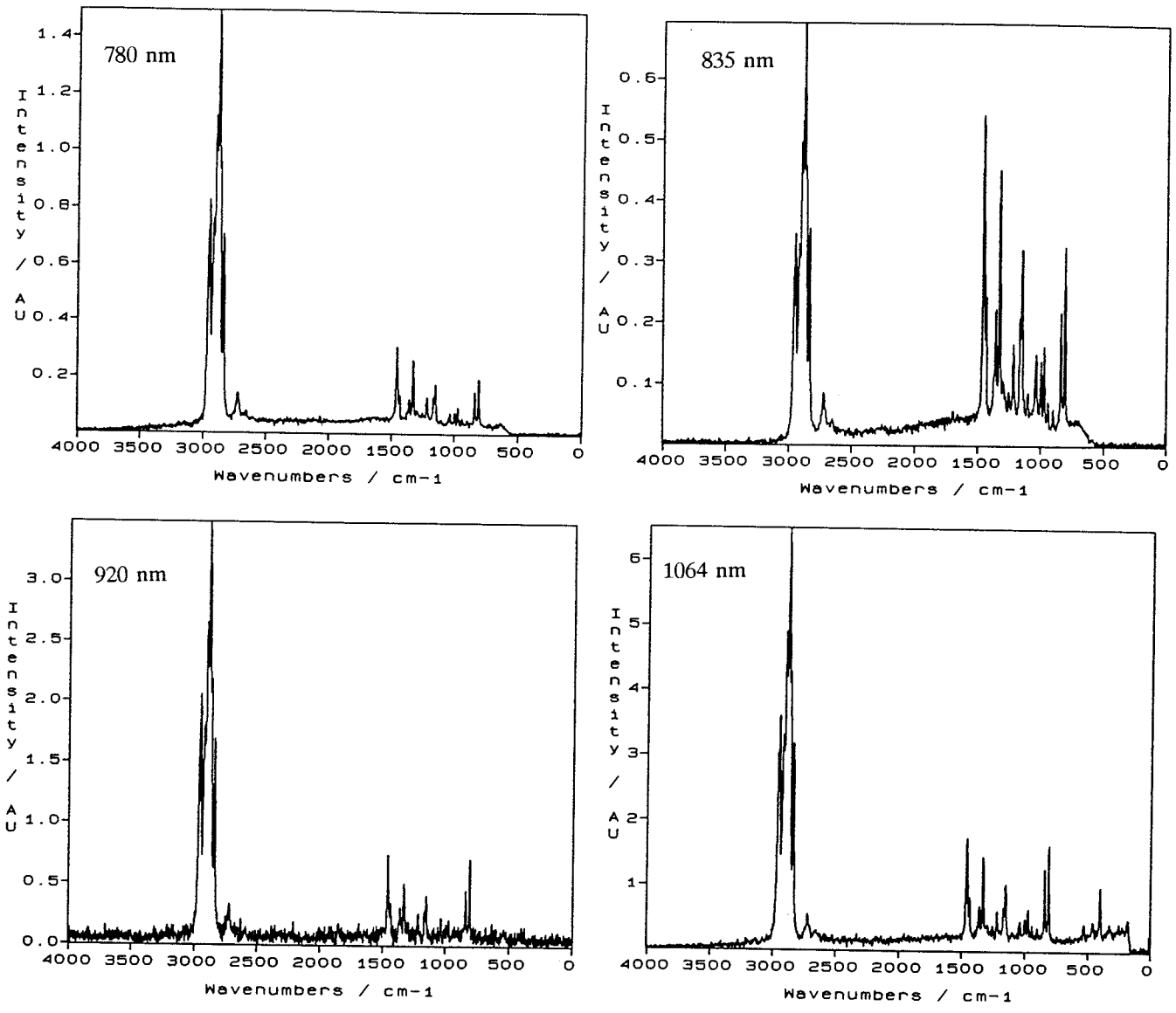

Figure 3.30 - Raman spectra of polypropylene.

polypropylene, poly(phenylene sulphide), nitrile rubber and isotactic polystyrene. The Raman spectra of these five compounds recorded at the four excitation wavelengths are shown in Figures 3.29 to 3.33.

Often in Raman spectroscopy the source of the fluorescence observed in a spectrum is due to an impurity that can in favourable cases be removed by a suitable purification process. Such purification processes are however time consuming and in the case of

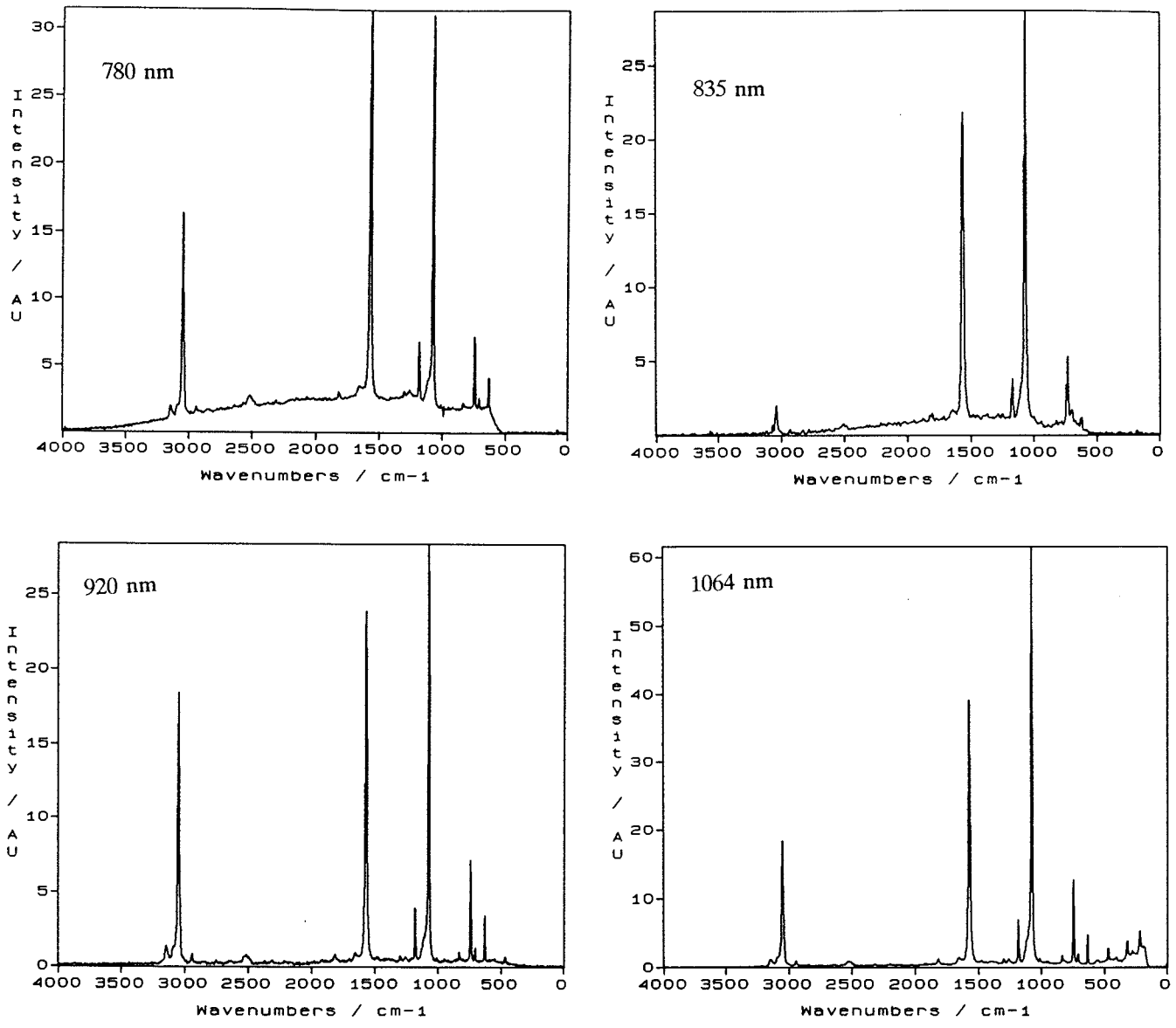

Figure 3.31 - Raman spectra of poly(phenylene sulphide).

polymers can cause unacceptable changes to the specimen. Hence, the avoidance of such processes is one of the major advantages of 1064 nm excitation in Raman spectroscopy. "Similar" samples of a polymeric or indeed any material can show completely different levels of fluorescence because different impurities are present in different amounts of the sample. Thus to overcome this problem the same sample of each polymer was used to record each spectrum shown here to ensure that the levels of fluorescence originate from the same source.

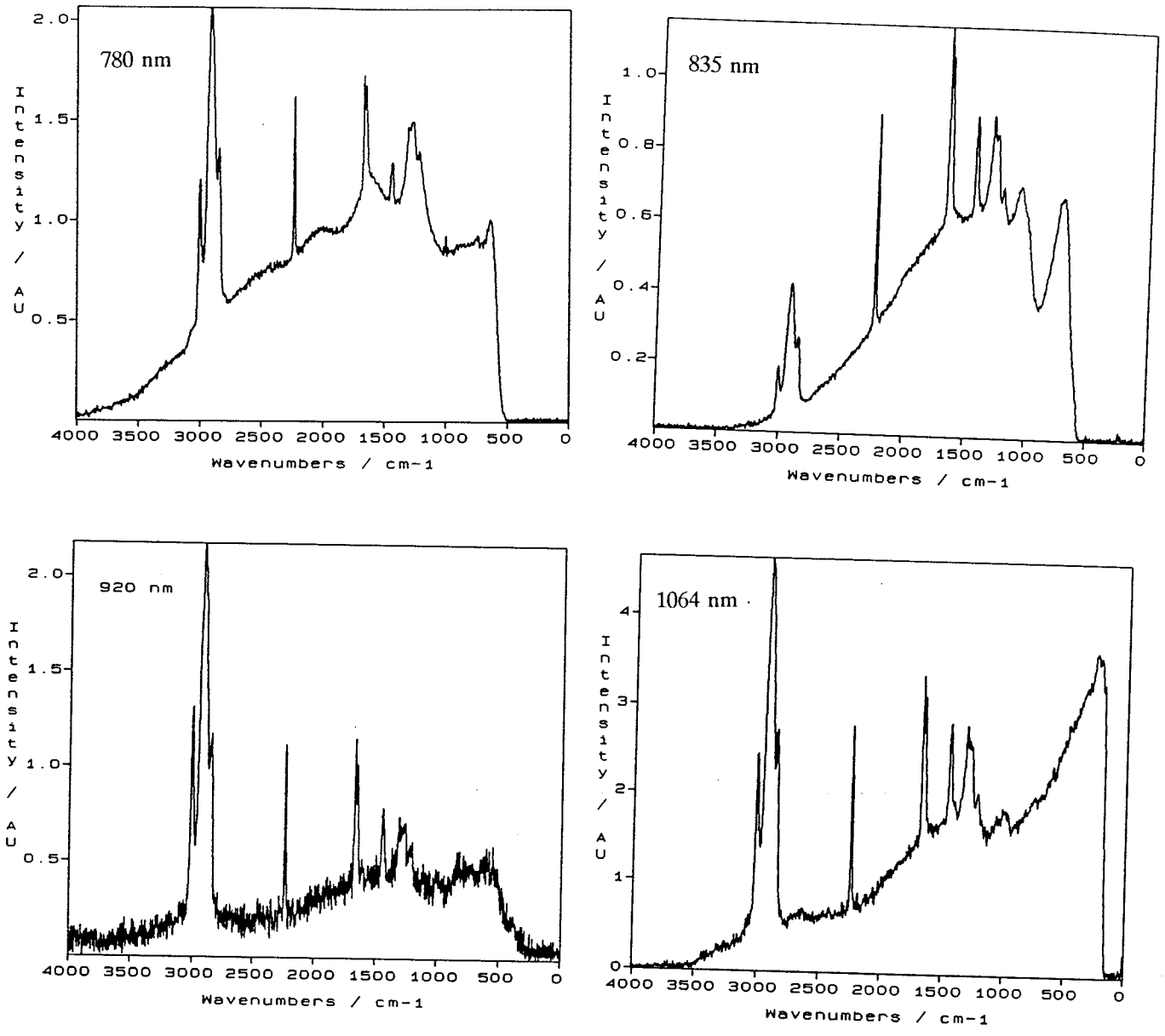

Figure 3.32 - Raman spectra of nitrile rubber.

Polyethylene (Figure 3.29) and polypropylene (Figure 3.30) are excellent Raman samples and can be successfully studied using blue or green sources. They both give good spectra at all the wavelengths used. Poly(phenylene sulphide) (Figure 3.31) is more problematic and shows some fluorescence at 780 and 825 nm but at 920 nm the fluorescence has disappeared giving a similar quality spectrum to that observed with 1064 nm excitation.

Nitrile rubber (Figure 3.31) without purification is hard to study and it shows poor spectra at all wavelengths. However the level of fluorescence is similar at each excitation wavelength.

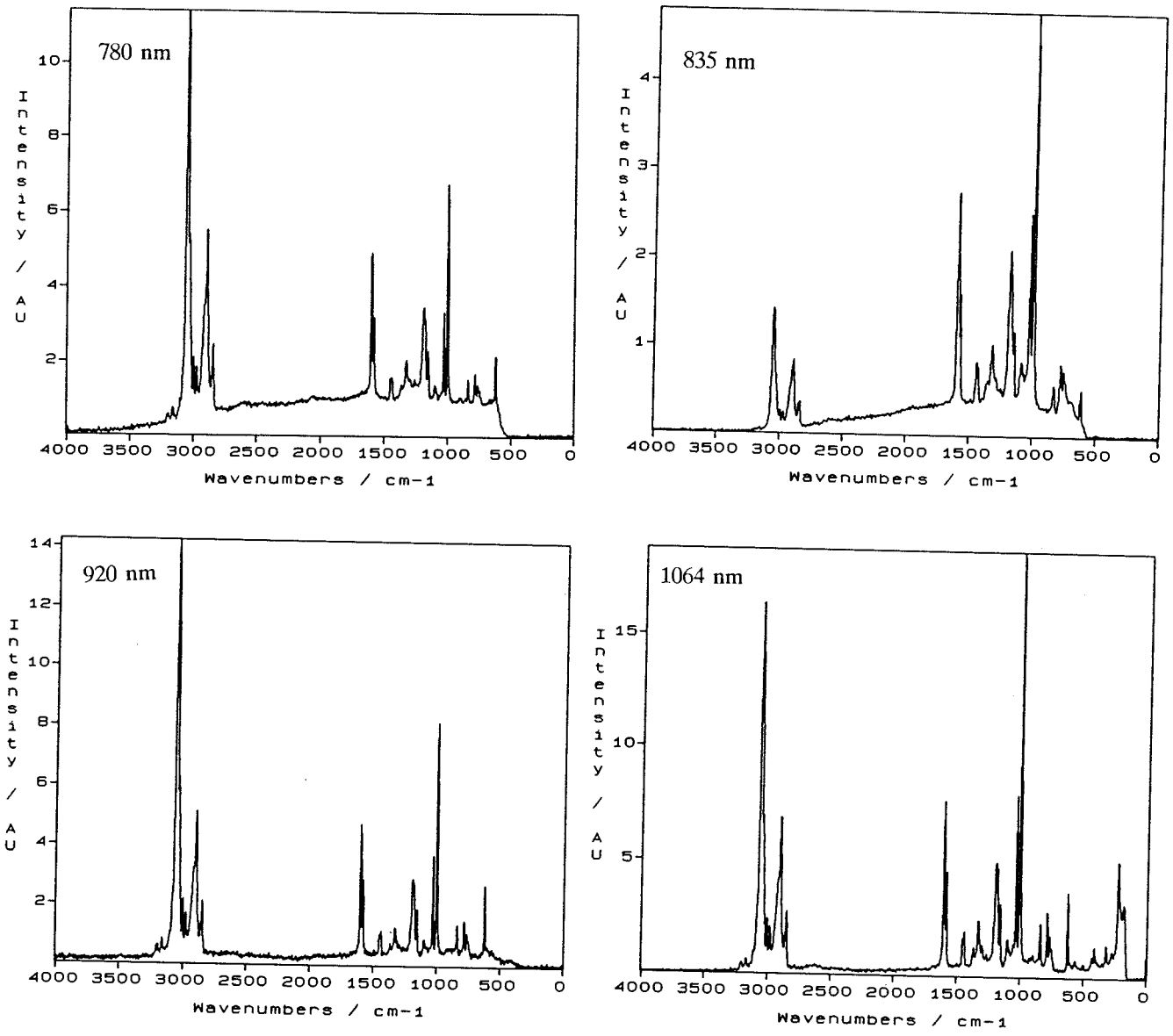

Figure 3.33 - Raman spectra of isotactic polystyrene.

Isotactic polystyrene yields good spectra at all wavelengths showing a small amount of fluorescence at 780 and 835 nm. No fluorescence is seen with 920 or 1064 nm.

As with organic samples the usefulness of 780 and 835 nm is limited with polymeric samples, 920 nm however shows excellent promise compared to 1064 nm and it is apparent that there is very little disadvantage in terms of increased sample fluorescence in adopting a source at 920 nm rather than 1064 nm.

3.5 SELECTED APPLICATIONS

The advantages of using shorter wavelength excitation in FT Raman are best shown with 780 nm excitation. Thus the following applications described below have all been examined using this excitation alone.

3.5.1 High temperatures

In Section 3.1.1 it was mentioned that the maximum possible temperature at which samples could be examined using FT Raman spectroscopy with 1.064 μm excitation (without a long wavelength cutoff filter) was about 200 ^{o}C. This is because the background emitted by a heated sample is seen by the interferometer because the source is coincident with the Raman sample. As the sample becomes hotter this so-called "blackbody radiation" becomes more intense at shorter wavelengths until eventually the detector is saturated. Equation (3.1) is the so-called Planck's equation which gives the theoretical emission from an ideal blackbody source.

$$L^{B}(\lambda,T)\, d\lambda = \frac{2hc^2}{\lambda^5} \frac{1}{\exp(hc/\lambda kT) - 1} d\lambda \; Wm^{-2}sr^{-1} \qquad (3.1)$$

where h = Planck's constant (J s)

c = speed of light (m s^{-1})

λ = wavelength (m)

k = Boltzmann constant (J K^{-1})

T = absolute temperature (K)

It can be deduced from Equation (3.1) that as T increases, the amount of radiation emitted at lower wavelengths increases thus increasing the likelihood of detector saturation. One consequence of using a Silicon detector is that the sample can be heated to a higher temperature without saturating it. In addition using the 780 nm source, the Raman spectrum is shifted away from the region of the heated background, thus a hotter sample can be examined.

Many polymer samples undergo transitions (annealing, melting etc.) at temperatures above 200 °C and these transitions are not accessible to FT Raman spectroscopy. If the polymer sample fluoresces when studied with Argon or Krypton ion lasers then effectively any transition above 200 °C cannot be studied with Raman unless an excitation wavelength is found where the polymer does not fluoresce and also the Raman spectrum is sufficiently far from the heated background produced by the sample.

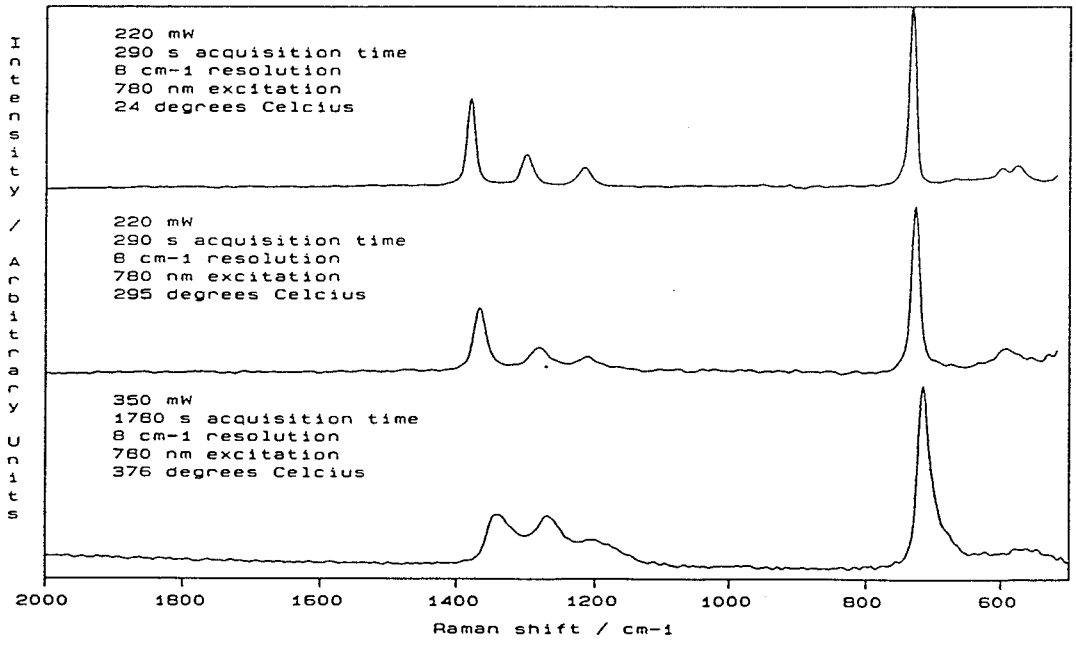

Figure 3.34: Raman spectra of polytetrafluoroethylene at various temperatures.

Figure 3.34 shows the Raman spectrum of polytetrafluoroethylene at room temperature, 295 °C and 376 °C. The spectra have not been corrected for the response of the instrument. At 376 °C the PTFE is in the molten phase. Unfortunately the cutoff of the Rayleigh filters occurs at 450 cm^{-1}, thus several important peaks cannot be seen. For the spectrum recorded at 376 °C a long wavelength cutoff filter was used to block the Raman radiation and the "blackbody radiation" beyond 2200 cm^{-1}.

These spectra demonstrate that it is possible to record Raman spectra of polymers at temperatures up to 376 °C and possibly higher using 780 nm excitation and a Silicon detector.

3.5.2 Aqueous samples

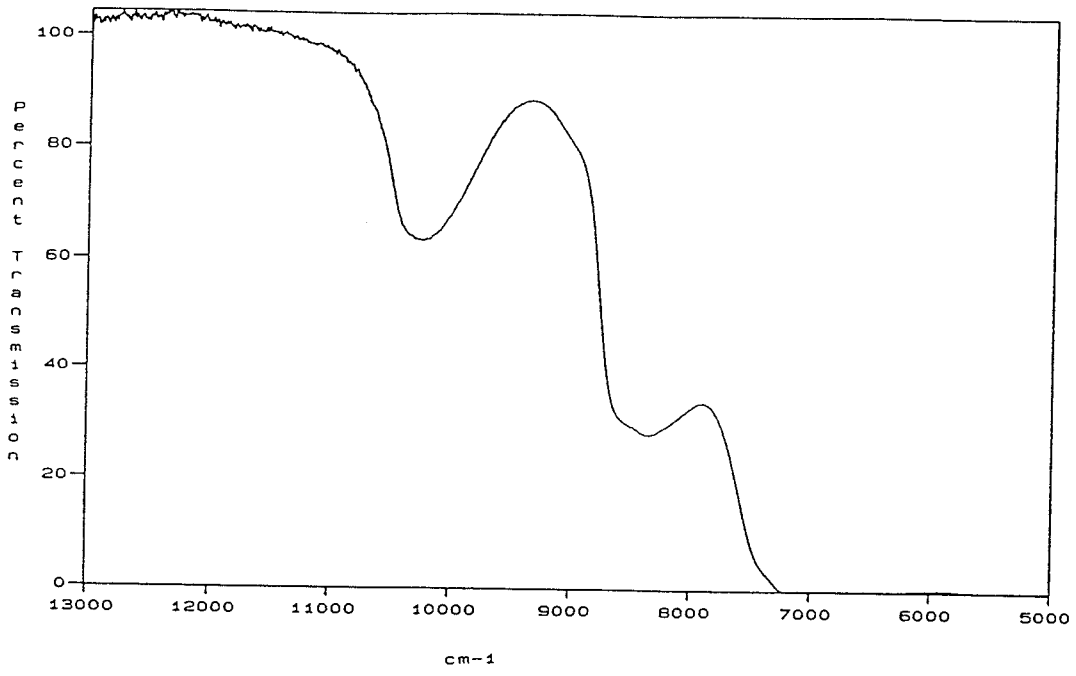

Figure 3.35: Infrared transmission spectrum of water.

Figure 3.35 shows the infrared transmission spectrum of water. This spectrum shows that any sample dissolved in water will suffer from self absorption of the Raman radiation when 1064 nm (9398 cm^{-1}) excitation is used. In general, the lack of sensitivity of the near infrared / FT approach leads to the design of multiple reflection, long pathlength cells (as have been recently demonstrated with gases[22]) but these are useless in this case because the Raman scatter will be self absorbed. Thus moving to shorter wavelengths has promise.

Figures 3.36, 3.37 and 3.38 show the Raman spectrum obtained using in each case a 1 cm quartz cuvette and a liquid cell consisting of a 2.5 cm glass tube of 1.4 mm internal diameter coated with gold internally. Figure 3.39 shows a diagram of this liquid cell. The liquid spectra obtained using the liquid cell each show an approximately fourfold improvement in signal to noise ratio over those recorded with the liquid in the quartz cuvette. Similar experiments with 1064 nm excitation revealed that while a Raman spectrum of a suitable sample dissolved in water may be recorded with the sample placed

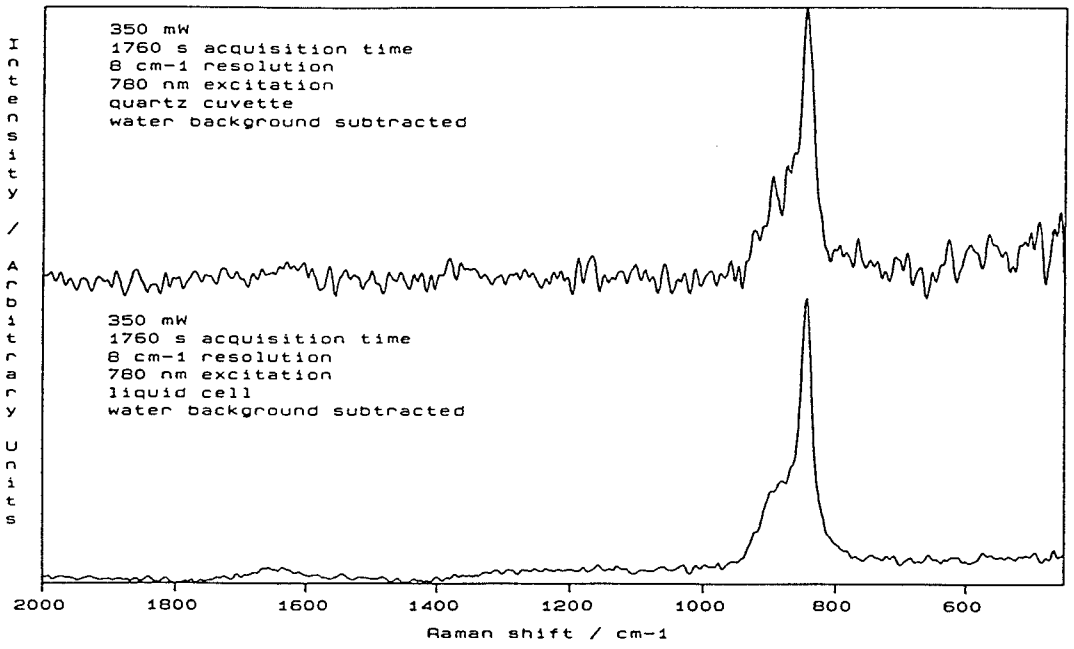

Figure 3.36: Raman spectra of 0.10 M Potassium Chromate in water.

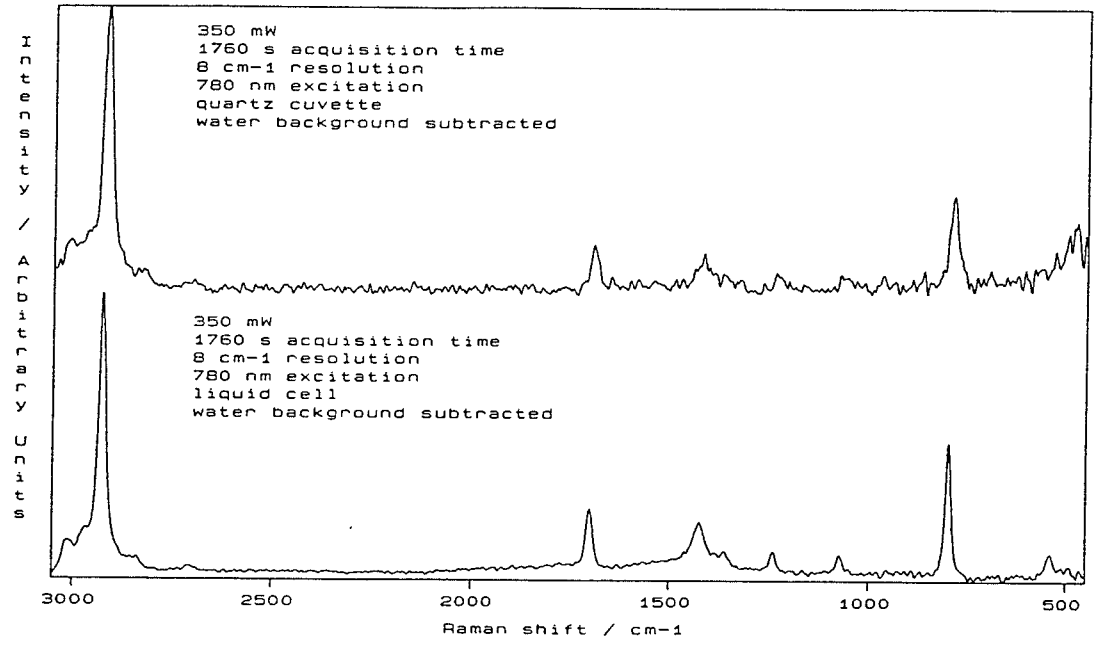

Figure 3.37: Raman spectra of 0.86 M Acetone in water.

in the quartz cuvette, when the sample was placed in the liquid cell virtually no Raman spectrum could be recorded from the sample.

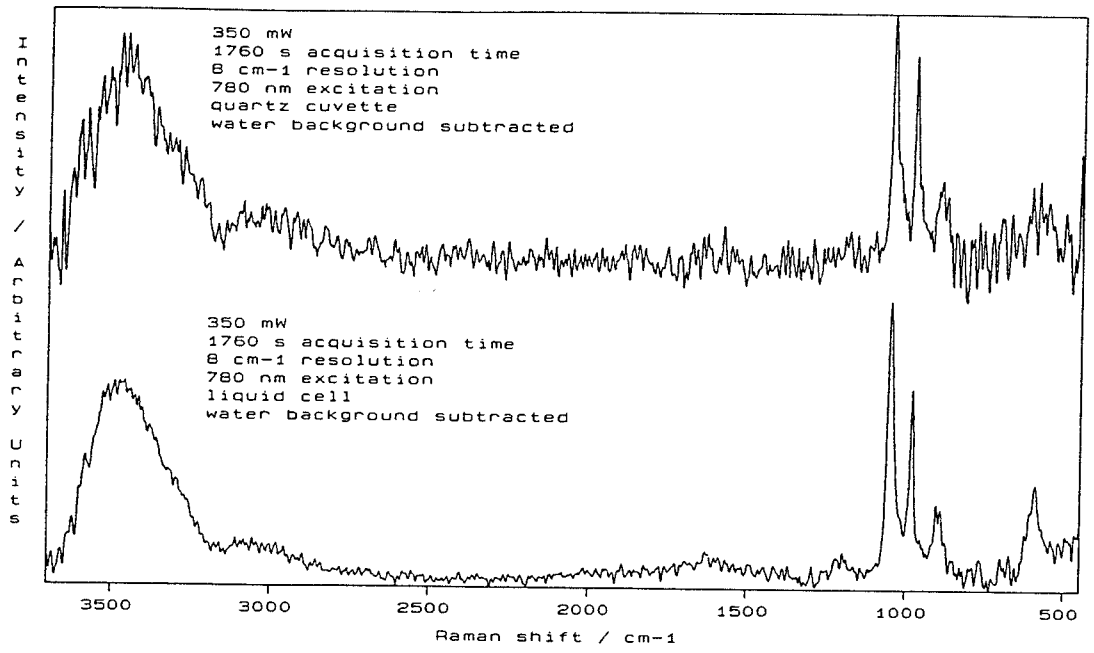

Figure 3.38: Raman spectra of 0.41 M Sulphuric Acid in water.

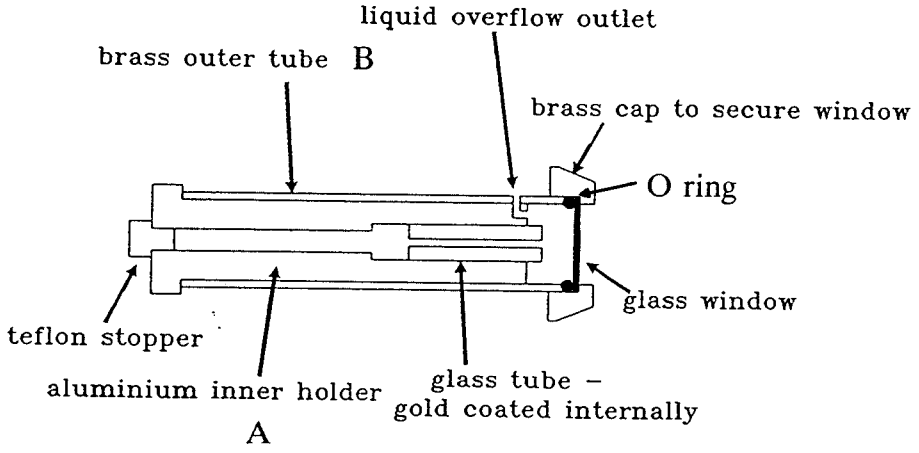

Rotation of A within tube B closes the liquid overflows outlet.

Figure 3.39: Schematic diagram of liquid cell.

The results shown here indicate that shorter wavelengths show considerable advantages over 1064 nm when examining aqueous samples however if the ultimate goal of obtaining

Raman spectra from dilute solutions without resonance Raman or SERS is to be achieved, then the sensitivity of the current setup will have to be vastly increased.

3.5.3 Self absorption by organic samples

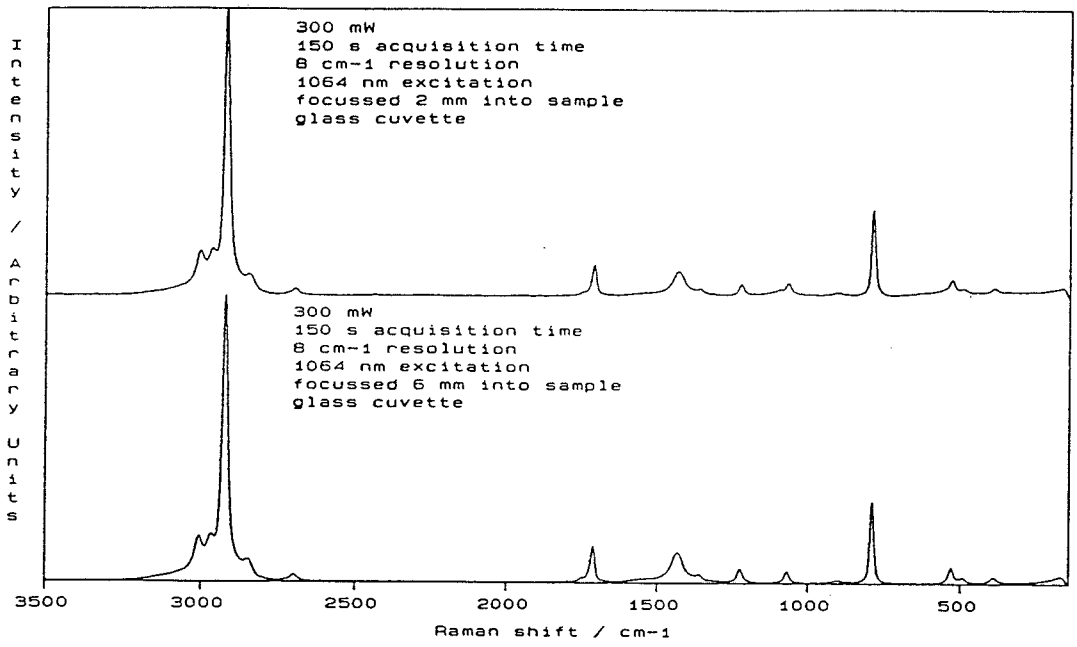

Figure 3.40: Raman spectra of Acetone.

Figures 3.40 and 3.41 show the Raman spectra of acetone and ethanol recorded with 1064 nm excitation in a glass cuvette. In each case in Figure (a) the focus of the collection optics was 2 mm into the liquid and in Figure (b) the focus was 6 mm behind the front window. In Figures 3.42 and 3.43 are the corresponding near infrared absorption spectra of acetone and ethanol. The absorption spectra were recorded in a 1 cm quartz cuvette and are shown in absolute shift.

Figure 3.43 clearly demonstrates that the severe attenuation of the C-H region for ethanol is due to self absorption of the Raman radiation by the ethanol. Acetone does not show strong absorptions in the C-H region of the Raman spectrum and thus Figure 3.40 does not show any attenuation in the C-H region. The example of tetrahydrofuran used by Petty[5] to demonstrate this self absorption effect shows that the band at 917 cm^{-1}

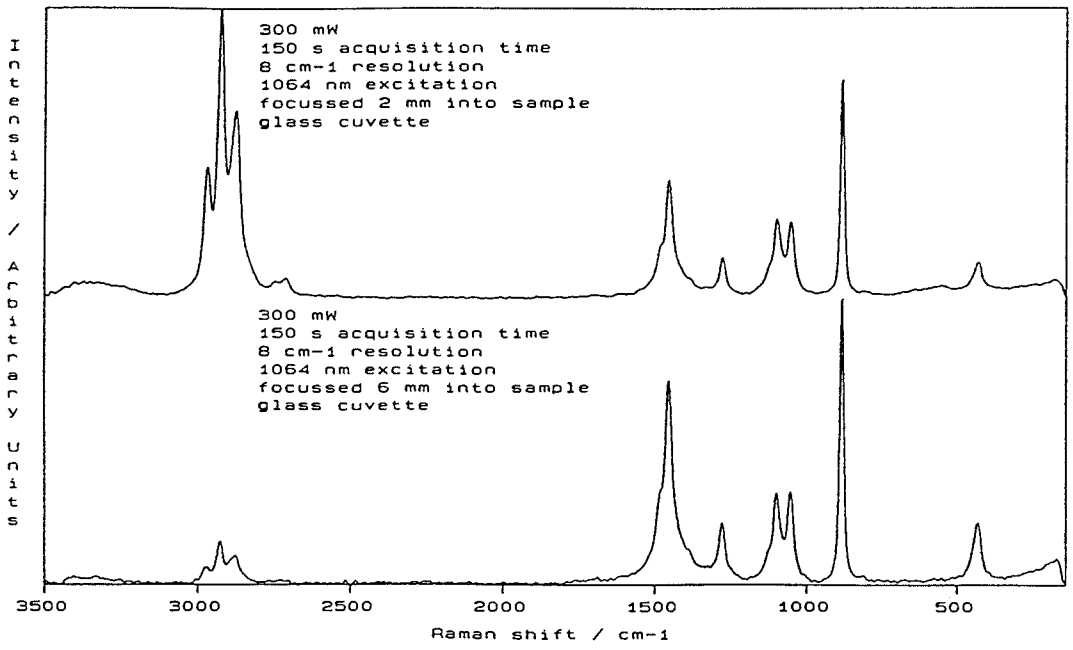

Figure 3.41: Raman spectra of Ethanol.

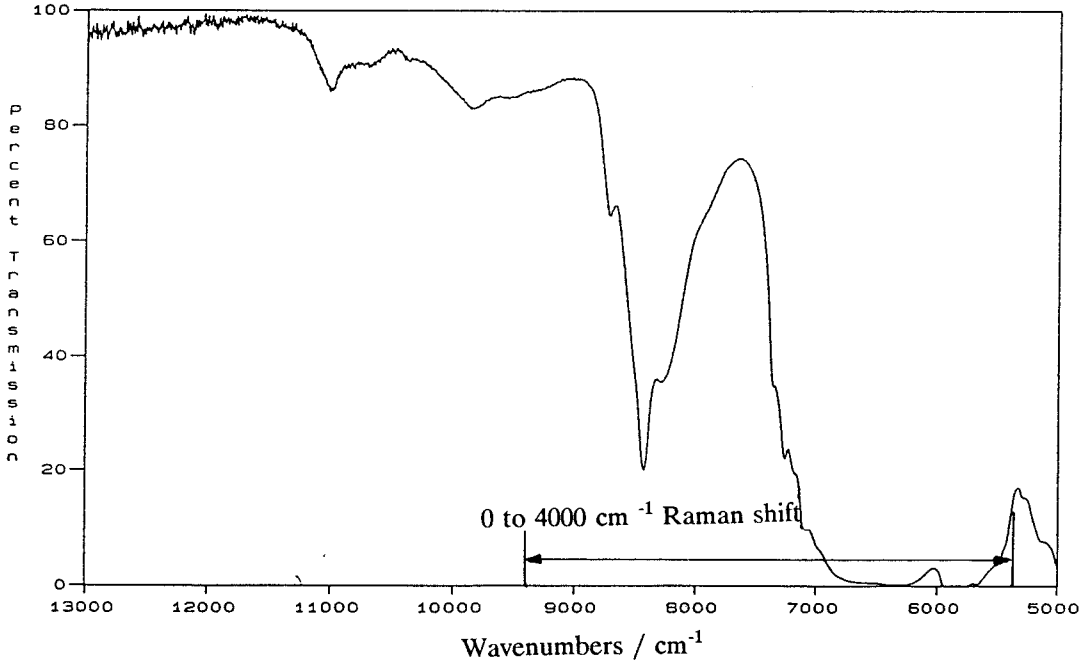

Figure 3.42: Infrared transmission spectrum of Acetone.

in tetrahydrofuran is self absorbed. The example of ethanol, also used by Schrader et al.[4] to demonstrate the possibility of self absorption of the Raman radiation, shows here that

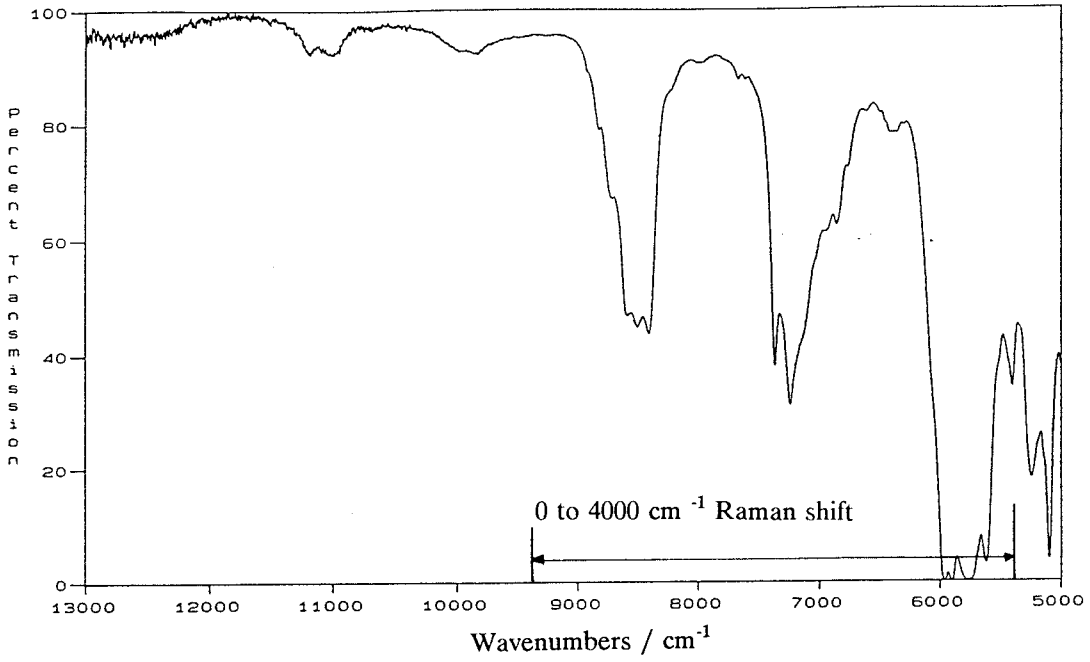

Figure 3.43: Infrared transmission spectrum of Ethanol.

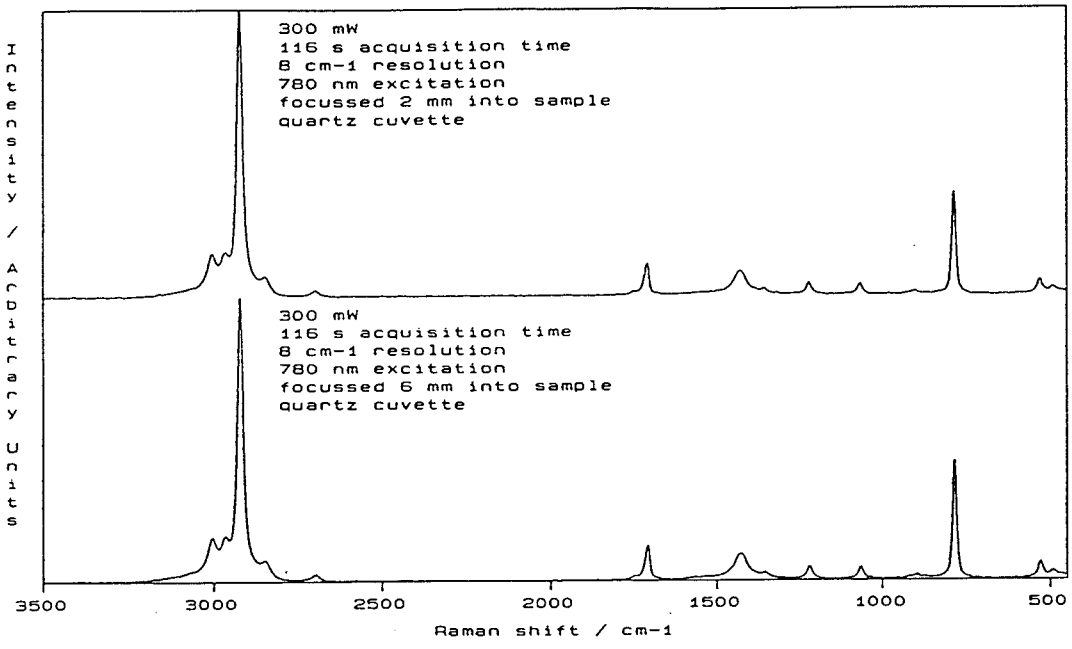

Figure 3.44: Raman spectra of Acetone.

self absorption can occur wherever a Raman peak coincides with a strong absorption in the infrared transmission spectrum.

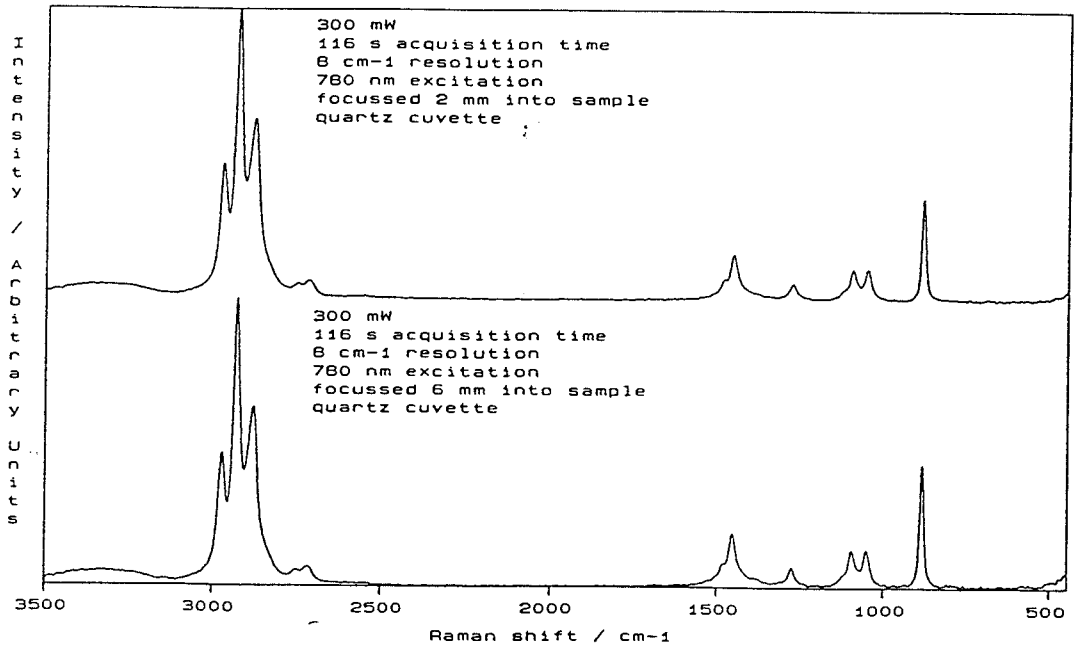

Figure 3.45: Raman spectra of Ethanol.

Figures 3.44 and 3.45 show analogous plots to Figures 3.40 and 3.41 recorded with 780 nm excitation. As expected, no attenuation of the C-H region occurs in either acetone or ethanol.

3.6 SHIFTED EXCITATION DIFFERENCE TECHNIQUE FOR REMOVING FLUORESCENCE

The fluorescence problem encountered by Raman spectroscopists is well known and becomes more serious as the excitation wavelength is reduced. Raman scattering is an inefficient process and thus unwanted spectral backgrounds such as fluorescence can seriously deteriorate the quality of a Raman spectrum. As pointed out earlier, fluorescence can result from sample impurities or from the sample itself via an intrinsic relaxation process resulting from an electronic absorption of the sample. Whatever the cause fluorescence is invariably seen as a nuisance by the Raman spectroscopist.

Thus far, an extremely effective way of overcoming fluorescence is to move the excitation wavelength to lower energies, such as has been done with FT Raman spectroscopy.

Another way that has been demonstrated is the use of fluorescence filters based on the time discrimination of the fluorescence from the Raman scatter[23]. This is in principle possible because the fluorescence processes obscuring Raman spectra have lifetimes in the nanosecond timescale whilst Raman processes occur in the sub-picosecond to sub-femtosecond timescale. Less promising are techniques attempting to remove fluorescence based on the passive optical separation of the Raman scatter from the fluorescence.[24] Passive optical separation of Raman light from fluorescence could, in principle, be achieved by using a property of a material (e.g. spatial focusing characteristics) which was different for short pulses (e.g. Raman light produced by a sample irradiated with a pulsed laser source) than for pseudo-continuous signals (e.g. fluorescence produced by the same sample irradiated with a pulsed laser).

Recently, a fluorescence rejection technique based on shifted excitation difference spectra has been described[25]. This technique requires that the Raman spectrum of the sample is collected using two excitation wavelengths relatively close to each other. In the publication mentioned here the wavelengths used were 10 cm^{-1} apart near 775 nm.

It can be assumed that the Raman spectrum of a sample $R(\bar{\nu})_1$ collected at a specific excitation frequency ($\bar{\nu}$) is made up of N Gaussian peaks, i.e:

$$R(\bar{\nu})_1 = \frac{1}{\sqrt{2\pi}} \sum_{i=1}^{N} \frac{A_i}{\sigma_i} \exp\left[\frac{-(\bar{\nu}-\bar{\nu}_{0i})^2}{2\sigma_i^2}\right] \qquad (3.2)$$

where each peak i is characterized by an area A_i, a centre position ν_{0i}, and a standard deviation σ_i. Suppose a second Raman spectrum $R(\bar{\nu})_2$ is collected using an excitation frequency close to the excitation frequency used to collect the first spectrum ($\bar{\nu}$ - σ). The difference between these two spectra given by $S(\bar{\nu}) = R(\bar{\nu})_1 - R(\bar{\nu})_2$ is:

$$S(\bar{\nu}) = \frac{1}{\sqrt{2\pi}} \sum_{i=1}^{N} \frac{A_i}{\sigma_i} \left\{ \exp\left[\frac{-(\bar{\nu}-\bar{\nu}_{0i}+\delta)^2}{2\sigma_i^2}\right] - \exp\left[\frac{-(\bar{\nu}-\bar{\nu}_{0i})^2}{2\sigma_i^2}\right] \right\} \qquad (3.3)$$

If Equation (3.3) is fitted to the spectrum $S(\bar{\nu})$ using an appropriate nonlinear least-squares fitting routine then the original Raman spectrum $R(\bar{\nu})$ can be generated. Because

the fluorescence background is essentially unaffected by the slight difference in excitation wavelength, the spectrum that is generated by fitting Equation (3.3) to the real difference spectrum, i.e. $R(\bar{\nu})_1$ - $R(\bar{\nu})_2$, has had the fluorescence background removed.

Preliminary experiments with this technique using the Titanium:Sapphire laser based FT Raman system showed some promise but the large changes in the instrument response over short differences in wavelength due to the characteristics of the transmission filters meant that the intensity of peaks at identical Raman shifts in the spectra $R(\bar{\nu})_1$ and $R(\bar{\nu})_2$ were not equal making the fitting of Equation (3.3) to $S(\bar{\nu})$ difficult as the choice of the number and choice of peaks to be fitted has to be decided by inspection of the original spectrum, a somewhat arbitrary method subject to an unknown error.

A refinement of the shifted excitation difference technique may show more promise. It is possible to alter the laser wavelength sinusoidally with a suitable driver on the birefringent filter. This will cause the Raman spectrum to oscillate at the same frequency as the excitation laser wavelength. If the instrument response is relatively uniform the intensity of the Raman peaks will not alter significantly, in addition the fluorescence background which is roughly independent of excitation wavelength will not oscillate. Thus it should be possible in principle to separate the Raman signal from the fluorescence.

3.7 REFERENCES

1. Chase, D.B. & Hirschfield, T., App. Spec., (1986), **40**, 133.
2. Schrader, B., Hoffmann, A. & Keller, S., Spectrochim. Acta, (1991), **47A** (9/10), 1135.
3. Cutler, D.J. & Petty, C.J., Spectrochim. Acta, (1991), **47A** (9/10), 1159.
4. Schrader, B., Hoffmann, A., Simon, A. & Sawatzki, J., Vib. Spec., (1991), **1** (1), 239.
5. Petty, C.J., Vib. Spec., (1991), **2**, 263.
6. Everall, N. & Lumsdon, J., Vib. Spec., (1991), **2**, 257.
7. Williams, K.P.J. & Gerrard, D.L, Optics and Laser Tech., (1985), **17** (5), 245.
8. Wang, Y. & McCreery, R.L., Anal. Chem., (1989), **61**, 2647.
9. Williamson, J.M., Bowling, R.J. & McCreery, R.L., App. Spec., (1989), **43** (3), 372.
10. Allred, C.D. & McCreery, R.L., App. Spec., (1990), **44** (7), 1229.
11. Ferris, N.S. & Bilhorn, R.B., Spectrochim. Acta, (1991), **47A** (9/10), 1149.
12. Schulte, A., Lenk, T.J., Hallmark, V.M. & Rabolt, J.F., App. Spec., (1991), **45** (3), 325.
13. Indralingum, R., Simeonson, J.B., Petrucci, G.A., Smith, B.W. & Winefordner, J.D., Anal. Chem., (1992), **64**, 964.
14. Baraga, J.J., Feld, M.S. & Rava, R.P., App. Spec., (1992), **46** (2), 187.
15. Newman, C.D., Bret, G.C. & McCreery, R.L., App. Spec., (1992), **46** (2), 262.
16. Horinaka, H., Yamamoto, N. & Hamaguchi, H., App. Spec., (1992), **46** (2), 379.
17. Schulte, A., App. Spec., (1992), **46** (6), 891.
18. Angel, S.M., Kulp, T.J. & Vess, T.M., App. Spec., (1992), **46** (7), 1085.
19. Iwata, K., Weaver, W.L. & Gustafson, T.L., J. Phys. Chem., (1992), **96**, 10219.
20. Klug, D.D., Singleton, D.L. & Walley, V.M., Lasers in Surgery and Medicine, (1992), **12**, 13.
21. Petty, C.J., Warnes, G.M., Hendra, P.J. & Judkins, M., Spectrochim. Acta, (1991), **47A** (9/10), 1179.
22. Dyer, C.D. & Hendra, P.J., The Analyst, (1992), **117**, 1393.
23. Chou, P., Martinez, M.L. & Studer, S.L., App. Spec., (1991), **45** (5), 918.
24. Carrol, M.K., Miller, R.M., Keller, R.A. & Hieftje, G.M., App. Spec., (1992), **46**

(3), 442.

25. Shreve, A.P., Cherepy, N.J. & Mathies, R.A., App. Spec., (1992), **46** (4), 707.

Chapter 4

THE DEPENDENCE OF RAMAN SIGNAL INTENSITY ON PARTICLE SIZE FOR CRYSTAL POWDERS

Chapter 4

THE DEPENDENCE OF RAMAN SIGNAL INTENSITY ON PARTICLE SIZE FOR CRYSTAL POWDERS

4.1 INTRODUCTION

A large number of samples examined in Fourier transform Raman spectroscopy are in the form of crystalline powders. It has long been known that the intensity of the Raman signal varies according to particle size when studying solids. In 1931 Kubelka and Munk[1] developed a theory of the optical properties of crystal powders. Schrader and Bergmann[2] later expanded the theory to include Raman scattering.

A consideration of the effect of particle size on the intensity of the observed Raman signals is essential if any quantitative measurements using crystal powders are to be made. Such quantitative measurements may involve a simple comparison of an unknown substance to a set of standard spectra (as is used in infrared spectroscopy) or measurement of absolute Raman cross sections where a sufficiently large crystal of the substance under examination is not easily obtained. Also if an internal standard is used, again particle size is crucial.

Quantitative measurements on crystal powders are made difficult by a lack of reproducibility. Work conducted in this study showed that when a powdered sample was not moved or touched, reproducible peak intensities could be obtained under the same scanning conditions for consecutively run spectra (less than one percent deviation). However if the sample is removed and replaced between consecutive scans under the same conditions then typical discrepancies between peak heights in consecutively run spectra can be of the order of ten percent. This is discussed later.

The work described here was initially aimed at investigating the characteristics of the Raman light collected by the collection optics of the second prototype Fourier transform Raman spectrometer developed in this research group at Southampton[3]. The spectrometer consisted of a Perkin Elmer 1720 FTIR spectrometer modified for the

Raman experiment. Excitation was provided by a Nd^{3+}:YAG laser and the data processed using conventional FTIR hardware.

Initial data showed marked variations in the intensity of the Raman peaks of potassium chromate, the sample initially used to examine the characteristics of the Raman light collected by the collection optics of the Raman spectrometer. Earlier work by Petty[4] also showed that the intensity of the collected Raman signal for various particle sizes of potassium chromate decreased as the particle size decreased and this observation was initially confirmed in this study. However, general experience suggested the reverse tendency - grinding a powder improves the spectra. No explanation was offered in Petty's thesis for his observation and we therefore initiated a further investigation of these phenomena.

The initial work carried out in examining the characteristics of the scattered Raman radiation collected by the prototype instrument's collection optics is presented followed by the work carried out on solids of different particle size. An explanation of the variation of the Raman signal intensity with particle size is offered making use of the theory developed by D'Orazio and Schrader[5] in 1976.

None of the spectra presented in this chapter have been corrected for the response of the instrument[6].

4.2 RESULTS AND DISCUSSION

4.2.1 The effect of collection angle on the strength of the collected Raman signal

Figure 4.1 shows a diagram of the collection optics of the FT Raman instrument used in this study. The collection angle of the front collection lens was varied by placing an iris diaphragm at the front of the collection lens as closely to its front surface as the design would allow. Table 4.1 shows the collection cone angle for each value of the iris diaphragm aperture used in this experiment. The distance of the sample from the collection lens was determined by finding the focus of the instrument (the intersection

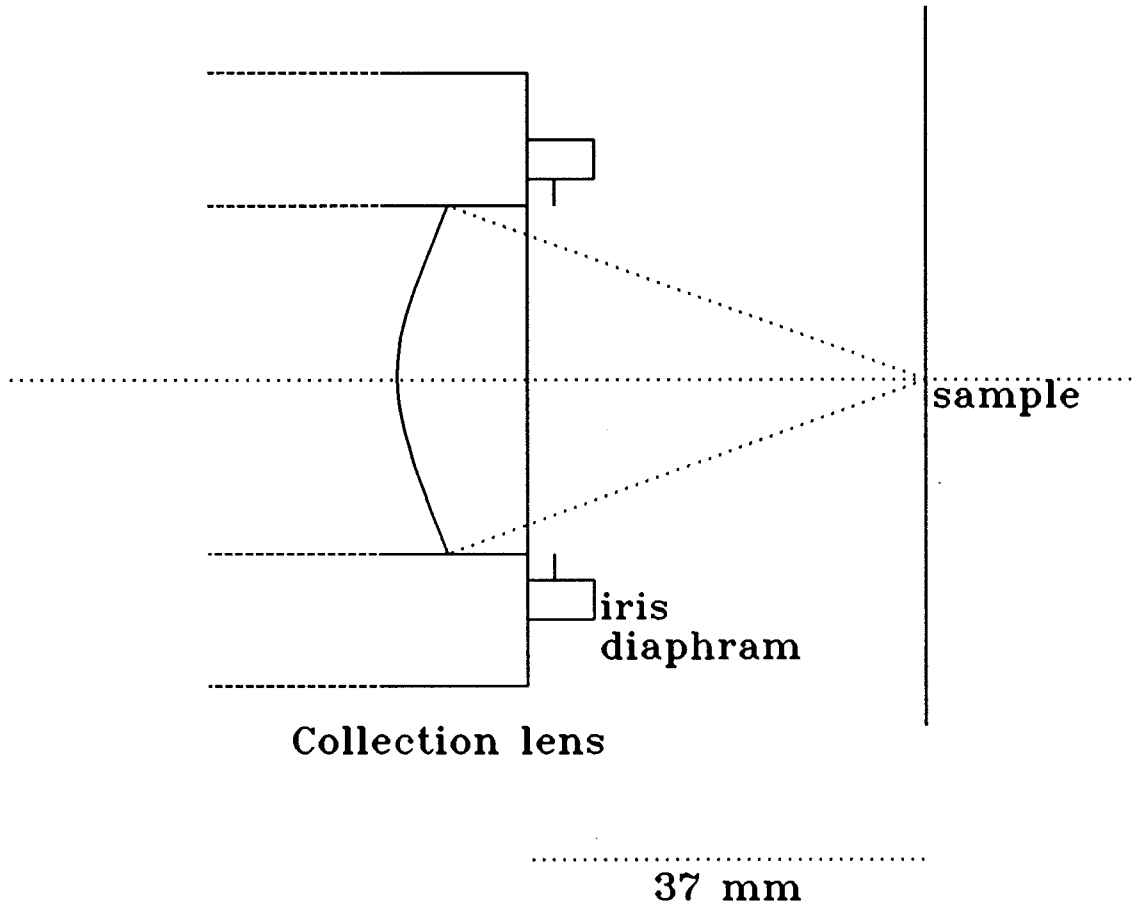

Figure 4.1 - Diagram of the collection optics of the FT Raman instrument used for this study indicating the position of the iris diaphragm.

Iris Aperture / mm	Collection Angle / degrees	Iris Aperture / mm	Collection Angle / degrees
40	56.8	20	30.2
37.5	53.7	17.5	26.6
35	50.6	15	22.9
32.5	47.4	12.5	19.2
30	44.1	10	15.4
27.5	40.8	7.5	11.6
25	37.3	5	7.7
22.5	33.8	2.5	3.9

Table 4.1 - Collection angle for each iris aperture.

of the well-known He-Ne "spots") then measuring the appropriate distance.

In this investigation it has been assumed that the total intensity of the Raman radiation emitted by the sample is proportional to the height of the largest peak in the spectrum of the compound under study. Figure 4.2 shows a plot of the height of the peak in the Raman spectrum of anthracene at ν = 1400 cm^{-1} versus the area of the aperture of the iris diaphragm.

It may be expected that ideally a plot such as Figure 4.2 would be a straight line passing through the origin of the plot. The line may be expected to "level off" once the maximum collection angle of the collection lens has been reached.

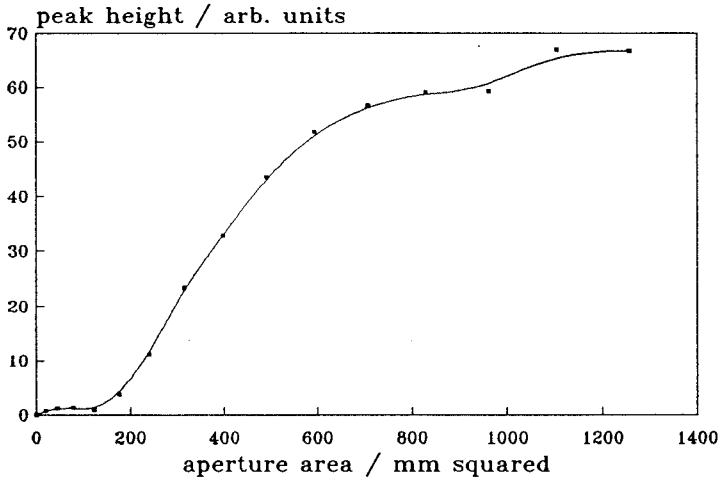

Figure 4.2 - Maximum peak height of Anthracene versus area of diaphragm.

However there are a number of reasons why this is not the case, as can be seen from Figure 4.2. At a collection angle of less than 20 degrees, the collection lens is illuminated by a comparatively low intensity of emitted Raman light. There are two reasons for this phenomenon.

a) The small prism on the front collection lens used to reflect the laser beam onto the sample creates an obstruction on the front collection lens which in turn causes a loss of collected Raman radiation.

b) The eighth wave plate placed inside the interferometer to change the polarisation of the He-Ne light passing down one portion of the interferometer causes an obstruction which also obscures a portion of the Raman radiation collected from the sample.

From Figure 4.1 it has been calculated that once the diaphragm has been opened to a

diameter of 40 mm, the collection lens is fully illuminated. Consequently no increase in the total intensity of Raman light collected can be achieved once this point has been reached. However a levelling off (i.e. point of maximum intensity) is reached before the diaphragm has been opened to 40 mm.

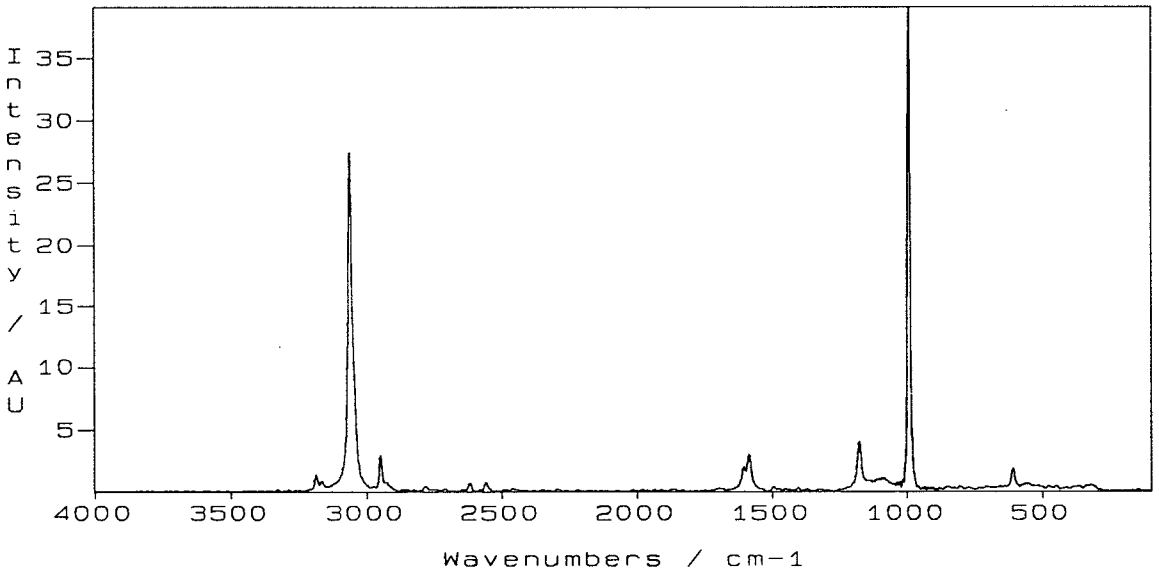

Figure 4.3 - Raman spectrum of benzene.

Figure 4.4 shows that a maximum point of collected radiation is reached when the diaphragm has been opened to 32.5 mm. This indicates that the maximum optical throughput of the instrument is attained at a collection angle of only 47 degrees. The throughput of the interferometer is thus not limited by the size of the collection optics but some other optical component, e.g. mirror or beamsplitter.

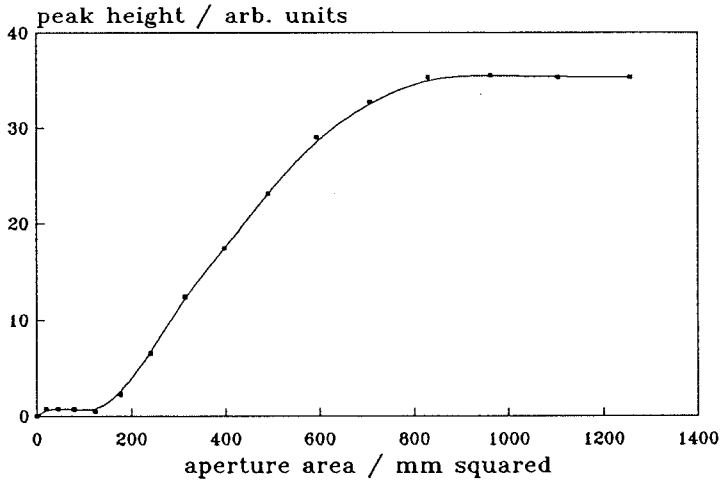

Figure 4.4 - Maximum peak height for benzene versus aperture area.

Examination of Figure 4.4 shows that the points between a collection angle of 19.2 and 47.4 degrees do not in fact lie on a straight line. A correction factor may be applied for radiation falling on an area dA indicated in Figure 4.5.

Figure 4.6 shows a plot of signal strength versus the area of the diaphragm with the intensities corrected for the angular variation of the intensity of the collected radiation. The plot shows good linearity for a collection angle between 22.9 and 44.1 degrees.

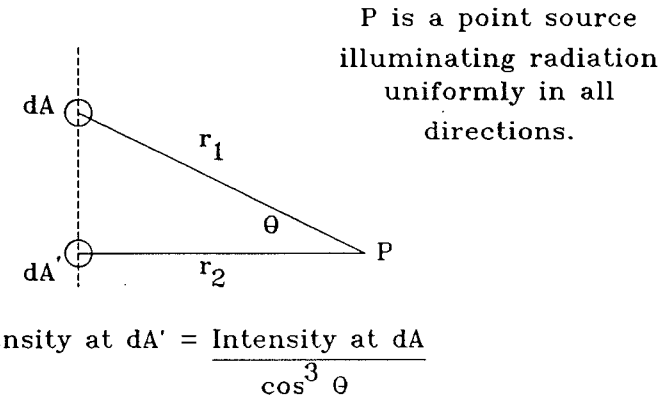

Figure 4.5 - Diagram indicating correction factor.

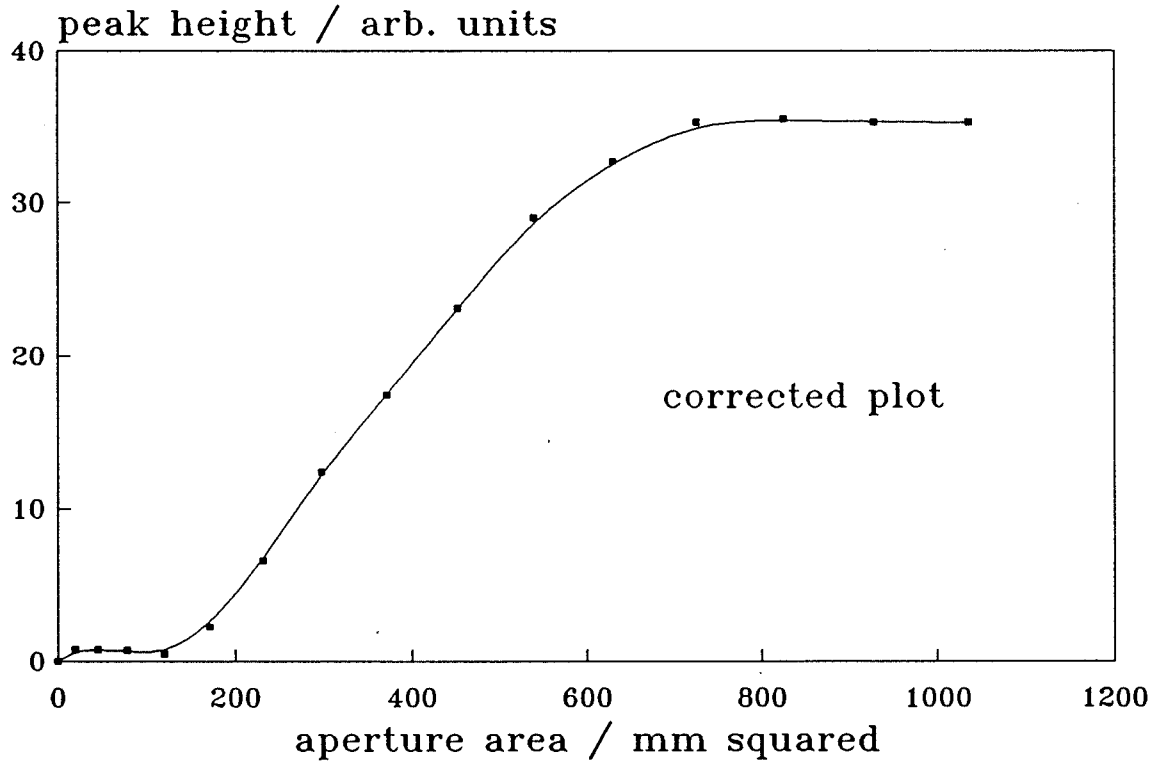

Figure 4.6 - Corrected plot of the maximum peak height for benzene versus the aperture area.

No account has been made of the increasing reflection losses caused as the angle of incidence of the collected Raman light with the front of the collection lens is increased.

4.2.2 Reproducibility of Raman signal intensities in the study of powdered samples

After an initial investigation of common inorganic laboratory reagents, four common compounds were selected as being suitable for this investigation. The compounds selected were non-hygroscopic, had an average diameter of crystals of 0.1 mm and gave "good" Raman spectra. Surprisingly few compounds met these three criteria. Barium nitrate, ammonium chloride, potassium chromate and lithium carbonate were selected as suitable.

The selected compounds were sorted into different particle sizes using standard sieves. The standard sieves were of mesh sizes 60, 80, 100, 120 and 140 wires per inch. Table 4.2 shows the "hole sizes" corresponding to the sieve size[7]. Using the sieves described in Table 4.2 it was possible to sort the selected compounds into a range of particle sizes.

Standard Sieve Size		"hole size" / mm
Wires / inch	wires / cm	
60	23.6	0.250
80	31.5	0.177
100	39.4	0.149
120	47.2	0.125
140	55.1	0.105

Table 4.2 - "Hole sizes" corresponding to standard sieve sizes.

The problem of lack of reproducibility in the measurement of peak intensities in an FT Raman experiment had to be investigated more fully before further quantitative measurements could be carried out using crystal powders.

Table 4.3 shows the results of 10 repeat spectra run on three of the compounds used in this investigation using a 1 x 4 cm quartz window cell with 2 mm thickness and silver backing.

Parti-cle Size	peak height $LiCO_3$ ν = 1091 cm^{-1}	Percent standard deviation $LiCO_3$	Max.peak height $Ba(NO_3)_2$ ν = 1048 cm^{-1}	Percent standard deviation $Ba(NO_3)_2$	Max.peak height NH_4Cl - ν = 3047 cm^{-1}	Percent standard deviation NH_4Cl
D > 250 μm	42.15	22.4	42.59	11.7	2.78	2.73
250 μm > D > 177 μm	37.49	19.5	43.73	5.54	2.83	4.01
177 μm > D > 149 μm	41.95	18.0	65.42	5.12	2.81	2.45
149 μm > D > 125 μm	37.53	7.24	67.33	2.71	2.78	2.83
125 μm > D > 105 μm	43.35	9.02	74.46	5.26	2.77	1.74
105 μm > D	34.49	6.87	78.84	3.48	2.71	0.105
laser power / mW	100	100	250	250	250	250

Table 4.3 - Percent Standard Deviation for K_2CrO_4, $Ba(NO_3)_2$, $LiCO_3$ and NH_4Cl. (20 scans, 8 cm^{-1} resolution).

A few brief observations can be made from the above table.

(a) As a general trend the percentage standard deviation for each compound shows a decrease as the particle size is reduced.

(b) For $Ba(NO_3)_2$ the maximum peak intensity increases as the particle size falls.

(c) For $LiCO_3$ and NH_4Cl the maximum peak intensities remain approximately the same for all particle sizes.

Observations (b) and (c) will be more fully discussed on Section 4.2.4.

Two possible explanations can be offered for the decrease in the percentage standard deviation as the particle size is reduced in Table 4.3. The first explanation is that the laser beam diameter at the focus of the collection optics is of a similar magnitude to the

size of the crystal particles under examination. Thus the path of the laser beam through the sample is likely to be greatly influenced by the orientation of the first crystal face it impinges upon. The implications of this is that different orientations of the first crystal may reflect and transmit different relative amounts of the laser light and the variation in the orientation of the first crystal that the laser beam strikes will produce a "scatter" of Raman intensities as a result. As the crystal size is reduced the likelihood that the laser strikes only one crystal initially is reduced and thus an average orientation of crystals is experienced by the laser beam at any one time. As a result smaller crystal sizes produce a smaller "scatter" of Raman intensities. In support of this explanation is the fact that the spot size of the laser beam at the focus of the collection optics has been calculated as 130 μm for the prototype instrument used in this work. The use of a system having a larger laser spot size at the sample should provide better reproducibility in the peak heights for spectra recorded with the same particle size samples. For this reason further experiments examining the dependence of Raman signal intensity with particle size (Section 4.2.4) were carried out using a system with a larger laser spot size at the sample position. For the commercial Perkin Elmer 1700 FT Raman spectrometer used to carry out the experiments in Section 4.2.4 the spot size has been calculated to be 250 μm.

The second explanation is that only a relatively small number of crystals are emitting the Raman radiation that is being viewed by the Raman instrument. Because each molecule in the crystal does not emit its Raman radiation uniformly in all directions, the relative orientation of the molecules and thus the crystals may affect the absolute intensity of the Raman radiation experienced by the instrument. However, this explanation is unlikely to be the cause of the non-reducible intensities experienced when examining crystal powders because it would be expected that the crystals (and thus the molecules) would be randomly orientated and that there would be sufficiently large number of crystals emitting the Raman radiation collected by the instrument to give an average orientation and thus negate any effect caused by the fact that each crystal may not emit its Raman radiation uniformly in all directions.

The relative peak intensities in a Raman spectrum generated by the Fourier transform

Raman instrument used in this investigation (and indeed all FT Raman spectrometers) need to be corrected by multiplication with a "correction curve"[6]. However, the problem is not solved as easily as would be hoped. Interferometers do show day-to-day variations in performance using the same scanning conditions if the instrument is allowed to become misaligned and the ambient temperature not kept constant[8]. The effect of these day-to-day variations can be minimised by ensuring that all quantitative work carried out on an FT Raman instrument is done in the shortest period of time possible. Throughout this report, any data presented on the same plot was carried out as quickly as possible in order to overcome this limitation.

It has been assumed that the different particle size samples of the same compound were of similar density. This was confirmed by density measurements on all the samples.

4.2.3 The effect of J-stop variation on the intensity of the collected Raman signal

The purpose of the J-stop or Jacquinot-stop is to act as an imaging element to reduce the amount of "off-axis" radiation passing into the interferometer in an FT Raman experiment.

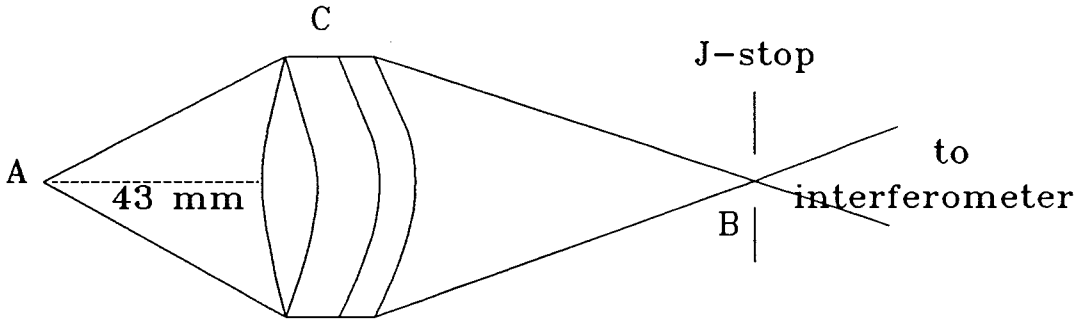

Figure 4.7 - The sample, collection optics and J-stop.

In the FT Raman instrument used in this investigation the focus of the collection optics is approximately 43 mm in front of the surface of the front collection lens. Figure 4.7 shows a sketch of the collection optics, the sample area and the J-stop.

If a sample is placed at the focus of the FT Raman instrument, any Raman radiation emitted at point A will pass through point B in the centre of the J-stop (neglecting lens abberation). Radiation emitted around point A may pass through the J-stop if the radiation is collected by lens C and if the J-stop is large enough. A "spot" of 1 mm diameter at the sample will produce a minimum beam width of 6 mm at the J-stop, i.e. an image at the J-stop will be six times the size of an object at the sample.

A study where the J-stop size is varied while all other conditions are held constant will provide a picture of the Raman signal intensity emerging from the sample at the laser focus.

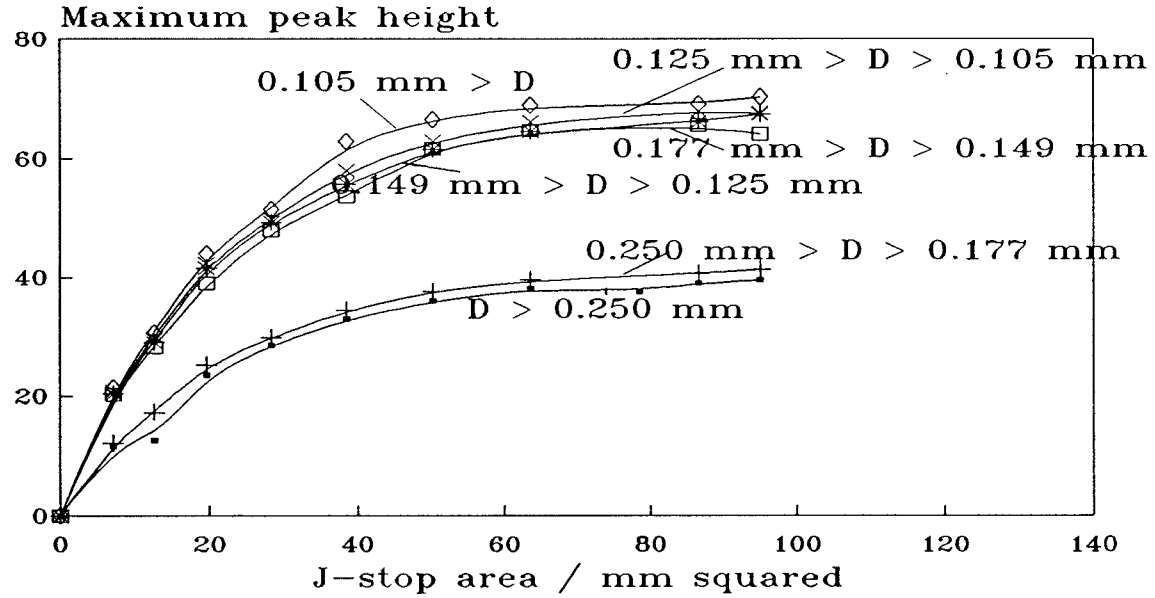

Figure 4.8 - Maximum peak height versus J-stop area for $Ba(NO_3)_2$.

Figure 4.8 shows a plot of maximum peak intensity versus the J-stop area for different particle sizes of $Ba(NO_3)_2$. Again the prototype 1720 FT Raman system was used with the samples placed in a 2 mm thick quartz cell. The maximum peak intensity increases as the particle size of the $Ba(NO_3)_2$ is increased. This phenomenon will be examined further in Section 4.2.5. The largest J-stop area at which a plot in Figure 4.8 is seen to "level off" corresponds to a diameter of approximately 9 mm. This would indicate that either the largest diameter of "glowing patch" on the sample is 9/6 mm or that the detector is being fully illuminated when the J-stop has been opened to 9 mm. The image at the detector is approximately the same size as the object in the sample area[12], the

detector has a diameter of 1 mm. This would indicate that the largest "glowing patch" on the sample that could be possibly be seen would be of the order of 1 mm in diameter, not 1.5 mm. A possible explanation is that the sample may be slightly out of focus. A simple calculation shows that a sample misalignment of 1.5 mm along the horizontal axis could account for this anomaly.

4.2.4 Raman signal intensity variation as a function of particle size

As indicated in Section 4.2.2, this study was carried out with various particle sizes of K_2CrO_4, $Ba(NO_3)_2$, $LiCO_3$ and NH_4Cl. Figure 4.9 shows the maximum peak height versus average particle size for the four different compounds with the maximum intensity in each data set normalised to one. It has been assumed that the peak height is proportional to the area of the peak, this has been verified.

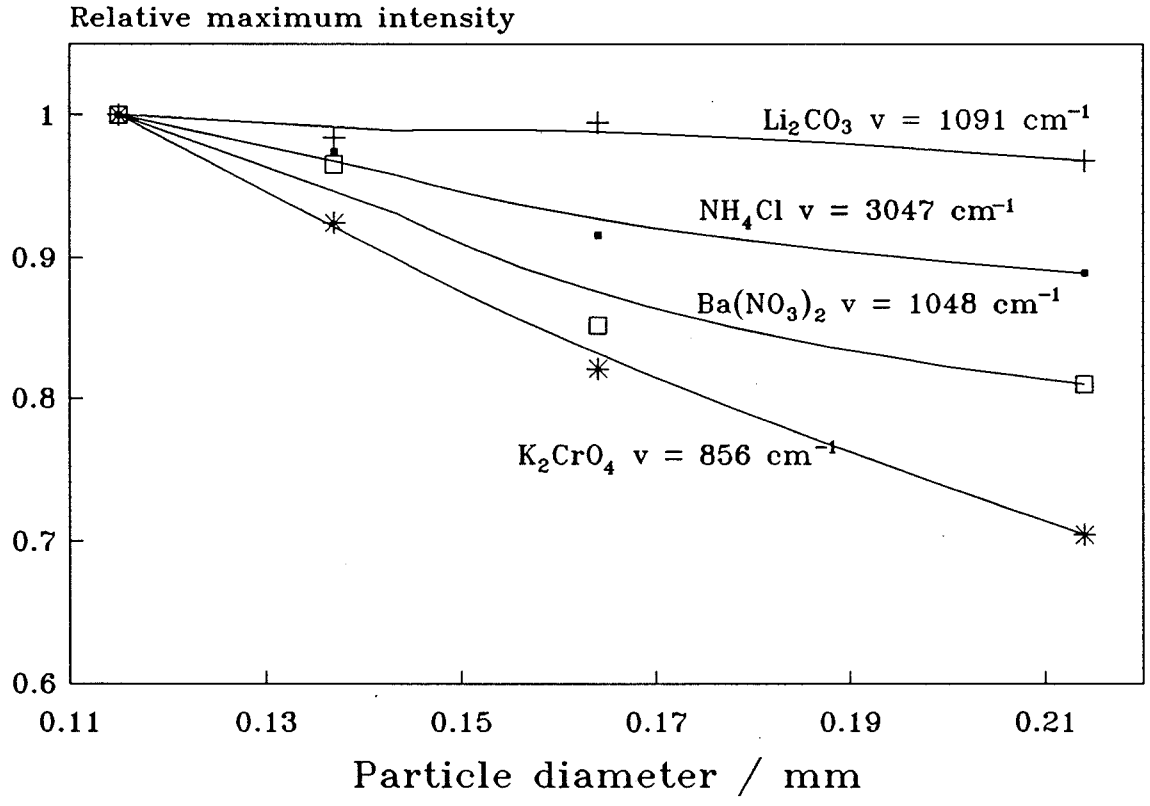

Figure 4.9 - Maximum peak height versus particle size.

In Figure 4.9 the average particle sizes have been estimated as being intermediate between the values of the "hole sizes" shown in Table 4.2. These experiments were carried out using the Perkin Elmer 1700 FT Raman spectrometer with a 1.064 μm Nd^{3+}:YAG laser and InGaAs detector at room temperature. The laser power was 200 mW, 2 scans were co-added and a resolution of 4 cm^{-1} was used. The samples were placed in a cell with dimensions 1 x 3 cm and thickness 1.75 mm. The cell had a glass front window and painted black metal backing. Each measurement was carried out in duplicate, the average standard deviation is of the order of 7 percent (calculated from 10 repeat measurements). Previous work examining the variation of Raman signal intensity with particle size has reported that the Raman signal intensity decreases as particle size increases[4,9,10]. Thus the data shown in Figure 4.9 is in direct disagreement with previously reported work. The implications of this are discussed in Section 4.2.6.

4.2.5 Theory of the dependence of Raman signal strength on particle size

D'Orazio and Schrader presented a theory[5] in 1976 which offers an explanation of the dependence of the Raman signal strength on solid particle size in terms of measurable physical quantities. This theory was developed from that of the multiple scattering processes in crystalline powders presented by Kubelka and Munk[1]. This latter theory has been generally accepted as reliable in the few literature reports dealing with the subject[5,9,10,11]. The argument developed by D'Orazio and Schrader will not be presented in detail in this report. However, the following equation was developed to calculate the Raman radiation emitted by a solid powdered sample when a monochromatic source of radiation is directed at the a sample.

$$\overleftarrow{\theta}_R = \overrightarrow{\theta}_o \frac{s\,k}{a}\left(\frac{k\sinh^2 kd + (a+r)\sinh kd\cosh kd - krd}{[(a+r)\sinh kd + \cosh kd]^2}\right) \qquad (4.1)$$

where

$$\overleftarrow{\theta}_R = \textit{flux of radiation emitted from the sample surface} \qquad (4.2)$$

$\vec{\theta}_O$ = *flux of radiation entering the front surface of the sample* (4.3)

$$r = c\ N\ q \tag{4.4}$$

r = *macroscopic scattering module* (4.5)

c depends on the angular distribution of scattered radiation inside the multiple scattering medium , where $1 < c < 2$ (4.6)

N = *number of particles per unit volume* (4.7)

q = *the optical cross section of the scattering particles* (4.8)

$$s = 2\ N\ \sigma \tag{4.9}$$

s = *Raman scattering cross section for the wavelength of Raman radiation under consideration* (4.10)

σ = *molecular absolute Raman cross section* (4.11)

d = *thickness of the crystal powder sample layer* (4.12)

a = *absorption module (defined in an equivalent manner to r) describing radiation loss by absorption* (4.13)

$$k = (\ 2\ a\ r + a^2\ )^{1/2} \tag{4.14}$$

The equation only applies if the average diameter of the crystals in the process examined is much greater than the wavelength of the radiation scattered by the particles (which does apply in this investigation). Assuming that $kd > 3$ then equation (4.1) becomes:

$$\overleftarrow{\theta_R} = \overrightarrow{\theta_O} \frac{s\,k}{a} \left(\frac{a + r + k - 2krde^{-kd}}{(a + r + k)^2} \right) \qquad (4.15)$$

Figure 4.10 shows the calculated total intensity of the Raman light emitted from a crystal powder sample using typical values for *a*, *r* and *s* calculated by D'Orazio and Schrader using Equation (4.1).

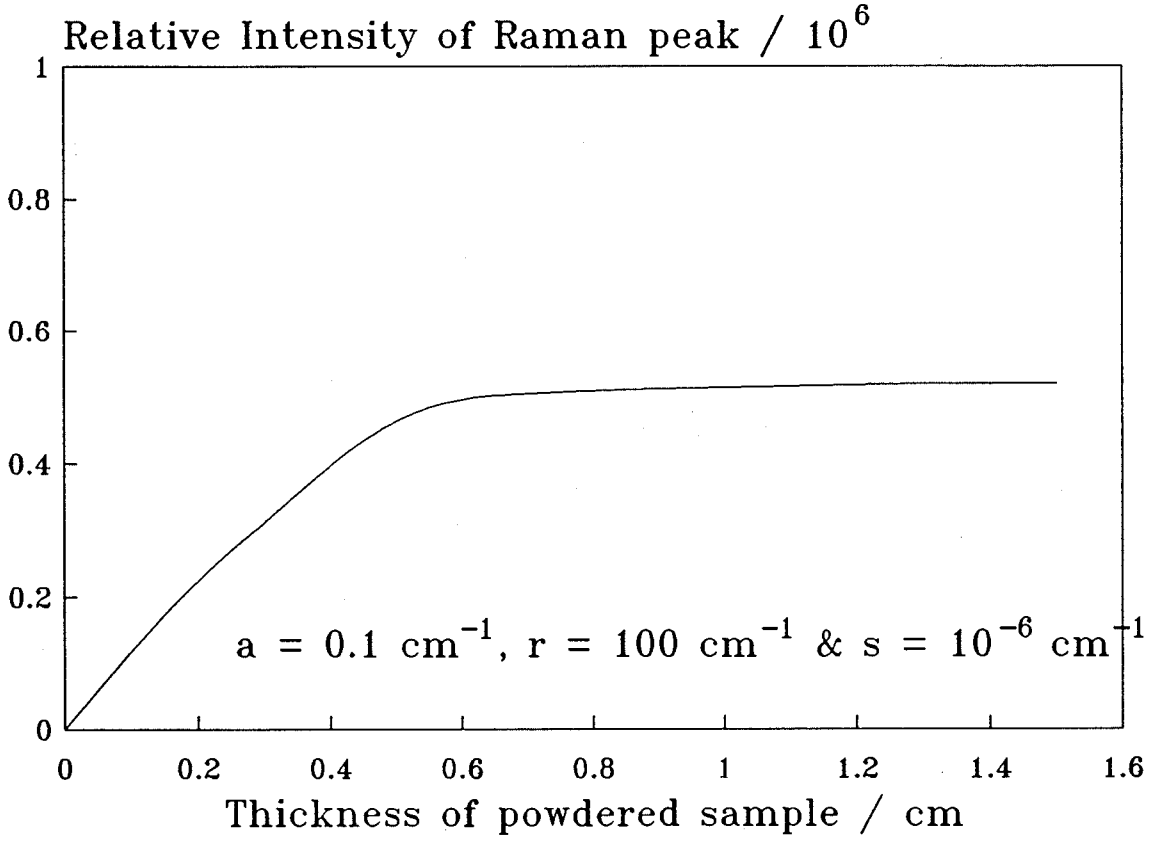

Figure 4.10 - Calculated relative intensities of remitted Raman radiation versus sample thickness.

If it is assumed that the intensity of a peak at a specific Raman shift (as measured by the maximum intensity of the peak in the Raman spectrum given by the FT spectrometer (I_R)) is proportional to the total Raman signal emitted by the sample at that shift (θ_R), Equation (3.15) can be modified to the following equation:

$$I_R = C_R \frac{s\,k}{a}\left(\frac{a + r + k - 2krde^{-kd})}{(a + r + k)^2}\right) \qquad (4.16)$$

where C_R is the proportionality constant relating I_R to θ_R.

D'Orazio and Schrader's publication made use of their theory to quantitatively explain the Raman intensity obtained in an investigation of thiourea using a conventional Raman spectrometer. The quantitative use of Equation (4.15) requires that the absolute spectral response of the spectrometer used in the investigation is calibrated[11]. The calculation of *a*, *r* and *s* using measurements made with the calibrated conventional Raman spectrometer is outlined in the publication presented by D'Orazio and Schrader. Using the calculated values the absolute intensities of the Raman radiation emitted by a solid powdered sample can be calculated and compared to the values obtained from the experimental measurements. The values of *a* and *r* are assumed to remain approximately constant over the wavelength range considered for each compound. Our experimental results in this work show that in each compound examined, the relative intensities of all of the Raman peaks for the same compound vary linearly with the particle size. This indicates that the assumption regarding *a* and *r* is valid, and also that each value of *s* for each Raman peak in the same compound varies in the same manner with particle size. Figures 4.11 and 4.12 show the results of an investigation carried out with K_2CrO_4 and $Ba(NO_3)_2$. In each case, the sample was sorted into four different particle sizes using standard sieves. A 1 x 3 cm cell with a glass window and painted black at the rear was used with the cell thickness varied between 0.50 and 1.75 mm. Measurements were carried out in duplicate using a laser power of 200 mW, 4 cm^{-1} resolution and 2 scans co-added. Figures 4.11 and 4.12 show plots of maximum peak intensity versus cell thickness for each particle size for both compounds. A 1700 FT Raman spectrometer with 1064 nm Nd^{3+}:YAG laser and InGaAs detector was used.

The solid lines indicate the best fit of Equation (4.16) to the experimental data obtained using a non-linear least squares fitting routine. The fit of Equation (4.16) is clearly excellent. Tables 4.4 (a) and (b) show the optimal values of $C_R s$, *a* and *r*

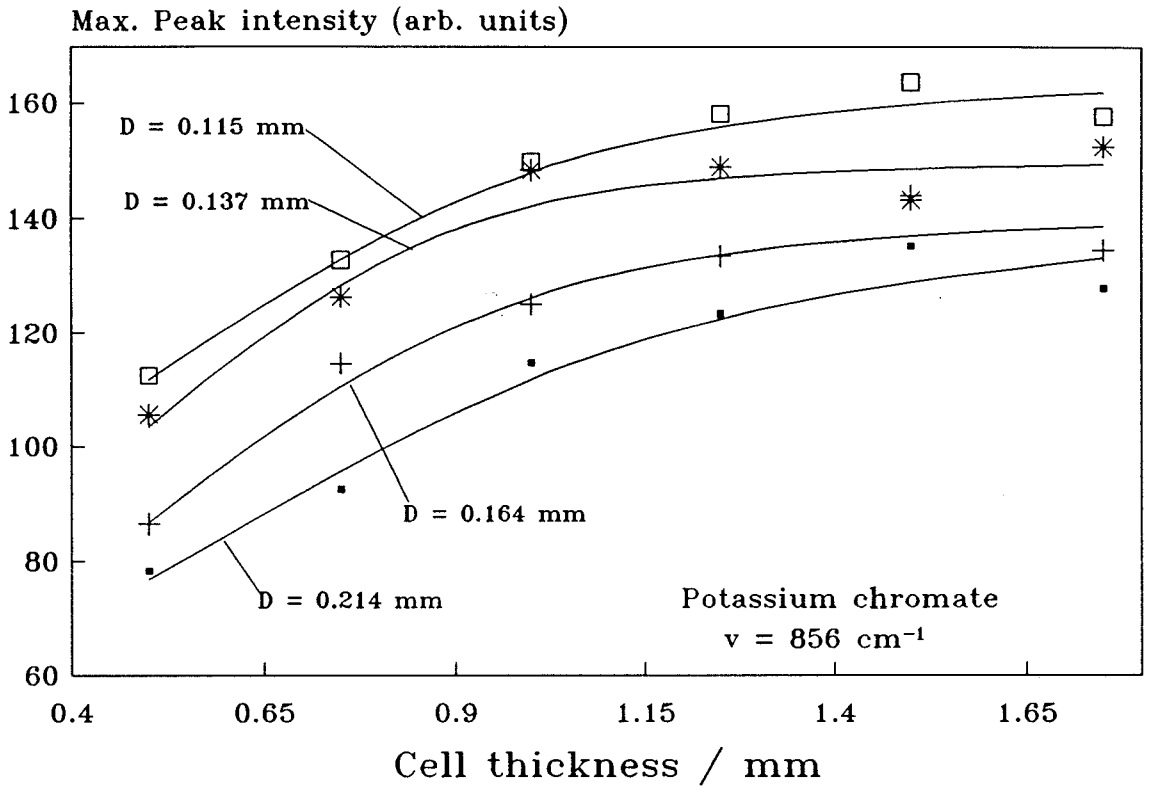

Figure 4.11 - Maximum peak intensity versus cell thickness for various particle sizes of K_2CrO_4.

Particle size / cm	0.0115	0.0137	0.0164	0.0214
Parameter				
a / cm	10.6	7.8	5.7	6.1
$C_R s$ / cm	4983	4983	3902	3117
r / cm	70.7	151.4	166.6	81.7

Table 4.4 (a) - Fitted parameters for K_2CrO_4.

Particle size / cm	0.0115	0.0137	0.0164	0.0214
Parameter				
a / cm	7.3	7.2	6.4	4.4
$C_R s$ / cm	1999	1898	1607	1259
r / cm	46.0	63.4	66.1	102.5

Table 4.4 (b) - Fitted parameters for $Ba(NO_3)_2$.

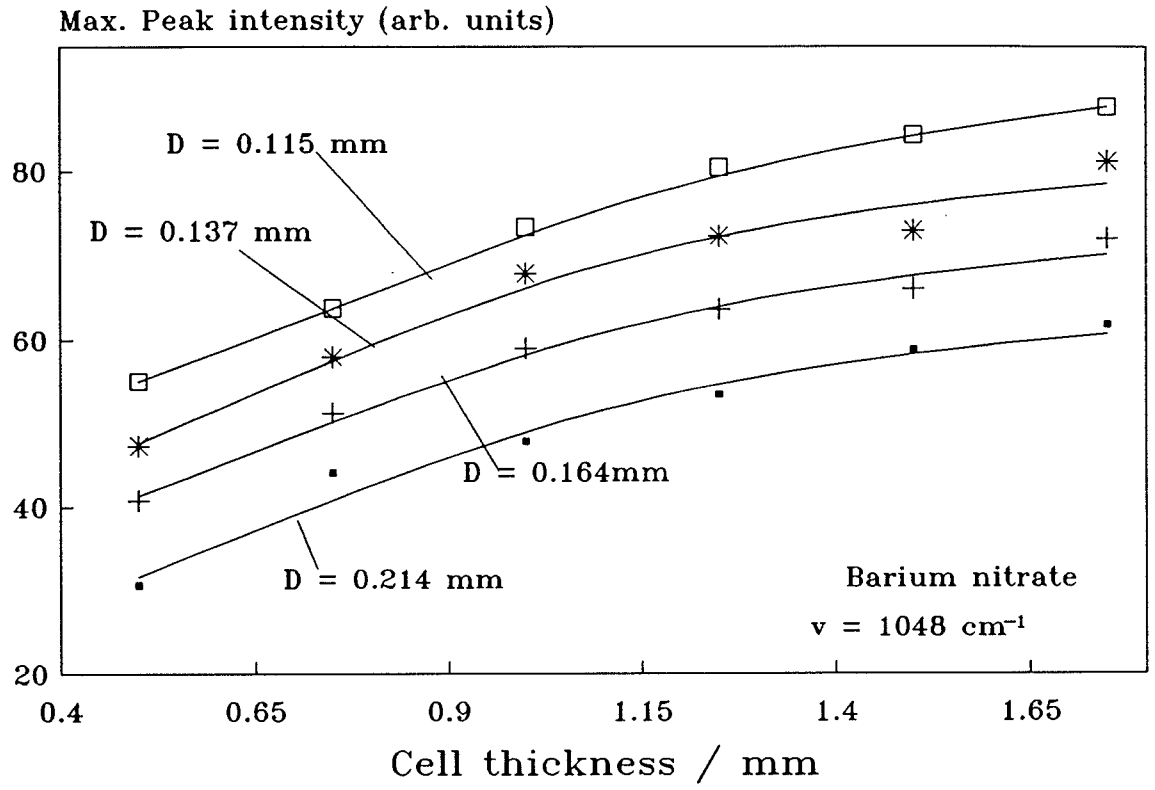

Figure 4.12 - Maximum peak intensity versus cell thickness for various particle sizes of $Ba(NO_3)_2$.

obtained for K_2CrO_4 and $Ba(NO_3)_2$.

From equation (4.4) r is proportional to N (the number of particles per unit volume) which is proportional to D^{-3}. Equation (4.4) also shows r is proportional to q (the optical cross section) which is proportional to D^2. Thus the value of r is approximately inversely proportional to the average diameter (D) of the particles under examination[12]. However this is not confirmed by Tables 4.4 (a) and (b), the slope of a logarithmic plot of r versus D is 0.095 (linear correlation coefficient of 0.058) and 1.21 (linear correlation coefficient of 0.97) for K_2CrO_4 and $Ba(NO_3)_2$ respectively. The expected slopes would be negative unity if r was inversely proportional to D. Thus either the values of r produced by the least squares fit of Equation (4.16) to the experimental data is not accurate enough to test the validity of the assumed inverse relationship of D to r or the theory used to derive Equation (4.16) is not accurate. The data presented thus far does not allow any conclusion to be drawn.

The value of a decreases as D increases[12], but the proportionality does not obey any simple relation, it depends on the natural extinction coefficient of the molecules in the crystal powder under examination. This is clearly the case for the values of a in Tables 4.4 (a) and (b). Logarithmic plots of a versus D give slopes of -0.89 (linear correlation coefficient of -0.85) and -0.81 (linear correlation coefficient of -0.93) for K_2CrO_4 and $Ba(NO_3)_2$ respectively. Thus a is approximately inversely proportional to D for these two compounds in this particle size range.

The value of s is approximately inversely proportional to D, assuming that C_R is constant for each particle size. This can be deduced from logarithmic plots of C_R versus D for K_2CrO_4 and $Ba(NO_3)_2$ which give slopes of -0.82 (linear correlation coefficient of -0.96) and -0.77 (linear correlation coefficient of -0.98) respectively.

4.3 CONCLUSIONS

The experimental data here are clearly in contradiction to the theory and previous reported work in the field. To the author's knowledge this work is the first study in which a powdered sample was actually sorted into different particle sizes to rigorously test the theory thus far accepted in the literature.

The work of Petty[4] has some precedence but work conducted in this laboratory as part of the study reported here using the same samples as Petty has thrown Petty's work into doubt. Using the samples prepared by Petty the observed trend of increasing Raman signal strength with increasing particle size was confirmed. However, when Petty's samples were sieved again the opposite trend was observed indicating an error in the labelling of samples was made in Petty's study. This contradiction was double checked to confirm the result.

The reliability of the parameters reported in Tables 4.4 (a) and (b) is unknown, the results for $Ba(NO_3)_2$ appear to follow a definite trend but the results with K_2CrO_4 show a large experimental scatter. Fitting routines such as the one used to fit Equation (4.16) to the data presented in Figures 4.11 and 4.12 are notoriously unreliable but the fact that

an excellent fit can be obtained yielding realistic values of r and a (the scattering and absorption parameters) using the appropriate equation means that the theory cannot be disproved.

Further work is undoubtedly needed in this field to answer the questions raised here. This may include attempts to provide an absolute calibration of the spectral response of the spectrometer used in the study. This is possible in principle but in reality the results may only be accurate to within the correct order of magnitude. In principle the value of the absorption parameter a may be calculated as outlined in Kortum[12]. The values of a yielded by the fit of Equation (4.16) to the data may then be verified.

4.4 REFERENCES

1. Kubelka, P. & Munk, F., Z. Tech. Physik, (1931), **11A**, 593.
2. Schrader, B. & Bergmann, G., Z. Anal. Chem., (1967), **225**, 230.
3. Hendra, P.J. & Mould, H.M., Int. Lab., (1988), **18**, 34.
4. Petty, C.J., Ph.D. thesis, (1991), Southampton.
5. D'Orazio, M. & Schrader, B., Journal of Raman Spectroscopy, (1976), **4**, 253.
6. Petty, C.J., Warnes, G.M., Hendra, P.J. & Judkins, M., Spectrochim. Acta, (1991), **47A** (9/10), 1179.
7. Lange's Handbook of Chemistry, (1978), McGraw-Hill, ed. Dean, J.A.
8. Griffiths, P.R. & De Haseth, J.A., Fourier Transform Infrared Spectrometry, (1986), Wiley, 344.
9. Schrader, B., Hoffmann, A. & Keller S., Spectrochimica Acta, (1991), **47A** (9/10), 1135.
10. Waters, D.N., Spectrochimica Acta, (1994), **50A** (11), 1833.
11. D'Orazio, B., & Schrader, B., J of Raman Spectroscvopy, (1974), **2**, 585.
12. Kortum, G., Reflectance Spectroscopy, Springer-Verlag, Berlin-Heidelberg, (1969).

Chapter 5

PYROLYSIS FOURIER TRANSFORM INFRARED SPECTROSCOPY WITH POLY(BUTYLENE TEREPHTHALATE) FORMULATIONS

Chapter 5

PYROLYSIS FOURIER TRANSFORM INFRARED SPECTROSCOPY WITH POLY(BUTYLENE TEREPHTHALATE) FORMULATIONS

5.1 INTRODUCTION

Normally, techniques (e.g. TGA-FTIR or TGA-MS) of examining the decomposition of polymers examine them at temperatures above their decomposition points. Experimental approaches such as these may provide information about the advanced decomposition of a polymer but often the compounds produced by a polymer below the temperature at which it decomposes completely, may be of considerable interest. This is particularly true in the case of applications where a polymeric material may be subject to a high temperature not sufficiently high to completely degrade the material but high enough to cause the emission of considerable amounts of unknown and possibly undesirable compounds.

As the legal requirements regarding the thermal performance of polymers become more stringent, experimental techniques which assay the thermal decomposition products of polymers, the temperature at which they are produced and the effect of various additives (such as flame retardants) on the decomposition process of interest, become more important. In this chapter a simple pyrolysis Fourier Transform infra red (FTIR) gas cell is used to compare the relative thermal performance of a model system of poly(butylene terephthalate) (PBT) polymers consisting of a virgin PBT sample, an extruded PBT sample, an extruded and moulded PBT specimen and two specially prepared formulations containing two different flame retardants.

Pyrolysis FTIR is a relatively straightforward technique that can easily evaluate the thermal performance of polymeric materials by examining the gases they release on heating. When compared to TGA-FTIR, a common technique to evaluate the thermal performance of polymers, pyrolysis FTIR displays several advantages. It requires

relatively little skill and because the IR beam passes just above the heated polymer, the possibility that some of the components released by the heated materials condense before they are analysed, as often happens with TGA-FTIR, is significantly reduced.
In previous studies on the thermal decomposition of PBT and PET[1-7], it has been shown that below 240 °C, physisorbed CO_2 and H_2O are released. Above 240 °C, PBT can degrade[1] leading to a reduction in molecular weight, increase in COOH endgroups[2] as well as the release of tetrahydrofuran, butan-1,4-diol, carbon dioxide, butadiene and cyclic oligomers of PBT[3]. Previous TGA-FTIR studies in this laboratory also indicate that when PBT is heated typically at a temperature rise rate of approximately 10 °C/min the onset of advanced decomposition occurs near 350 °C.

5.2 EXPERIMENTAL

5.2.1 Experimental Setup

All infrared spectra recorded in this investigation were recorded on a Bomem FTIR spectrometer (model Michelson M100, Quebec, Canada) operated using Lab Calc software. The gas cell used had a 3 cm path length with 5 mm thick KBr windows and a 0.5" pyroprobe insert. The pyroprobe consisted of a Pt wire flash pyrolysis probe with power supply (model CDS 120, CDS Analytical Inc., Oxford, PA, USA).

Figure 5.1 shows a schematic diagram (not to scale) of the pyrolysis gas cell with the pyrolysis probe inserted. In each pyrolysis experiment, about 10 mg of the sample to be studied was placed in a 25 mm x 1 mm quartz tube with glass wool plugs in both ends of the tube. The quartz tube was placed inside the Pt coils of the pyrolysis probe and positioned at its centre. The cell was then flushed for ten minutes with dry nitrogen and then sealed closed. The glass wool plugs prevented the pyrolysing sample from leaving the sample tube but allowed the gases produced by the decomposing sample to escape from the sample tube into the cell.

The pyrolysis probe unit was heated very rapidly (normally at a rate of 20 °C s^{-1}) to the preset temperature which was maintained until the end of the experiment. In each

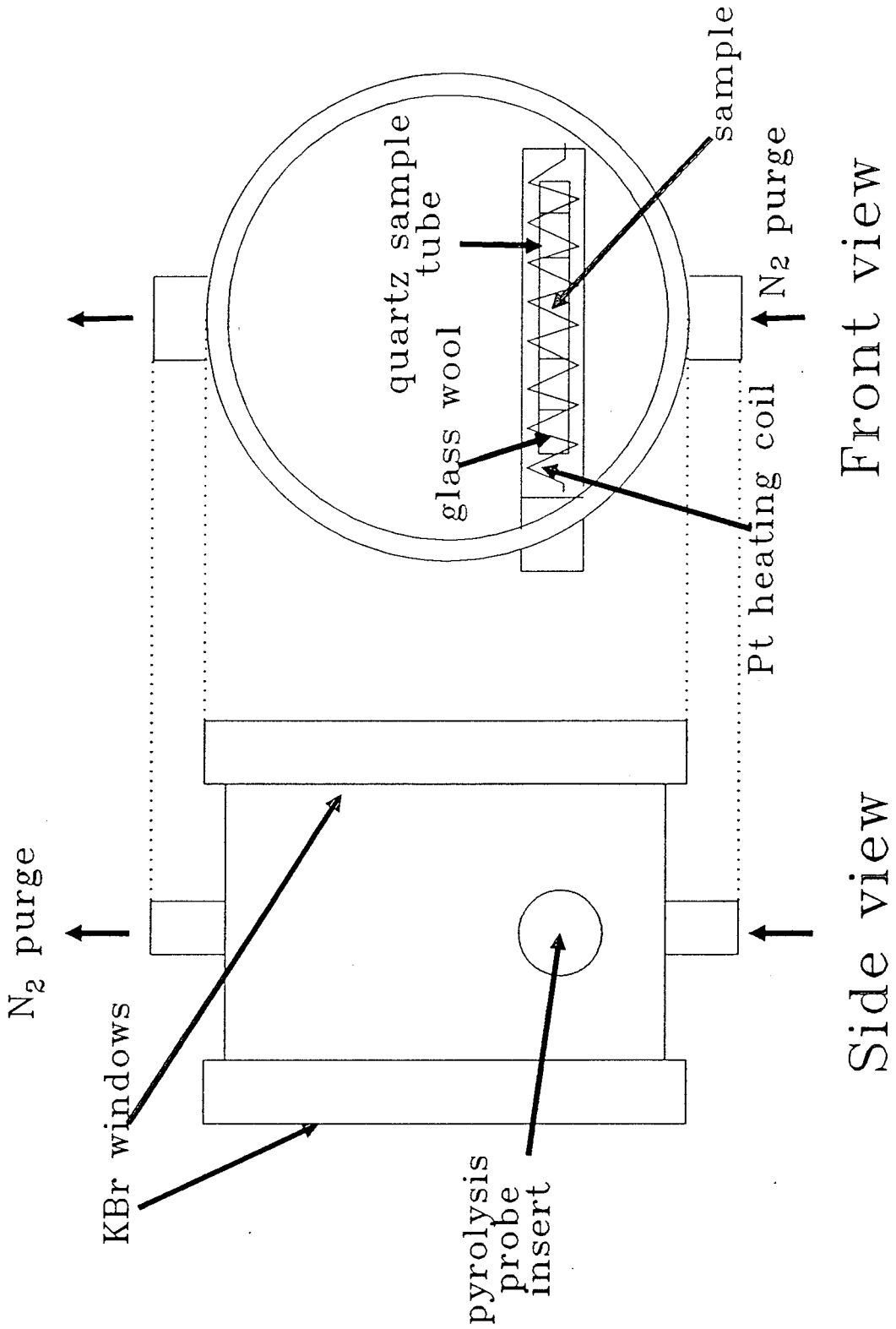

Figure 5.1: Schematic diagram of pyrolysis cell.

pyrolysis experiment 10 spectra (scanning time for each spectrum was 66 seconds) were collected consecutively at 4 cm^{-1} resolution. Each experiment thus lasted a total of 660 seconds.

Because of the small internal diameter of the quartz tube in which the test sample was placed, it was not possible to carry out each pyrolysis experiment with a thermocouple measuring the temperature of the sample. The temperature dial on the power supply unit for the pyrolysis probe was thus calibrated in a series of separate experiments with a k-type thermocouple and these measured temperatures taken to be the temperatures the sample experienced for each corresponding temperature dial setting on the pyrolysis probe power unit.

5.2.2 Sample Specifications

Table 5.1 shows the specifications of the samples used in the evaluation of the pyrolysis gas cell. Five different PBT based polymeric samples were studied using the pyrolysis gas cell. Samples 1, 2 and 3 consisted of pure PBT (Figure 5.2) subject to the treatment indicated in the table. Samples 4 and 5 were specially prepared PBT formulations predominantly composed of PBT. Both formulations also contain a heavily brominated aromatic compound as flame retardant: tetrabromobisphenol A oligomer (TBBA) in sample 4 and 1,2-di(pentabromophenyl)-ethane (DPBE) in 5 (Figure 5.3).

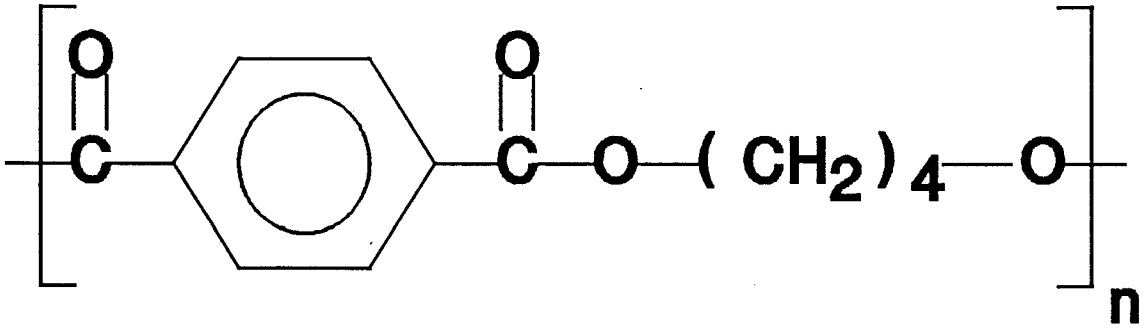

Figure 5.2: Poly(butylene terephthalate).

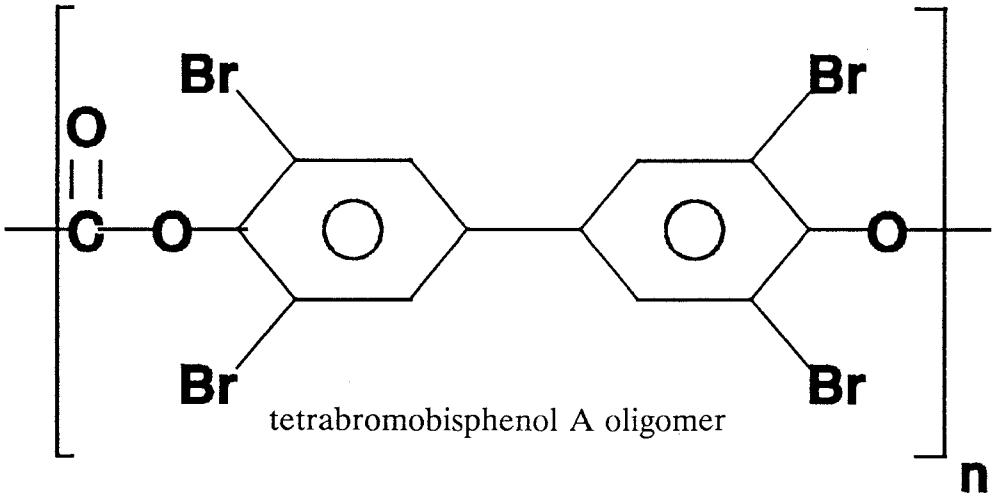

tetrabromobisphenol A oligomer

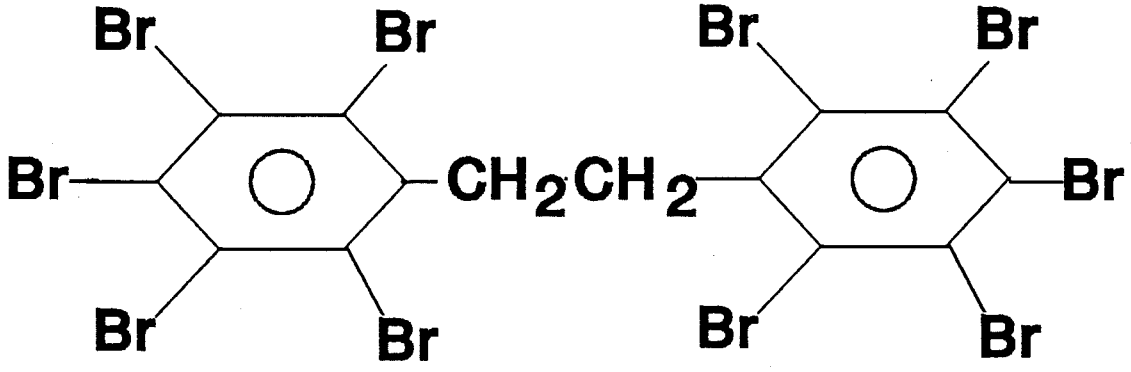

1,2-di(pentabromophenyl)-ethane

Figure 5.3: TBBA oligomer (n =4, dispersion ± 1) and DPBE.

Both formulations contained other additives but because of the competitive nature of the work performed at General Electric Plastics, these additives are not specified.

Sample Number	Sample Name	Composition
1	Pure PBT Resin	Virgin PBT
2	Extruded PBT	Extruded PBT
3	Moulded PBT	Extruded and Moulded PBT
4	Compounded PBT formulation	54.75 % PBT 11 % TBBA

5	Compounded PBT formulation	57.75 % PBT 7.5 % DPBE

Table 5.1 - Specifications of PBT samples used.

Samples 2 to 5 were ground into powder form under liquid nitrogen to suppress thermal degradation in the grinder. Sample 1 was already in powder form and did not need to be ground. All samples were dried at 130 °C for at least two hours before testing and stored in a dessicator. The removal of excess water (ca. 0.3 % v/v) was carried out to ensure that the baseline in each FTIR spectrum was as stable as possible and to allow the discrimination between physisorbed water and water released from polycondensation at relatively moderate temperatures and decomposition reactions at higher temperatures.

5.3 RESULTS AND DISCUSSION

5.3.1 Temperature calibration of the pyrolysis probe

Three different experiments were conducted in order to gain as accurate as possible a picture of the sample temperature inside the pyrolysis probe. The heating rate of the pyrolysis probe as indicated by the power supply unit was 20 $^{o}C\ s^{-1}$. Assuming that the polymer sample in the pyrolysis probe is heated to its maximum temperature at this rate, it would take approximately 10 seconds for the sample to be heated from room temperature to 275 ^{o}C. The experiments described below show that the sample is not in fact heated to its maximum temperature in this time but in a considerably longer time.

(a) The pyrolysis probe was set up as normal but without a sample and with only one glass wool plug in the quartz tube. The thermocouple was placed in the centre of the quartz tube through the hole in the top of the cell usually used as an exit position for the nitrogen purge. Figure 5.4 shows the results of this experiment. It was apparent from this experiment that the temperature inside the quartz tube took 3 minutes to reach a final value. The heating rate on the pyrolysis power unit indicates that the time to reach the maximum should be between 6 and 18 seconds. Figure 5.4 shows that this is not the case.

(b) The pyrolysis probe was removed from the gas cell and set up with a quartz tube

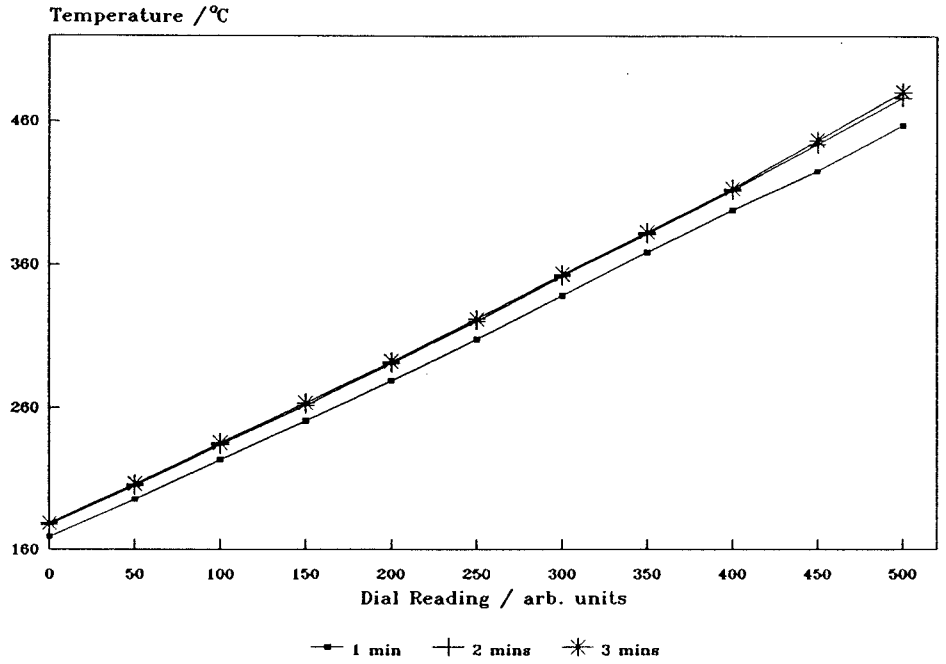

Figure 5.4: Plot of thermocouple temperature versus pyrometer dial reading.

inside stoppered with glass wool on one side (i.e. exactly as in (a)). The thermocouple was used to determine the temperature at three positions in the glass tube. Figure 5.5 shows the results of this experiment. When the pyrolysis probe was removed from the gas cell, it was noticeable that the thermocouple reached its maximum temperature in approximately 1 minute. This indicates that there is a degree of thermal inertia inside the gas cell, no doubt because the pyrolysis unit loses heat to the cell body.

(c) Again with the pyrolysis probe removed from the cell, the temperature profile inside the 25 mm quartz tube was examined for three different dial settings, the results of this experiment are shown in Figure 5.6. An unfortunate (and unavoidable) aspect of the use of the thermocouple is that any measurement made to determine the temperature the sample experiences in the gas cell alters the system in an unknown way. It is likely that with two glass wool stoppers, the sample is better insulated than when the temperature readings were made and will thus maintain a higher average temperature in the quartz tube than is observed with thermocouple measurements (i.e. Figure 5.6 will have a more level and possibly higher profile). In the absence of a more satisfactory solution the only course is to assume that the temperature that the sample experiences during a pyrolysis

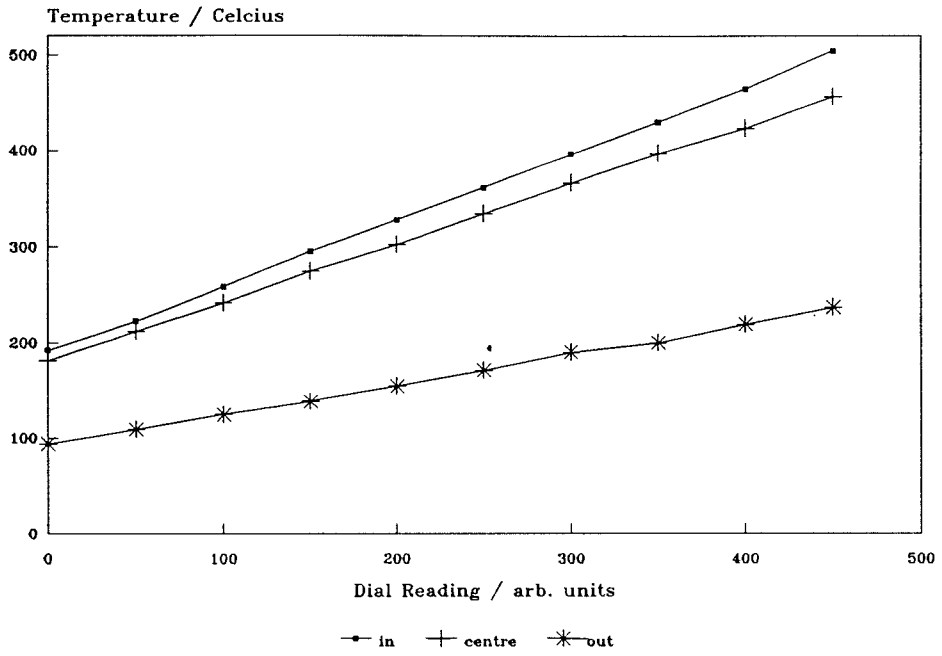

Figure 5.5: Plot of thermocouple temperature versus pyrometer dial reading.

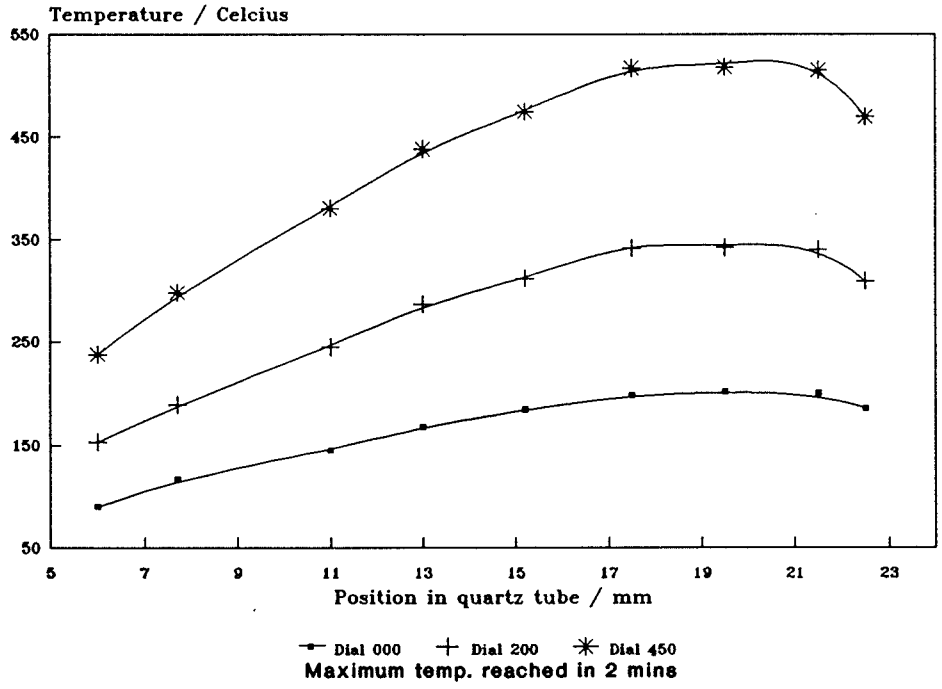

Figure 5.6: Plot of thermocouple temperature versus position in quartz tube.

experiment is the highest temperature observed for each dial setting in Figure 5.5, at the same time keeping in mind that it is possible that the true sample temperatures may

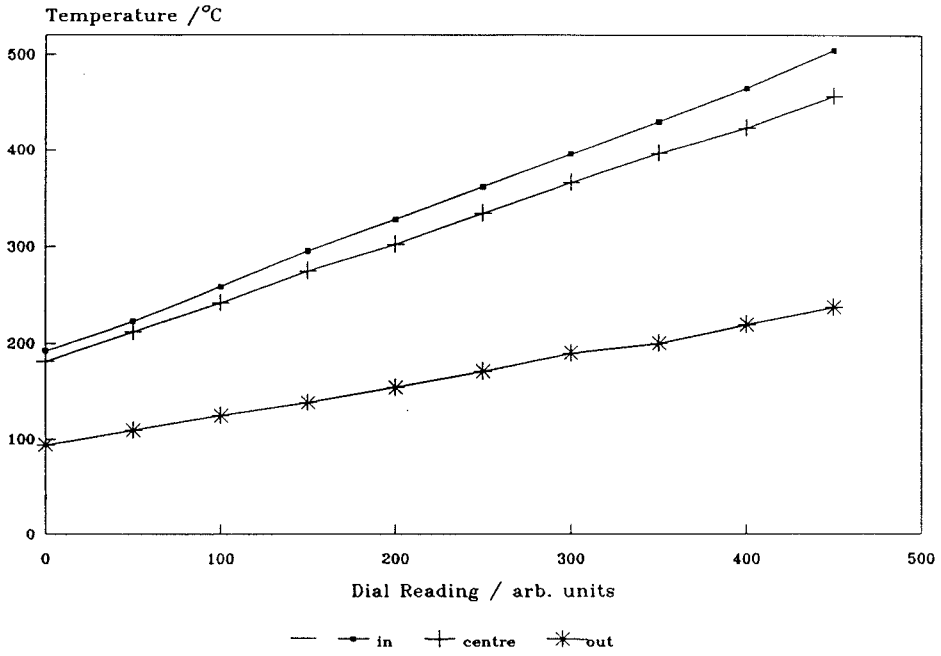

Figure 5.5: Plot of thermocouple temperature versus pyrometer dial reading.

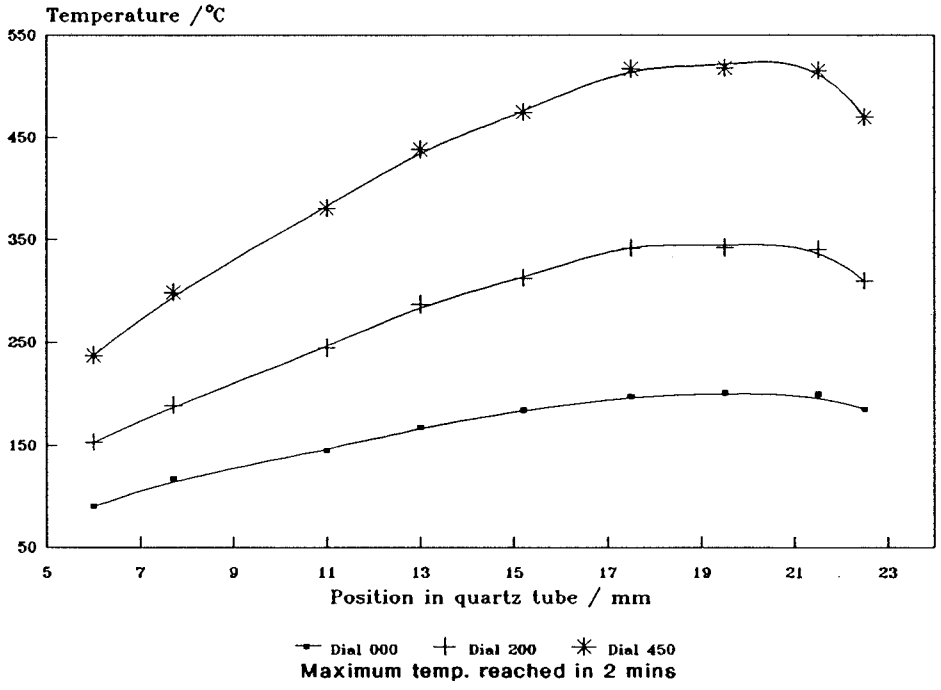

Figure 5.6: Plot of thermocouple temperature versus position in quartz tube.

experiment is the highest temperature observed for each dial setting in Figure 5.5, at the same time keeping in mind that it is possible that the true sample temperatures may

deviate considerably from the assigned values.

5.3.2 Pyrolysis experiments from 225 to 430 °C

Each sample shown in Table 5.1 was pyrolysed under the same conditions at temperatures of 225, 260, 295, 330, 360, 395 and 430 °C. These temperatures were selected to give an indication of the volatiles released by the different polymeric materials below and slightly above the temperature of total decomposition as determined by TGA studies (i.e. approximately 350 °C). The result of each pyrolysis experiment was a series of 10 FTIR spectra (4 cm^{-1} resolution between 4500 and 550 cm^{-1}) recorded over a period of 11 minutes e.g. Figure 5.2. The final (i.e. tenth) spectra in each series of ten spectra collected during each pyrolysis experiment was used to compare the volatile materials released by each sample.

Figures 5.8 to 5.13 show a comparison of the tenth spectrum in each pyrolysis experiment for each material at the different temperatures selected.

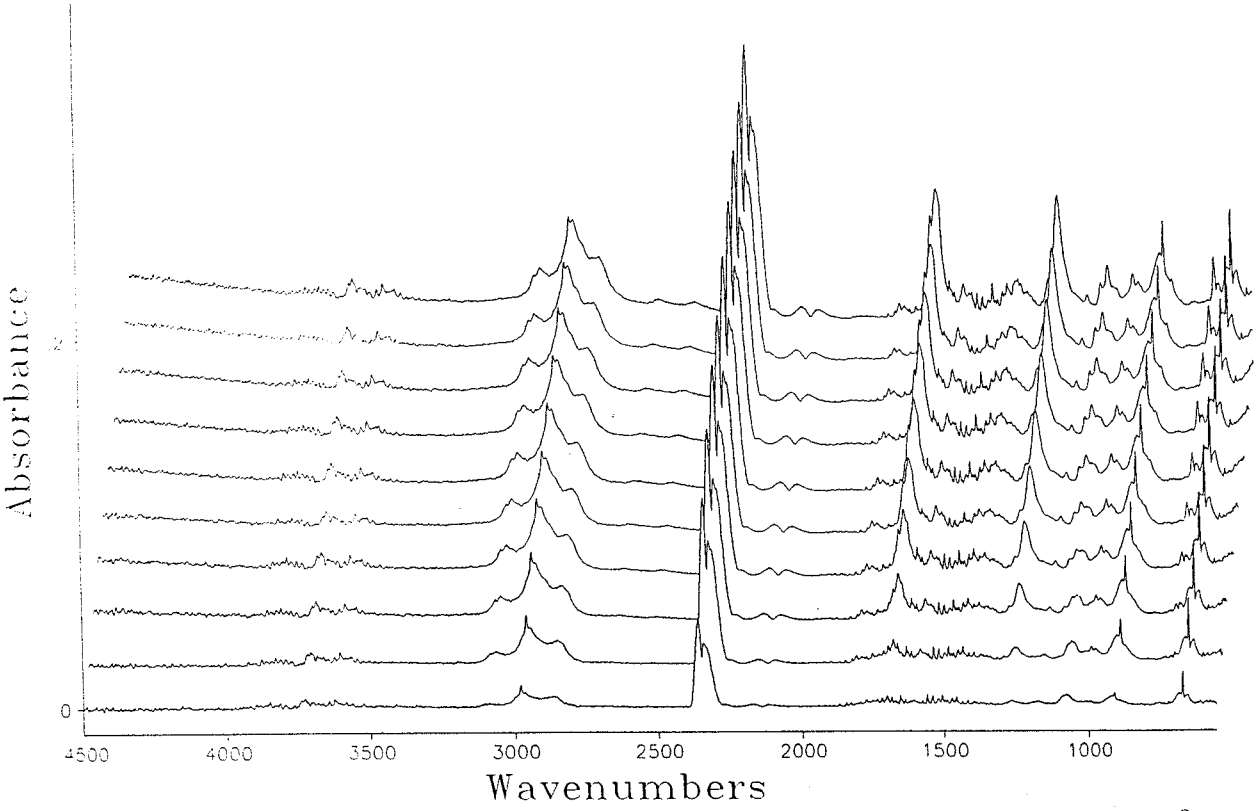

Figure 5.7: Typical series of spectra from pyrolysis experiment (sample 4 at 360 °C).

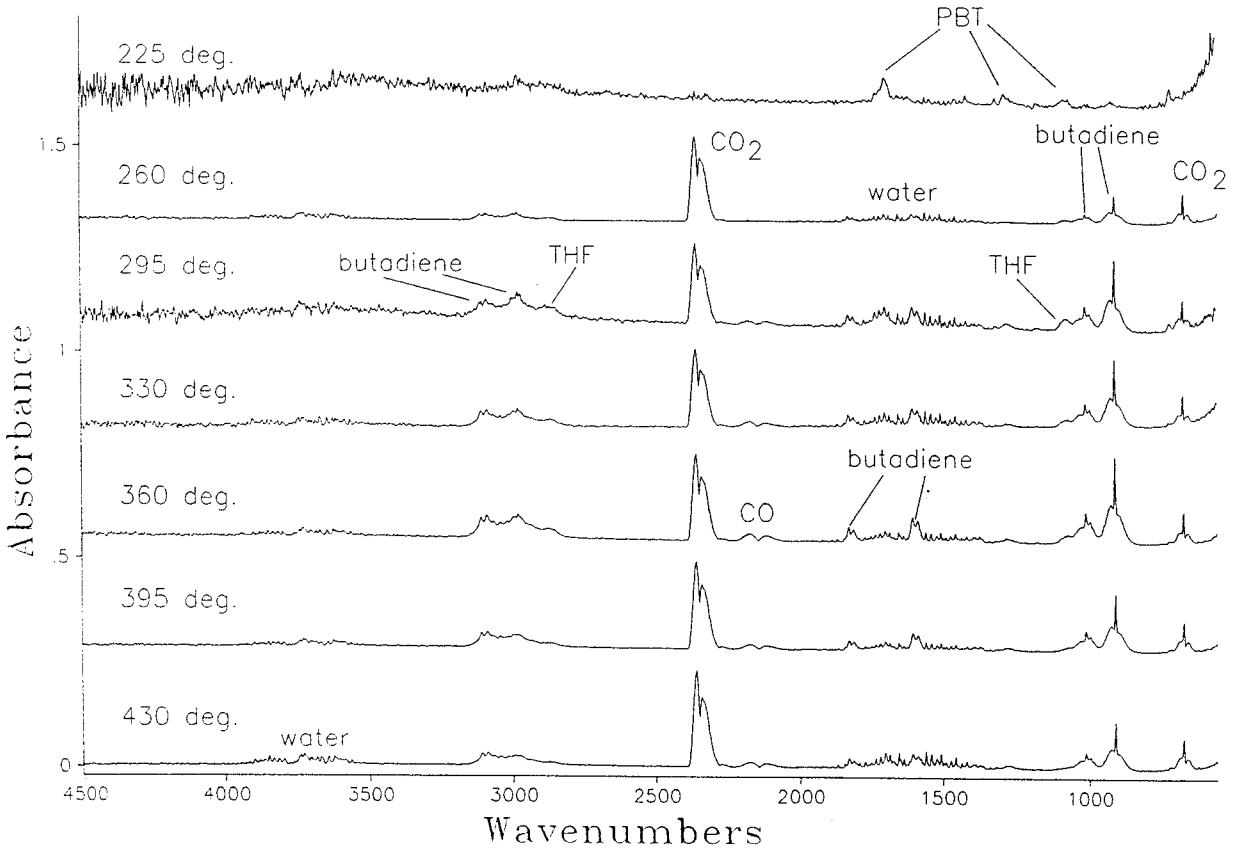

Figure 5.8: Comparison of the last spectra (i.e. #10) for pure PBT resin at different temperatures.

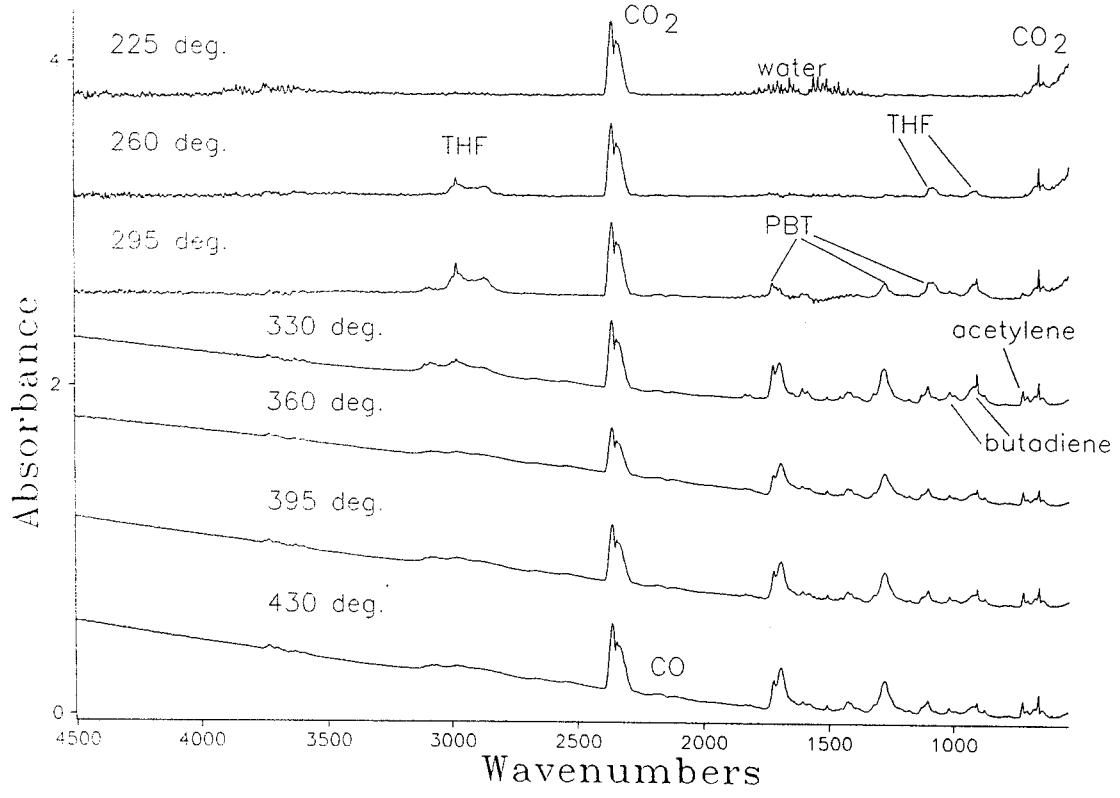

Figure 5.9: Comparison of spectrum #10 for extruded PBT at different temperatures.

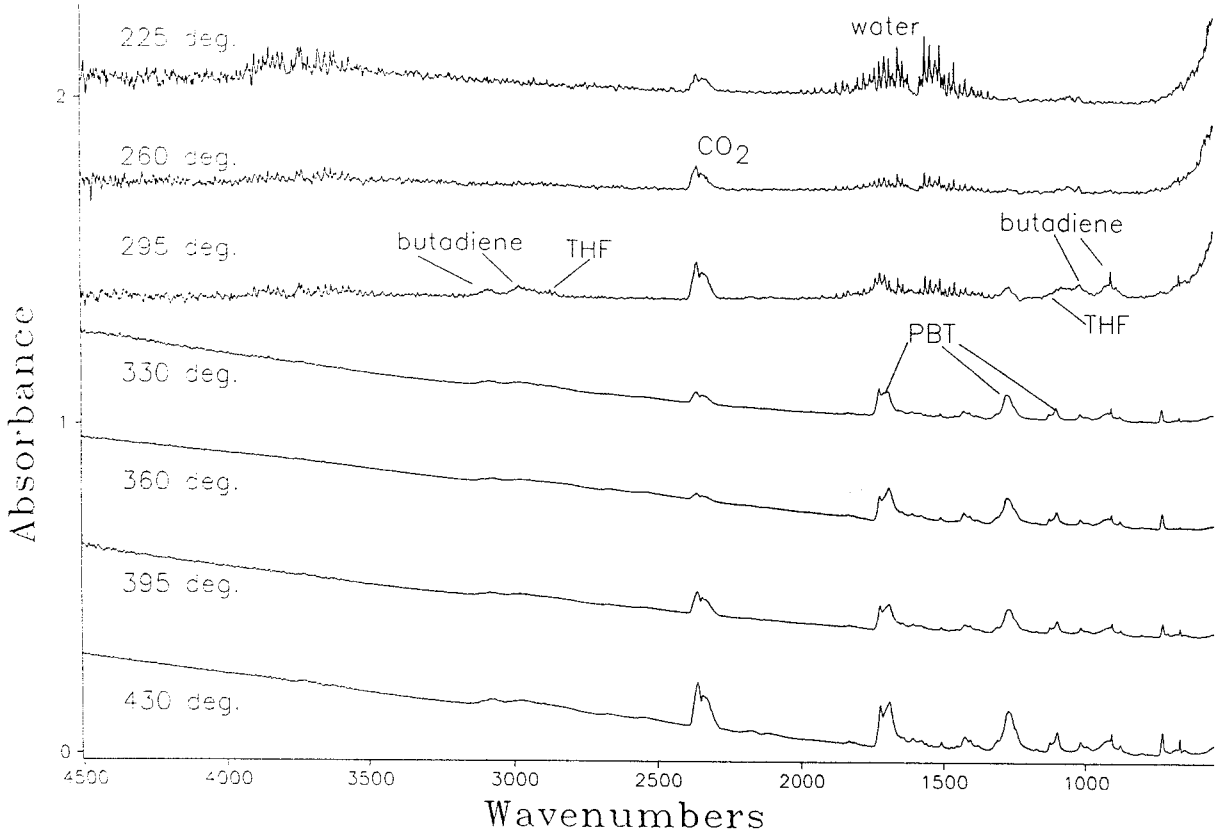

Figure 5.10: Comparison of spectrum #10 for moulded PBT at different temperatures.

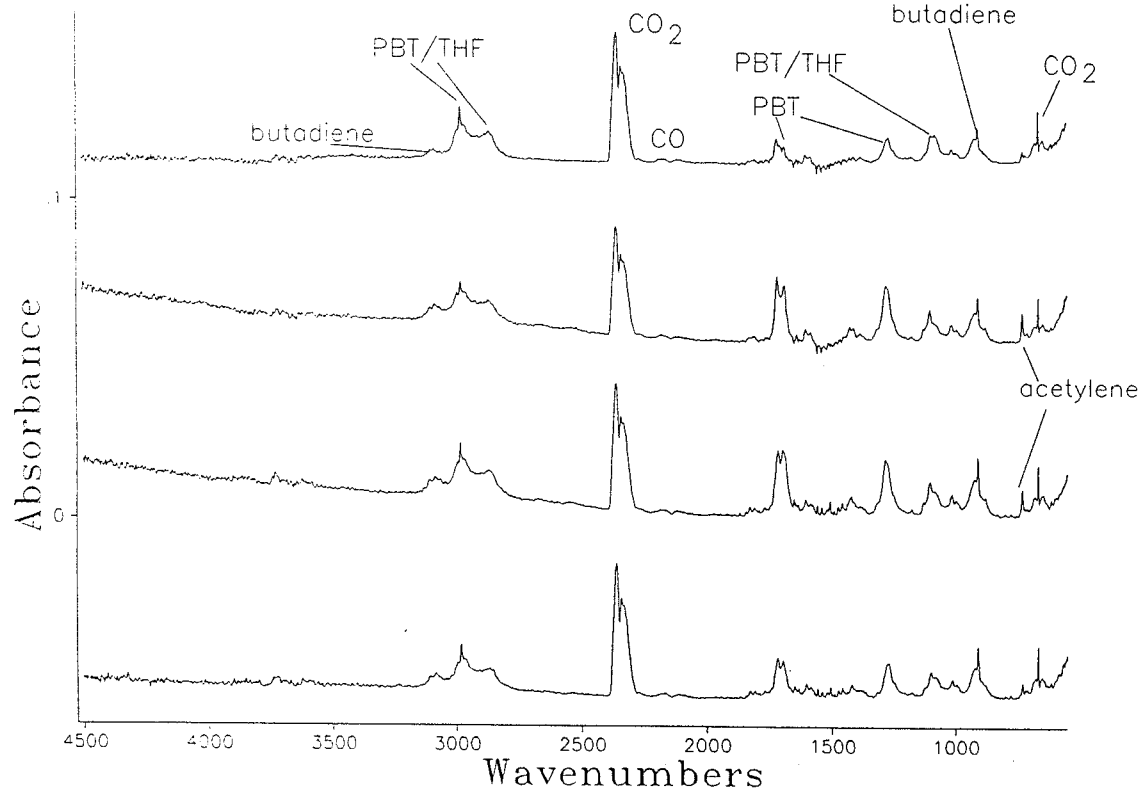

Figure 5.11: Comparison of spectrum #10 for 4 repeat pyrolysis experiments with extruded PBT.

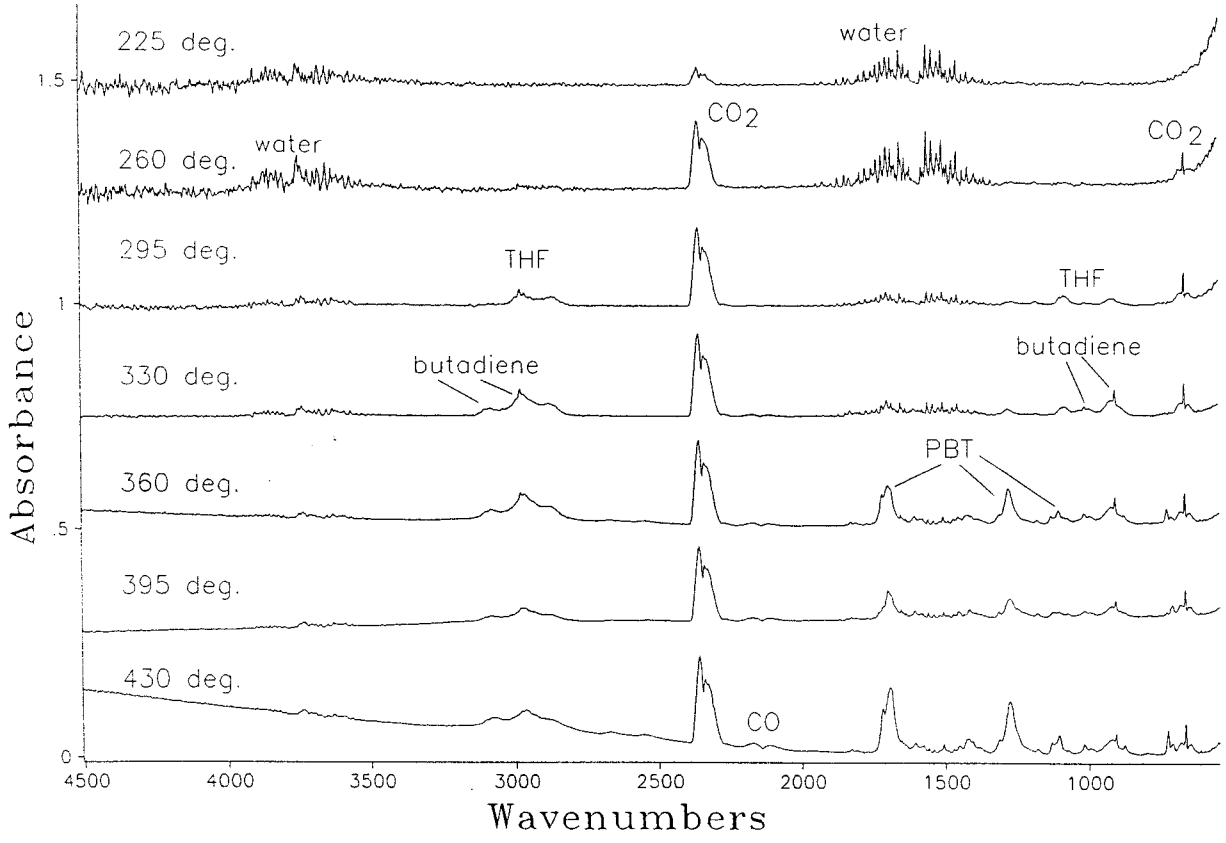

Figure 5.12: Comparison of spectrum #10 for sample #4 at different temperatures.

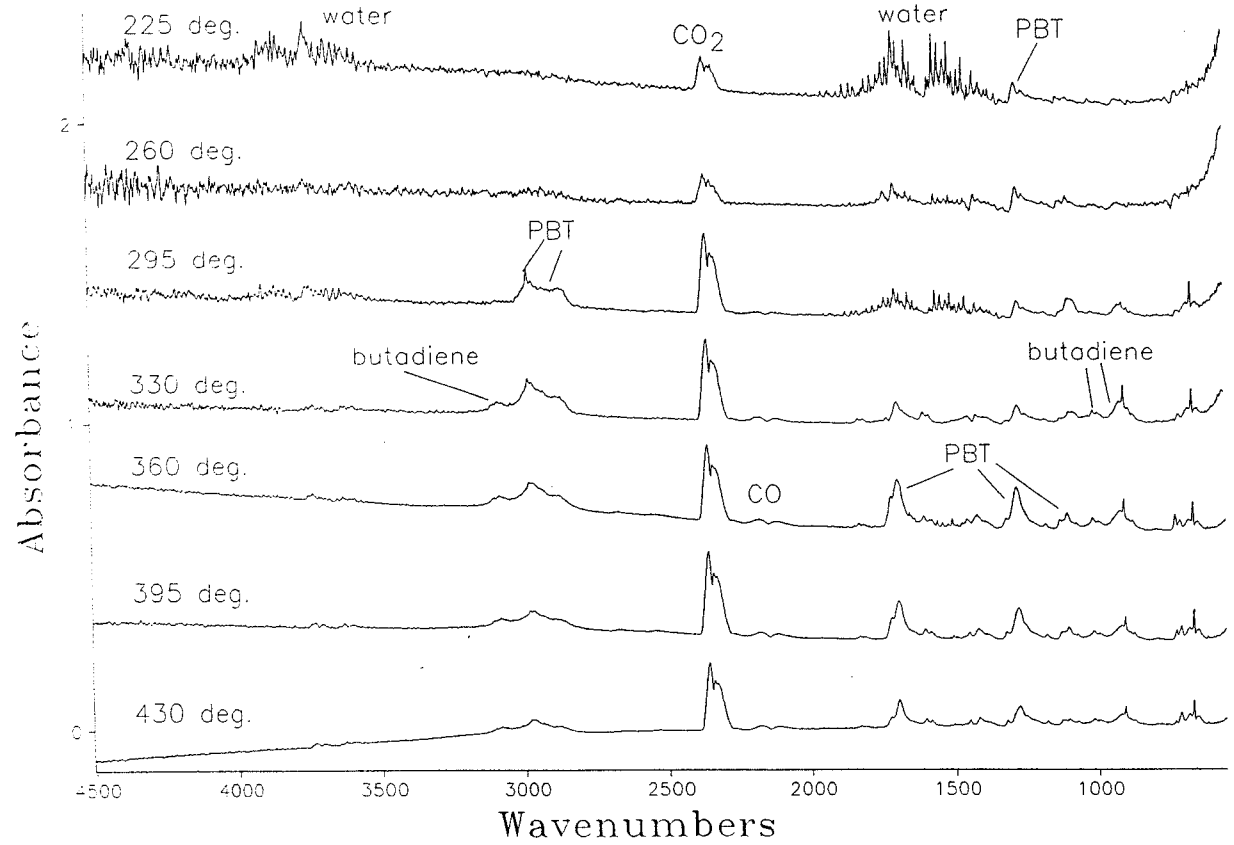

Figure 5.13: Comparison of spectrum #10 for sample #5 at different temperatures.

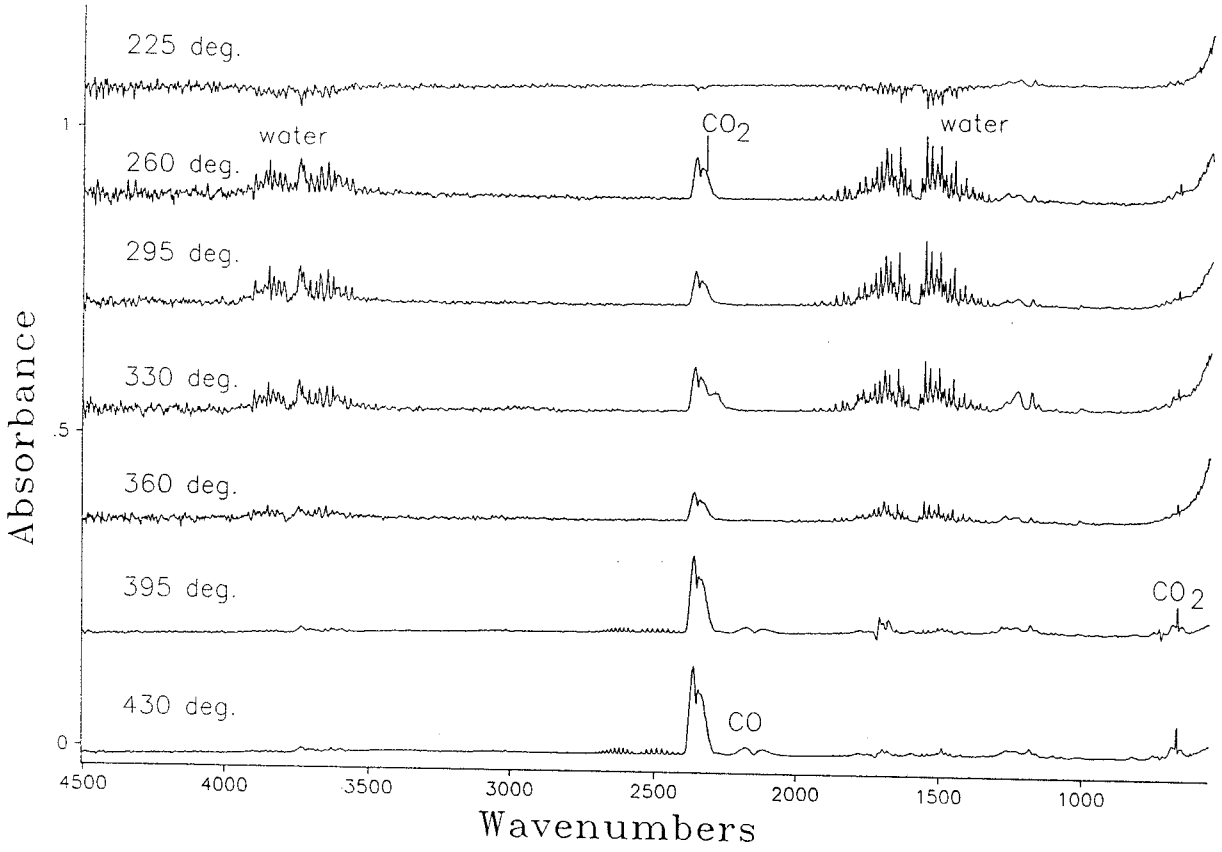

Figure 5.14: Comparison of spectrum #10 for TBBA oligomer at different temperatures.

The identification of the compounds produced in each pyrolysis experiment was accomplished by comparison with the appropriate spectrum obtained from a Sadtler reference library of IR spectra and identifying at least two of the major peaks.

Tetrahydrofuran (THF) and butan-1,4-diol have their main absorption bands very close together (2982 cm^{-1}, 2897 cm^{-1} and 1072 cm^{-1} for butan-1,4-diol and 2993 cm^{-1}, 2871 cm^{-1} and 1079 cm^{-1} for THF) thus it was difficult to distinguish between these two compounds if either or both were present in the gaseous decomposition products of a particular sample. The Sadtler reference spectra for THF and butandiol have been recorded using liquid samples, this also means that some differences in the exact shifts of the absorption bands can be expected from the values given in the Sadtler spectra. Thus whenever THF has been identified as a component of the pyrolysis products of a sample, it is possible that butan-1,4-diol was also present.

Poly(butylene terephthalate) has its three strongest absorption bands at 1715 cm^{-1}, 1271

cm^{-1} and 1104 cm^{-1}. Where PBT or PBT oligomers have been identified in pyrolysis products of samples used here, the main absorption bands do not appear at precisely these frequencies e.g. the strongest peak in the gas decomposition spectra attributed to PBT or PBT oligomers is usually at 1697 cm^{-1}. These differences were attributed to the difference in the state of PBT from its usual solid polymeric state. It may be expected that only PBT in the gaseous state would contribute to the PBT observed in each pyrolysis experiment but examination of the IR cell after each pyrolysis experiment showed the presence of a white powder on the KBr windows which was found to be PBT, thus is was concluded that PBT could be released by the test sample in the form of small particles in addition to oligomers.

Figure 5.7 shows a typical series of spectra obtained from a single pyrolysis experiment using sample 4 heated at 360 °C for 11 minutes. An impression can be gained of order in which specific compounds are produced in a particular experiment. In Figure 5.7 it can be seen that at lower temperatures CO_2, H_2O and some THF are produced. PBT is released in large amounts together with butadiene and CO as the pyrolysis reaction continues (i.e. at higher temperatures). The sample is completely degraded at this temperature giving mainly CO_2, PBT, PBT oligomers and butadiene. It is possible to extract plots of peak areas versus time for the series of ten spectra thus giving a picture of the evolution profile of a specific component. However time profiles such as this were found to be of little value because they usually indicated that the concentration of most components increased rapidly in the first few minutes of a pyrolysis experiment and this was also the period where the temperature in the quartz tube was rising to its set value.

In Figures 5.8 to 5.10 and 5.12 to 5.14 the absorbance scale for each spectrum is not constant. This is readily indicated by the noise level in each spectrum which differs vastly. If each spectrum in each figure were presented with a similar absorbance intensity scale then the spectra recorded at lower temperatures would appear almost flat when compared to the spectra recorded at the higher temperatures. Thus the differences in the y-axis scale must be taken into account for any semi-qualitative comparison of the relative amounts of each component produced at each temperature.

Comparison of Figures 5.8, 5.9 and 5.10 indicates that the virgin PBT sample (sample 1) degrades (i.e. releases compounds other than CO_2 and H_2O) at a lower temperature (between 260 and 295 °C) than the extruded and compounded PBT samples (samples 2 and 3). The PBT resin (sample 1) appears to degrade mainly by producing THF and butadiene while the extruded and moulded PBT polymer samples (samples 2 and 3) produce THF, PBT, PBT oligomers and butadiene.

Both samples 2 and 3 produce a higher concentration of PBT oligomers than the PBT resin (sample 1). This observation is surprising because the PBT resin (sample 1) certainly contains a higher proportion of PBT oligomers than the other two PBT samples (samples 2 and 3) because it has not been thermally processed. The PBT resin is seen to give off PBT oligomers at 225 °C while the extruded and moulded PBT samples (samples 2 and 3) do not. This indicates that the PBT given off by sample 1 at lower temperatures are the oligomers remaining in the PBT resin after polymerization, they are presumably lost in the extrusion process where temperatures are in excess of 270 °C. The PBT and PBT oligomers seen released in Figures 5.9 and 5.10 must originate from the degradation of the bulk polymer itself and not simply from the release of PBT oligomers present in the polymer. Samples 2 and 3 behave in a similar manner above 330 °C, the major difference between Figures 5.9 and 5.10 is that the extruded PBT (sample 2) releases THF at a lower temperature than the moulded PBT (sample 3), the extruded PBT (sample 2) also releases CO_2 at a lower temperature than the moulded PBT (sample 3).

Figure 5.11 shows the final spectra in each series for a set of pyrolysis experiments carried out under similar conditions at 295 °C to check the reproducibility of the pyrolysis technique. All four spectra have a similar scale for the y-axis. All four spectra reveal the presence of similar amounts of CO_2, the major difference between the four spectra is in the relative amounts of PBT and PBT oligomers and THF produced. The relative amounts of THF and PBT and PBT oligomers produced are an indication of the temperature experienced in the pyrolysis probe. The samples producing relatively more PBT and PBT oligomers than THF must experience a higher temperature than the samples producing relatively less PBT / PBT oligomers than THF. Thus some variation

of "average temperature" does occur during any series of pyrolysis experiments, however the reproducibility of the technique as demonstrated by Figure 5.11 is as good as can be expected from such a simple technique.

Figures 5.12 and 5.13 reveal that samples 4 and 5 degrade primarily into CO_2, PBT or PBT oligomers and butadiene. However, sample 4 degrades at a significantly higher temperature than sample 5. Sample 5 releases PBT or PBT oligomers at 225 °C while sample 4 only starts degrading at 295 °C. Comparison of Figures 5.9 and 5.10 with Figures 5.12 and 5.13 reveals that sample 4 comfortably outperforms samples 2 and 3 (the extruded and moulded PBT samples) while sample 5 only narrowly outperforms them.

Figure 5.14 shows the results of a similar series of pyrolysis experiments conducted with samples 1 to 5 conducted with pure TBBA. TBBA apparently starts to degrade at 395 °C, another interesting feature of Figure 5.14 is the presence of a gas phase spectrum of HBr seen to appear near 395 °C. The spectra shown in Figure 5.14 reveal little about the mode of action of the flame retardant. The temperature at which the polymer samples degrade is around 300 °C, however the gas spectra of the flame retardant shows that it starts to degrade around 395 °C. It is likely that the flame retardant functions by releasing bromine containing compounds which consume any free radicals produced by a flame close to the decomposing material, thus it is unlikely that the flame retardants have any great influence on the decomposition temperature of the test materials.

The absorptions seen in Figure 5.14 at 1231 cm^{-1} and 1181 cm^{-1} could not be assigned to any compound, neither could the feature seen at higher temperatures at 1688 cm^{-1}. Many compounds were checked (using the Sadtler reference library) to see if they matched these frequencies e.g. various mono- and poly-brominated phenols and benzaldehydes but no definite match could be found.

5.3.3 Pyrolysis experiments at 800 °C

The sample was placed in the cell as in the experiments described for the pyrolysis

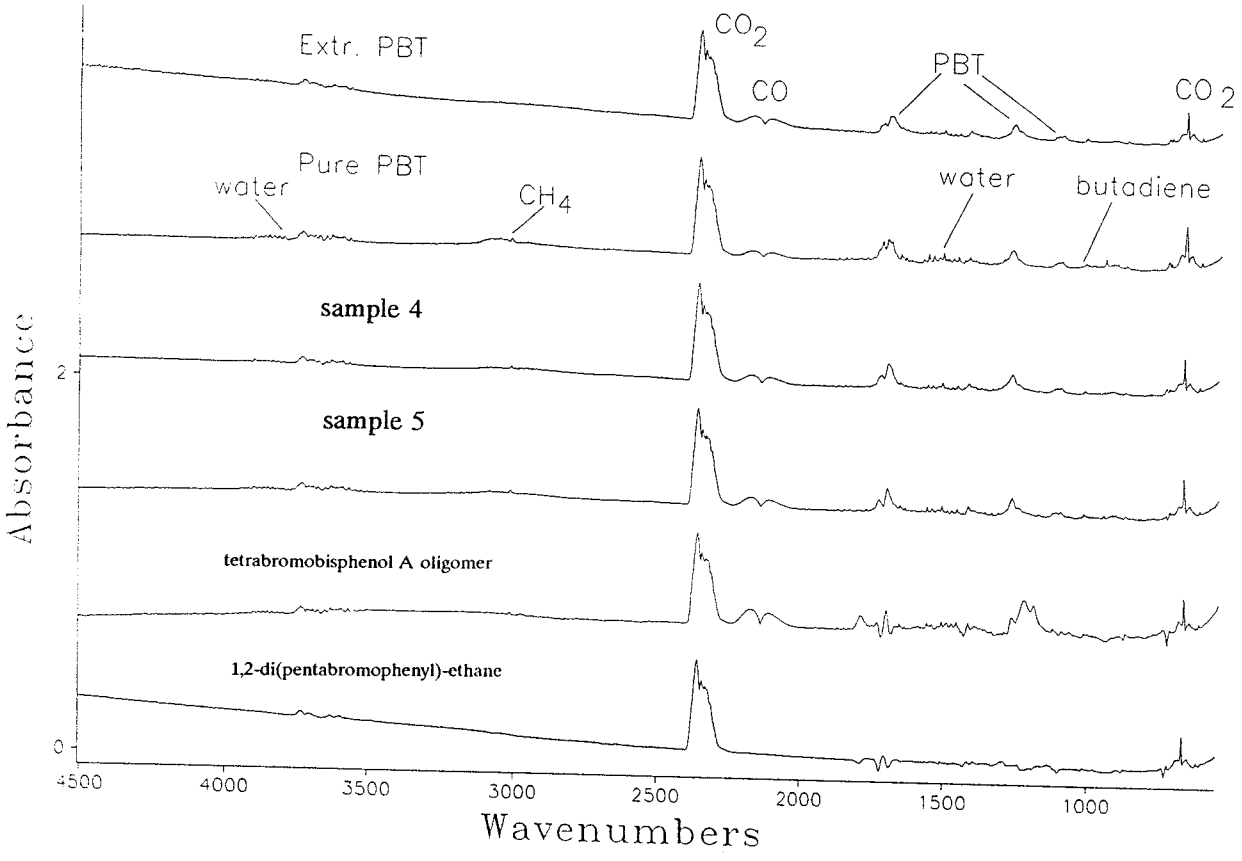

Figure 5.15: Comparison of Spectrum #10 for each test material at 800 °C in N_2.

between 225 °C and 430 °C and the cell flushed for 10 minutes with dry nitrogen. Figure 5.15 shows the final spectrum in each series of 10 spectra collected during each experiment lasting 11 minutes.

Two major problems are associated with pyrolysis at such high temperatures. Most of the sample in the quartz tube is released as gases or fine particles. These fine particles cause an increase in the background of the IR spectra recorded and reduce the quality of the spectra obtained. In addition the heated platinum wire in the pyrolysis unit starts to give off an appreciable thermal background, some of this radiation enters the interferometer and causes an error in the interferogram seen by the detector of the FTIR instrument and thus a source of error in each FTIR spectrum recorded at the high temperature.

The samples heated to 800 °C give off mainly CO_2, CO and PBT oligomers. In the initial

period of each pyrolysis experiment butadiene is also released but by the end of the reaction its concentration is too low to be identified in each final spectrum. A similar series of experiments was carried out with the test materials as shown in Figure 5.15 in air. The final FTIR spectrum from each pyrolysis experiment revealed that all the polymers decomposed almost completely into CO_2.

5.4 CONCLUSION

Pyrolysis FTIR has been shown to be a useful technique when used to compare the high temperature performance of different polymeric materials. The various decomposition products can be identified with some limitations.

The pyrolysis experimental setup described here has the advantage that a minimum of operator skill is required to provide rapid qualitative information about the decomposition products given off by a polymeric material.

It is likely that the sample temperature in the quartz tube is very sensitive to factors such as the length of the quartz tube, its exact position in the heating coil, the amount of glass wool plug used in the tube and the exact configuration of the platinum heating coil. In view of this it is important that a system of reference materials be used in any series of pyrolysis experiments and that care should be taken to test each material as closely as possible under identical conditions.

A further drawback is the fact that due to the cell windows and exterior not being heated, it is likely that some of the decomposition products of the polymer pyrolysis condense on the windows of the cell. One advantage of this technique is that the infrared beam of the spectrometer passes directly adjacent to the source of the gaseous volatile material thus the possibility that any decomposition products condense before their presence is recorded by the spectrometer is minimised. In many more expensive commercially available cells suitably for temperature programmed FTIR this problem is addressed by providing heated cell windows.

The pyrolysis cell is unsuitable for extremely high temperature pyrolysis (e.g. 800 °C) because the pyrolysis probe (and therefore the test material in the cell) takes approximately five minutes to reach this temperature (as opposed to a maximum of three minutes to reach the preset temperature below 430 °C). It is likely that during this time most of the sample has already decomposed and the decomposition products sampled do not represent the decomposition products of the sample at the selected temperature.

Five different PBT polymeric materials have been compared using the pyrolysis FTIR technique and the compounds identified which the materials produce when heated between 225 and 430 °C. All of the test materials start to release decomposition products between 295 and 330 °C, this is consistent with previous work carried out with TGA. It is apparent that the formulation containing TBBA (sample 4) has a superior thermal performance when compared to the sample containing DPBE (sample 5). The technique has thus provided a qualitative answer to the question of whether or not the formulation containing the new flame retardant is superior to the formulation containing its predecessor. Very little has been revealed about the mode of action of the flame retardants. This is not surprising since the purpose of the flame retardant is in fact to help the formulation resist burning in a flame and not to significantly stabilise the formulation at temperatures below its decomposition temperature.

5.5 REFERENCES

1. Devaux, J., Godard, P. & Mercier, J.P., Polym. Eng. & Sci., (1982), **22** (4), 229.
2. Devaux, J., Godard, P. & Mercier, J.P., Makromol. Chem., (1978), **179**, 2201.
3. Montaudo, G., Puglisi, C. & Samperi, F., Polym. Degrad. & Stab., (1993), **42**, 13.
4. Buxbaum, L.H., Agnew Chemistry (International Edition), (1968), **7**, 182.
5. Adams, R.E., J. Polym. Sci., Polym. Chem. Ed., (1980), **20**, 119.
6. Foti, S., Giuffrida, M., Maravinga, P. & Montaudo, G., J. Polym. Sci., Polym. Chem. Ed., (1984), **22**, 1201.
7. McNeill, I.C. & Bounekhel, M., Polym. Degrad. & Stab., (1991), **34**, 187.

Chapter 6

THE EVALUATION OF A HIGH TEMPERATURE AND HIGH PRESSURE INFRARED GAS CELL FOR THE MONITORING OF POLY(BUTYLENE TEREPHTHALATE) POLYCARBONATE TRANSESTERIFICATION

Chapter 6

THE EVALUATION OF A HIGH TEMPERATURE AND HIGH PRESSURE INFRARED GAS CELL FOR THE MONITORING OF POLY(BUTYLENE TEREPHTHALATE) POLYCARBONATE TRANSESTERIFICATION

6.1 INTRODUCTION

The goal of the work described in this chapter was twofold. Firstly, the aim of the work described here was to evaluate the performance of the Graseby Specac high temperature / high pressure IR cell accessory with automatic temperature controller. The second purpose of the work described was to use the IR cell to gain some insight into the undesirable reactions known to occur in PBT/PC blends when they are heated for prolonged periods above 270 ^{o}C.

The Graseby Specac IR cell is an FTIR cell designed for the analysis of samples in transmission, specular reflectance and gas decomposition modes. The cell can be heated to 800 ^{o}C and can be pressurized up to a pressure of 1000 psi. The cell windows (ZnSe) can be heated up to 200 ^{o}C to prevent the condensation of unwanted materials on the cell windows. The cell temperature is controlled by a dedicated electronics unit (which can itself be by controlled from a computer) and this enables the sample to be heated at a desired heating rate to any preset temperature. The sample can be heated to 800 ^{o}C in 40 minutes from room temperature at its maximum heating rate. The sample, set and cell window temperatures are displayed at all times. When used in "gas decomposition mode" the sample is positioned in a cup slightly below the IR beam. The gases evolved by the sample during a predetermined temperature rise can then be analysed. Switching between gas decomposition/ transmission and specular reflectance mode is done by changing the cell baseplate which allows the cell to be positioned sideways to allow the IR beam to be reflected from the sample position in the cell.

In spite of the large number of polymers potentially available only a few are used in the

manufacture of commercial products on a large scale. One of these materials is produced by General Electric Plastics by blending bisphenol A polycarbonate (PC) and poly(butylene terephthalate) (PBT), and is extensively use for moulded automobile parts. PC is tough, stable to 300 °C but has poor solvent resistance, its T_g is approximately 145 °C. PBT has relatively good solvent resistance, a low T_g (approximately 43 °C), a high T_m (> 220 °C) and a high decomposition temperature (PBT starts to decompose at approximately 350 °C). Above 30 °C PBT exhibits a decrease in mechanical properties due to its low T_g value. An alloy formed with PBT and PC produces a material with good chemical resistance as well as good heat and impact resistance.

Certain processes may occur during the manufacture of a PBT/PC blend at elevated temperature (> 270 °C) of which a potential blend manufacturer should be aware. The most important of these processes is the formation of a PBT/PC copolymer catalysed by the residual titanium[1-3] used as a catalyst in the polymerisation of the PBT component of the blend. Initially, the reaction between the PBT and PC, usually referred to in the literature as transesterification, will produce block copolymers and finally random copolymers. Not only will the chemical resistance, mechanical strength and thermal resistance of the blend be reduced by transesterification, but the final product may contain transparent portions (due to reduced crystallinity), orange-yellow portions (due to formation of titanium complexes) and CO_2 gas bubbles formed by the decomposition of alkyl carbonate transesterification products[1].

To reduce the transesterification process, stabilisers are added to the blend which complex the residual titanium catalyst and thus reduce the transesterification reaction. Phosphites have been shown to be effective in this respect in stabilising PBT/PC blends to prevent these transesterification reactions[1,2].

The transesterification between PBT and PC as well as between PET and PC has been extensively studied using infrared, mass spectrometry, proton and carbon(13) nuclear magnetic resonance and differential scanning calorimetry[1-13]. Transesterification is thought to occur via three pathways: alcoholysis, acidolysis and direct transesterification[3,6,7,8]. Figure 6.1 shows a schematic diagram of these three pathways. Devaux et al[3,13] have

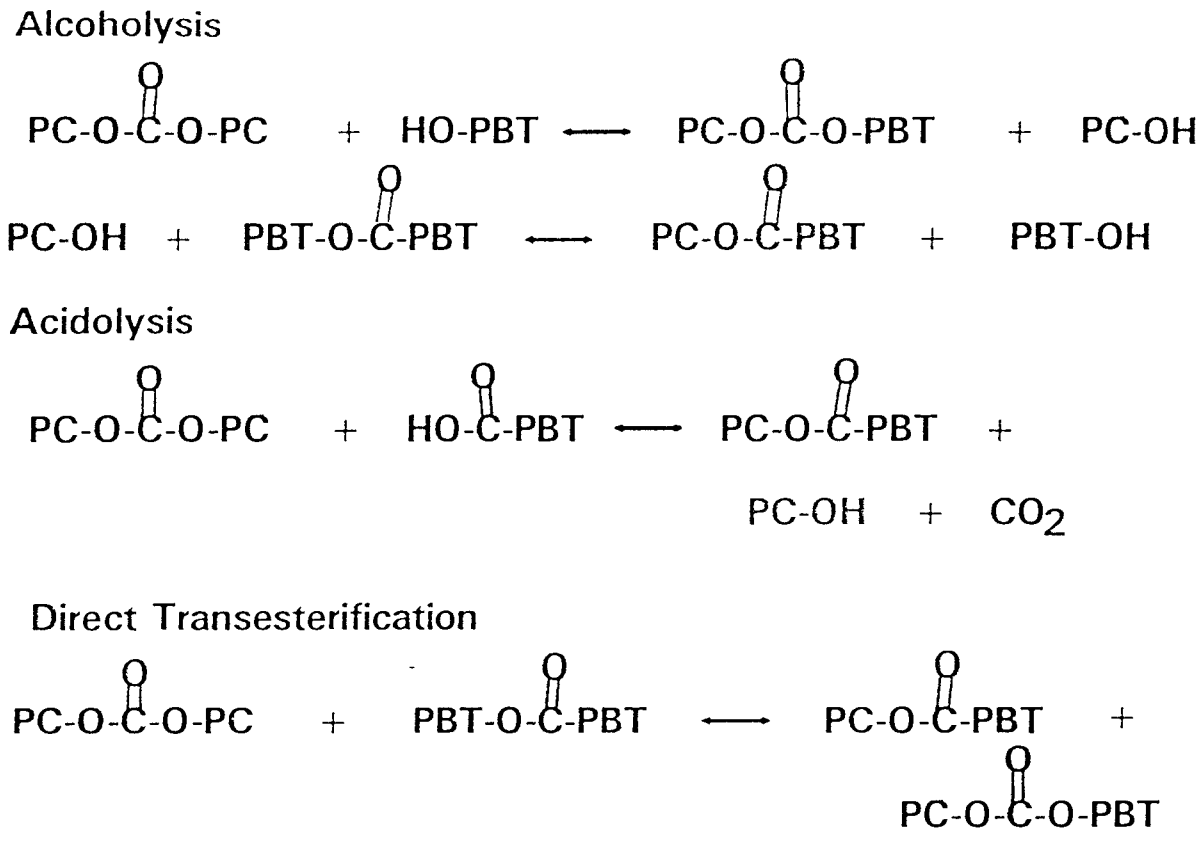

Figure 6.1: Possible transesterification reactions for PBT/PC.

concluded that the direct transesterification reaction is the predominant mechanism in transesterification in PBT/PC blends. Any information about the effect of additives in the PBT/PC blends which could promote or reduce the transesterification process would be of particular interest to their manufacturers for commercial applications. A study examining the effect of molecular weight of the components on PBT/PC mixtures concluded as expected that the miscibility of PBT/PC blends increases with decreasing molecular weight of the components[1]. Although the transesterification process has been extensively studied, little has been reported about the behaviour of PBT/PC blends heated above temperatures where transesterification starts up to temperatures where the PBT component starts to decompose (i.e. 350 °C).

In this study it was decided to examine the processes occurring in PBT/PC blends by preparing blends using different grades of PBT in each blend. Thus possible correlations between the thermal processes occurring in a PBT/PC blend and the physical properties

of the PBT used in the blend could be revealed.

The PBT/PC formulations used to evaluate the Specac accessory consisted of six samples made with 50:50 PBT:PC. In samples #1 to #6 a different grade of PBT was used. Samples #7 to 11 were analogues with PBT/PC #1, #2, #4, #5 & #6 but with 0.08% 45% H_3PO_3 in H_2O being added during blending as a stabiliser to prevent the transesterification reaction. The main object in examining the various formulations was to try and correlate trends seen in the thermal behaviour of the formulations with the differences between the PBT used in the samples i.e. end group concentration, molecular weight and catalyst content. The formulations used in this work were compounded by extrusion at a relatively low temperature (240 ^{o}C) to try and avoid any reactions prior to testing with the IR accessory.

6.2 EXPERIMENTAL

6.2.1 The experimental setup

All of the infrared spectra presented here were recorded on a Bomem FTIR spectrometer (model Michelson M 100, Bomem) fitted with the Graseby Specac high temperature / high pressure FTIR accessory and automatic temperature controller (Graseby Specac).

6.2.2 Sample specifications

Table 6.1 shows the composition of the PBT/PC samples used in this work.

PBT/PC Sample Number	Sample Composition				
		M_w(g/mol),vs polystyrene	COOH content (μeq/g)	OH content (μeq/g)	Ti (ppm)
1	50 % PBT 1 & 50 % PC	60200	75	28	110
2	50 % PBT 2 & 50 % PC	63900	31	85	105

3	50 % PBT 3 & 50 % PC	67000	42	72	67
4	50 % PBT 4 & 50 % PC	48900	27	130	69
5	50 % PBT 5 & 50 % PC	90000	± 45	± 60	105
6	50 % PBT 6 & 50 % PC	90000	60	35-40	105
7	sample 1 with 0.04 % H_3PO_3				
8	sample 2 with 0.04 % H_3PO_3				
9	sample 4 with 0.04 % H_3PO_3				
10	sample 5 with 0.04 % H_3PO_3				
11	sample 6 with 0.04 % H_3PO_3				

Table 6.1 - Composition of poly(butylene terephthalate) /polycarbonate formulations 1 to 11.

In each formulation the same grade of PC was used. The figures given in Table 6.1 are for the different PBT grades used in each sample.

6.2.3 Experimental specifications

6.2.3.1 Gas decomposition experiments

All the samples examined were dried at 130 °C for 2 hours and then stored over dried silica. When using the IR cell in its gas decomposition mode, approximately 100 mg of the sample was placed in the sample cup and fitted into the cell. The cell was then heated to 150 °C from room temperature (10 °C/min heating rate) and then left at 150 °C for 10 minutes while flushing the cell with dry nitrogen. The cell was then sealed and the lid placed on the interferometer and the sample area around the cell flushed for 30 minutes with dry nitrogen, (necessary to stabilize the interference from atmospheric water and carbon dioxide during the course of an experiment). The background was then recorded and the sample heated to 350 °C (5 °C/min heating rate). Thirty IR spectra were them collected at the rate of one spectrum (5 scans at 4 cm^{-1} 33 s scanning time) every minute starting at 200 °C. The last spectrum was thus collected when the sample

was at a temperature of approximately 348 °C. The cell windows were maintained at a temperature of 150 °C throughout each experiment.

6.2.3.2 Specular reflectance experiments

For these experiments, films were pressed from PBT/PC #1, #2, #7 & #8 at 210 - 215 °C and 235 - 240 °C at the maximum and minimum thickness possible with the Graseby Specac film press (i.e. 30 and 100 μm). The pressed films were each cut into circles of 1 cm diameter then placed in the IR cell. The cell was heated at 10 °C/min to 150 °C then flushed to 30 minute with dry N_2. The cell was sealed then heated to 350 °C at a heating rate of 5 °C/min. One spectrum (5 scans) was collected every minute between 200 and 350 °C. Throughout the experiment the cell windows were kept at 150 °C. The reference spectrum was collected with no sample in the IR cell and the cell heated at a temperature of 150 degrees.

6.2.3.3 Polymer films

Two different experiments were carried out with the IR cell in its transmission mode. Firstly, films of the PBT/PC samples were pressed (30 - 40 μm thickness, one minute at 5000 KPa and 240 °C and quenched into water) and placed in the IR cell with a KBr disk as backing. The PBT/PC blends melt at approximately 240 °C and without a KBr disk as backing it is not possible to record spectra of the films above this temperature. The cell was heated from room temperature to 200 °C at 20 °C/min then at 5 °C/min to 240 °C while the cell was flushed with dry nitrogen through one of the cell inlet ports. It was assumed that this heating treatment would drive off any excess water in the film. The cell was then sealed and the film heated to 350 °C at a rate of 2.5 °C/min. Twenty spectra (10 scans each at 4 cm^{-1} 66 s acquisition time) were collected at intervals of 2 minutes between 250 and 350 °C.

6.2.3.4 Polymer diluted in KBr

Secondly, approximately 10 mg of each blend (dried for 2 hours at 130 °C and stored over dried silica) was pressed in a KBr disk (5 minutes at 5000 KPa). An identical series of experiments was carried out with these KBr disks as were completed with the pure films described above.

6.3 RESULTS AND DISCUSSION

6.3.1 Gas decomposition experiments

6.3.1.1 Problems experienced

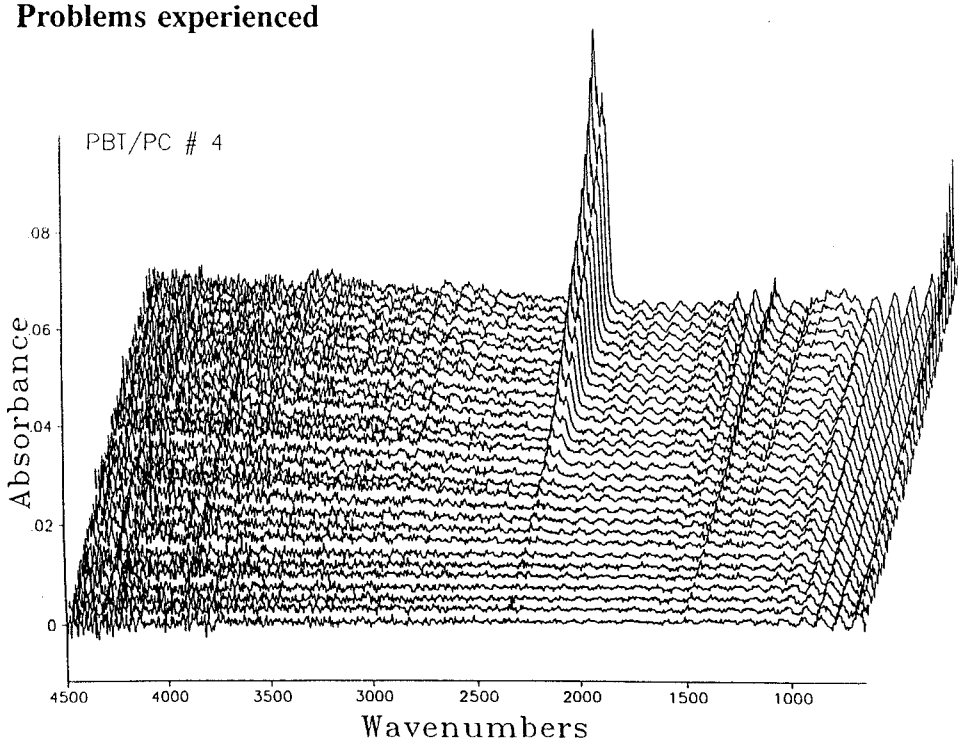

Figure 6.2: Multiple spectra of gas transmission experiment showing interference patterns, 200 to 350 °C in 30 minutes.

In many of the initial spectra recorded using the cell, a very severe interference pattern was present. Figure 6.2 shows a multiple spectrum collected using PBT/PC #4. It is evident that the interference pattern completely obscures each spectrum below 2000 cm^{-1} and thus is a major problem, particularly at higher temperature. A brief experiment with an alternative FTIR instrument (Digilab) also showed a similar interference pattern.

Possible causes such as: (i) electrical interference from the cell temperature controller, (ii) effect of apodisation function due to unusually strong absorption at low wavenumbers, (iii) some type of etalon effect between cell windows, were considered.

Finally it was concluded that it must be a simple interference pattern[16], using the appropriate formula a film thickness of 0.06 mm could be responsible for this type of pattern. It is likely that the interference pattern is caused by (iii) above. Calculations using the thermal coefficient of iron as being that of the cell support this view. It was found that by angling one of the cell windows with respect to the other the pattern was not produced. The suppliers produce an angled window for the cell for use in the specular reflectance mode and this window was used for the remainder of the cell trial.

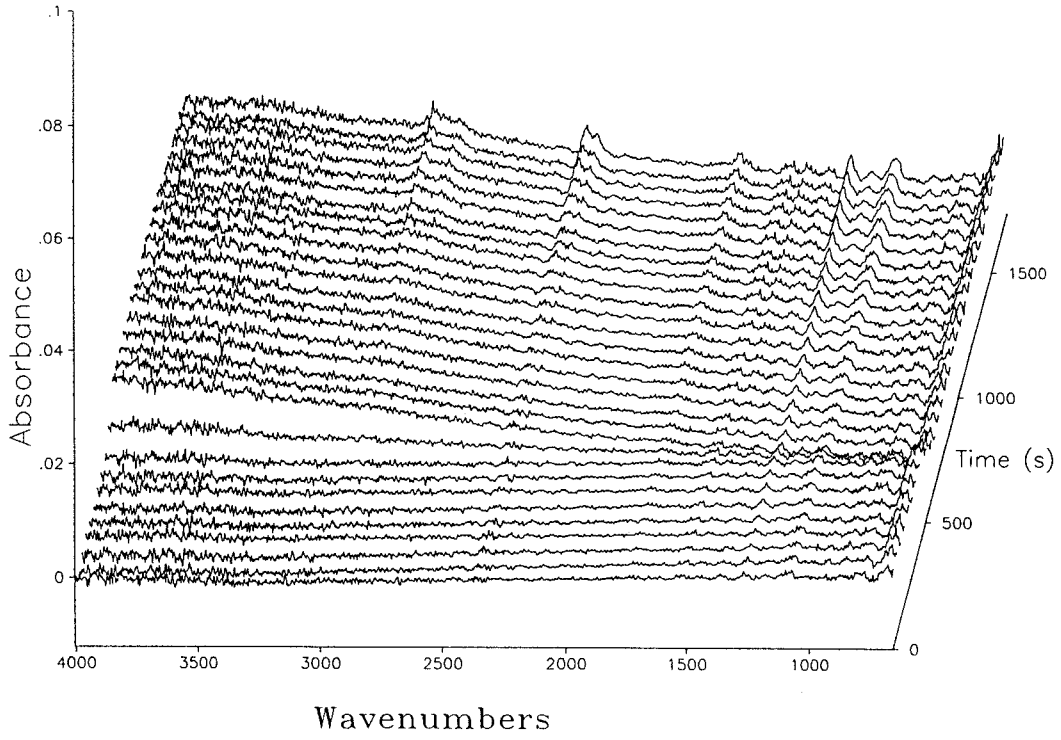

Figure 6.3: Multiple spectra of gas transmission experiment showing baseline shift, 200 to 350 °C in 30 minutes.

Figure 6.3 shows the results of a typical gas decomposition experiment. Apart from the presence in the IR spectra of the components given off by the sample in the IR cell, the most noticeable feature of the spectra is the shift in baseline at a temperature corresponding to 240 °C. This is the approximate temperature at which the polymer blend melts. The most likely cause of this phenomenon is that the sample in the sample

cup reflects some of the radiation that is seen by the FTIR detector. The wavelength dependence of this reflection depends on the form of the sample thus when the sample melts a shift in the baseline occurs. Positioning an additional iris in the IR beam reduces this baseline shift and any baseline shift that is not eliminated can be removed using the appropriate Lab Calc software.

6.3.1.2 Experimental results

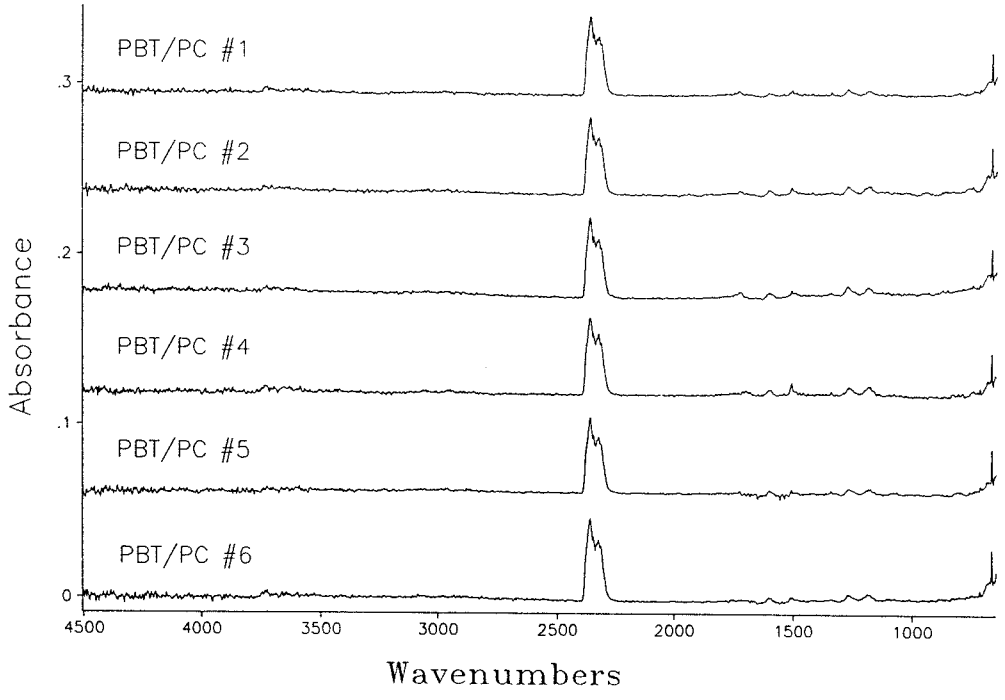

Figure 6.4: Final spectra in multiple series, PBT/PC #1 to 6, i.e. IR spectra of all gaseous compounds given off by samples when heated from 200 to 350 °C in 30 minutes.

Figures 6.4 and 6.5 show the final spectra collected in each of the gas decomposition experiments carried out with the unstabilised formulations (samples 1 to 6) and the unstabilised formulations (samples 7 to 11), respectively.

Table 6.2 shows the band positions of some of the compounds likely to be seen in Figures 6.4 and 6.5. Figure 6.4 shows the gas decomposition products of the unstabilised materials heated in N_2 and Figure 6.5 shows the decomposition products of the stabilised materials heated in N_2. The most remarkable difference between the stabilised and unstabilised formulations is that the unstabilised materials start to produce CO_2 at

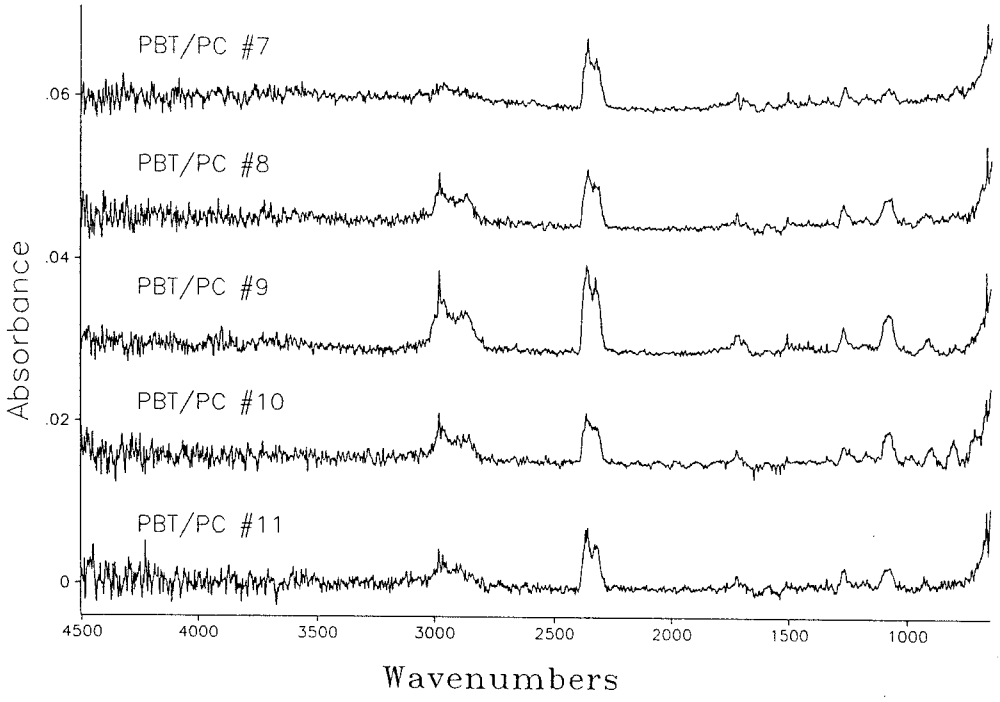

Figure 6.5: Final spectra in multiple series, PBT/PC #7 to 11, as for Figure 6.4.

between 270 and 290 °C (Figure 6.6), while a similar plot to Figure 6.6 for the stabilised materials shows that they start to produce CO_2 at around 300 °C, producing 20 percent of the CO_2 generated by the unstabilised materials during the course of an experiment.

Compound	position/cm-1	Compound	position/cm-1
Butan-1,4-diol	2982 1072	Tetrahydro-furan	2993 1079 916
Bisphenol A	3348 1509 1237 1220 826	PC	1765 1494 1210 1177 1146
Phenol	3648 1601 1182 747	PBT	1715 1271 1104

Table 6.2 - Band positions for expected compounds in decomposition products of PC and PBT.

The compounds produced by the unstabilised and stabilised formulations (besides CO_2) also differ markedly. The unstabilised formulations (Figure 6.4) produce mainly

bisphenol A and phenol and possibly also PC and PBT oligomers. The stabilised formulations produce mainly THF (or butandiol) and PBT oligomers. The stabilised formulations thus appear to produce PBT breakdown products while the unstabilised formulations produce decomposition products of PC[14]. The stabiliser is thought to act (i.e. reduce the amount of transesterification taking place in a blend) by complexing the titanium catalyst residue from the PBT component of the PC/PBT blend, thus the fact that different compounds are released by the two groups of formulations (stabilised and unstabilised) must be related to the degree to which transesterification is taking place in the two groups of blends (i.e. stabilised and unstabilised). The large difference in the CO_2 release between the two groups of compounds must also be related to the transesterification process occurring in the PBT/PC blends.

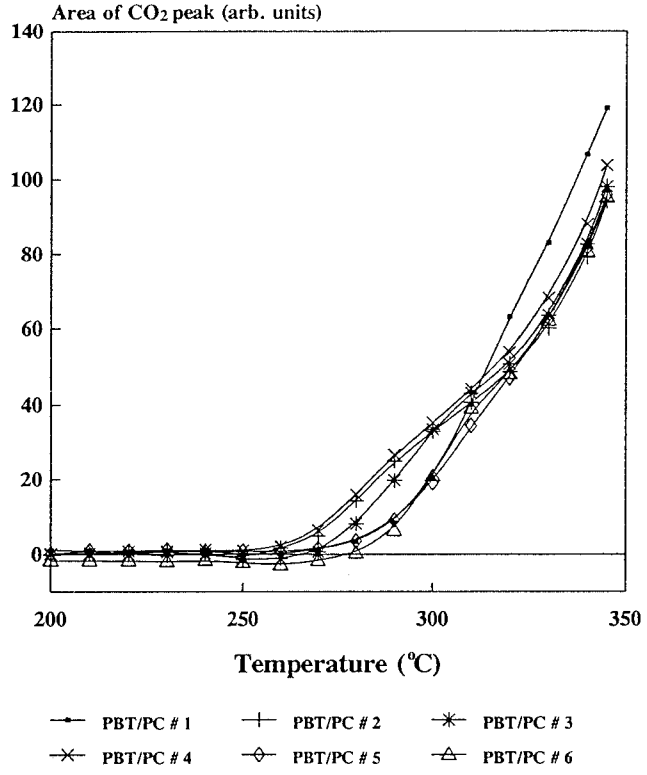

Figure 6.6: Extract of CO_2 peak area versus temperature for PBT/PC #1 to 6, 200 to 350 °C in 30 minutes.

Figure 6.6 shows plots of the area of the CO_2 peak versus time for each gas decomposition experiment for the unstabilised formulations (i.e. the evolution of CO_2 versus temperature for each material). From Figure 6.6 it is apparent that the formulations #1 to #6 release CO_2 in the order #4,#2 > #3 > #5,#1 > #6 over the temperature range 270 to 290 °C. An examination of the PBT parameters (Table 6.1)

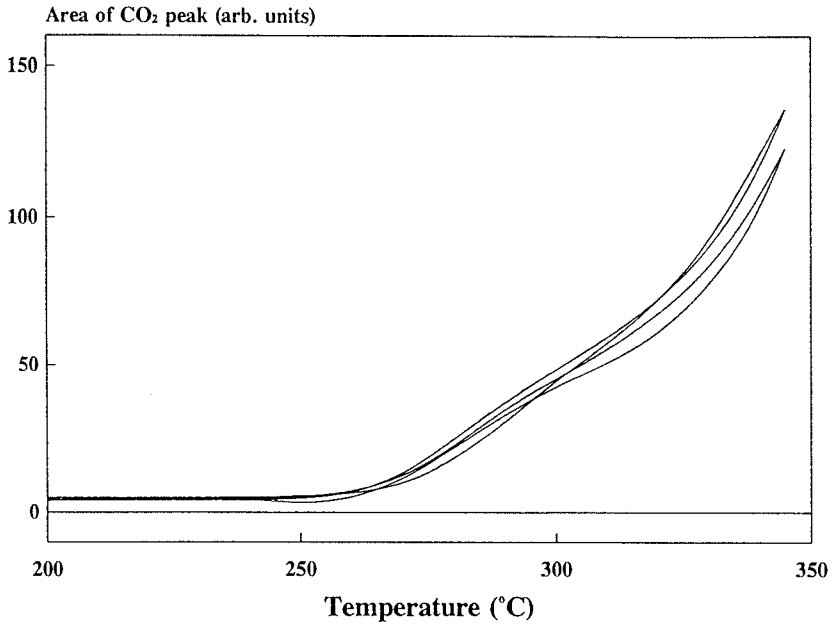

Figure 6.7: Reproducibility check for PBT/PC #4, CO_2 extraction curves.

reveals that this order correlates best with the increasing concentration of the OH end-groups: #4 > #2 > #3 > #5 > #6 > #1. In this ranking order only #1 : the sample containing PBT #1 - lowest [OH] = 28 μeq/g, mismatches the CO_2 release order in Figure 6.6. One has to consider that #5 and #6 have a significantly higher molecular weight, 90000 g/mol versus 45000 - 65000 g/mol for all the other PBT's. Nevertheless, the pattern of CO_2 release by the unstabilised formulations PBT/PC # 1 to #6 does not correlate with the increasing molecular weight of the PBT polymers in the order #3 < #1,#2 < #4 < #5,#6. This is at variance with earlier work[15] which showed that CO_2 release showed a good correlation to molecular weight in experiments carried out with pure PBT.

The CO_2 release shown by the stabilised formulations (i.e. a similar plot to Figure 6.6 obtained using the stabilised formulations) revealed that, within the experimental uncertainty, all the stabilised formulations released similar amounts of CO_2.

Figure 6.8 shows a comparison of the CO_2 release of PBT/PC samples 1 and 2 and the pure PBT components of each blend. It is apparent from this figure that the CO_2

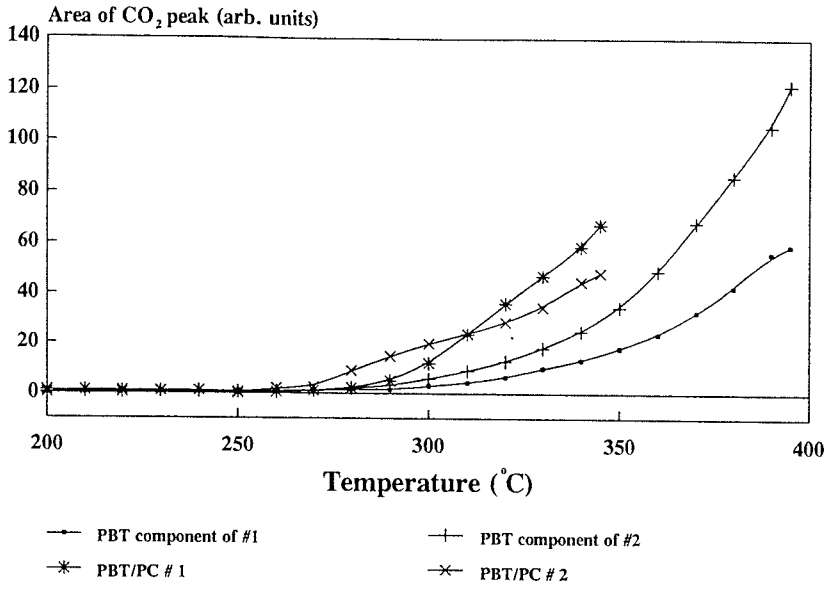

Figure 6.8: Comparison of PBT with PBT/PC, CO_2 extraction curves.

released by the unstabilised formulations is not due to PBT degradation but rather results from some reaction that occurs between PBT and PC in each blend or due to PC decomposition. Evidence that the CO_2 released by the PBT/PC blends on heating originates from some reaction product of PBT and PC is that the stabilised materials show virtually no CO_2 release. The stabiliser is thought to act by complexing the titanium in the PBT not by preventing the thermal decomposition of PC.

6.3.2 Specular reflectance experiments

The optical efficiency of this accessory even when empty was quite low, typically less than 10 percent of the radiation that the detector sees when there is no cell or sample in the IR beam pathway. The metal plate used for a sample backing in the specular reflectance mode blackened on heating and once black it was not possible to restore the shine. This probably also contributed to poor cell performance.

As mentioned in Section 6.2.3.2, attempts were made to record specular reflectance spectra using PBT/PC #1, #2, #7 and #8. Various types and thicknesses of films were

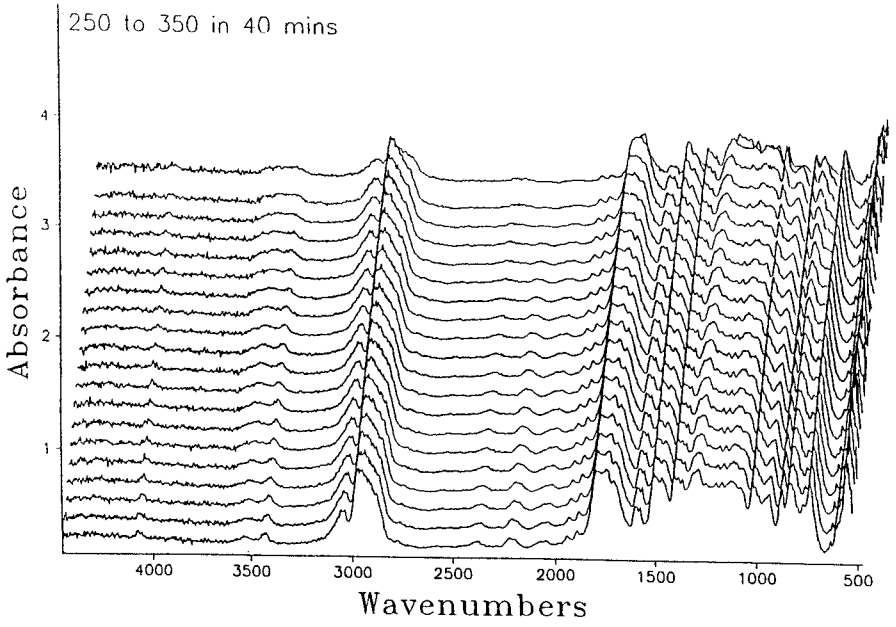

Figure 6.9: Multiple specular reflectance spectra of PBT/PC #1 film, 250 to 350 °C in 40 minutes.

used in this part of the trial. Pressing films between 210 and 215 °C resulted in white films, the thicker films gave barely no spectrum and the thinnest films (30 - 40 μm) gave poor ones. No success either was achieved with the thick film pressed between 235 and 240 °C. Figure 6.9 shows an example of one of the best series of spectra collected with the cell in specular reflectance mode. No resolution of the C=O region above 1700 cm^{-1} is seen, thus the transesterification reactions cannot be followed.

It would appear that the IR radiation seen by the detector passes through the polymer sample, is reflected off the metal backing then passes back through the sample so this setup of the cell has no advantage over the normal cell transmission mode. Thus the nature of the samples are not suitable for specular reflectance measurements. It is likely that if the samples were less transparent and less strong IR absorbers that some useful information could be gained from specular reflectance measurements. No further measurements were performed with the cell in specular reflectance mode.

6.3.3 Normal transmission experiments

6.3.3.1 Polymer films

Experiments conducted with the accessory in its transmission mode showed good potential in following the changes in the carbonyl absorption of the PBT and PC, however there were several problems. The absorbance of the PBT/PC films was too high and problems were experienced in producing films thin enough thus the error in the absorbance values in the spectra of the films was large making relative comparison between the various materials difficult. The use of polymer samples pressed into KBr disks gave good qualitative information regarding the changes in carbonyl absorption as a blend was heated but again the errors in the determination of absolute absorbances were too large to allow quantitative comparison to be made between the various blends.

Table 6.3 shows the characteristic IR absorption frequencies of the carbonyl peaks in PBT, PC and the transesterification products of PBT and PC.

Description	Structure	IR absorption frequency / cm^{-1}
Aliphatic ester	PBT-Ph-(C=O)-O-CH_2-PBT	1720
Aromatic ester	PBT-Ph-(C=O)-O-Ph-PC	1740 1070
Aromatic carbonate	PC-Ph-O-(C=O)-O-Ph-PC	1774
Aliphatic-aromatic carbonate	PC-Ph-O-(C=O)-O-CH_2-PBT	1770

Table 6.3 - Characteristic IR absorption frequencies of C=O peaks in PBT and PC transesterification[3.11].

Figure 6.10 shows an expansion of the carbonyl region for a typical series of spectra collected as a PBT/PC film on a KBr disk backing was heated from 250 to 350 °C.

Qualitatively the disappearance of the carbonate C=O absorption from the PC is the most notable feature of Figure 6.10. Figures 6.11 and 6.12 show the first and final spectra

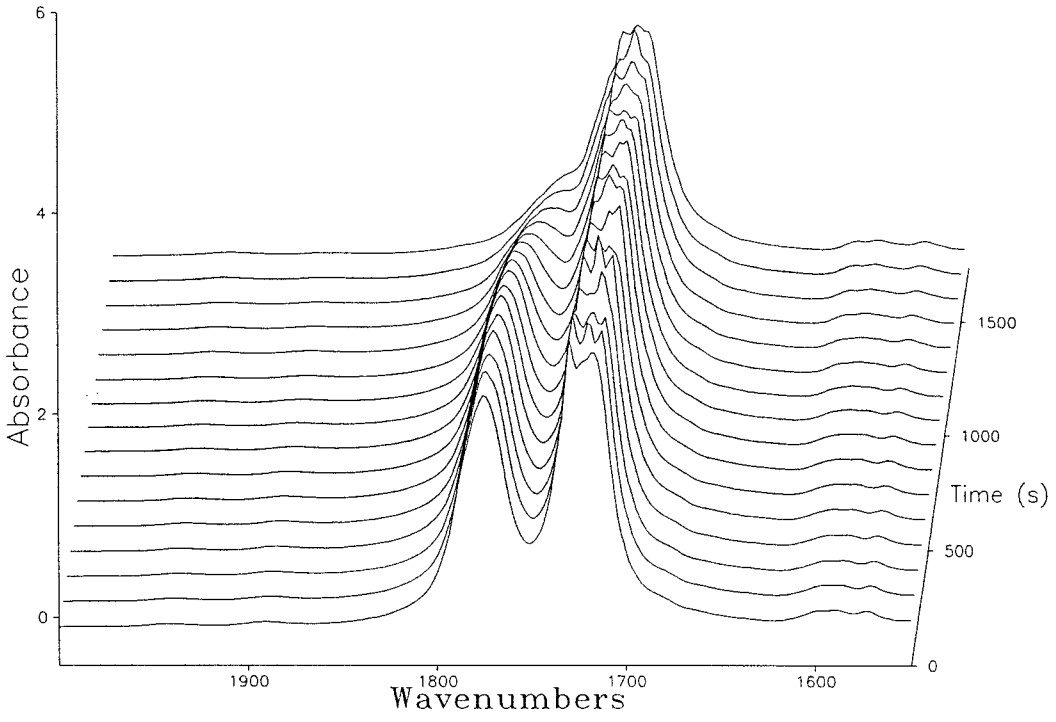

Figure 6.10: Carbonyl region (1550 cm^{-1} to 2000 cm^{-1}) for PBT/PC #5, film on KBr disk, 250 to 350 °C in 30 minutes.

collected for each unstabilised formulation (i.e. samples 1 to 6). Each spectrum in Figure 6.11 shows the strong C=O absorptions due to the PBT (1720 cm^{-1}) and the PC (1774 cm^{-1}). In the final spectra shown in Figure 6.12 the peak at 1774 cm^{-1} due to the PC has almost entirely disappeared and the 1720 cm^{-1} absorption is still relatively strong. A band also appears at 1070 cm^{-1} corresponding to the formation of the aromatic-ester transesterification product. The fact that the carbonate C=O peak of the PC disappears indicates that the view expressed earlier that the CO_2 production monitored in Figure 6.6 originates from the PC component of the blend. A simple calculation shows that at STP (standard temperature and pressure) 50 mg of PC would produce approximately 4.5 cm^3 of CO_2.

Figures 6.13 and 6.14 show analogous plots to Figures 6.11 and 6.12 for the formulations 7 to 11. It is noticeable from these plots that the stabilised formulations do not show the same reduction in the carbonate C=O peak (1774 cm^{-1}) seen in Figures 6.11 and 6.12. This agrees with the earlier observation that the stabilised PBT/PC blends produce far less CO_2 than the unstabilised blends, and is further evidence that the origin of the CO_2 produced by the unstabilised blends in the gas decomposition experiments was the PC

component of the PBT/PC blend.

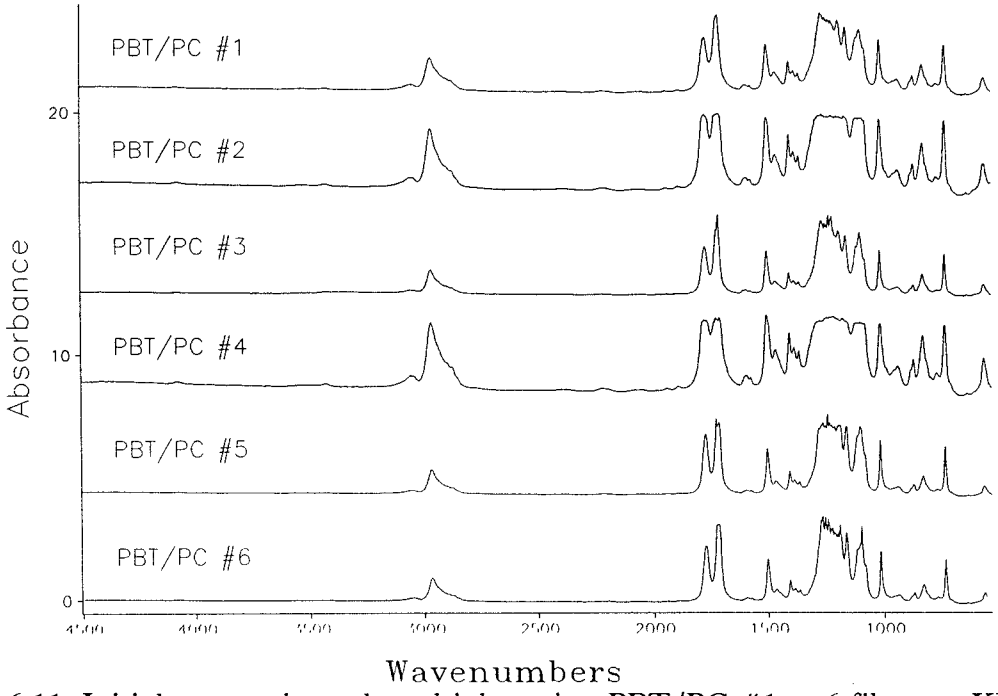

Figure 6.11: Initial spectra in each multiple series, PBT/PC #1 to 6 films on KBr disks, 250 to 350 °C in 40 minutes.

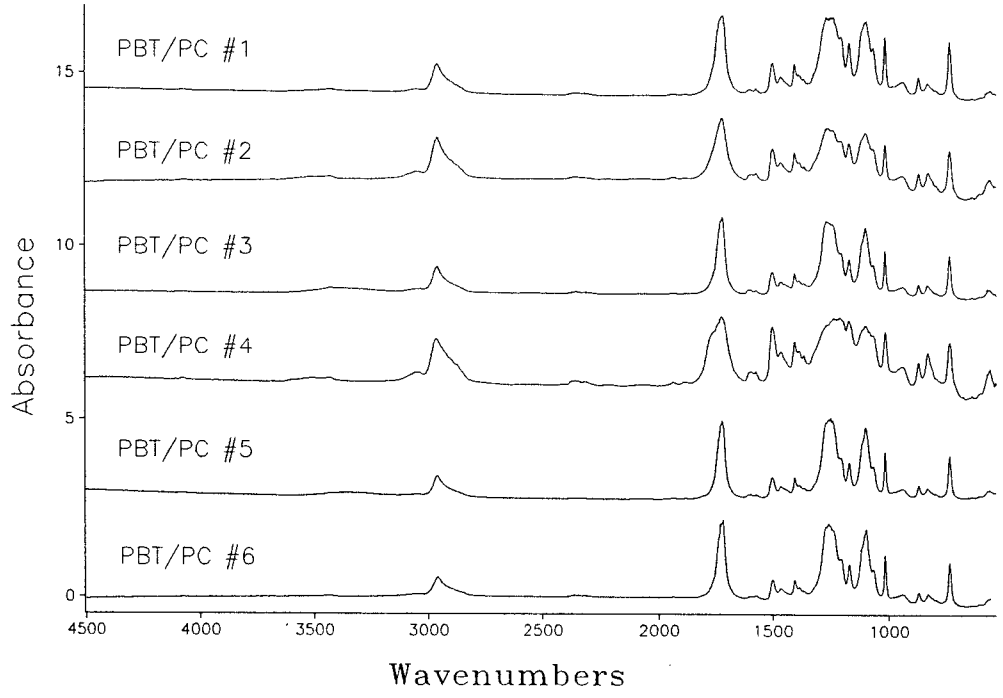

Figure 6.12: Final spectra in each multiple series, PBT/PC #1 to 6 films on KBr disks, 250 to 350 °C in 40 minutes.

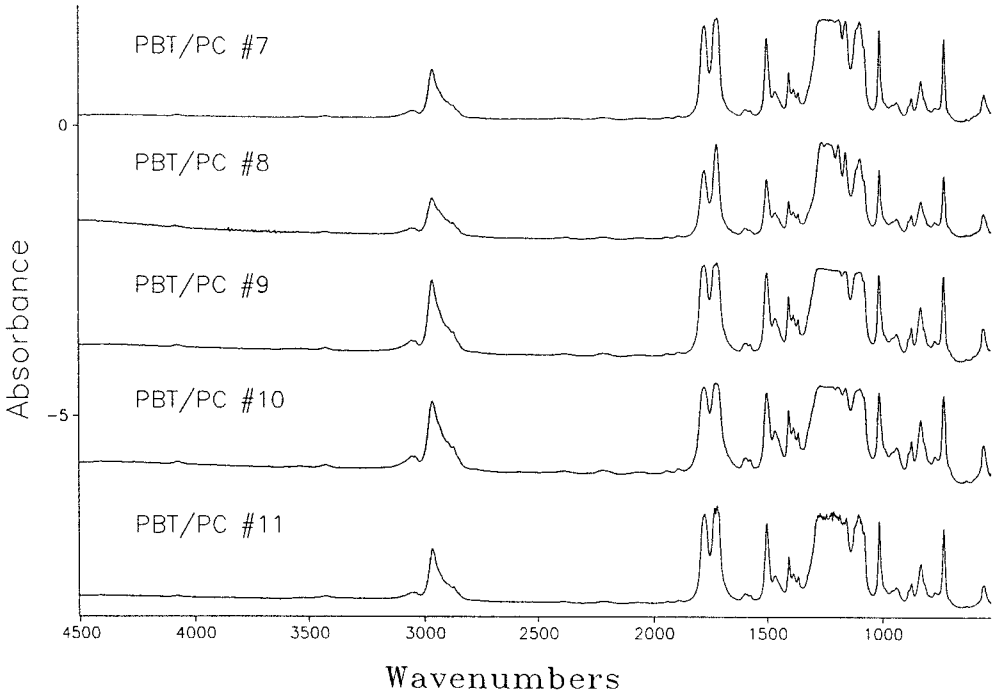

Figure 6.13: Initial spectra in each multiple series, PBT/PC #7 to 11 films on KBr disks, 250 to 350 °C in 40 minutes.

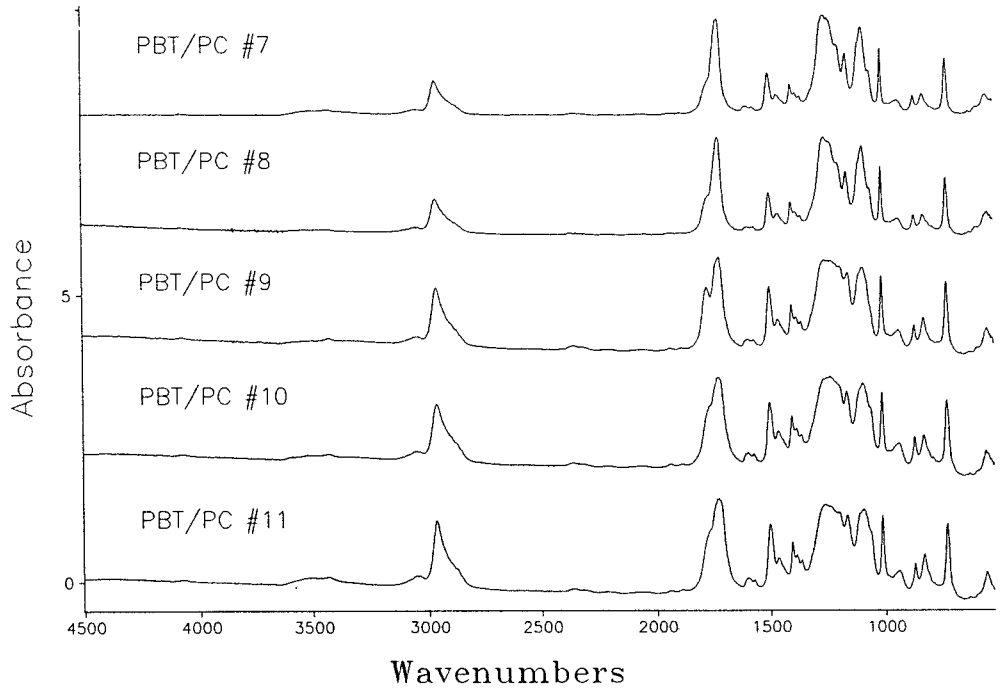

Figure 6.14: Final spectra in each multiple series, PBT/PC #7 to 11 films on KBr disks, 250 to 350 °C in 40 minutes.

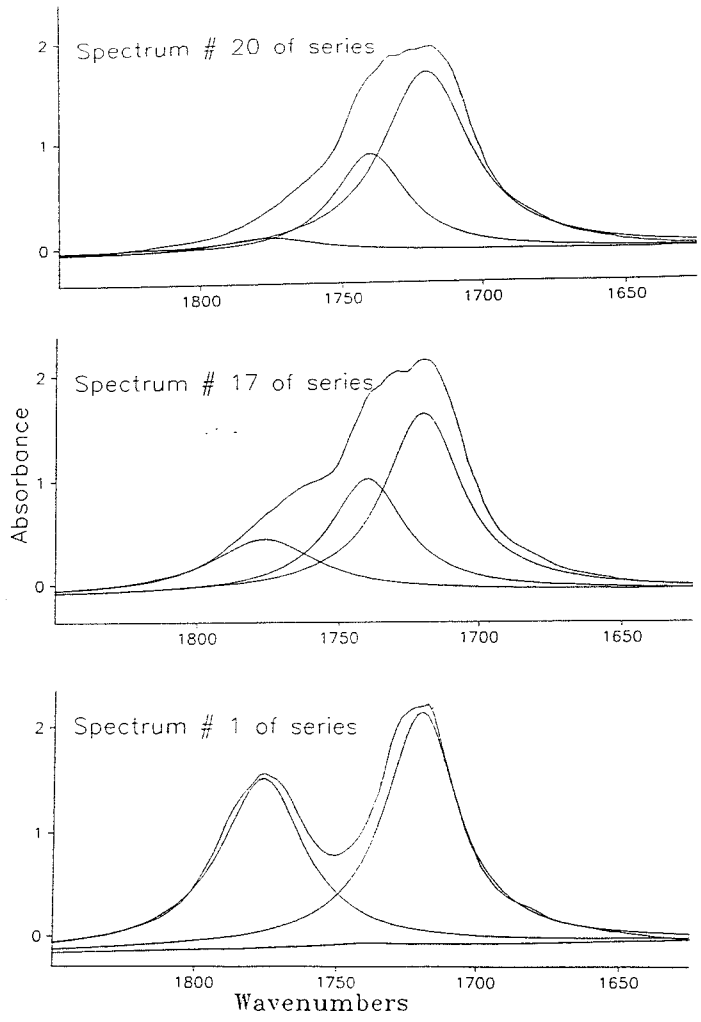

Figure 6.15: Results of curvefitting of peaks in C=O region of spectra #1, 17 & 20 for PBT/PC #1, 250 to 350 °C in 40 minutes.

Attempts to deconvolute the C=O region (1650 cm^{-1} to 1850 cm^{-1}) of the IR spectra collected of the PBT/PC films as they were heated from 250 to 350 °C revealed only qualitative information about the possible individual peaks in the C=O stretching region. Invariably the C=O region in the initial spectra (in Figures 6.11 and 6.13) could be described by two Gaussian peaks centred at 1774 cm^{-1} and 1720 cm^{-1}, the final spectra (Figures 6.12 and 6.14) could be described by three Lorentzian peaks centred at 1774 cm^{-1}, 1740 cm^{-1} and 1720 cm^{-1}. Figure 6.15 shows the results of a deconvolution using the results obtained for sample 1. The figure indicates that initially at 250 °C no transesterification product corresponding to the aromatic ester transesterification product (i.e. C=O peak at 1740 cm^{-1} and 1070 cm^{-1} peak) has occurred in this blend, but that after heating to 350 °C, the aromatic ester transesterification product contributes significantly to the C=O region. The peak due to the carbonate C=O in PC (1774 cm^{-1})

has almost completely disappeared. Earlier work with transesterification of PC/PBT found evidence for two transesterification products (1740 and 1770 cm^{-1}), these results indicate that either only one transesterification product is formed or, more likely, the aryl aryl transesterification product (1770 cm^{-1}) does not survive the heating process to 350 °C. The latter assumption is more likely since if the carbonate moiety of the PC decomposes before 350 °C then it is unlikely that the carbonate moiety of the aryl aryl transesterification product would be stable under similar conditions.

6.3.3.2 Polymer diluted in KBr

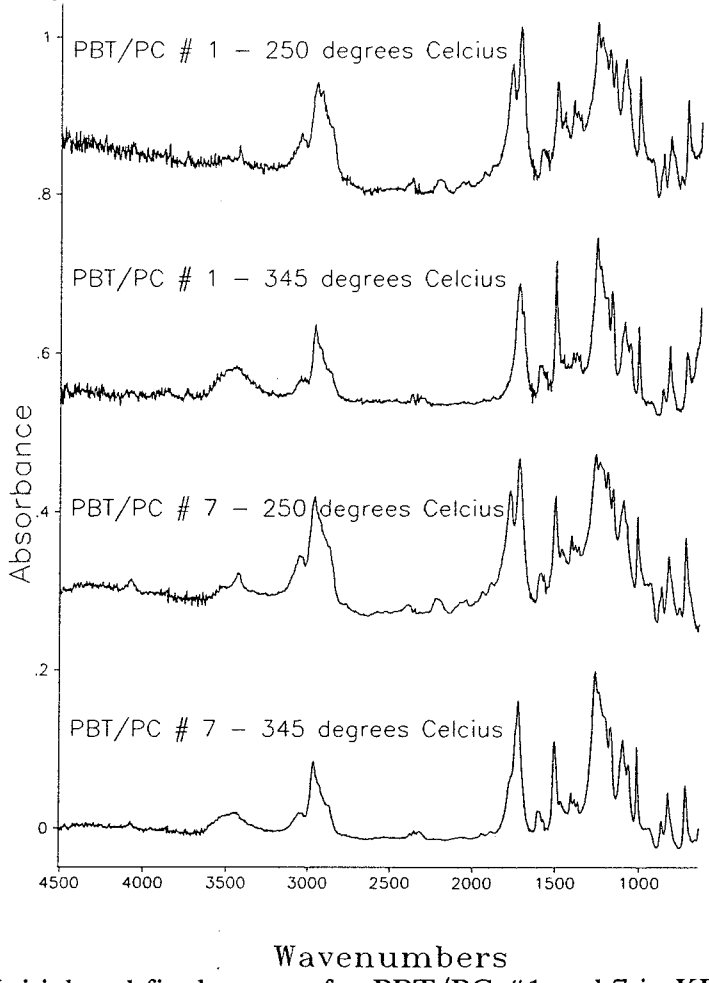

Figure 6.16: Initial and final spectra for PBT/PC #1 and 7 in KBr disks, 250 to 350 °C in 40 minutes.

Similar heating experiments were conducted with the polymer blends pressed in KBr disks. Figure 6.16 shows the initial and final spectra collected in the experiments conducted with PBT/PC formulations 1 and 7 (i.e. unstabilised and stabilised blends using a similar PBT component). The reduction in the carbonate C=O peak at 1774 cm^{-1}

for the unstabilised formulation is noticeable, the carbonate C=O peak at 1774 cm^{-1} in the stabilised formulation does not decrease to the same extent, a shoulder remains on the side of the 1720 cm^{-1} PBT carbonyl band.

6.4 CONCLUSIONS

6.4.1 Evaluation of gas cell

The cell is well designed and functions well in the gas transmission and normal transmission modes. Its throughput is about fifty percent compared with the energy the detector sees when the sample area of the Bomem is empty. This is sufficient for normal transmission studies of polymer films or KBr disks but when using the cell in the gas transmission mode this low throughput meant longer scanning times to obtain acceptable signal to noise ratios. A loss of half of the intensity of a band represents a fourfold increase in the collection time to obtain the same quality spectrum as before. The relatively high loss of energy through the cell was probably a result of the relatively small diameter of the windows (about 10 mm) and their thickness of the windows (13 mm). These windows have been designed for extremely high pressure work but for work of this nature at moderate pressures, a wider and thinner set of windows would have been adequate and have a better throughput.

The use of the angled window solved the problem of interference but the throughput of the cell was reduced by 15% and this represents a further, possibly unnecessary, reduction in the performance of the cell.

The system used to examine the performance of the cell was possibly not ideally suited to highlight its usefulness in gas transmission and normal transmission modes. The PBT/PC formulations released relatively small concentrations of gases in the temperature ranges used in this investigation. The polymer samples were not ideally suited for examination in normal transmission either. Possibly with another system of polymers the cell would have yielded better results concerning the thermal performance of the materials studied.

No useful results were obtained from the cell in its "specular" reflectance mode. Possible with a sample more suitable for specular reflectance measurements useful results could be obtained.

The most outstanding feature of the cell was the temperature programmable heating unit. It was extremely simple to use and maintained a reproducible heating rate over a wide temperature range. No checks were made to determine how accurate the dial readings on the unit were but throughout the experiment there was no indication that the actual sample temperature differed substantially from the dial readings of the unit.

6.4.2 Transesterification process

Quantitatively the differences between the performance of the stabilised and unstabilised formulations was extremely clear. In all aspects, the stabilised formulations (samples 7 to 11) outperformed the unstabilised blends (samples 1 to 6) in thermal stability.

Transmission experiments showed that the most noticeable change in the IR transmission spectra of the films and KBr disks made with the blends was the fact that the 1774 cm^{-1} carbonate C=O of the PC disappeared almost completely when any of the unstabilised blends were heated to 350 °C. Deconvolution routines showed that after heating an unstabilised PBT/PC film on a KBr disk to 350 °C, no transesterification product corresponding to the aliphatic aromatic carbonate (i.e. the transesterification product with a carbonyl peak at 1770 cm^{-1}) could be found. This appeared to contradict the findings of Devaux et. al.[3] that the direct transesterification product was the most likely mechanism for the transesterification reaction between PBT and PC. It is likely that the carbonate moiety of the PC and of the aliphatic aromatic ester is not thermally stable at these temperatures[1,14] and thus when the blend is heated to 350 °C no band at 1770 cm^{-1} can be seen.

The only correlation that has been established by this work is the rate at which a blend releases CO_2 and the OH end-group concentration of the PBT in the blend. A high OH end-group content concentration of PBT showed earlier release in CO_2 in the linear

temperature program, starting at 260 °C for [OH] = 130 μeq/g and 280 °C for [OH] ≈ 35 μeq/g. It seems that CO_2 release is linked to a reaction between PC and the OH end-groups of the PBT. Probably alcoholysis will be the most reactive initial reaction in the PBT/PC blend. However, the fact that no aryl-alkyl carbonates, resonance species at 1770 cm^{-1}, could be detected in the film indicates a fast secondary degradation reaction of these species into more stable PC-OH and enhanced release of CO_2. No correlations were observed between thermal behaviour of the blends and the other parameters of the PBT i.e. Ti catalyst content, molecular weight and COOH end-group concentration.

Gas transmission experiments revealed that besides releasing much less CO_2 than the unstabilised materials, the stabilised blends also released completely different volatiles. The unstabilised materials release primarily breakdown products of PC (i.e. phenol, bisphenol A and PC oligomers)[14] while the stabilised materials release primarily THF, a breakdown product of PBT and methane from PC. The phosphite stabiliser is thought to prevent transesterification by complexing the titanium catalyst in the PBT, the fact that the PC appears to be more thermally stable in the presence of the catalyst indicates that the breakdown of PC is linked to the presence of the titanium catalyst, either because the breakdown of PC occurs as a result of transesterification or less likely because the titanium directly influences the decomposition of PC.

6.5 REFERENCES

1. Hamilton, D.G. & Galucci, R.R., J. App. Polym. Sci., (1993), **48**, 2249.
2. Miley, D.M. & Runt, J., Polym., (1992), **33** (21), 4643.
3. Devaux, J., Godard, P. & Mercier, J.P., Polym. Eng. & Sci., (1982), **22** (4), 229.
4. V.d. Velden, G., Kolfschoten-Smitsmans, G. & Veermans, A., Polym. Comm., (1987), **28**, 169.
5. Remiro, P.M. & Nazabal, J., J. App. Polym. Sci., (1991), **42**, 1639.
6. Porter, R.S., & Wang, L.H., Polym., (1992), **33** (10), 2019.
7. Kotliar, A.M., J. Polym. Sci.: Macromol. Rev., (1981), **16**, 367.
8. Espinosa, E., Fernandez-Berridi, M.J., Maiza, I. & Valero, M., Polym., (1993), **34** (2), 382.

9. Kimura, M. & Porter, R.S., J. of Polym. Sci.: Polym. Phys. Ed., (1983), **21**, 367.
10. Devaux, J., Godard, P., Mercier, J.P., Touillaux, R. & Dereppe, J.M., J. Polym. Sci.: Polym. Phys. Ed., (1982), **20**, 1875.
11. Devaux, J., Godard, P. & Mercier, J.P., J. Polym. Sci.: Polym. Phys. Ed., (1982), **20**, 1881.
12. Devaux, J., Godard, P. & Mercier, J.P., J. Polym. Sci.: Polym. Phys. Ed., (1982), **20**, 1895.
13. Devaux, J., Godard, P. & Mercier, J.P., J. Polym. Sci.: Polym. Phys. Ed., (1982), **20**, 1901.
14. Montaudo, G. & Puglisi, C., Polym. Degrad. & Stab., (1992), **37**, 91.
15. Internal Report, General Electric Plastics, (1993).
16. An Infrared Spectroscopy Atlas for the Coatings Industry, Federation of Societies for Coatings Technology, Philadelphia, Penn., (1980).

Chapter 7

POLY(BUTYLENE TEREPHTHALATE) POLYCARBONATE TRANSESTERIFICATION: MONITORING ITS PROGRESS WITH FOURIER TRANSFORM RAMAN SPECTROSCOPY

Chapter 7

POLY(BUTYLENE TEREPHTHALATE) POLYCARBONATE TRANSESTERIFICATION: MONITORING ITS PROGRESS WITH FOURIER TRANSFORM RAMAN SPECTROSCOPY

7.1 INTRODUCTION

Poly(butylene terephthalate) / polycarbonate blends are known to undergo transesterification reactions when they are heated (T > 270 °C) for long periods[1,2,3]. In the previous chapter (Chapter 6) describing the evaluation of the Graseby Specac cell using a system of stabilised and unstabilised PBT/PC blends, this transesterification reaction was studied. The known transesterification pathways yield two main transesterification products: the aromatic ester (C=O at 1740 cm^{-1} in IR) and the aliphatic-aromatic carbonate (C=O at 1770 cm^{-1} in IR). The aromatic ester also gives rise to a new band in the IR at 1070 cm^{-1}. These transesterification products have been previously identified with IR but previous work at GE Plastics[4] was unable to show the presence of the aliphatic aromatic carbonate in heated PBT/PC blends, evidence for the presence of the aromatic ester was however found.

The goal of the work described in this chapter was to evaluate the potential of FT Raman spectroscopy as a technique to monitor the amount of transesterification occurring in a PBT/PC blend. There are two approaches that may be adopted. Firstly, a commercial FT Raman instrument using 1064 nm Neodymium:YAG laser excitation may be used to record spectra of heat treated PBT/PC samples. Secondly, the developmental instrument using 780 nm Ti:Sapphire laser excitation described in Chapter 3 has shown potential in recording spectra of heated polymer samples[5], this instrument may offer the possibility of following the transesterification reaction while the reaction is occurring.

Neodymium:YAG 1064 nm excitation offers the advantage that polymer (and other

samples) are less likely to show fluorescence because of the relatively long laser wavelength used. However, the practical limit for obtaining spectra from heated samples is 200 °C because the heated background given off by the sample saturates the detector used in the instrument (InGaAs). The Ti:Sapphire laser providing 780 nm excitation effectively moves the Raman spectrum further away from the heated background and it has been demonstrated that Raman spectra of polymers at temperatures up to 370 °C can be obtained[5]. However, the use of shorter wavelength radiation raises the likelihood of more persistent sample fluorescence.

Two different PBT/PC samples were used in this investigation. Both blends contained equal amounts of poly(butylene terephthalate). The first of the two was an unstabilised blend, the second was a similar one to which 0.08 % of 45 % phosphorous acid in water was added while blending the PBT and PC in an extruder. Phosphorous acid is known to retard the transesterification reaction[6].

7.2 EXPERIMENTAL

7.2.1 Experimental setup

All the Raman spectra presented in this chapter were recorded using a Perkin Elmer 1720 FT Raman Spectrometer with Spectron Nd^{3+}:YAG laser operating at 1064 nm. The infrared spectra presented here were recorded using a Perkin Elmer 1720 FTIR Spectrometer with Graseby Specac Specular Reflectance IR accessory.

7.2.2 Sample specifications

Two of the blends specially prepared for the investigation described in Chapter 6 were selected as test materials for this work. They are described again in the table below.

PBT/PC Sample Number*	Sample Composition
#1	50 % PBT, 50 % PC

*Sample numbers used as in Chapter 6.

#7	as #1 plus 0.08 % 45 % H_3PO_3 in water

Table 7.1 - Composition of Samples # 1 and 7.

7.2.3 Experimental procedures

7.2.3.1 Heating PBT/PC blends

PBT/PC samples # 1 and # 7 were heated at 260, 275, 290, 305 and 320 °C for one hour in an oven exposed to air to cause transesterification in each blend. The samples were placed in the oven as granulates on an aluminium foil backing. Crude plaques of each sample were thus formed since the pellets melted. They were subsequently allowed to cool slowly in air on removal from the oven and examined cold.

7.2.3.2 FT Raman spectra of heat treated PBT/PC blends

FT Raman spectra were recorded of the heat treated PBT/PC blends described in 7.2.3.1. In addition, spectra were recorded of PBT/PC # 1 and # 7 pellets that were not heat treated and also of a pure powdered polycarbonate sample. The spectra presented in this report have not been corrected for the response of the spectrometer. In all the Raman spectra presented in this report 1064 nm excitation was used at 4 cm^{-1} resolution and 50 scans co-added.

7.2.3.3 Specular reflectance spectra of heat treated PBT/PC blends

Specular reflectance spectra were recorded of the heat treated PBT/PC samples described in 7.2.3.1. Spectra were also recorded of the unheated PBT/PC # 1 and # 7. The resulting specular reflectance spectra were processed with the Kramers Kronig algorithm. All spectra were recorded with 4 cm^{-1} resolution and 100 scans were co-added.

7.3 RESULTS AND DISCUSSION

7.3.1 FT Raman spectra of heat treated PBT/PC blends

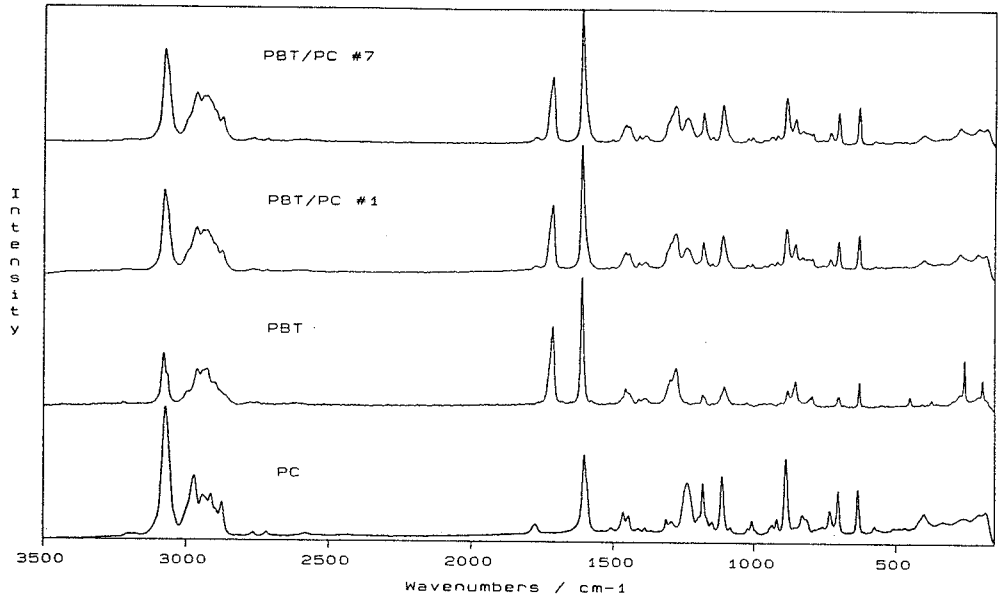

Figure 7.1: Raman spectra of PBT/PC #1, PBT/PC #7, PC and PBT.

Figure 7.1 shows FT Raman spectra of PBT/PC # 1, PBT/PC # 7, PC and PBT that have not undergone any heat treatment. It is apparent that the spectra of the PBT/PC blends are very similar. It was found that this was the case for all the PBT/PC blends referred to in the work described in Chapter 6. No differences could be seen in the spectra of different PBT/PC blends whether stabilised or unstabilised (with H_3PO_3) or with different grades of PBT (i.e. with different molecular weights or end-groups).

Also shown in Figure 7.1 is the FT Raman spectrum of the polycarbonate contained in the PBT/PC blends used in this work. It is apparent from Figure 7.1 that the C=O band for the PC is relatively weak while the C=O bands due to the PBT are relatively strong. Figure 7.2 shows an expanded view of the carbonyl and C=C regions of Figure 7.1. The Raman spectra of the PBT/PC blends are dominated by the bands from PBT, this is because the Raman spectrum of PBT at 1.064 μm is approximately three times as intense as the Raman spectrum of PC using 1.064 μm excitation. Only the most intense bands

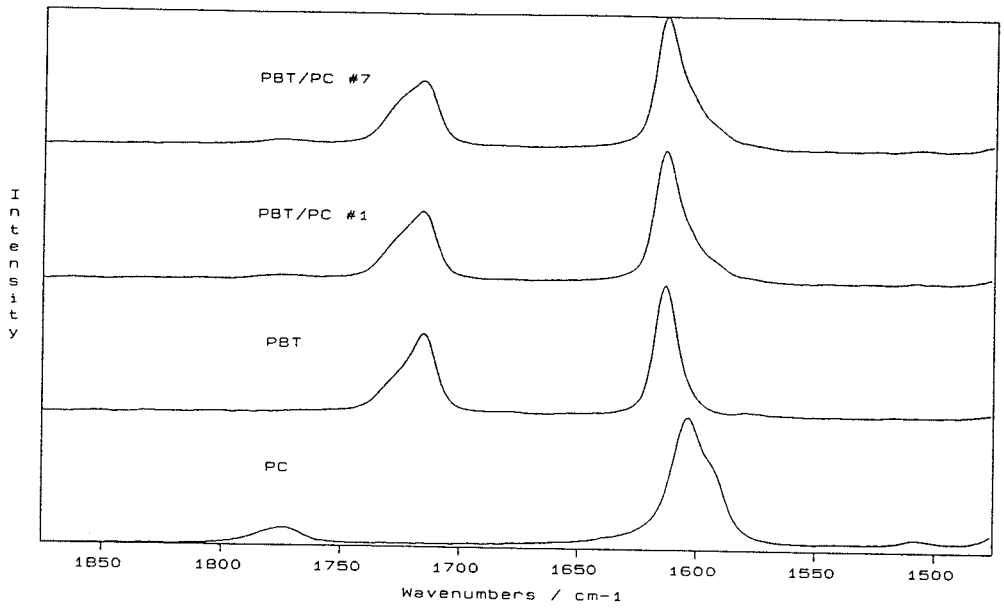

Figure 7.2: Expanded view of Figure 7.1.

from the PC are seen in the Raman spectra of the blends i.e. the bands at 3074, 1236, 1180, 889 and 706 cm^{-1}. The C=O band from the PC (1775 cm^{-1}) is extremely weak in the PC spectrum and even weaker in the spectra of the blends. Transesterification work in Chapter 6 using IR showed that the main changes in the IR spectra of a PBT/PC blend undergoing transesterification occur with the carbonyl stretches. It is thus expected that evidence for transesterification using Raman would most likely be in the form of changes in C=O band intensities or band positions. Figure 7.3 shows the FT Raman spectra of a PBT/PC blend and a blend that has been heated to 270 °C then quenched in water. The PBT carbonyl stretch of the unheated sample consists of a main peak at 1716 cm^{-1} and a shoulder at higher frequency. The carbonyl stretch of the quenched material consists solely of a peak at 1722 cm^{-1}. The peak at 1716 cm^{-1} corresponds to the C=O of the crystalline form of PBT. The shoulder on the 1716 cm^{-1} peak is due to the C=O amorphous form of the PBT in the blend. The peak at 1722 cm^{-1} of the quenched material is due to the C=O of the amorphous form of PBT.

Figures 7.4 and 7.5 show the series of FT Raman spectra collected from heat treated

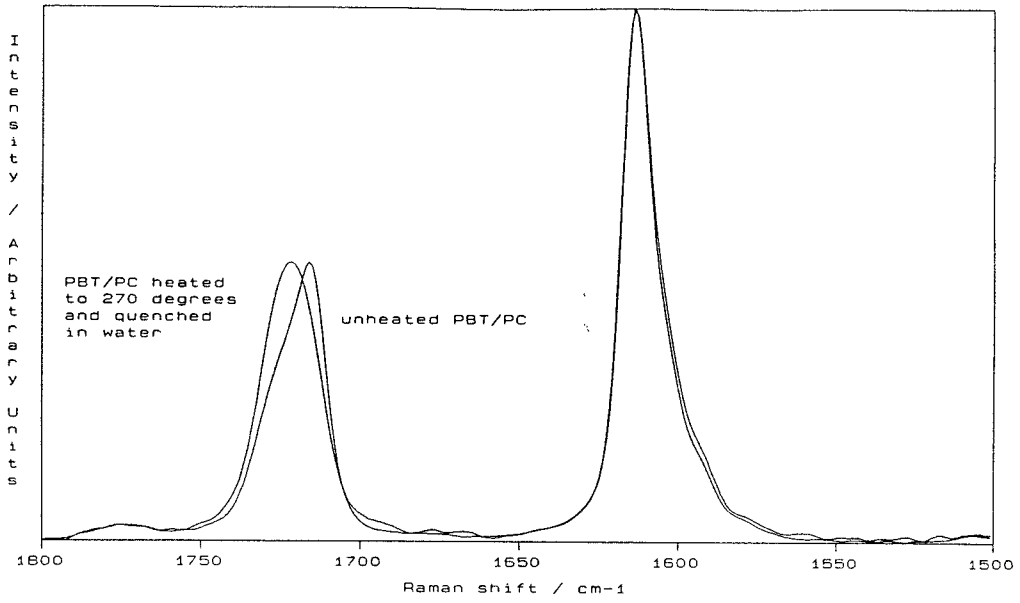

Figure 7.3: Carbonyl region of crystalline and amorphous PBT/PC blends.

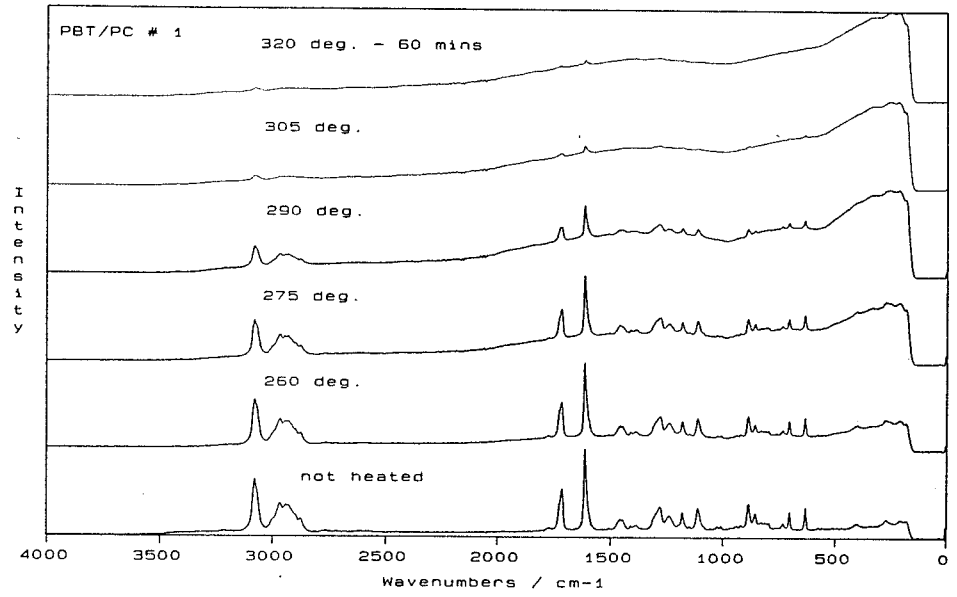

Figure 7.4: Raman spectra of heat treated PBT/PC #1.

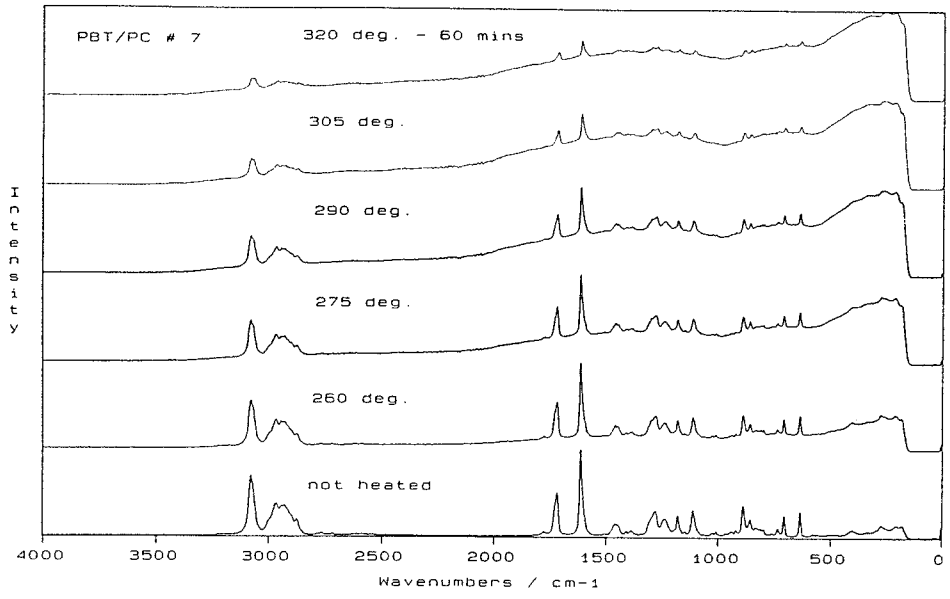

Figure 7.5: Raman spectra of heat treated PBT/PC #7.

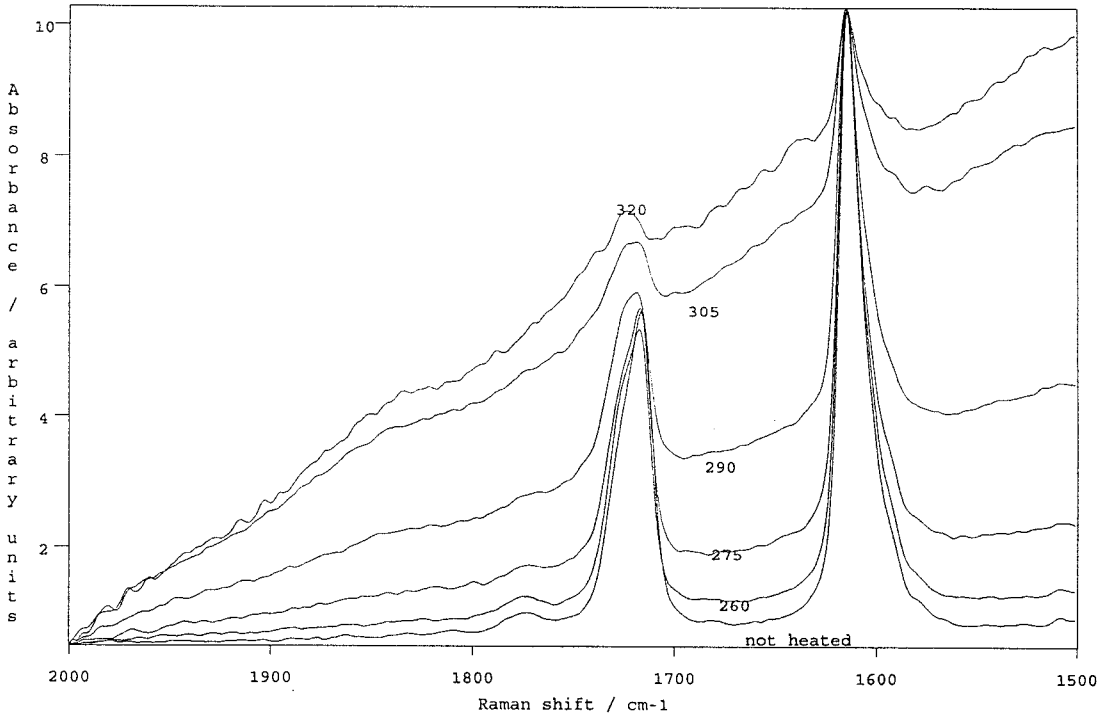

Figure 7.6: Expanded view of Figure 7.4.

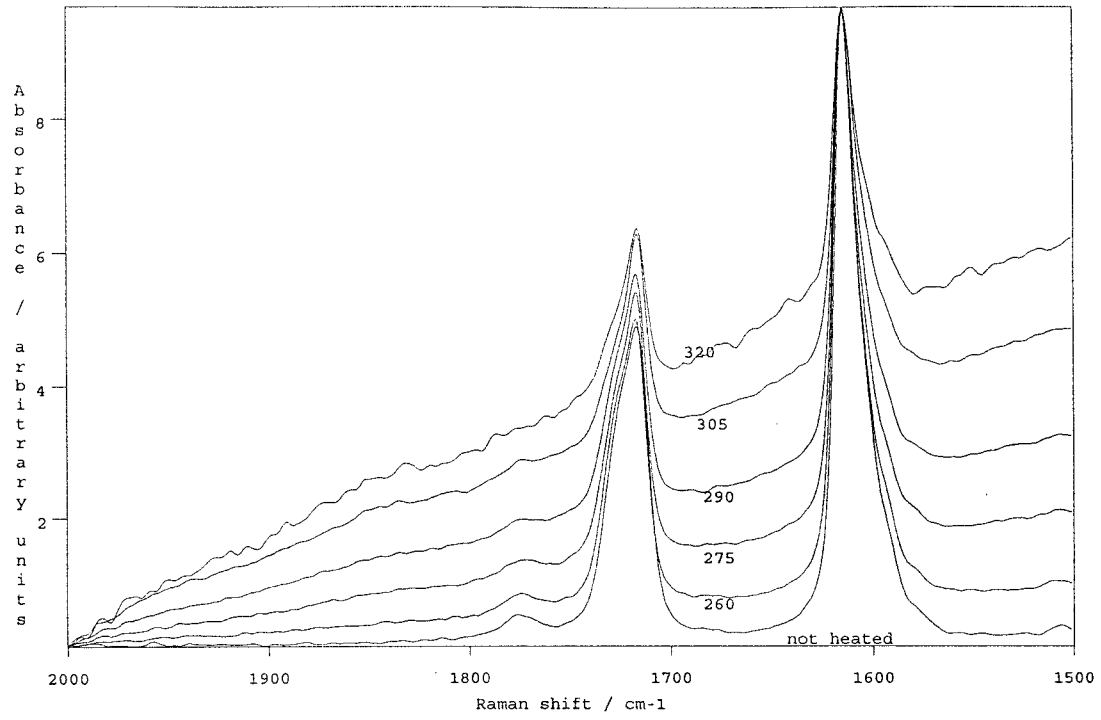

Figure 7.7: Expanded view of Figure 7.5.

PBT/PC specimens as in 7.2.3.1. Figures 7.6 and 7.7 show the expanded carbonyl region for the same heat treated samples. The Raman spectra of the unheated PBT/PC blends shows distinctly the C=O bands from the PBT (1716 cm^{-1}) and less intensely the C=O due to the PC (1774 cm^{-1}). As the PBT/PC samples are heated at ever higher temperatures for one hour the level of fluorescence in each Raman spectrum increases and the intensity of the PBT C=O Raman bands decreases. Eventually the C=O band from the PBT disappears almost completely. In Figure 7.6 the C=O band due to the PBT component of the blend (1716 cm^{-1}) in the unheated sample has a shoulder at higher Raman shift. As the blend is heated for longer periods the intensity of the shoulder appears to increase while the intensity of the main peak at 1716 cm^{-1} is decreasing. Since the transesterification products do not have C=O absorptions around 1720 cm^{-1} these spectral changes cannot be directly attributed to the formation of transesterification products. In the spectrum of the PBT/PC #1 blend heated at 320 ^{o}C, the very weak feature at 1740 cm^{-1} may be due to the formation of a transesterification product, but it is not possible to positively identify the expected transesterification product bands known from infrared results to have C=O frequencies at 1740 cm^{-1} and 1770 cm^{-1}. Either the transesterification products are not formed or, more likely, the

C=O bands from the transesterification products are relatively weak features in the Raman thus they are not seen. Figure 7.7 does not show the changing band shape of the C=O band at 1716 cm^{-1}, the weak feature at 1740 cm^{-1} is also not seen. The presence of the stabilizer has apparently had some influence on the C=O band profile of the PBT.

It was proposed in Chapter 6 that the transesterification reaction acts as a pathway for the thermal degradation of the PBT/PC blend by forming thermally unstable transesterification products. The addition of a stabilizer that prevents transesterification would thus remove a pathway for thermal degradation and thus act as a thermal stabilizer for PBT/PC blends. Visual evidence confirms this view. After identical thermal treatments the stabilised blends invariably showed less colour changes (i.e. darkening) than the unstabilised blends. The changes in the C=O band shape of the PBT seen in Figure 7.6 occur because transesterification between PBT and PC in the blend while PBT is above its T_M reduces the ability of PBT in a PBT/PC blend to crystallize once the blend is cooled to room temperature. A similar reduction in crystallinity is not displayed by a change in the C=O band intensity in Figure 7.7 because transesterification is not occurring in the blend and the PBT is able to crystallize once the blend cools. This change in C=O profile of the PBT is thus indirect evidence for transesterification.

7.3.2 Specular reflectance IR spectra of heat treated PBT/PC blends

Specular reflectance IR spectra of the heated PBT/PC samples described in 7.2.3.1 were recorded to compare to the Raman spectra shown in 7.3.1 above and thus provide experimental confirmation as to whether or not transesterification had, in fact, occurred. Figures 7.8 and 7.9 show the specular reflectance IR spectra of heat treated PBT/PC # 1 and # 7 treated with the Kramers Kronig algorithm. Figures 7.10 and 7.11 show the corresponding expanded C=O regions. Figure 7.12 shows a comparison of the unheated PBT/PC blend with the sample of the same blend that has subsequently been heated at 320 °C for one hour. It is possible to see that the C=O band at 1775 cm^{-1} has shifted to 1770 cm^{-1} and a shoulder at 1740 cm^{-1} has appeared on the side of the C=O band due to the PBT. This is weak evidence that both transesterification products have formed in the heated blend. The uncertainty in the identification of the aromatic-aliphatic

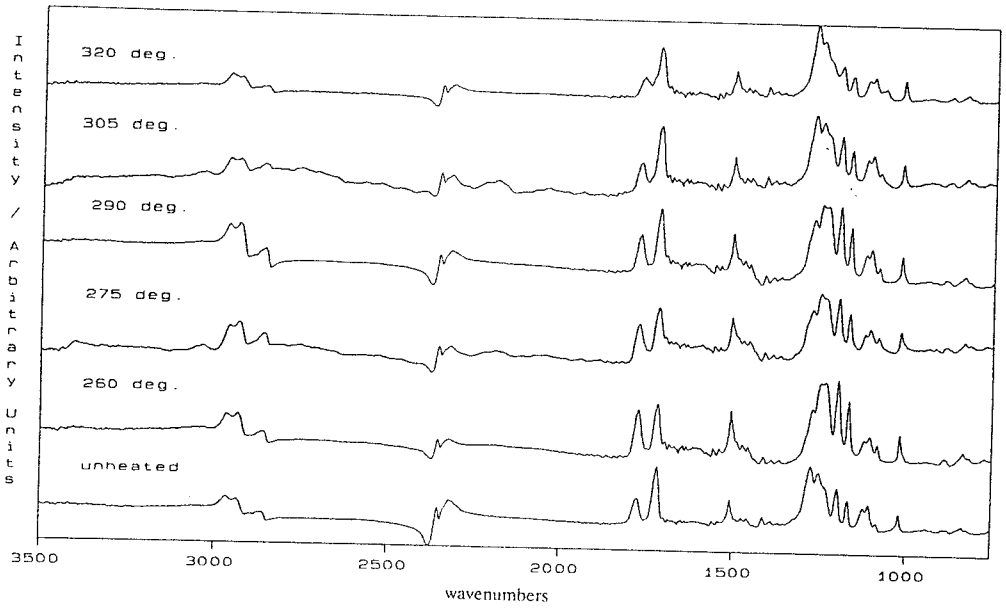

Figure 7.8: Specular reflectance infrared spectra of heat treated PBT/PC #1.

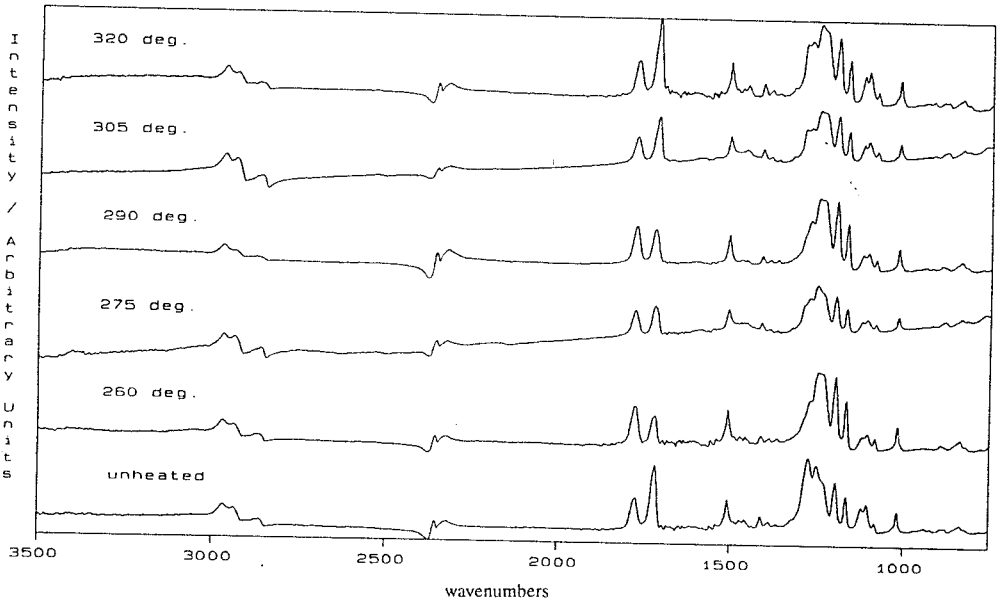

Figure 7.9: Specular reflectance infrared spectra of heat treated PBT/PC #7.

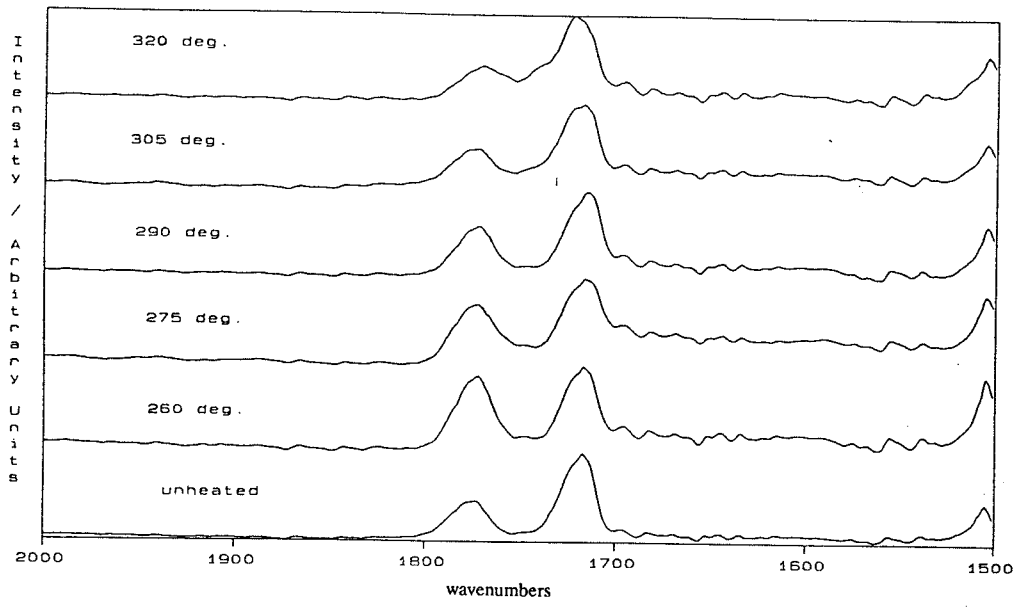

Figure 7.10: Expanded view of Figure 7.8.

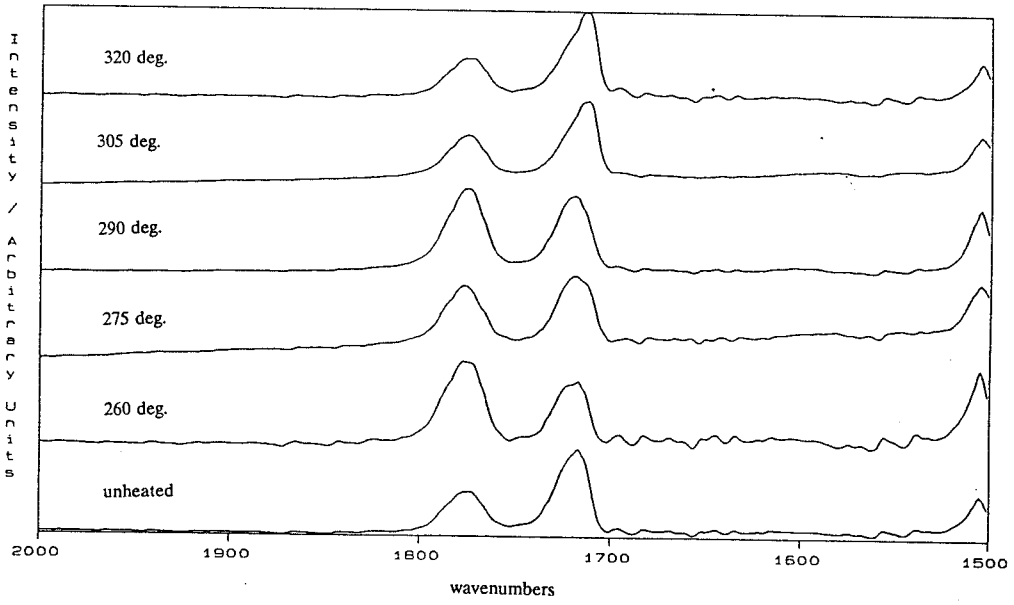

Figure 7.11: Expanded view of Figure 7.9.

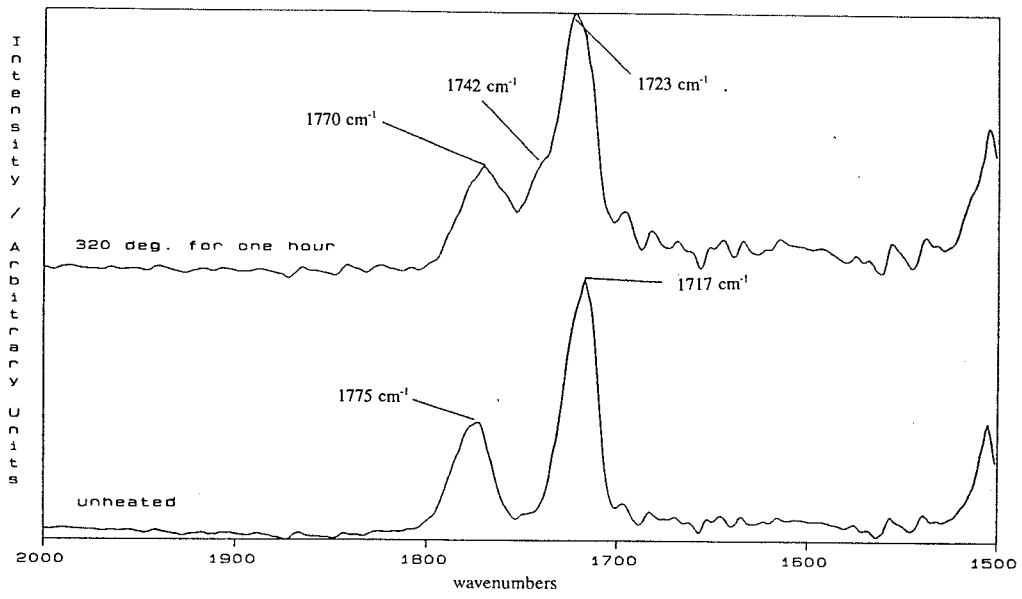

Figure 7.12: Comparison of unheated PBT/PC #1 with PBT/PC #1 heated at 320 °C for one hour.

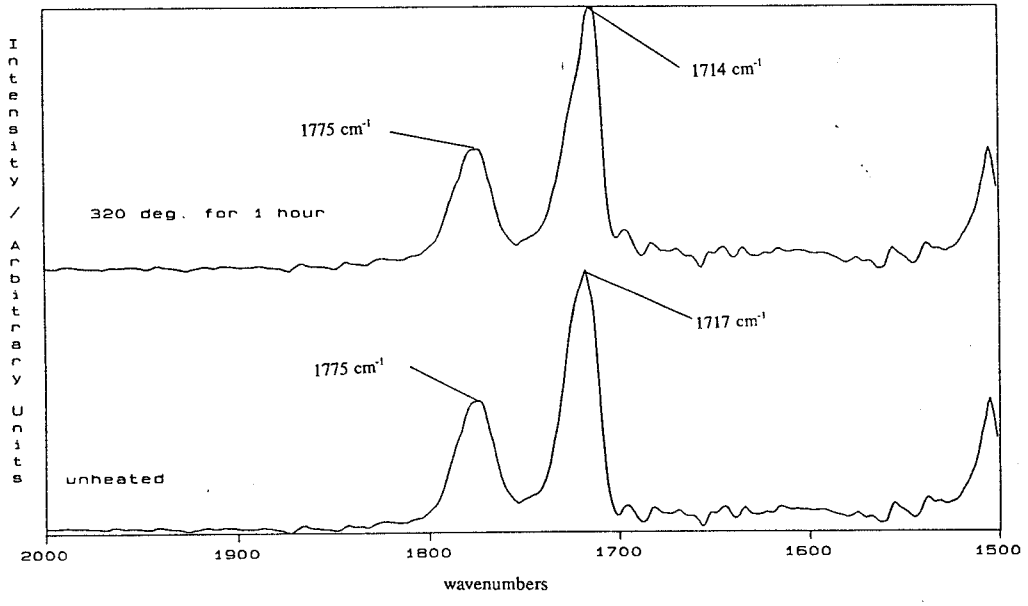

Figure 7.13: Comparison of unheated PBT/PC #7 with PBT/PC #7 heated at 320 °C for one hour.

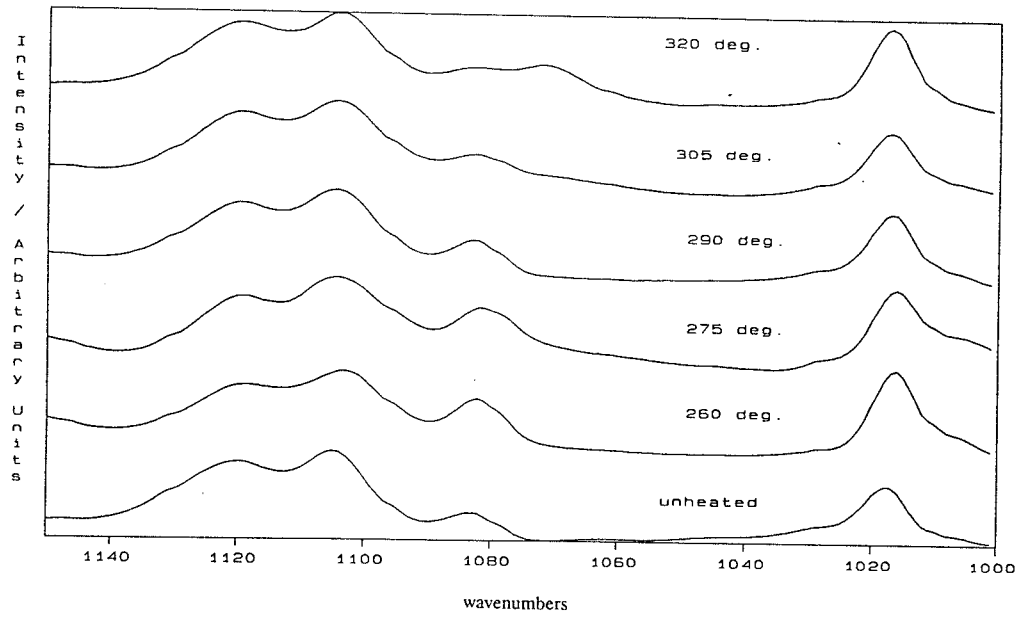

Figure 7.14: Expanded view of Figure 7.8.

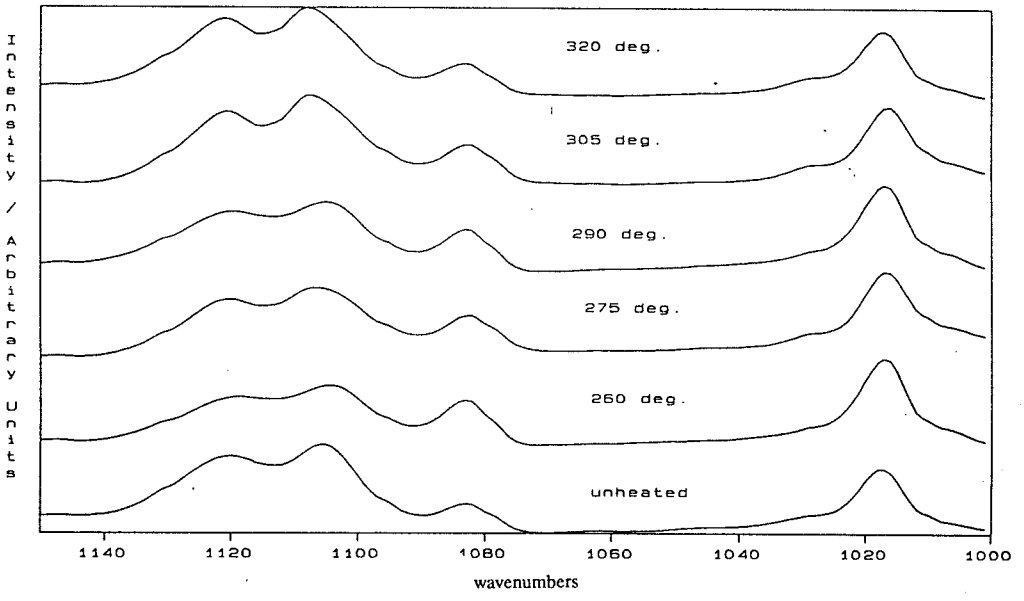

Figure 7.15: Expanded view of Figure 7.9.

carbonate (C=O at 1770 cm^{-1}) is due to the fact that the quality of the IR spectra is not adequate enough to be able to attribute the observed change in vibration frequency (i.e. 1774 cm^{-1} to 1770 cm^{-1}) to the formation of the aromatic-aliphatic carbonate transesterification product. Figure 7.13 shows a similar plot to Figure 7.12 for PBT/PC # 7. In Figure 7.12 the changes in the C=O peak positions are not apparent. This must be evidence that transesterification has not occurred to as great an extent as for the unstabilised PBT/PC blend. Figures 7.14 and 7.15 show the region of the IR spectra where the 1070 cm^{-1} peak due to the aromatic ester should appear. As before the aromatic ester can be identified in Figure 7.14 in the PBT/PC sample that has been heated at 320 °C for one hour but cannot be seen in Figure 7.15.

7.4 CONCLUSIONS

As expected in all the PBT/PC samples heated some discolouration of the sample occurs, the more aggressive the thermal treatment, the darker the discolouration.

Indirect evidence for transesterification was obtained using FT Raman spectroscopy. This was in the form of a change in the band shape of the C=O due to the changing crystallinity of the PBT component of the unstabilised blend. This change has been attributed to the retardation of crystallization caused by transesterification between PBT and PC while the PBT is above its T_M. The monitoring of the reduction in the crystallinity of the PBT component of a PBT/PC blend using Differential Scanning Calorimetry is one of the main techniques to provide evidence that transesterification has occurred in a blend[7].

No direct evidence for the transesterification products was observed. This is not surprising because carbonyl stretches do not usually give rise to strong bands in Raman spectroscopy as opposed to the strong absorptions which carbonyl stretches potentially yield in infrared spectroscopy. Specular reflectance spectra obtained from the same samples examined with FT Raman showed evidence that advanced transesterification had in fact occurred. Evidence for the aliphatic-aromatic carbonate (C=O at 1770 cm^{-1}) and the aromatic ester (C=O at 1740 cm^{-1}) was obtained for the unstabilised PBT/PC blends

heated at 320 °C for one hour. The corresponding stabilised blend showed no evidence for the transesterification products.

It is unlikely that heating the PBT/PC blends at higher temperatures or for longer periods will allow the transesterification products of the PC and PBT to be directly identified with Raman spectroscopy. The quality of the Raman spectra seen in the PBT/PC blends heated at 320 °C is already extremely poor (due to fluorescence) and thus more aggressive heating regimes will only yield Raman spectra of worse quality due to thermal degradation reactions which become more predominant at higher temperatures.

It was originally envisaged that if the results of the FT Raman work at 1064 nm was encouraging then some work would be carried out with 780 nm excitation in an attempt to follow the transesterification reaction directly while the blend is heated at temperatures above 270 °C. However work with 1064 nm showed that the level of fluorescence in the heat treated PBT/PC blends makes it unattractive to attempt to carry out any work at 780 nm since invariably samples fluorescing at 1064 nm show far more at the lower wavelength.

The inability of FT Raman to directly show the transesterification products is not surprising because the selection rules for infrared and Raman spectroscopy are such that bands which are relatively strong in the infrared are usually relatively weak in the Raman and vice versus. The fact that the major change in the spectra (IR and Raman) of the PBT/PC blends is in the C=O region and C=O stretches are relatively strong IR features will mean that IR should be a better technique than Raman to follow transesterification in PBT/PC blends.

7.4 REFERENCES

1. J.Devaux, P.Godard and J.P.Mercier, J. Polym. Sci.: Polym. Phys. Ed., (1982), **20**, 1895.
2. J.Devaux, P.Godard and J.P.Mercier, J. Polym. Sci.: Polym. Phys. Ed., (1982), **20**,

1901.

3. J.Devaux, P.Godard, J.P.Mercier, P.Touillaux and J.M.Dereppe, J. Polym. Sci.: Polym. Phys. Ed., (1982), **20**, 1875.
4. Martin Pellow-Jarman and Martin Hetem, Internal Report General Electric Plastics Europe, Evaluation High T & P Graseby Specac IR Cell for PBT/PC Transesterification Monitoring, (1993).
5. P.J.Hendra, M.V.Pellow-Jarman and R.Bennett, Vib. Spec., (1993), **5** (3), 311.
6. D.G.Hamilton and R.R.Gallucci, Journal of Applied Polymer Science, (1993), **48**, 2249.
7. Internal Report, General Electric Plastics Europe.

Chapter 8

THE EVALUATION OF A SOLVENT ELIMINATION LIQUID CHROMATOGRAPHIC - FOURIER TRANSFORM INFRARED SPECTROSCOPY INTERFACE

Chapter 8

THE EVALUATION OF A SOLVENT ELIMINATION LIQUID CHROMATOGRAPHIC - FOURIER TRANSFORM INFRARED SPECTROSCOPY INTERFACE

8.1 INTRODUCTION

The interfacing of FTIR with liquid chromatography (LC) has been a subject of growing interest in recent years. In general the types of interfaces can be separated into two groups: those which make use of simple flow cells[1-9] and those which eliminate the solvent before the infrared spectrum of the eluent is recorded[10-30]. The main drawback of the flow cell design is that most solvents commonly used in LC possess intense IR absorptions in certain wavelength regions rendering some spectral region opaque. Thus the cell pathlength must be kept small to allow a sufficiently high IR transmittance in these regions. This in turn imposes a limitation on the sensitivity obtainable using LC-FTIR interfaces incorporating a flow cell design. Solvent elimination LC-FTIR interfaces overcome this disadvantage in that the common LC solvent systems can be used with good sensitivity. A major drawback of LC-FTIR interfaces using a solvent elimination design in the past has been that the interfaces usually could not remove water and other high boiling point liquids at moderately high flow rates (above 0.1 mL/min). Work in the field of LC-FTIR interfaces has reached the point where commercial systems are now available. A recent commercially available piece of equipment developed for interfacing[13,14] FTIR with LC is the "LC-Transform", an instrument showing promise in eliminating water from a chromatographicly separated sample.

8.1.1 The LC-Transform

The "LC-Transform" is a commercially available piece of equipment (Lab Connections, Marlborough, USA) that allows Liquid Chromatography (LC) and Fourier Transform Infrared (FTIR) spectroscopy to be interfaced. The components separated by LC can be detected by FTIR and a continuous series of IR spectra generated corresponding to the

chromatographic output of the column. The solvents used in the chromatographic separation are eliminated before the FTIR spectra are recorded thus solvent spectral interference is removed. The advantages of chromatographic separation are thus combined with the ability of IR to provide detailed information regarding the identity of the substances corresponding to the eluted peaks.

The LC-Transform consists of a sample collection module and a scanning accessory stage for the FTIR instrument. In principle it is possible to obtain good IR spectra from sample quantities down to 100 ng (if a cooled MCT detector is used). The eluent from a column is collected as a thin track around the edge of a slowly rotating IR reflective mirror. The IR collection disk can be rotated at 3, 5, 10 or 20 °/min. The sample is deposited on the disk through a nebulizer nozzle system which has appropriate temperature and flow controls. Figure 8.1 shows the basic principle of operation.

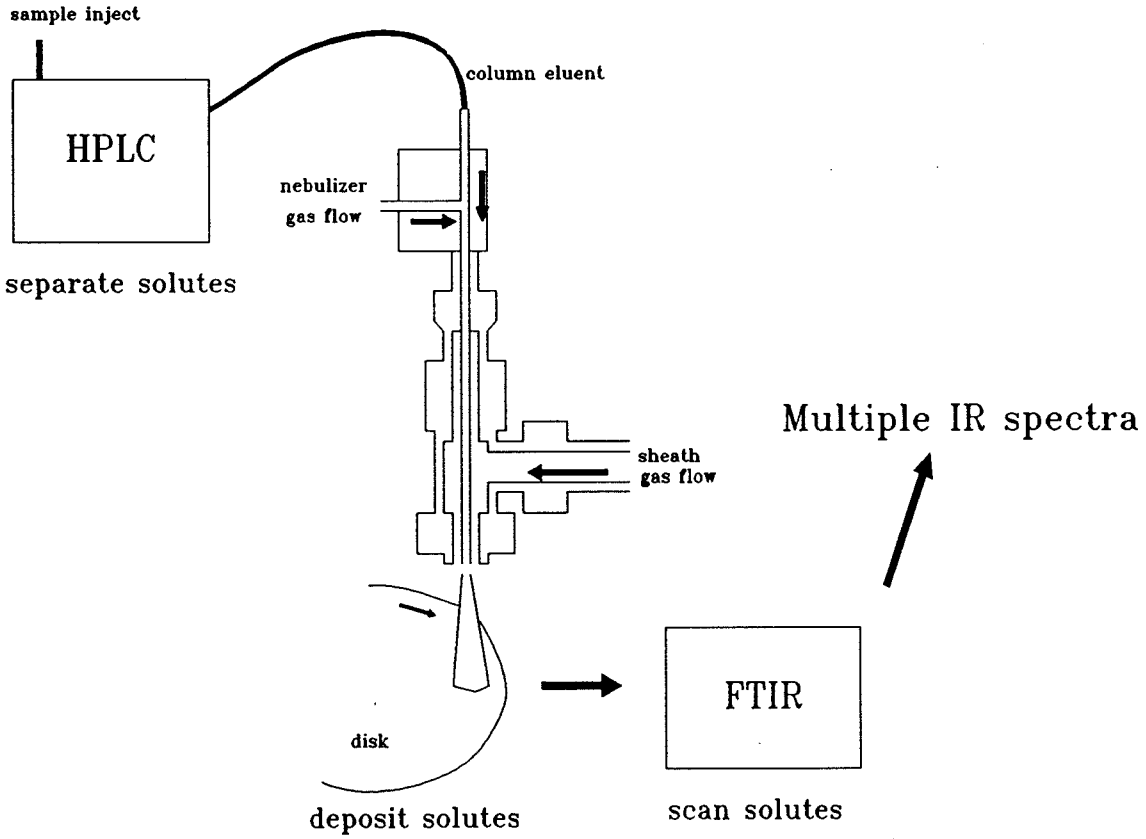

Figure 8.1: Basic operating principle of the LC-Transform.

The eluent from the column is mixed with nitrogen or dry air within the nozzle assembly of the column to form an aerosol jet. The aerosol is then passed through thin tubing and out of the nozzle orifice where it comes into contact with a heated sheath gas flow which volatilizes most of the mobile phase of the column eluent. The sheath gas also restricts the nebulizer spray to a narrow jet which is coated onto the sample collection disk rotating at a chosen constant rate during a chromatographic run. The flow leaving the LC column is split between waste, the nebulizer and the usual detection system of the LC system. If required the LC-Transform can be placed after the usual detection system of the column. The nebulizer and sheath gas are capable of evaporating a flow of typically 100 μl/min. The nebulizer and sheath gas flows are regulated by needle valves located beneath flow indicator tubes. Typical flow settings during an experiment are between 20 and 25 which correspond to nebulizer and sheath gas flow rates of approximately 0.025 and 4 l/min respectively.

During a gradient chromatographic run the composition and hence volatility of the solvent changes, the temperature of the sheath gas can be changed to correspond to the varying solvent composition. Any solvent material not evaporated by the sheath gas is removed by a 15 watt stage heater placed under the disk directly beneath the nebulizer nozzle. The entire chromatogram is deposited as a single dried circular track on the collection disk.

The collection disk is then scanned in an FTIR instrument either by rotating the disk at a preset rate giving time resolved FTIR (3, 5 10 or 20 ^{o}/min) or by moving the disk stepwise to a desired location on the disk to allow the IR spectrum of each component to be recorded. The IR beam is focused onto the sample track that has already been deposited onto the disk. The IR beam at the disk surface is approximately 2 mm wide. The beam travels through the sample and is then reflected back through the sample by the disk then passed onto the IR detector of the spectrometer. The slower the speed the disk is scanned, the greater is the spectral resolution given and as said before the disk can also be stopped at a required position to allow the collection of multiple scans.

The collection disks are made of germanium 2 mm thick and the rear surface of the disk

is coated with aluminium. As a result disks reflect 90 percent of the IR radiation incident. Germanium is chemically resistant and IR transparent. The 2 mm thickness of the disks prevents interference between the beam reflected from the disk and the incident beam on the disk. The disks may be cleaned and reused.

8.1.2 Size exclusion chromatography with extracts from polycarbonate / acrylonitrile-butadiene-styrene

8.1.2.1 Polycarbonate extract of polycarbonate / acrylonitrile-butadiene-styrene

Size exclusion chromatography (SEC), or gel permeation chromatography (GPC), is used here as a technique to determine the molecular weight distribution of polycarbonate (PC) in polycarbonate / acrylonitrile-butadiene-styrene (PC/ABS) by comparison with narrow molecular weight distribution polystyrene standards. The PC portion of the PC/ABS is extracted in tetrahydrofuran (THF).

The LC-Transform can be used to compare the chromatographic separation of the PC extracts of three commercial samples of PC/ABS (designated as PC/ABS #1; PC/ABS #2 & PC/ABS #3) using Gram-Schmidt* profiles taken from the time resolved FTIR spectra of the deposited chromatograms.

8.1.2.2 Free styrene-acrylonitrile extract of polycarbonate / acrylonitrile-butadiene-styrene

SEC is also used to determine the molecular weight distribution of the free poly(styrene-acrylonitrile) (SAN) in PC/ABS. The free SAN in PC/ABS is extracted from the mix with acetone and dimethylamine, the butadiene portion of the sample is not extracted with the SAN. The solvent is then evaporated off and the extracted sample dissolved in THF. Again a high molecular weight column set is used with a THF solvent in the GPC.

---

*Gram-Schmidt plots are plots of total peak area under each IR spectrum versus time.

Again the LC-Transform can be used to compare the SAN extracts of PC/ABS to give qualitative information about the free styrene-acrylonitrile copolymers used in the PC/ABS samples studied.

8.1.3 Size exclusion chromatography with high impact polystyrene rubbers

Four rubber samples were chosen for this series of experiments. They were designated as HIPS #1, HIPS #2, HIPS #3 and HIPS #4.

HIPS #1 and #2 belong to a class of rubbers that are thermoplastic rubbers and designed for use without vulcanisation. They consist of block segments of styrene and rubber monomer units. These block copolymers form a two phase system because the polystyrene and elastomeric blocks are incompatible. The polystyrene (PS) domains are below their T_g at normal temperatures while the polybutadiene domains are above their T_g. During processing the PS is heated above its T_g and thus softens to permit flow. After cooling the PS domains harden and effectively lock the rubber network in place.

HIPS #4 is a similar material to the first two rubber samples. It is comprised of a two phase system of thermoplastic blocks (PS) and rubbery blocks (polybutadiene or polyisoprene). The rubbery phase forms a continuous 3-D network through which the submicron sized polystyrene domains are dispersed which act as crosslinks to hold the rubber network in place.

HIPS #3 is also a high impact polystyrene (HIPS) material of similar composition to the other test samples referred to in this section.

8.1.4 Identification of unknown compound in bisester diamide

Bisester diamide (BEDA) $[\text{-NH-(CH}_2)_4\text{-NH-CO-Ph-CO}]_n$, a product synthesized at General Electric Plastics from butylamine and terephthalic acid (1:2), contains an unknown component of higher molecular weight than BEDA. Chloroform SEC is expected to be able to separate the unknown compound from the BEDA and provide an

FTIR spectrum of the compound to aid in its identification.

8.2 EXPERIMENTAL

8.2.1 Size exclusion chromatography with polycarbonate / acrylonitrile-butadiene-styrene extracts

8.2.1.1 Polycarbonate extract of polycarbonate / acrylonitrile-butadiene-styrene

Three samples of PC/ABS were chosen as test samples. They were PC/ABS #1, PC/ABS #2 and PC/ABS #3. A sample of the PC component of each sample was prepared by extracting the PC/ABS sample in THF. Chromatographic runs of each sample were carried out using the GPC with THF as solvent. The concentration of PC extract in each sample was approximately 0.1% in THF. The injection volume of the sample was 150 μl. The chromatographically separated column eluent was collected on the germanium disk at a liquid flow rate of approximately 100 μL/min. The N_2 gas flow rates to the sheath and nebulizer were 35 and 25 (arbitrary units) respectively with a sheath gas temperature of 65 ^{o}C. The nozzle height was 6 mm above the collection disk (the same nozzle height was used for all the data presented in this report) and the collection disk was rotated at 10^{o}/min. The first five minutes of the chromatographic run was not collected on the collection disk. The FTIR examination of the collection disk was carried out using the Bomem M100 FTIR operating with Lab Calc software at 4 cm^{-1} resolution. This interferometer was used to collect all the FTIR spectra shown in this report. The FTIR instrument recorded a series of 60 spectra with each spectrum taking approximately 26.4 seconds to collect (i.e. the average of 4 scans), the collection disk was rotated at 3^{o}/min. The background spectrum was recorded by using a portion of the disk where no sample had been deposited. Backgrounds were recorded in the same way for all the spectra presented in this report. Before the FTIR examination of the disk the sample compartment of the Bomem was degassed with helium for approximately 30 minutes to reduce interference from CO_2 and water vapour. This was done for all the spectra collected in this investigation.

8.2.1.2 Styrene-acrylonitrile extract of polycarbonate / acrylonitrile-butadiene-styrene

The same three samples referred to in Section 8.2.1.1 were used in this series of GPC experiments with the LC-Transform. A sample of the free SAN extract of each sample was prepared by extracting free SAN from the PC/ABS with acetone and dimethylamine. Chromatographic runs of each sample were carried out using the GPC with THF as a solvent. The concentration of free SAN extract in each sample was approximately 0.1% in THF. The injection volume of the sample was 150 μL. The flow rate of solvent from the GPC to the disk was 100 μL/min, N_2 gas flow rates to the LC-Transform, nozzle height, sheath gas temperature and the collection disk rotation speed were the same as in Section 8.2.1.1. The first five minutes of each chromatographic run was not collected on the disk. FTIR examination of the disks were carried out as in Section 8.2.1.1.

8.2.2 Size exclusion chromatography with high impact polystyrene rubbers

Four different samples of PS/HIPS rubbers were used in this set of experiments. Samples were dissolved in chloroform to give 0.1% solutions by mass, 100 μl of each sample was injected onto the polyamide GPC using chloroform as a solvent.

The flow from the column to the LC-Transform was 100 μl/min. The sheath temperature was kept at a constant temperature of 65 ^{o}C. The sheath gas and nebulizer gas flow rates were 35 and 25 arbitrary units in all the experiments carried out in this section. The stage heater was not used and sample collection on the disk was started five minutes after the injection was made. The collection disk was rotated at 10^{o}/min during the chromatographic run. FTIR examination was carried out as before with 50 spectra of ten scans each (each spectrum taking 66 s to collect), the collection disk was rotated at 3^{o}/min.

8.2.3 Identification of unknown compound in bisester diamide

The sample was dissolved in chloroform to give a solution of 2 % concentration, 100 μl of each sample was injected onto the column. The flow from the LC-Transform to the

disk was 100 μl/min. The sheath temperature was 65 °C and the gas flow rates to the sheath and nebulizer were 35 and 25 arbitrary units respectively. The usual disk rotation rate was 10 °/min during the deposition of the chromatogram on the disk. FTIR examination of the disk was carried out by collecting multiple spectra of the disk of 10 scans each (collection time 66 s) with the disk rotating at 3 °/min or by scanning the disk while the disk was stationary to obtain a better spectrum of the desired compound.

8.3 RESULTS AND DISCUSSION

8.3.1 Correction of baselines in recorded spectra

A significant feature of all the series of spectra collected of the samples deposited in the germanium disks was the shifting of the baseline. In general the baseline shift was approximately dependent on the amount of sample deposited on the disk at any particular time. As a result all of the spectra shown in this report have been baseline corrected. A typical baseline correction involved firstly the use of a Lab Calc program written in Array Basic which was able to carry out a multiple point baseline correction using the same points for each spectrum in the series. When this is done care should be taken that the chosen baseline points do not correspond to any peak in one of the spectra in the multiple spectra file. Once the multiple point baseline correction has been carried out then another modified Lab Calc program is used to carry out a baseline correction on each spectrum to ensure that the baseline of each spectrum has approximately the same abscissa value.

Similar baseline corrections can be carried out using Grams 386 software. The usual Grams 386 software is capable of performing the multiple point baseline correction and the autolevel baseline correction can be performed using a slightly modified version of the Lab Calc program.

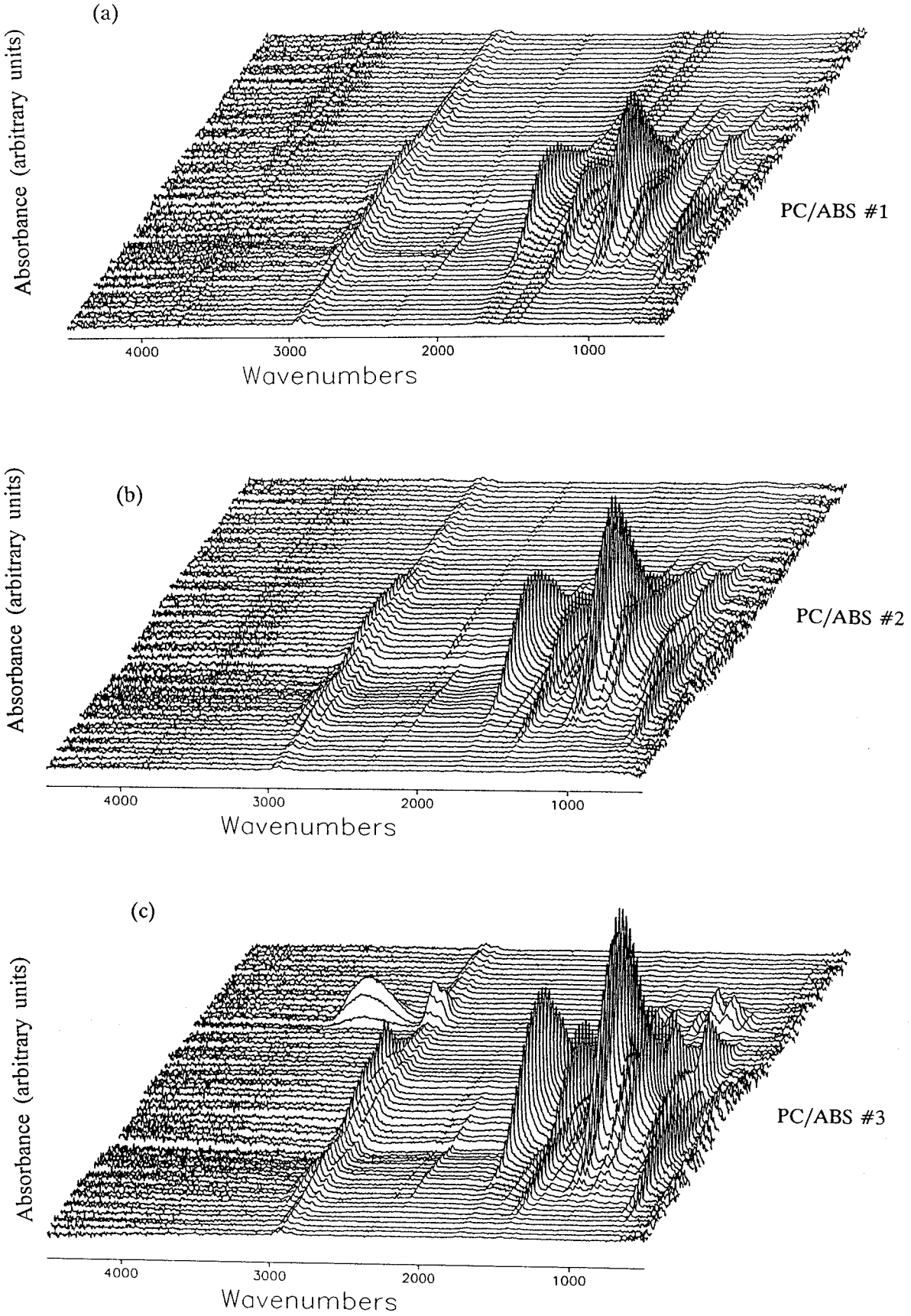

Figure 8.2: Time resolved FTIR spectra for PC extracts of the three PC/ABS test material.

8.3.2 Size exclusion chromatography with polycarbonate / acrylonitrile-butadiene-styrene extracts

8.3.2.1 Polycarbonate extract of polycarbonate / acrylonitrile-butadiene-styrene

Figures 8.2 (a), (b) and (c) show the time resolved FTIR spectra collected for the PC extracts of the three PC/ABS test materials. Figures (a), (b) and (c) are similar in appearance. Each series of spectra is basically a profile of the PC as it is eluted during the SEC separation. Also present in each figure is a small amount of SAN copolymer which is extracted with the PC in the sample preparation. The most noticeable difference between the three figures is that there is a peak eluting towards the end of the chromatographic run for the PC/ABS #3 sample corresponding to the elution time of a nonpolymeric material. A spectral library search shows that this material is hydrogenated bisphenol-A. Figures 8.2 (a), (b) and (c) are unsuitable for any quantitative comparison of the three test materials. It is necessary to extract peak area chromatograms from each figure for the compound of interest to allow any semi-quantitative comparison between the test materials.

Table 8.1 shows the results of the characterization of the three PC/ABS samples. This data was generated at General Electric Plastics using H^1 nmr and GPC using polystyrene standards of known molecular weights.

	PC/ABS #1	PC/ABS #2	PC/ABS #3
% polycarbonate	63.8	64.0	53.8
% acrylonitrile	7.2	7.4	11.8
% polybutadiene	6.4	7.9	10.3
% styrene	22.5	20.8	24.2
% free SAN	23.5	23.1	27.9
M_W - PC	40 000	52 000	55 200
M_W - SAN	143 000	168 000	122 000

Table 8.1 - Composition parameters for PC/ABS #1, PC/ABS #2 and PC/ABS #3.

Figures 8.3 (a), (b) and (c) show the various extracted profiles of specific peaks areas

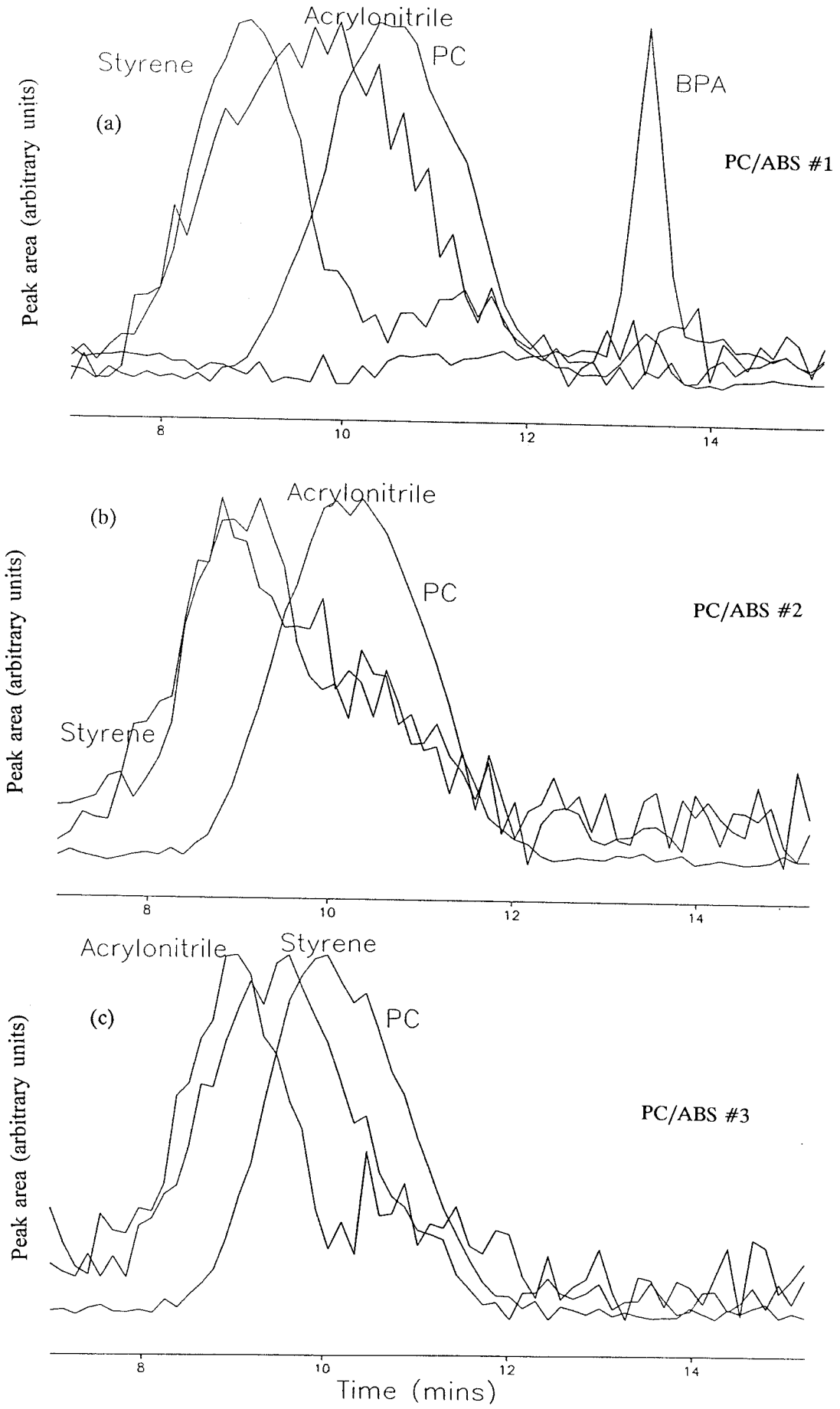

Figure 8.3: Time extracted peak area profiles for the three PC/ABS test materials.

corresponding to the compounds present in the chromatogram. The sample preparation followed here is designed to allow the calculation of the molecular weights of the PC component of the PC-ABS material thus the PC component of the test material has been extracted preferentially to the ABS. However an appreciable concentration of styrene and acrylonitrile is injected together with the PC in each chromatographic separation. This allows the styrene and acrylonitrile components of the test materials to be compared to each other and to the PC component.

With SEC the lower the molecular weight the longer the elution time, thus higher molecular weight polymers elute earlier in each chromatogram. In all cases (i.e. Figure 8.3 (a), (b) and (c)) the styrene and acrylonitrile components of the blend have higher molecular weights than the PC component. This is confirmed from Table 8.1. It is apparent from Figure 8.3 (using the extract profile of the styrene peak) that the molecular weights of the three SAN copolymers increase in the order PC/ABS #3 < PC/ABS #1 < PC/ABS #2. This is in agreement with the data in Table 8.1. The poor signal to noise ratios of the extracted profiles of the acrylonitrile and the styrene are due to the fact that the sample preparation was designed to preferentially extract PC and not PS and polyacrylonitrile.

The relative elution times of the three PC peaks for the three samples are in agreement with the values given for the molecular weights in Table 8.1 i.e. the molecular weight of the PC components increases in the order PC/ABS #1 < PC/ABS #2 < PC/ABS #3.

The molecular weights given in Table 8.1 are expressed relative to the molecular weights of the narrow band molecular weight polystyrene standards and are not the actual molecular weights.

8.3.2.2 Styrene acrylonitrile extract of polycarbonate / acrylonitrile-butadiene-styrene

Figures 8.4 (a), (b) and (c) show the time resolved FTIR spectra collected for the SAN extracts of the three PC/ABS samples used as test materials in this part of the trial. Qualitatively each figure looks similar. Each series of spectra is basically a profile of the

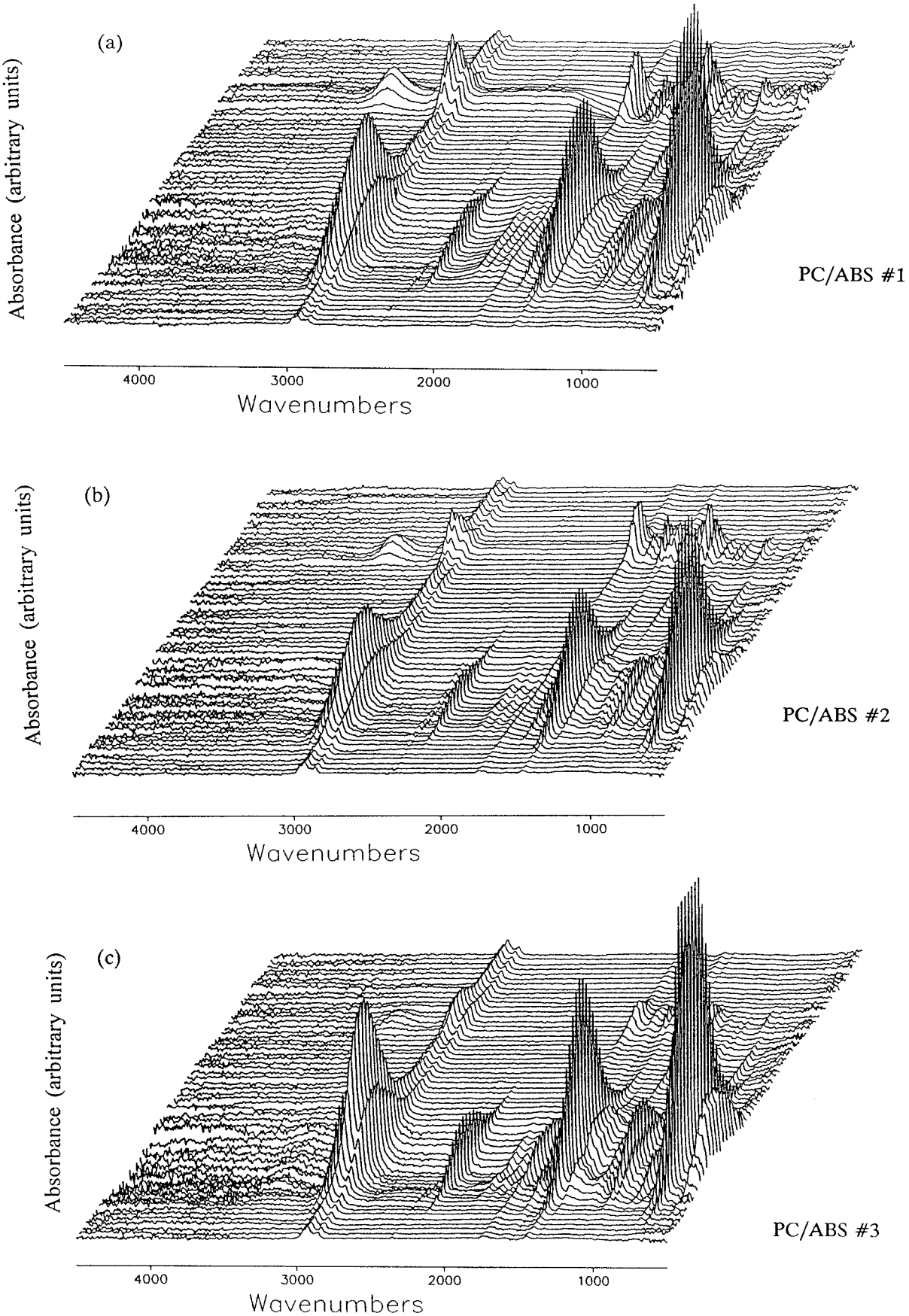

Figure 8.4: Time resolved FTIR spectra for SAN extracts from PC/ABS samples.

SAN copolymer as it is eluted during the SEC separation. Also seen in each figure corresponding to low molecular weight material is some hydrogenated bisphenol-A. To allow a semi-qualitative comparison of the styrene and acrylonitrile components it is necessary to extract chromatograms from the time resolved IR spectra. Figures 8.5 (a), (b) and (c) show the ratio of styrene to acrylonitrile peak area extracts across the elution time for the different PC/ABS samples. The absolute values of the ratios of styrene to acrylonitrile shown in Figure 8.5 are purely relative values generated by ratioing the chromatographic extracts of the peak areas for the styrene and the acrylonitrile. It is apparent from Figure 8.5 that the sample with the highest amount of styrene relative to acrylonitrile is the PC/ABS #1, then comes the PC/ABS #2 closely followed by the PC/ABS #3. This is confirmed by the data given in Table 8.1 in Section 8.3.2.1.

8.3.3 Size exclusion chromatography with high impact polystyrene rubbers

Figures 8.6 (a) & (b) and 8.7 (a) & (b) show the results obtained with the LC-Transform from the HIPS rubbers HIPS #2 & HIPS #1 and HIPS #3 and HIPS #4 respectively. The relatively low intensity of the IR spectra for the HIPS #3 sample is due to the fact that this sample was not completely soluble in chloroform and because identical masses of each sample were dissolved to make up the solutions to be injected not all the HIPS #3 sample weighed out was injected.

Figures 8.8 (a), (b), (c) and (d) show a comparison of Gram Schmidt plots for the 4 test materials. This gives an impression of the relative molecular weight distributions of the four materials. From the results shown in Figure 8.8 the molecular weights of the test materials increase in the order HIPS #1 > HIPS #4 > HIPS #2 > HIPS #3. Known data concerning the molecular weights of samples #1 and #2 confirms the order of the molecular weights of these two materials. HIPS #1 is known to have a similar molecular weight to HIPS #4.

Figures 8.9 (a), (b), (c) and (d) show a comparison of the FTIR spectra at the peak absorbance for 4 test materials. These spectra can give a relative impression of the differences in the composition of the different materials. HIPS #4 is a styrene-butylene-

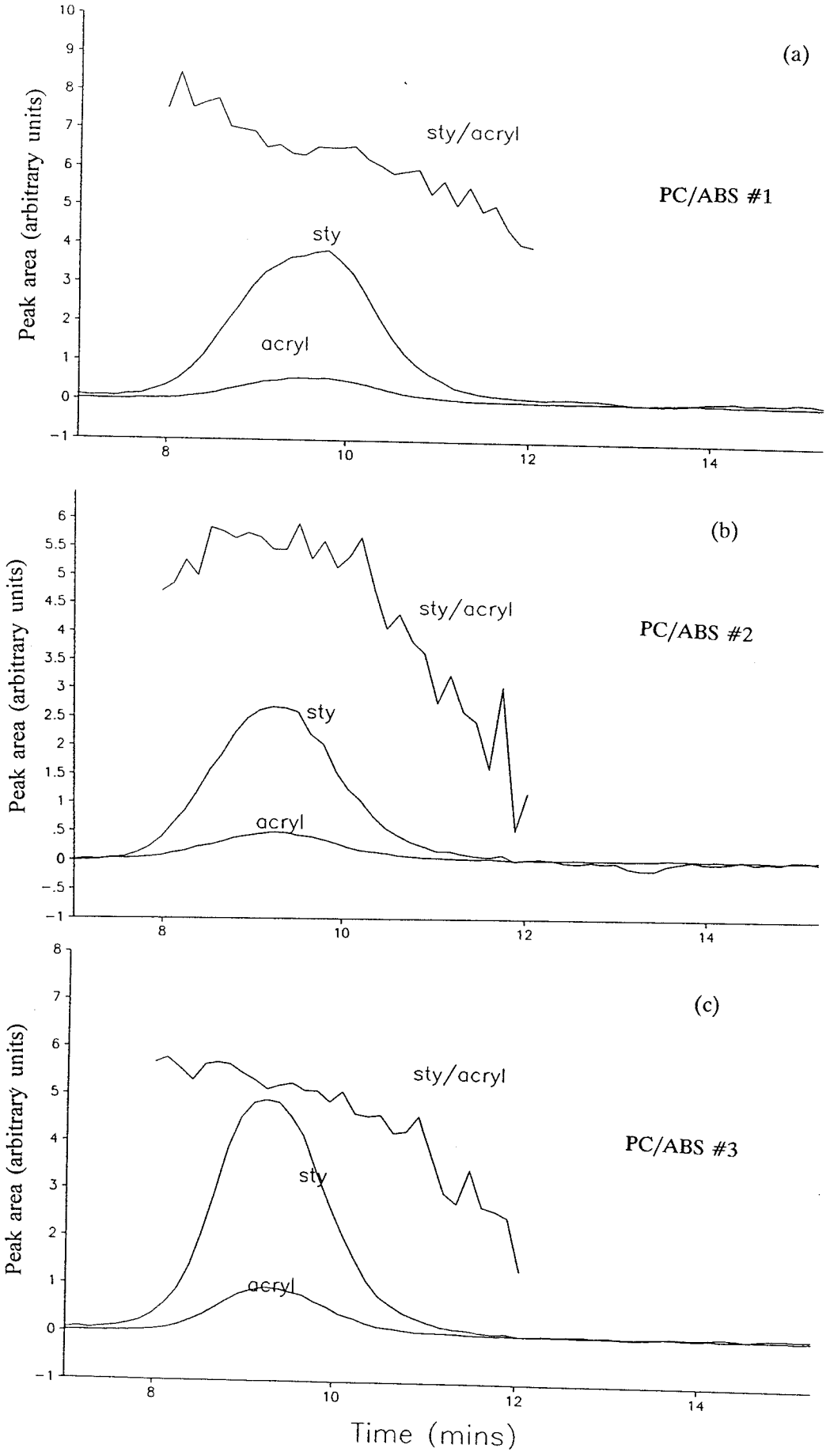

Figure 8.5: Styrene to acrylonitrile ratios for SAN extracts of PC/ABS samples.

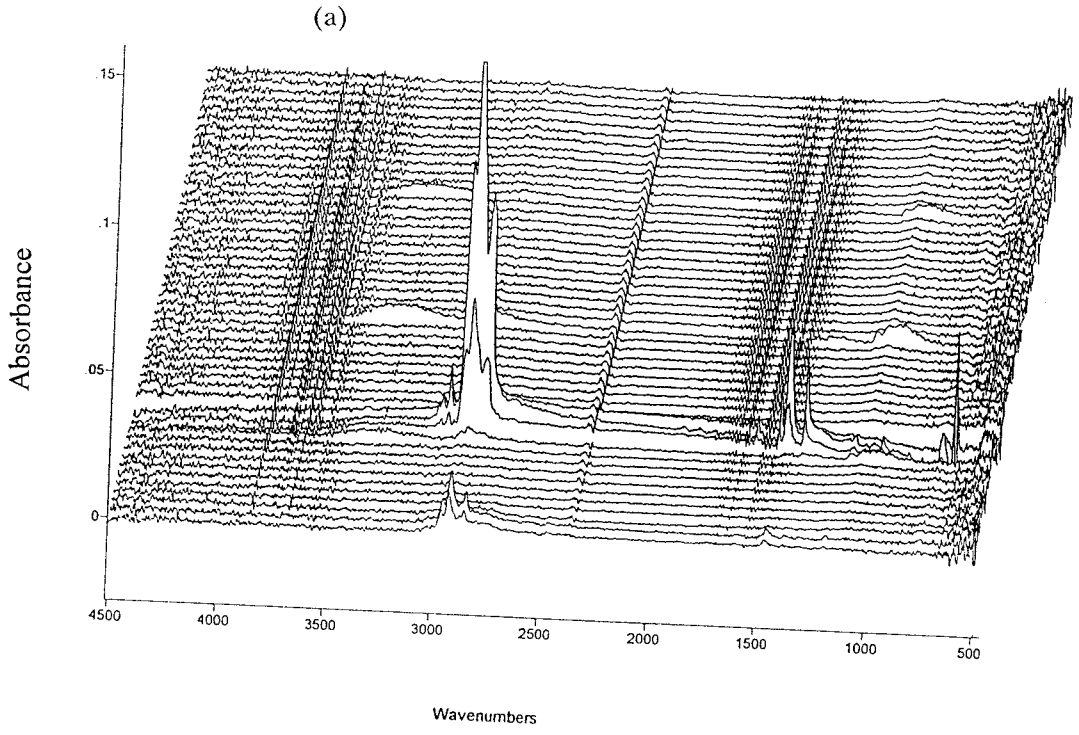

HIPS #2

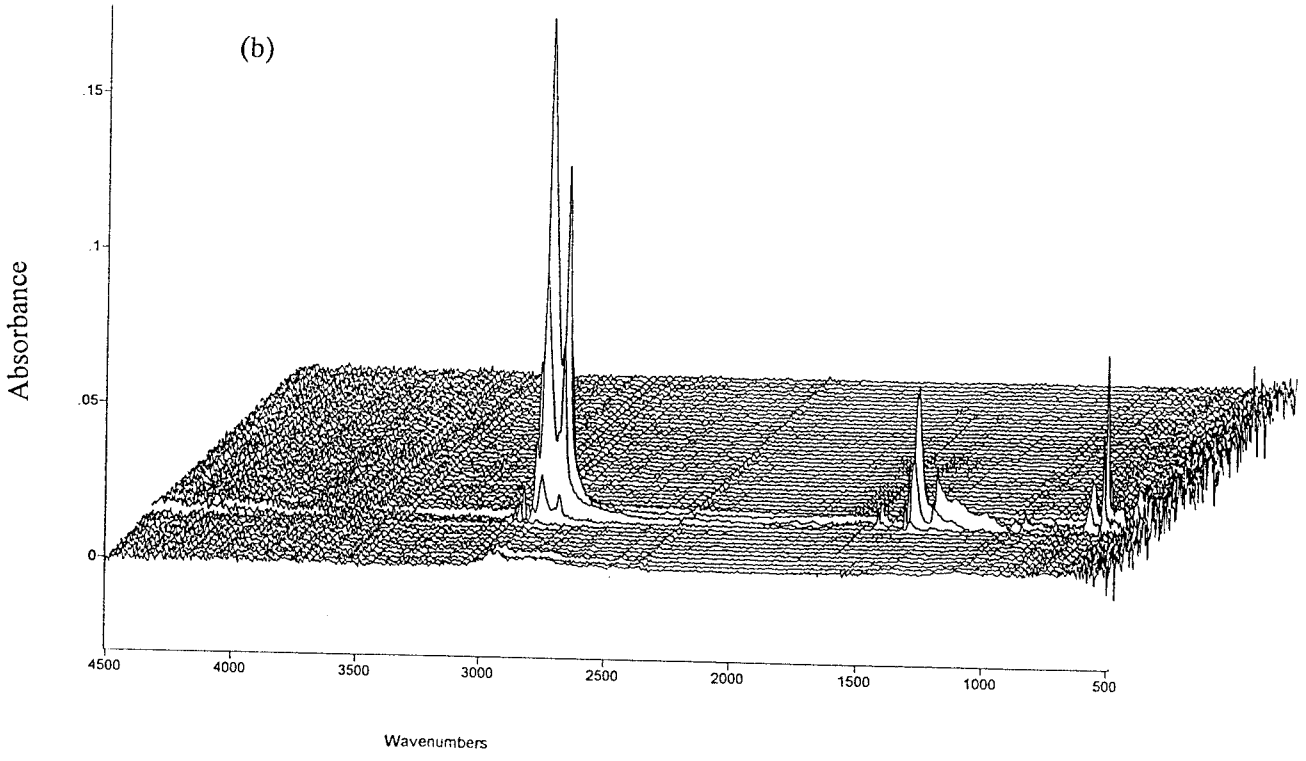

HIPS #1

Figure 8.6: Time resolved FTIR spectra for HIPS #1 and HIPS #2 samples.

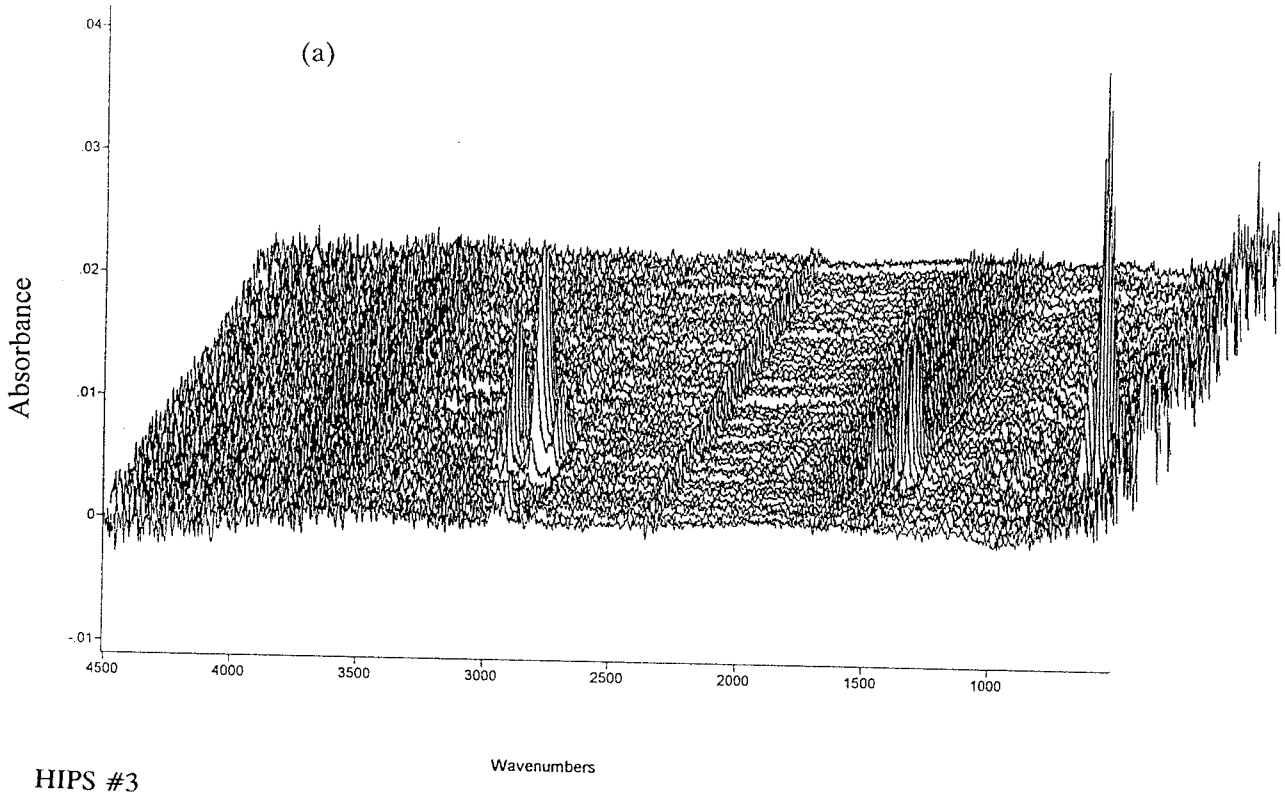

HIPS #3

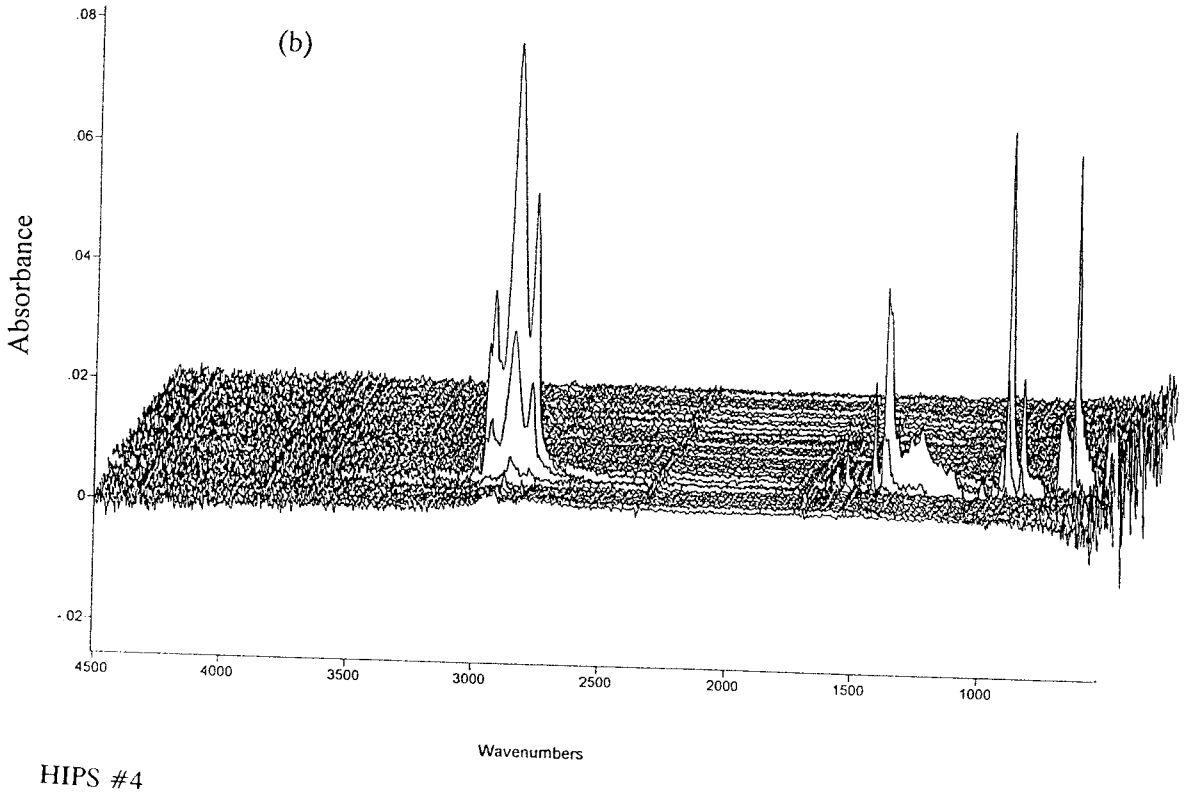

HIPS #4

Figure 8.7: Time resolved FTIR spectra for HIPS #3 and HIPS #4 samples.

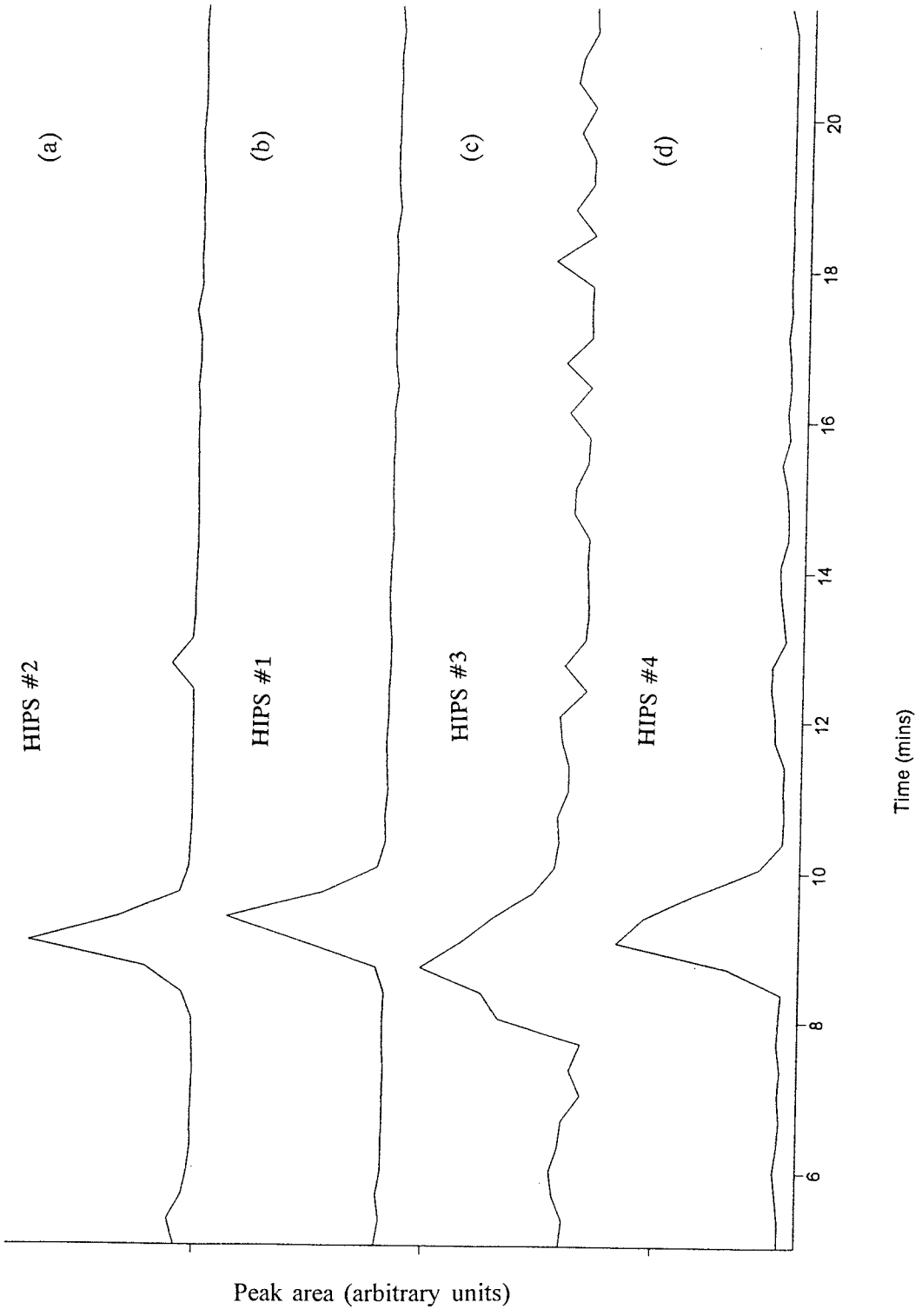

Figure 8.8: Comparison of Gram-Schmidt plots for HIPS test materials.

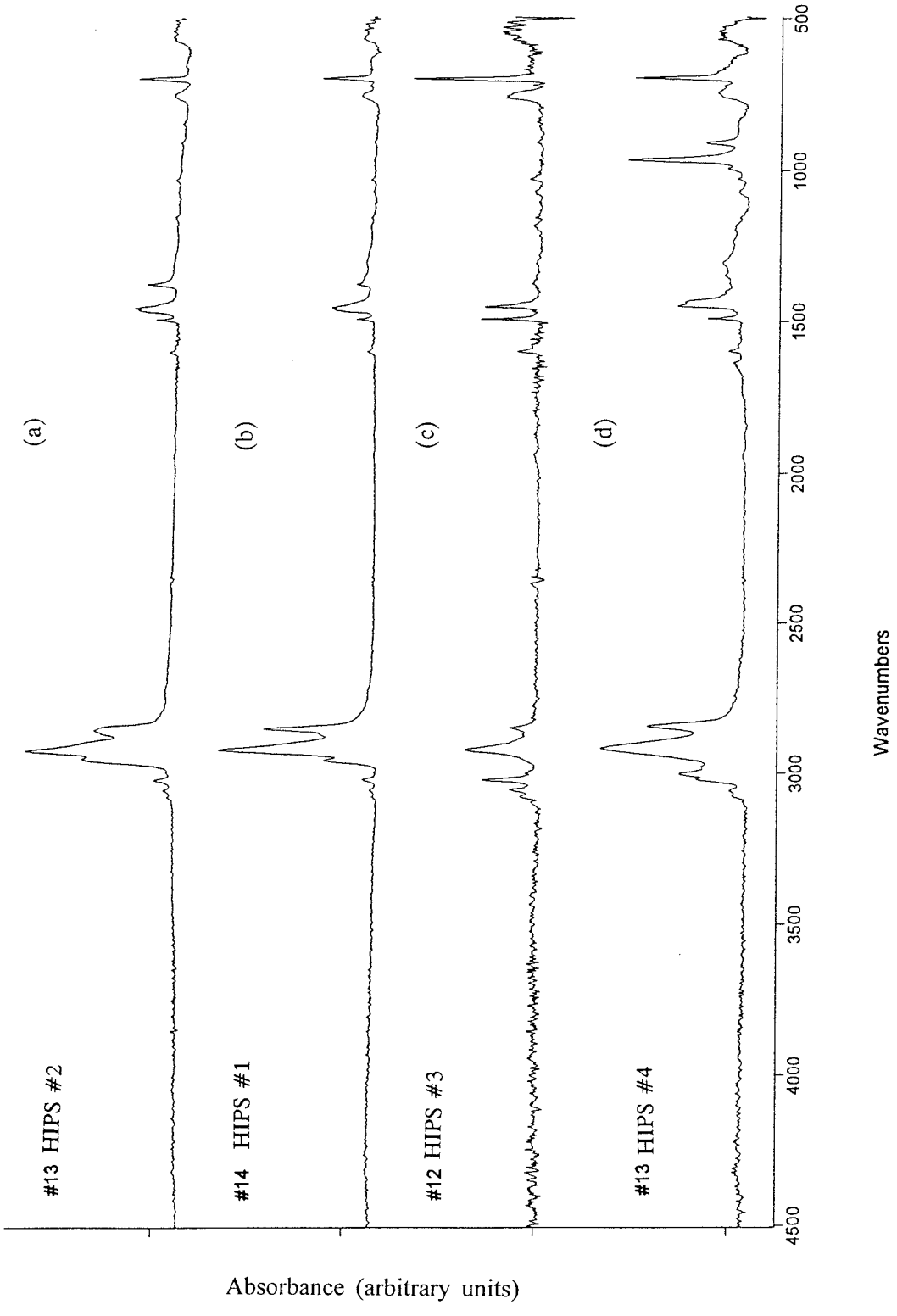

Figure 8.9: Comparison of FTIR spectra at peak absorbance for HIPS test materials.

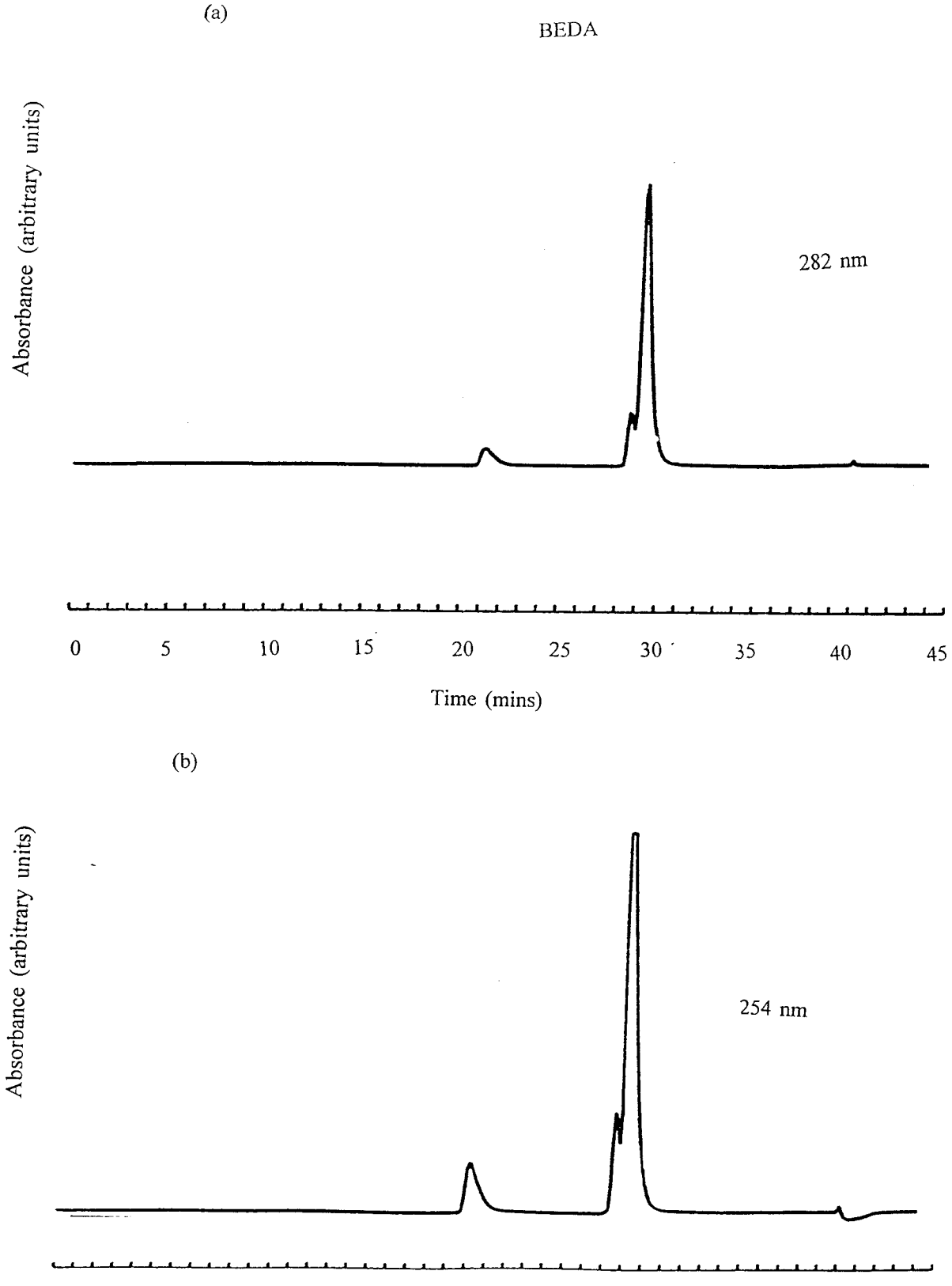

Figure 8.10: UV transmission for BEDA sample and unknown at 282 and 254 nm.

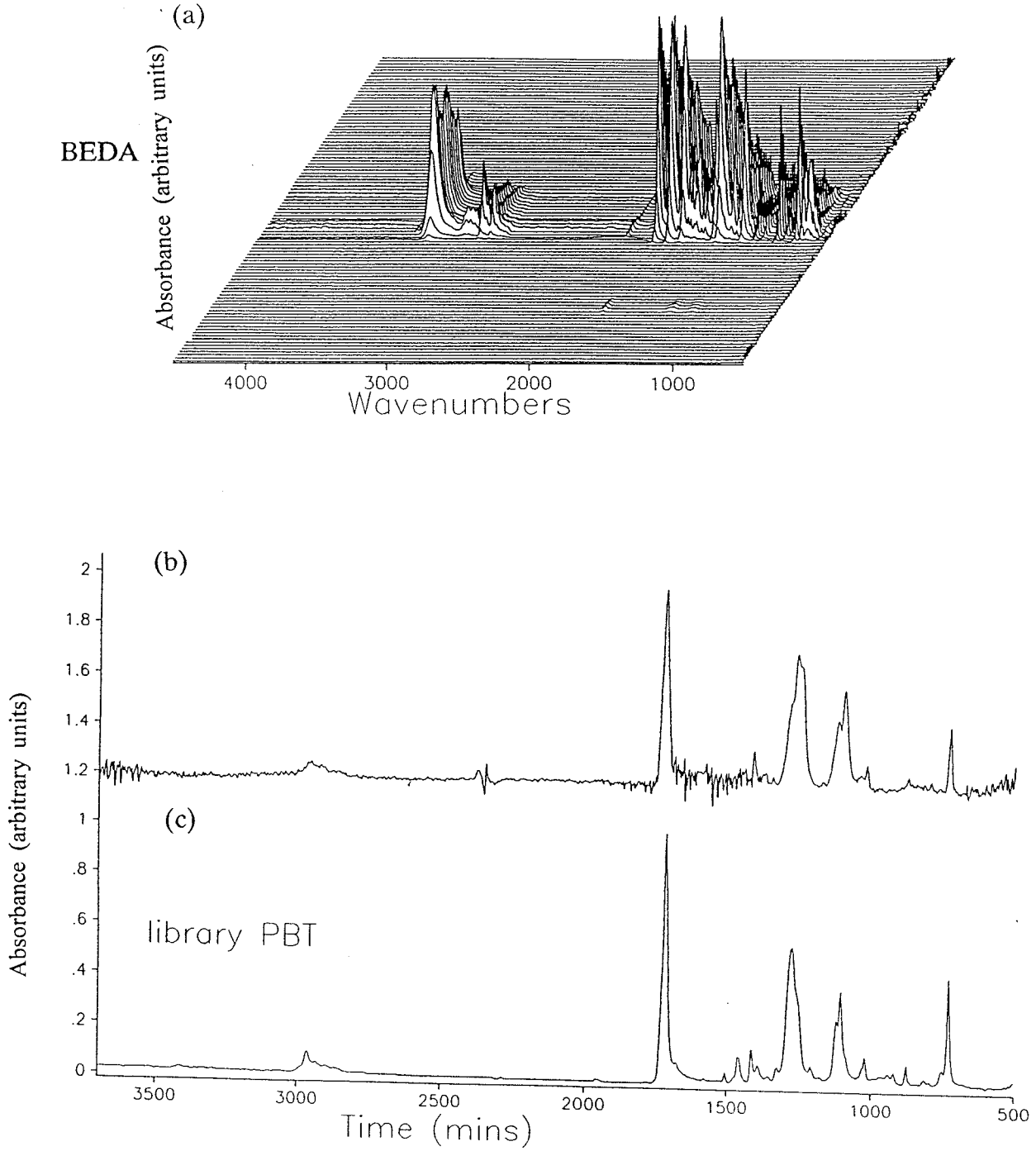

Figure 8.11 (a): Time resolved infrared spectra obtained for BEDA sample. (b): Unknown compound. (c): Library PBT spectrum.

styrene block copolymer. The HIPS #1 rubber is a styrene-ethylene/butylene-styrene block copolymer, the HIPS #2 rubber is a styrene-ethylene/propylene block copolymer. The composition of the HIPS #3 sample is unknown.

8.3.4 Identification of unknown compound in bisester diamide

Figures 8.10 (a) and (b) show the uv chromatograms produced with chloroform SEC at 282 and 254 nm respectively. The first peak is the peak of the unknown higher molecular weight compound. Figure 8.11 (a) shows the result produced by the LC-Transform using the chloroform SEC using the BEDA sample. Figure 8.11 (b) is the spectrum of the unknown. Figure 8.11 (c) is the spectrum of PBT showing that the unknown compound is PBT.

8.4 CONCLUSIONS

The LC-Transform has been assessed and shown be an excellent instrument for interfacing FTIR with SEC and RP-HPLC. The nebulizer and heated sheath gas part of the accessory designed to eliminate the solvent eluted with the components of interest operate well and have little difficulty in removing cresol and water from the compounds deposited on the disk.

However a significant problem with the FTIR spectra produced when using the LC-Transform is the baseline shifts described in Section 8.3.1. With the use of the appropriate software this problem can be overcome quite satisfactorily i.e. by applying various baseline corrections.

A severe limitation in this case of the LC-Transform was the performance of the FTIR spectrometer itself. Experiments with a Biorad FTS 40 infrared spectrometer have shown the performance of that instrument to be 3 to 4 times better in performance (i.e. it produces a signal to noise ratio 3 to 4 times better in the same collection time from the same sample) than the Bomem interferometer when both instruments use a DTGS detector. The poor performance of the Bomem means that long sampling times have to

be used to examine the collection disks and the number of spectra that can be collected of each peak on the disk is reduced. In spite of this drawback adequate results were obtained with the Bomem and the LC-Transform with every system examined.

The reproducibility of the LC-Transform in terms of the position of the peaks in the Gram-Schmidt plots was very good. However there is some variation in the absolute intensity of the FTIR spectra recorded for repeat runs, thus for semi-quantitative work an internal standard must be used.

8.5 REFERENCES

1. Dinunzio, J.E., J. Chrom., (1992), **626** (1), 97.
2. Jinno, K., Detectors for Liquid Chromatography, Yeung, E.S. (Ed.), Wiley, New York, (1986), 74.
3. Griffiths, P.R. & De Haseth, J.A., Fourier Transform Infrared Spectroscopy, Winefordner, J.D. & Elving, P.J. (Ed.), Wiley, New York, (1986), 611.
4. Hellgeth, J.W. & Taylor, L.T., Anal. Chem., (1987), **59**, 295.
5. Sabo, M., Anal. Chem., (1985), **57**, 1822.
6. Johnson, C.C. & Taylor, L.T., Anal. Chem., (1984), **56**, 2642.
7. Brown, R.S., Hausler, D.W., Taylor, L.T. & Carter, B.C., Anal. Chem., (1981), **53**, 197.
8. Gotoh, Y., Usami, T. & Takayama, S., First International Symposium on Polymer Analysis and Characterization, (1988) University of Toronto, Toronto, Canada, June 2-3.
9. Asada, N. & Toyoda, A., Fifth International Symposium on Polymer Analysis and Characterization, (1992), Inuyama, Aichi, Japan, June 2-4.
10. Kuehl, D. & Griffiths, P.R., J. Chrom. Sci., (1979), **17**, 471.
11. Wood. D.J., Spec. Int., (1990), **2**, 36.
12. Fujimoto, C., Oosuka, T. & Jinno, K., Anal. Chim. Acta, (1985), **178**, 159.
13. Gagel, J.J. & Biemann, K., Anal. Chem., (1987), **59**, 1266.
14. Gagel, J.J. & Biemann, K., Mikrochim. Acta, (1988), **2**, 185.
15. Somson, G.W., Van de Nesse, R.J., Gooijer, C., Brinkman, U.A.Th., Velhorst, N.H.,

Visser, T., Kootstra, P.R. & De Jong, A.P.J.M., J. Chrom., (1991), **552**, 635.
16. Robertson, R.M., De Haseth, J.A. & Browner, R.F., App. Spec., (1990), **44**, 8.
17. Robertson, A.M., Wylie, L., Littlejohn, D., Watling, R.J. & Dowle, C.J., Anal. Proc., (1991), **28**, 8.
18 Kalasinsky, V.F., Whitehead, K.G., Kenton, R.C., Smith, J.A.S. & Kalasinsky, K.S., J. Chrom. Sci., (1987), **25**, 273.
19. Kuehl, D. & Griffiths, P.R., Anal. Chem., (1980), **52**, 1384.
20. Conroy, C.M., Griffiths, P.R. & Jinno, K., Anal. Chem., (1985), **57**, 822.
21. Griffiths, P.R. & Conroy, C.M., Adv. Chrom., (1986), **25**, 105.
22. Conroy, C.M., Griffiths, P.R., Duff, P.J. & Ararraga, L.V., Anal. Chem., (1984), **54**, 2636.
23. Kalasinsky, K.S., Smith, J.A. & Kalasinsky, V.F., Anal. Chem., (1985), **57**, 1969.
24. Fujimoto, C., Morita, T. & Jinno, K., High Res. Chrom., (1988), **11**, 810.
25. Robertson, R.M., De Haseth, J.A., Kirk, J.D., Browner, R.F., App. Spec., (1988), **42**, 1365.
26. Lange, A.J., Griffiths, P.R. & Fraser, D.J.J., Anal. Chem., (1991), **63**, 782.
27. Cheung, P., Balke, S.T., Schunk, T.C. & Mourey, T.H., J. App. Polym. Sci.: App. Polym. Sym., (1993), **52**, 105.
28. Lange, A.J., Griffiths, P.R., App. Spec., (1993), **47** (4), 403.
29. Lange, A.J., Griffiths, P.R., J. Chrom. Sci., (1992), **30** (3), 93.
30. Schunk, T.C., Balke, S.T. & Cheung, P., J. Chrom. A, (1994), **661** (1-2), 227.

8.6 ACKNOWLEDGEMENTS

The assistance of colleagues at General Electric Plastics who made possible the work reported in this chapter is gratefully acknowledged.

Jeanette Ubels who assisted with the work describing size exclusion chromatography with HIPS rubbers.

Ben Baars who assisted with the identification of PBT in BEDA.

Chapter 9

SUMMARY OF CONCLUSIONS

Chapter 9

SUMMARY OF CONCLUSIONS

Over the last seven years the spectroscopy research group at Southampton University has developed a reputation for its pioneering work in developing applications of Raman spectroscopy, primarily as a results of its early involvement in the development of the instrumentation required for Fourier transform Raman spectroscopy.

The early involvement of the group at Southampton caused a flurry of activity which lead to a large number of publications in the first few years after the publication of Bruce Chase and co-workers demonstrating the feasibility of Fourier transform Raman spectroscopy. This activity was reflected in three special editions of Spectrochimica Acta published which contain many applications of FT Raman spectroscopy developed by the group and other workers in the field. A book was also published by three research group members in 1991 entitled *"Fourier transform Raman spectroscopy"* describing most of the early work performed by the group.

Further work in the group has continued at a more leisurely pace concentrating mainly on expanding the horizons of many of the applications opened up by previous members of the group active in the field. Because of the complementary nature of FT Raman and infrared spectroscopy, the group has always emphasized the two techniques together to avoid falling into the trap of attempting solve every problem with Raman when infrared could possibly have more to offer. Hence the focus of the work described in this thesis is not exclusively FT Raman spectroscopy.

The work presented in this thesis can be divided into two main sections. The first section consists of Chapter 3. This chapter gives an almost chronological account of the development of a Titanium:Sapphire laser based Fourier transform Raman spectrometer. The instrument, once operational, was used to examine as fully as possible the advantages and disadvantages of deep red laser sources (i.e. between 700 and 950 nm)

in Raman spectroscopy to provide a holistic impression of the commercial possibilities of using a deep red laser source for routine Raman spectroscopy.

The second main sections of this thesis deals which various selected applications of FT vibrational spectroscopy. These are dealt with in Chapters 4 to 8. Chapter 4 examines the often ignored problem of the dependence of Raman signal intensity with particle size dealing with particle sizes of the order of 0.1 mm. Some interesting results are presented and unfortunately more questions than answers are raised in this field. Chapters 5, 6 and 8 describe three separate projects carried out over a six month work period at General Electric Plastic Europe in Holland evaluating three analytical techniques using different model polymer systems based on Fourier transform infrared spectroscopy. Chapter 7 looks at the application of FT Raman spectroscopy to a problem examined in some detail in Chapter 6, i.e. the transesterification reactions occurring in heated poly(butylene terephthalate) polycarbonate blends.

9.1 THE CONSTRUCTION, DEVELOPMENT AND ASSESSMENT OF A TITANIUM:SAPPHIRE LASER BASED FOURIER TRANSFORM RAMAN SPECTROMETER

A working instrument was constructed using three wavelengths covering the region of interest between commonly used visible wavelengths (i.e. Krypton and Argon ion and Helium Neon laser wavelengths) popular with conventional Raman spectroscopy and the near infrared wavelength (Nd^{3+}:YAG at 1064 nm) routinely used in Fourier transform Raman spectroscopy. These wavelengths were 780, 835 and 920 nm, selected to take maximum advantage of the power output of the excitation laser used and to explore as fully as possible the advantages of excitation wavelengths in this region over 1.064 μm.

The shortest wavelength used showed excellent promise in minimizing the absorption problem experienced with water based and organic samples. In addition, Raman spectra can be collected from samples heated to temperatures some 200 ^{o}C higher than with 1.064 μm excitation. The use of 780 nm in FT Raman instruments also offers significant cost advantages over commercial systems in terms of laser source and detector.

Unfortunately the problem of sample fluorescence is probably unacceptable for most applications. The use of 835 nm excitation does not show any advantages over 780 nm besides a slight reduction in the level of sample fluorescence.

Moving to 920 nm loses the high temperature and lower liquid sample self absorption advantages of 780 nm and also the cost advantage offered by using a silicon detector. However 920 nm displays a similar levels of fluorescence to 1064 nm and in combination with an InGaAs detector offers an extremely high long wavelength cutoff of the Raman spectrum.

The work presented in this chapter demonstrates that, in principle, a working FT Raman instrument can be produced using 780 nm and 920 nm diode lasers as excitation wavelengths. Further it could be manufactured for lower cost than the commercially available instrument using 1064 nm. None of the advantages offered by 1064 nm excitation would be lost and all of the advantages demonstrated here would be available to the spectroscopist.

9.2 APPLICATIONS OF FOURIER TRANSFORM VIBRATIONAL SPECTROSCOPY

9.2.1 Chapter 4 : The dependence of Raman signal intensity on particle size for crystal powders

Previous work in the field examining Raman signal intensity with powdered samples with particle size in the 0.1 mm region invariably makes use of the theory developed by Schrader and co-workers from the more general Kubelka Munk theory of scattering by powdered samples. More serious is the fact that it is usually accepted that the Raman signal intensity decreases as particle size decreases with some apparently intuitive deductions made from the theory used as evidence.

This study shows for the first time that, at least with the four samples examined (potassium chromate, barium nitrate, lithium carbonate and ammonium chloride), the

intensity of the emitted Raman signal increases as the particle size is reduced. This observation is in apparent agreement with intuitive experience in the group, i.e. grinding powdered samples usually gives stronger Raman spectra.

Experimental data obtained with barium nitrate and potassium chromate is used to calculate values for the scattering and absorption parameters referred to in the generally accepted theory of Schrader and co-workers. Again an interesting point is raised concerning the previously assumed dependence of the scattering parameter on particle size.

Further work is undoubtedly required to clarify the points raised this chapter. This work should involve calculating the absolute spectral response of the spectrometer used, calculating the particle size more accurately and obtaining more experimental data to calculate the scattering and absorption parameters more accurately. In principle, Raman scattering cross-sections can also be calculated to allow verification with previously calculated values.

9.2.2 Chapter 5 : Pyrolysis Fourier transform infrared spectroscopy with poly(butylene terephthalate) formulations

This chapter describes the evaluation of a simple pyrolysis FTIR cell used to examine the compounds released by different PBT and PBT formulations containing flame retardants. PBT is shown to decompose releasing THF, CO_2, CO and PBT oligomers. Some observations can be made concerning the relative thermal performance of the different formulations. The main value of the technique is that it can easily reveal the decomposition products of a material with a minimum of operator skill.

9.2.3 Chapter 6 : The evaluation of a high temperature and high pressure infrared gas cell for the monitoring of poly(butylene terephthalate) polycarbonate transesterification

The transesterification reaction known to occur in heated blends of PBT and PC was

examined in some detail in this chapter using a commercially available high temperature and high pressure FTIR gas cell accessory. Eleven specially prepared stabilised and unstabilised PBT/PC blends were used as a model system. Phosphorous acid is known to retard the transesterification reaction and this was used as a stabiliser. In addition to the presence of stabiliser the parameters of the PBT component of the blend (i.e. end-group content, Ti catalyst content, molecular weight) were also varied in each of the stabilised and unstabilised formulations.

The experiments revealed that no transesterification occurred in the stabilised blends. The transesterification reaction was also shown to contribute to the degradation of the PC component of the blend. This degradation could be monitored by the fall in intensity of the C=O band at 1774 cm^{-1} and the release of CO_2 from the blends during heating. A correlation of the temperature at which a formulation released CO_2 to OH end-group concentration was deduced.

9.2.4 Chapter 7 : Poly(butylene terephthalate) polycarbonate transesterification monitoring with Fourier transform Raman spectroscopy

FT Raman spectroscopic evidence of transesterification between PBT and PC in unstabilised heated PBT/PC blends is presented in the form of the shift in position of the C=O band of the PBT component to higher frequency. This shift in frequency is shown to be a result of the reduction in crystallinity of PBT in a blend which occurs as a result of transesterification. No corresponding band shift is displayed by heating PBT/PC blends stabilised with phosphorous acid.

9.2.5 Chapter 8 : The evaluation of a solvent elimination liquid chromatographic - Fourier transform infrared spectroscopy interface

This chapter presents an evaluation of a commercially available interface between liquid chromatography and FTIR, this accessory is known as the LC-Transform. Several different model polymer systems were used to evaluate the performance of the LC-Transform. The interface relies on solvent elimination to remove the strong solvent

background which usually hinders on-line flow systems interfacing LC with FTIR. The LC-Transform displayed an excellent capability for eliminating high boiling solvents such as cresol and water. A detection limit of 500 ng was displayed. This limit should be considerably lowered if a more sensitive FTIR instrument were used.

9.3 GENERAL CONCLUSIONS

After the initial frenzy of activity in the development of FT Raman research has slowed to a more normal pace. However the technique has become relatively widely accepted and has justified the confidence that a comparatively small number of people showed in its initial development. Every major manufacturer of FTIR instruments now offers an FT Raman modification of their infrared interferometer or in one case a dedicated FT Raman bench.

The research group at Southampton continues its close co-operation with Perkin Elmer and hopefully some financial benefit will be obtained by Perkin Elmer as a result of the development of the Titanium:Sapphire laser based FT Raman system. Whether this will result in diode lasers being used in FT Raman instruments as sources or not is another matter. At the present time it is apparent that a CCD combined with a spectrograph is the system of choice using deep red laser sources because of the sensitivity advantages of CCD based instruments over FT systems. However, it should be remembered that although a dedicated Raman instrument based on a CCD using a spectrograph with a diode laser does have a sensitivity advantage over a dedicated FT Raman instrument, the FT Raman instrument would always offer the option of a combined FTIR instrument for a relatively small increase in capital outlay.

The work described here indicates that developments in applications of FT Raman and FT infrared are by no means reaching a plateau and their development is likely to continue as researchers attempt new analytical problems and devise methods to examine them and also instrumentation continues to develop as a result of new ideas and general advances in technology.

APPENDIX I

SEMINAR PRESENTATIONS

Since commencing my PhD I have had the opportunity to present numerous seminars. In May 1992 while on holiday in South Africa I was invited to present a series of seminars on FT Raman spectroscopy at various universities and companies, the companies and seminar dates are listed below:

"New Applications of Fourier Transform Raman Spectroscopy"

- University of South Africa (Pretoria), 26 May 1992.
- African Explosives and Chemical Industries (Johannesburg), 27 May 1992.
- Vacutec Ltd. (Johannesburg), 28 May 1992.
- University of Natal (Durban), 30 May 1992.

During my second three month work period at General Electric Plastics Europe I was invited to prepare and present a course to the members of the Technology group in which I worked covering all aspects of Fourier transform infrared spectroscopy. The course consisted of eight one hour lectures and two three hour practical sessions. The title and dates of the course are given below:

"The Theory and Applications of Fourier Transform Infrared Spectroscopy" General Electric Plastics Europe, Bergen op Zoom, 21 - 27 June 1994.

APPENDIX II

PUBLISHED WORK

Since commencing my PhD studies I have personally written four papers. One has been published, one has been accepted and two are currently being considered for publication. These papers are listed below and reproduced in this section.

COMPLETE LIST OF PUBLICATIONS

"Fourier Transform Raman Spectroscopy with 780 nm Ti:Sapphire Laser Excitation", P.J. Hendra, M.V. Pellow-Jarman, R. Bennett, Vibrational Spectroscopy, 1993, **5** (3), 311-323.

"The Effect of the PBT Constituent on the Reactions Occurring in PBT/PC Blends below their Decomposition Temperature", M.V. Pellow-Jarman, M.J.J. Hetem, accepted Plastics, Rubber and Composites: Processing and Applications.

"Comparison of the Thermal Degradation Products of Poly(butylene terephthalate) and flame retardant Poly(butylene terephthalate) using a pyrolysis FTIR Cell", M.V. Pellow-Jarman, M.J.J. Hetem, submitted to Journal of Thermal Analysis.

"The Dependence of Raman Signal Intensity of Particle Size for Crystal Powders", M.V. Pellow-Jarman, P.J. Hendra & R.J. Lehnert, submitted to Vibrational Spectroscopy.

The following published papers were included in the bound thesis. These have not been digitised due to copyright restrictions, but their doi are provided.

P.J. Hendra, M.V. Pellow-Jarman, R. Bennett (1993) **Fourier transform Raman spectroscopy with 780 nm Ti: Sapphire excitation** Vibrational Spectroscopy: 5 (3), 311-323 https://doi.org/10.1016/0924-2031(93)87007-G

Pellow-Jarman, M. & Hetem, M. (1995) **Comparison of the thermal degradation products of poly(butylene terephthalate) and flame retardant poly(butylene terephthalate) formulations using a pyrolysis FTIR cell.** Polymer Degradation and Stability, 47(3), pp.413–421. Available at: http://dx.doi.org/10.1016/0141-3910(95)00006-2

Martin V. Pellow-Jarman, Patrick J. Hendra, Ralph J. Lehnert (1996) **The dependence of Raman signal intensity on particle size for crystal powders** Vibrational Spectroscopy, 12(2), pp.257–261. Available at: https://doi.org/10.1016/0924-2031(96)00023-9

ABSTRACT

The effect of the properties of the poly[butylene terephthalate] (PBT) component (varying molecular weight, end-group and titanium contents) on the thermal processes occurring between 200 and 350 °C in stabilised and unstabilised blends (phosphorous acid stabiliser) of PBT and polycarbonate (PC) is studied using a temperature programmable Fourier Transform infrared cell in gas decomposition and transmission modes. The total amount of CO_2 released by the PBT/PC blends is found to be greatly reduced by the presence of a phosphorous acid stabiliser in the blend. Transesterification is also observed between the PBT and PC components of the blends, this reaction is also significantly reduced by the presence of the stabiliser.

KEYWORDS

poly(butylene terephthalate), polycarbonate, transesterification.

THE EFFECT OF THE POLY(BUTYLENE TEREPHTHALATE) CONSTITUENT ON THE REACTIONS OCCURRING IN POLY(BUTYLENE TEREPHTHALATE)/POLYCARBONATE POLYMER BLENDS BELOW THEIR DECOMPOSITION TEMPERATURE

Martin Pellow-Jarman
Department of Chemistry
University of Southampton
SO9 5NH
England

Martin Hetem
General Electric Plastics Europe
Plasticslaan 1
4600 AC Bergen op Zoom
The Netherlands

INTRODUCTION

In spite of the large number of polymers potentially available, a relatively smal number are used in the manufacture of commercial products on a large scale. Or of these products is produced by blending bisphenol A polycarbonate (PC) ar poly(butylene terephthalate) (PBT). This blend is extensively used for moulde automobile parts.

Polycarbonate is tough and stable to 300 °C but has poor solvent resistance, it T_g is approximately 145 °C. Poly(butylene terephthalate) has relatively goc solvent resistance, a low T_g (approximately 43 °C), a high T_m (> 220 °C) and a hig decomposition temperature (poly(butylene terephthalate) starts to decompose a approximately 350 °C). An alloy formed with poly(butylene terephthalate) an polycarbonate produces a material with good chemical resistance as well as goc heat and impact resistance.

Certain processes may occur during the manufacture of a poly(butylen terephthalate)/polycarbonate blend at elevated temperature (> 250 °C) of which potential blend manufacturer should be aware. The most important of thes processes is the formation of a poly(butylene terephthalate)/polycarbonat copolymer catalysed by the residual titanium[1-3] present in the catalyst used in th polymerisation of the poly(butylene terephthalate) component of the blend Initially the reaction between the poly(butylene terephthalate) and polycarbonate usually referred to in the literature as transesterification, will produce bloc copolymers and finally random copolymers. Not only will the chemical resistance mechanical strength and thermal resistance of the blend be reduced b transesterification, but the final product may contain transparent portions (du to reduced crystallinity), orange-yellow portions (due to formation of titaniu complexes) and CO_2 gas bubbles formed by the decomposition of alkyl carbonat transesterification products[1].

To reduce the transesterification process, stabilisers are added to the blen which complex the residual titanium in the poly(butylene terephthalate) Phosphates have been shown to be effective in stabilising poly(butylen terephthalate)/polycarbonate blends to prevent these transesterificatio reactions[1,2].

The transesterification between poly(butylene terephthalate) and polycarbonate a well as between poly(ethylene terephthalate) and polycarbonate has bee extensively studied using infrared, mass spectrometry, proton and carbon(13 nuclear magnetic resonance and differential scanning calorimetry[1-13] Transesterification is thought to occur via three pathways: alcoholysis acidolysis and direct transesterification[1,6,7,8]. Figure 1 shows a schematic diagra of these three possible transesterification pathways. Devaux et al[1,13] hav concluded that the direct transesterification reaction is the predominan mechanism in transesterification of poly(butylene terephthalate)/polycarbonat blends.

Any information regarding the properties of the components in the poly(butylen

terephthalate)/polycarbonate blend which could promote or reduce the transesterification process would be of particular interest to manufacturers of poly(butylene terephthalate)/polycarbonate blends for commercial applications. A study examining the effect of molecular weight of the components on poly(butylene terephthalate)/polycarbonate concluded that the miscibility of poly(butylene terephthalate)/polycarbonate blends increased with decreasing molecular weight of the components[1]. Although the transesterification process has been extensively studied, little has been reported about the behaviour of poly(butylene terephthalate)/polycarbonate blends heated above temperatures where transesterification starts up to temperatures where the poly(butylene terephthalate) component starts to decompose (i.e. 350 °C).

In this study it was decided to examine the processes occurring in poly(butylene terephthalate)/polycarbonate blends prepared with different grades (different molecular weight, end-group content and titanium content) of poly(butylene terephthalate) in each blend as they were heated to determine if there was a correlation between the thermal processes occurring in a poly(butylene terephthalate)/polycarbonate blend and the physical properties of the poly(butylene terephthalate) used in the blend.

The polymer samples used in this investigation were either specially prepared samples of poly(butylene terephthalate) or blends of 50:50 (w/w) poly(butylene terephthalate) and polycarbonate. The first six poly(butylene terephthalate)/polycarbonate samples were unstabilised samples containing the same grade of polycarbonate and different grades of poly(butylene terephthalate) (i.e. different molecular weights, end group content and catalyst content). The second five poly(butylene terephthalate)/polycarbonate samples were analogous samples to the unstabilised samples but contained a phosphorous acid stabiliser. The poly(butylene terephthalate)/polycarbonate formulations used were compounded by extrusion at 240 °C to try and avoid transesterification before studying the samples. Although it is likely that optimal mixing between the two components of the blend will not be achieved at 240 °C, extrusion of the poly(butylene terephthalate)/polycarbonate blend at a higher temperature could cause undesirable transesterification thus an extrusion temperature of 240 °C was selected as a compromise.

EXPERIMENTAL

All the IR spectra presented here were recorded on a Bomem FTIR spectrometer (model Michelson M 100, Bomem) using the Graseby Specac high temperature / high pressure FTIR cell accessory with an automatic temperature controller (Graseby Specac).

Table 1 shows the composition of the poly(butylene terephthalate)/polycarbonate samples used in this work.

PBT/PC Sample Number	Sample Composition				
		M_w(g/mol),vs polystyrene	COOH content (μeq/g)	OH content (μeq/g)	Ti (ppm)
1	50 % PBT 1 & 50 % PC	60200	75	28	110
2	50 % PBT 2 & 50 % PC	63900	31	85	105
3	50 % PBT 3 & 50 % PC	67000	42	72	67
4	50 % PBT 4 & 50 % PC	48900	27	130	69
5	50 % PBT 5 & 50 % PC	90000	± 45	± 60	105
6	50 % PBT 6 & 50 % PC	90000	60	35-40	105
7	sample 1 with 0.04 % H_3PO_3				
8	sample 2 with 0.04 % H_3PO_3				
9	sample 4 with 0.04 % H_3PO_3				
10	sample 5 with 0.04 % H_3PO_3				
11	sample 6 with 0.04 % H_3PO_3				

Table 1 - Composition of Poly(butylene terephthalate)/Polycarbonate Formulations 1 to 11

When using the IR cell in a gas decomposition experiment, approximately 100 mg of the sample was placed in the sample cup and fitted into the cell. All the samples examined were dried at 130 °C for 2 hours and then stored over dried silica. The cell was then heated to 150 °C from room temperature (10 °C/min heating rate) and then left at 150 °C for 10 minutes while flushing the cell with dry nitrogen. The cell was then sealed and the lid placed on the interferometer and the sample area around the cell flushed for 30 minutes with dry nitrogen, this was necessary to reduce the interference from atmospheric water and carbon dioxide during the course of an experiment. The background was then recorded and the sample heated to 350 °C (5 °C/min heating rate). Thirty IR spectra were then collected at the rate of one spectrum (5 scans at 4 cm^{-1} 33 s scanning time) every minute starting at 200 °C. The last spectrum was thus collected when the sample was at a temperature of approximately 348 °C (±1 °C). The cell windows were maintained at a temperature of 150 °C throughout each experiment.

Two different experiments were carried out with the IR cell in its transmission

mode. Firstly, films of the poly(butylene terephthalate)/polycarbonate samples were pressed (30 - 40 μm thickness, one minute at 5000 KPa and 240 °C quenched in water) and placed in the IR cell with a KBr disk as backing. The poly(butylene terephthalate)/polycarbonate blends melt at approximately 240 °C and without a KBr disk as backing it is not possible to record spectra of the films above this temperature. The cell was heated from room temperature to 200 °C at 20 °C/min then at 5 °C/min to 240 °C while the cell was flushed with dry nitrogen through one of the cell inlet ports. It was assumed that this heating treatment would drive off any excess water in the film. The cell was then sealed and the film heated to 350 °C at a rate of 2.5 °C/min. Twenty spectra (10 scans each at 4 cm^{-1} 66 s acquisition time) were collected at intervals of 2 minutes between 250 and 350 °C.

Secondly, approximately 10 mg of each blend (dried for 2 hours at 130 °C and stored over dried silica) was pressed in a KBr disk (5 minutes at 5000 KPa). An identical series of experiments was carried out with these KBr disks as were carried out with the films above.

RESULTS AND DISCUSSION

Gas Decomposition Experiments

Figure 2 shows the results of a typical gas decomposition experiment. Apart from the presence in the IR spectra of the components given off by the sample in the IR cell, the most noticeable feature of the spectra is the shift in baseline at a temperature corresponding to 240 °C. This is the approximate temperature at which the polymer blend melts. The most likely cause of this phenomenon is that the sample in the sample cup reflects some of the radiation that is seen by the FTIR detector. The wavelength dependence of this reflection depends on the form of the sample thus when the sample melts a shift in the baseline occurs. Positioning an additional iris in the IR beam reduces this baseline shift and any baseline shift that is not eliminated can be removed using the appropriate Lab Calc software.

Figures 3 and 4 shows the final spectra collected in each of the gas decomposition experiments carried out with the unstabilised formulations (samples 1 to 6).

Table 2 shows the band positions of some of the compounds likely to be seen in Figure 2 and 3.

Figure 3 shows the gas decomposition products of the unstabilised materials heated in N_2 and Figure 4 shows the decomposition products of the stabilised materials heated in N_2. The most remarkable difference between the stabilised and unstabilised formulations is that the unstabilised materials start to produce CO_2 at between 270 and 280 °C while the stabilised materials start to produce it at 300 °C and only produce 20 percent of the CO_2 generated by the unstabilised materials during the course of an experiment.

Compound	position/cm-1	Compound	position/cm-1
Butan-1,4-diol	2982 1072	Tetrahydro-furan	2993 1079 916
Bisphenol A	3348 1509 1237 1220 826	PC	1765 1494 1210 1177 1146
Phenol	3648 1601 1182 747	PBT	1715 1271 1104

Table 2 - Band Positions for Expected Compounds in Decomposition Products of Polycarbonate and Poly(butylene terephthalate).

The compounds produced by the unstabilised and stabilised formulations (beside CO_2) also differ markedly. The unstabilised formulations (Figure 3) produce mainl bisphenol A and phenol and possibly also polycarbonate and poly(butyler terephthalate) oligomers and methane from polycarbonate The stabilise formulations produce mainly tetrahydrofuran (or butandiol) and poly(butyler terephthalate) oligomers. The stabilised formulations thus appear to produc poly(butylene terephthalate) breakdown products while the unstabilise formulations produce decomposition products of polycarbonate[14]. The stabiliser i thought to act (i.e. reduce the amount of transesterification taking place in blend) by complexing the titanium catalyst residue from the poly(butyler terephthalate) component of the polycarbonate/poly(butylene terephthalate) blend thus the fact that different compounds are released by the two groups c formulations (stabilised and unstabilised) must be related to the degree to whic transesterification is taking place in the two groups of blends (i.e. stabilise and unstabilised). The large difference in the CO_2 release between the two group of compounds must also be related to the transesterification process occurring i the poly(butylene terephthalate)/polycarbonate blends.

Figure 5 shows plots of the area of the CO_2 peak versus time for each ga decomposition experiment for the unstabilised formulations i.e. the evolution o CO_2 versus temperature for each material. From Figure 5 it is apparent that th formulations #1 to #6 release CO_2 in the order #4,#2 > #3 > #5,#1 > #6. A examination of the poly(butylene terephthalate) parameters (Table 1) reveals tha this order correlates best with the increasing concentration of the OH end-groups #4 > #2 > #3 > #5 > #6 > #1. In this ranking order only #1 : the sample containin poly(butylene terephthalate) #1 - lowest [OH] = 28 μeq/g, doesn't completely matc the CO_2 release order in Figure 5. One has to consider that #5 and #6 have significantly higher molecular weight, 90000 g/mol versus 45000 - 65000 g/mol fo all the other poly(butylene terephthalate)'s. Nevertheless, the pattern of C release by the unstabilised formulations poly(butylen terephthalate)/polycarbonate # 1 to #6 does not correlate with the increasin molecular weight of the poly(butylene terephthalate) polymers in the order #3 #1,#2 < #4 < #5,#6. This is at variance with earlier work[15] which showed that C release showed a good correlation with molecular weight in experiments carried ou with pure poly(butylene terephthalate).

The CO_2 release shown by the stabilised formulations (i.e. a similar plot to Figur 5 obtained using the stabilised formulations) revealed that, within th experimental uncertainty, all the stabilised formulations released similar amount of CO_2.

Figure 7 shows a comparison of the CO_2 release of poly(butylen terephthalate)/polycarbonate samples 1 and 2 and the pure poly(butylen terephthalate) components of each blend. It is apparent from this figure that th CO_2 released by the unstabilised formulations is not due to poly(butylen terephthalate) degradation but due to some reaction that occurs betwee poly(butylene terephthalate) and polycarbonate in each blend or due t polycarbonate decomposition. Evidence that the CO_2 released by the poly(butylen terephthalate)/polycarbonate blends on heating originates from some reactio product of poly(butylene terephthalate) and polycarbonate is that the stabilise materials show virtually no CO_2 release and the stabiliser is thought to act b complexing the titanium in the poly(butylene terephthalate) not by preventing th thermal decomposition of polycarbonate.

Normal Transmission Experiments

Problems were experienced in attempting to follow the changes in carbony absorption of the poly(butylene terephthalate) and polycarbonate. The absorbanc of the poly(butylene terephthalate)/polycarbonate films was too large and problem were experienced in getting films thin enough thus the error in the absorbanc values in the spectra of the films was large making relative comparison betwee the various materials difficult. The use of polymer samples pressed into KBr disk gave good qualitative information regarding the changes in carbonyl absorption a a blend was heated but again the errors in the determination of absolut absorbances were too large to allow quantitative comparison to be made between th various blends.

Table 3 shows the characteristic IR absorption frequencies of the carbonyl peaks in poly(butylene terephthalate), polycarbonate and the transesterification products of poly(butylene terephthalate) and polycarbonate.

Description	Structure	IR absorption frequency / cm^{-1}
Aliphatic ester	PBT-Ph-(C=O)-O-CH_2-PBT	1720
Aromatic ester	PBT-Ph-(C=O)-O-Ph-PC	1740 1070
Aromatic carbonate	PC-Ph-O-(C=O)-O-Ph-PC	1774
Aliphatic-aromatic carbonate	PC-Ph-O-(C=O)-O-CH_2-PBT	1770

Table 4 - Characteristic IR Absorption Frequencies of C=O peaks in Poly(butylene terephthalate) and Polycarbonate Transesterification[3,11], R_1 and R_2 represent the Poly(butylene terephthalate) or Polycarbonate Polymer Chain.

Figure 8 shows an expansion of the carbonyl area for a typical series of spectra collected as a poly(butylene terephthalate)/polycarbonate film on a KBr disk backing was heated from 250 to 350 °C. Qualitatively the disappearance of the carbonate C=O absorption due to the polycarbonate is the most notable feature of Figure 8. Figures 9 and 10 show the first and final spectra collected for each unstabilised formulation (i.e. samples 1 to 6). Each spectrum in Figure 9 shows the strong C=O absorptions due to the poly(butylene terephthalate) (1720 cm^{-1}) and the polycarbonate (1774 cm^{-1}). In the final spectra shown in Figure 10 the peak at 1774 cm^{-1} due to the polycarbonate has almost entirely disappeared yet the band near 1720 cm^{-1} is still relatively strong. A band also appears at 1070 cm^{-1} corresponding to the formation of the aromatic-ester transesterification product. The fact that the carbonate C=O peak of the polycarbonate disappears indicates that the view expressed earlier that the CO_2 production monitored in Figures 5 originates from the polycarbonate component of the blend. A simple calculation shows that at STP (standard temperature and pressure) 50 mg of polycarbonate would produce approximately 4.5 ml of CO_2.

Figures 11 and 12 show analogous plots to Figures 9 and 10 for the formulations 7 to 11. It is noticeable from these plots that the stabilised formulations do not show the same reduction in the carbonate C=O peak (1774 cm^{-1}) seen in Figures 9 and 10. This agrees with the earlier observation that the stabilised poly(butylene terephthalate)/polycarbonate blends produce far less CO_2 than the unstabilised blends, and is further evidence that the origin of the CO_2 produced by the unstabilised blends in the gas decomposition experiments was the polycarbonate component of the poly(butylene terephthalate)/polycarbonate blend.

Attempts to curvefit the C=O region (1650 cm^{-1} to 1850 cm^{-1}) of the IR spectra collected of the poly(butylene terephthalate)/polycarbonate films as they were heated from 250 to 350 °C revealed only qualitative information about the possible individual peaks in the C=O stretching region. Invariably the C=O region in the initial spectra (in Figures 9 and 11) could be described by two Gaussian peaks centred at 1774 cm^{-1} and 1720 cm^{-1}, the final spectra (Figures 10 and 12) could be described by three Lorentzian peaks centred at 1774 cm^{-1}, 1740 cm^{-1} and 1720 cm^{-1}. Figure 13 shows the results of a curvefitting attempt using the results obtained for sample 1. The figure indicates that initially at 250 °C no transesterification product corresponding to the aromatic ester transesterification product (i.e. C=O peak at 1740 cm^{-1} and 1070 cm^{-1} peak) is present in the blend, after heating to 350 °C, the aromatic ester transesterification product contributes significantly to the C=O region. The peak due to the carbonate C=O in polycarbonate (1774 cm^{-1}) has almost completely disappeared. Earlier work with transesterification of polycarbonate/poly(butylene terephthalate) found evidence for two transesterification products (1740 and 1770 cm^{-1}), these results indicate that either only one transesterification product is formed or, more likely, the aryl aryl transesterification product (1770 cm^{-1}) does not survive the heating process to 350 °C. The latter assumption is more likely since if the carbonate moiety of the polycarbonate decomposes before 350 °C then it is unlikely that the carbonate moiety of the aryl aryl transesterification product would be stable under similar conditions.

Similar heating experiments were conducted on polymer blends diluted with KBr as disks. Figure 14 shows the initial and final spectra collected in the experiments conducted with poly(butylene terephthalate)/polycarbonate formulations 1 and 7 (i.e. unstabilised and stabilised blends using a similar poly(butylene terephthalate) component). The reduction in the carbonate C=O peak at 1774 cm^{-1} for the unstabilised formulation is noticeable, the carbonate C=O peak at 1774 cm^{-1} in the stabilised formulation does not decrease to the same extent, a shoulder remains on the side of the 1720 cm^{-1} poly(butylene terephthalate) carbonyl band.

CONCLUSIONS

Quantitatively the differences between the performance of the stabilised and unstabilised formulations was clear. In all aspects, the stabilised formulations (samples 7 to 11) outperformed the unstabilised blends (samples 1 to 6) in thermal stability.

Transmission experiments show that the most noticeable change in the IR transmission spectra of the films and KBr disks made with the blends is the fact that the 1774 cm^{-1} carbonate C=O of the polycarbonate disappears almost completely when any of the unstabilised blends are heated to 350 °C. Curvefitting attempts show that after heating an unstabilised poly(butylene terephthalate)/polycarbonate film on a KBr to 350 °C, no transesterification product corresponding to the aliphatic aromatic carbonate (i.e. the transesterification product with a carbonyl peak at 1770 cm^{-1}) can be found. This appears to contradict the findings of Devaux et. al.[3] that the direct transesterification product is the most likely mechanism for the transesterification reaction between poly(butylene terephthalate) and polycarbonate. It is likely that the carbonate moiety of the polycarbonate and of the aliphatic aromatic ester is not thermally stable at these temperatures[1,14] and thus when the blend is heated to 350 °C no band at 1770 cm^{-1} can be seen.

The only correlation that has been established by this work is the rate at which a blend releases CO_2 and the OH end-group concentration of the poly(butylene terephthalate) in the blend. Blends with a high OH end-group content of terephthalate) release CO_2 earlier in the linear temperature program, starting at 260 °C for [OH] = 130 µeq/g and 280 °C for [OH] ≈ 35 µeq/g. It seems that CO_2 release is linked to a reaction between polycarbonate and the OH end-groups of the poly(butylene terephthalate). Probably alcoholysis will be the most reactive initial reaction in the poly(butylene terephthalate)/polycarbonate blend. However, the fact that no aryl-alkyl carbonates (C=O at 1770 cm^{-1}), could be detected in the film indicates a fast secondary degradation reaction of these species into more PC-OH and enhanced release of CO_2. No correlations were observed between thermal behaviour of the blends and the other parameters of the poly(butylene terephthalate) i.e. Ti catalyst content, molecular weight and COOH end-group concentration.

Gas transmission experiments revealed that besides releasing much less CO_2 than the unstabilised materials, the stabilised blends also released completely different volatiles. The unstabilised materials release primarily breakdown products of polycarbonate (i.e. phenol, bisphenol A and polycarbonate oligomers)[14] while the stabilised materials release primarily tetrahydrofuran, a breakdown product of poly(butylene terephthalate) and methane from the polycarbonate. The phosphate stabiliser is thought to prevent transesterification by complexing the titanium catalyst in the poly(butylene terephthalate), the fact that the polycarbonate appears to be more thermally stable in blends containing titanium catalyst indicates that the breakdown of polycarbonate is linked to the presence of the titanium catalyst, either because the breakdown of polycarbonate occurs as a result of transesterification or because the titanium directly influences the decomposition of polycarbonate.

ACKNOWLEDGEMENTS

One of the authors, Martin Pellow-Jarman, wishes to thank the directors of General Electric Plastics Europe for the opportunity to work in their laboratories and carry out the work described in this publication. The authors also wish thank Dr Gert de Wit and Arno Hagenaars for their assistance in this work.

The authors also wish to thank Dr P.J. Hendra for his invaluable input.

LIST OF FIGURES

REFERENCES

1. Hamilton, D.G. & Galucci, R.R., Journal of applied Polymer Science, (1993), 48, 2249 - 2252.

2. Riley, D.M. & Runt, J., 33(21), (1992), 4643 - 4646.

3. Devaux, J., Godard, P. & Mercier, J.P., Polymer Engineering and Science, 22(4), (1982), 229 - 233.

4. V.d. Velden, G., Kolfschoten-Smitsmans, G. & Veermans, A., Polymer Communications, (1987), 28, 169 - 171.

5. Remiro, P.M. & Nazabal, J., Journal of Applied Polymer Science, (1991), 42, 1639 - 1645.

6. Porter, R.S., & Wang, L.H., Polymer, 33(10), (1992), 2019 - 2030.

7. Kotliar, A.M., Journal of Polymer Science: Macromolecular Review, 16, (1981), 367.

8. Espinosa, E., Fernandez-Berridi, M.J., Maiza, I. & Valero, M., Polymer, 34(2), 382 - 388.

9. Kimura, M. & Porter, R.S., Journal of Polymer Science: Polymer Physics Edition, 21, (1983), 367 - 378.

10. Devaux, J., Godard, P., Mercier, J.P., Touillaux, R. & Dereppe, J.M., Journal of Polymer Science: Polymer Physics Edition, 20, (1982), 1881 - 1894.

11. Devaux, J., Godard, P. & Mercier, J.P., Journal of Polymer Science: Polymer Physics Edition, 20, (1982), 1895 - 1880.

12. Devaux, J., Godard, P. & Mercier, J.P., Journal of Polymer Science: Polymer Physics Edition, 20, (1982), 1895 - 1900.

13. Devaux, J., Godard, P. & Mercier, J.P., Journal of Polymer Science: Polymer Physics Edition, 20, (1982), 1901 - 1907.

14. Montaudo, G. & Puglisi, C., Polymer Degradation and Stability, 37, (1992), 91 -96.

15. Internal Report, General Electric Plastics, 1993.

Alcoholysis

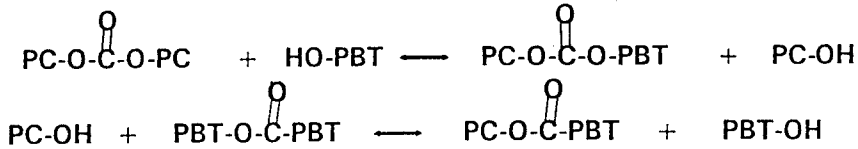

Acidolysis

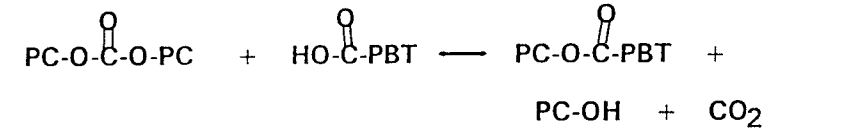

Direct Transesterification

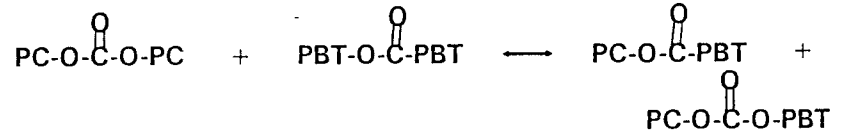

Figure 1

Figure 2

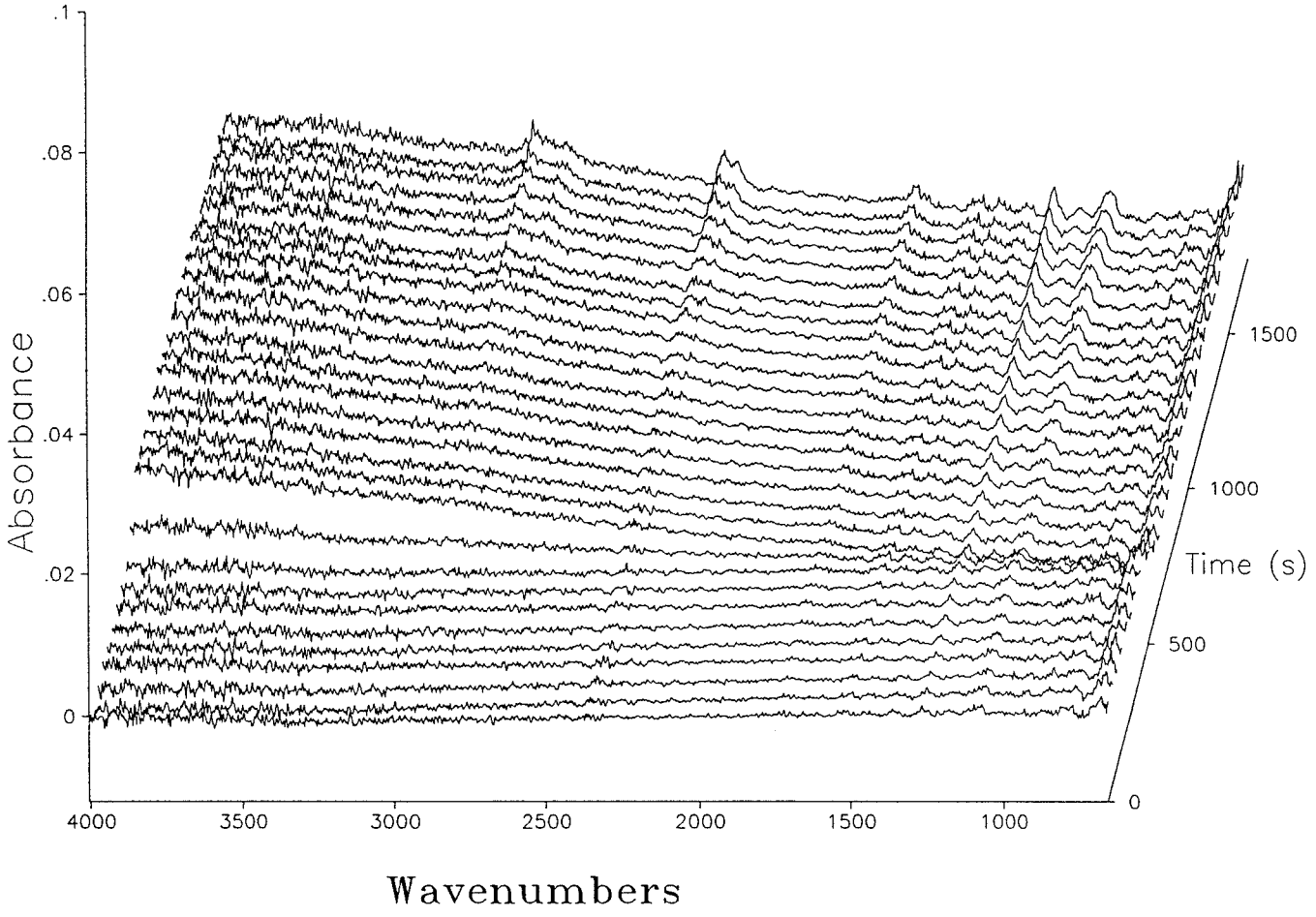

Figure 3

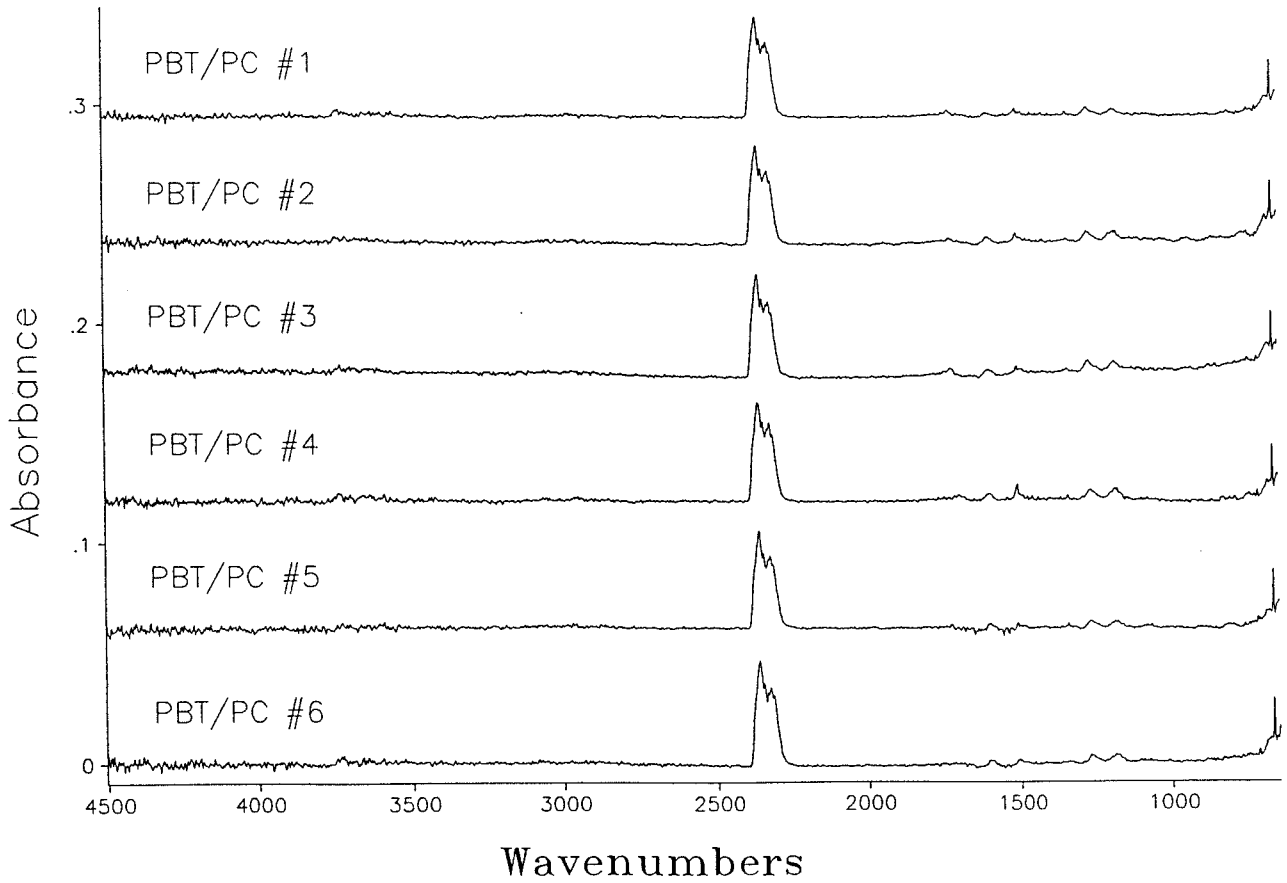

Figure 4

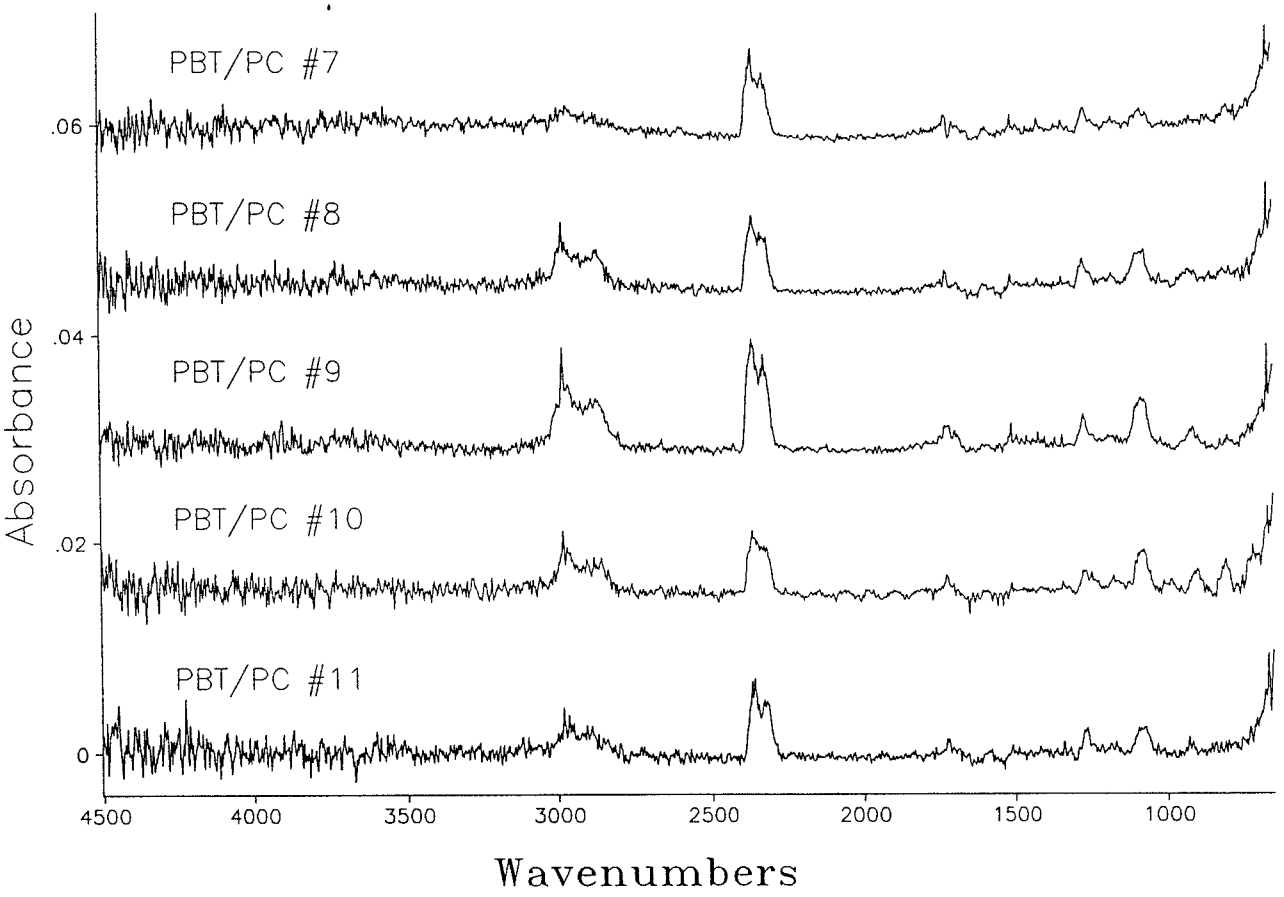

Figure 5

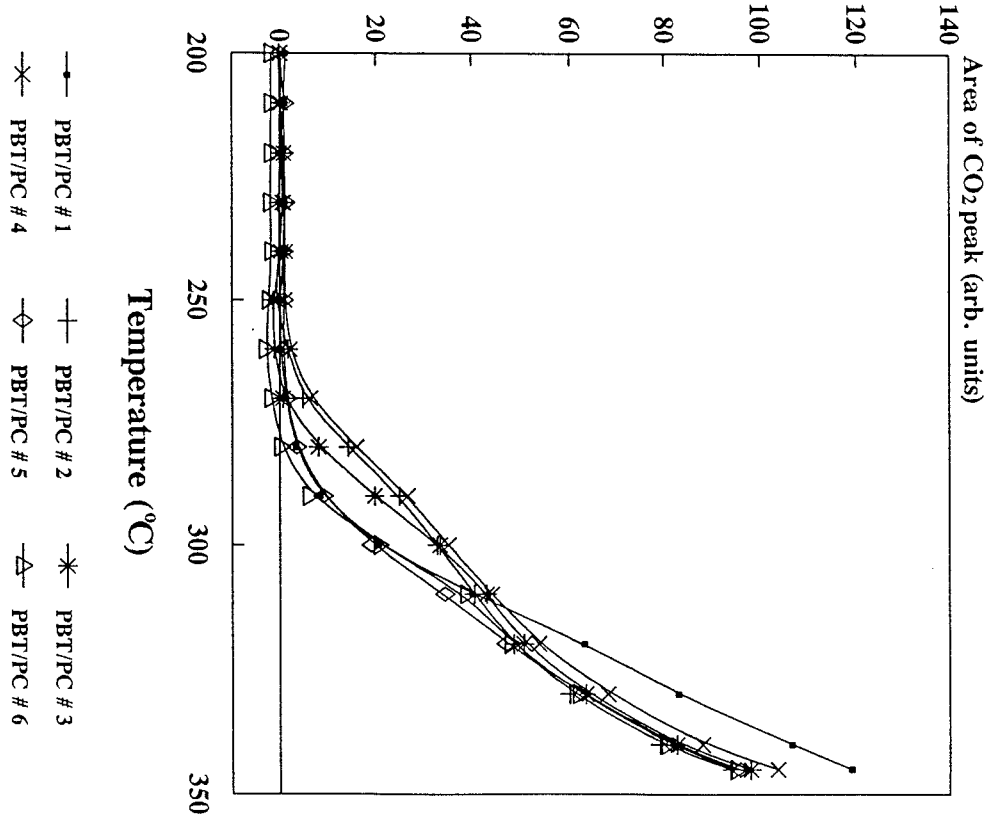

Figure 6

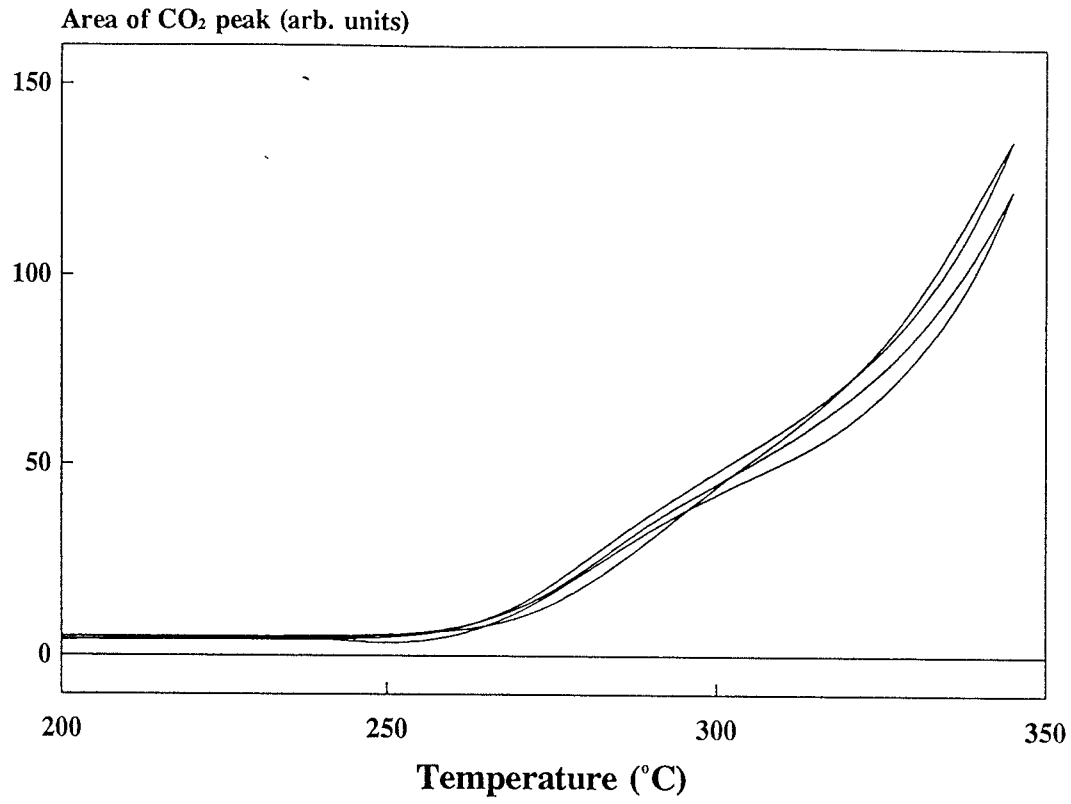

Figure 7

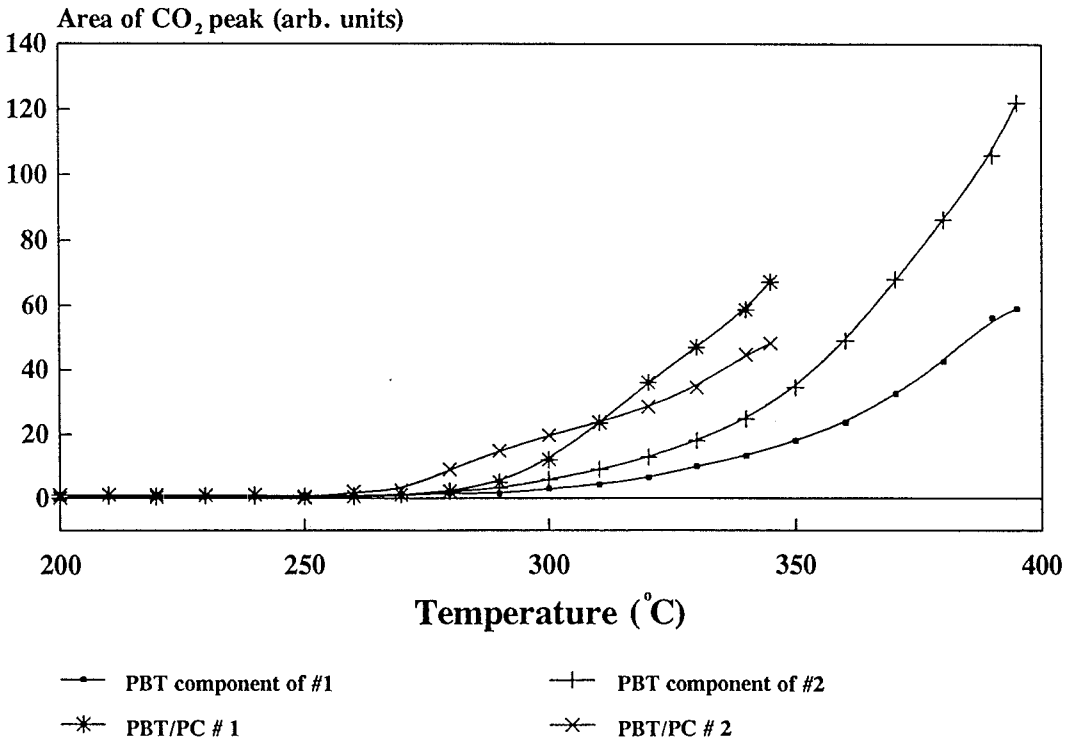

Figure 8

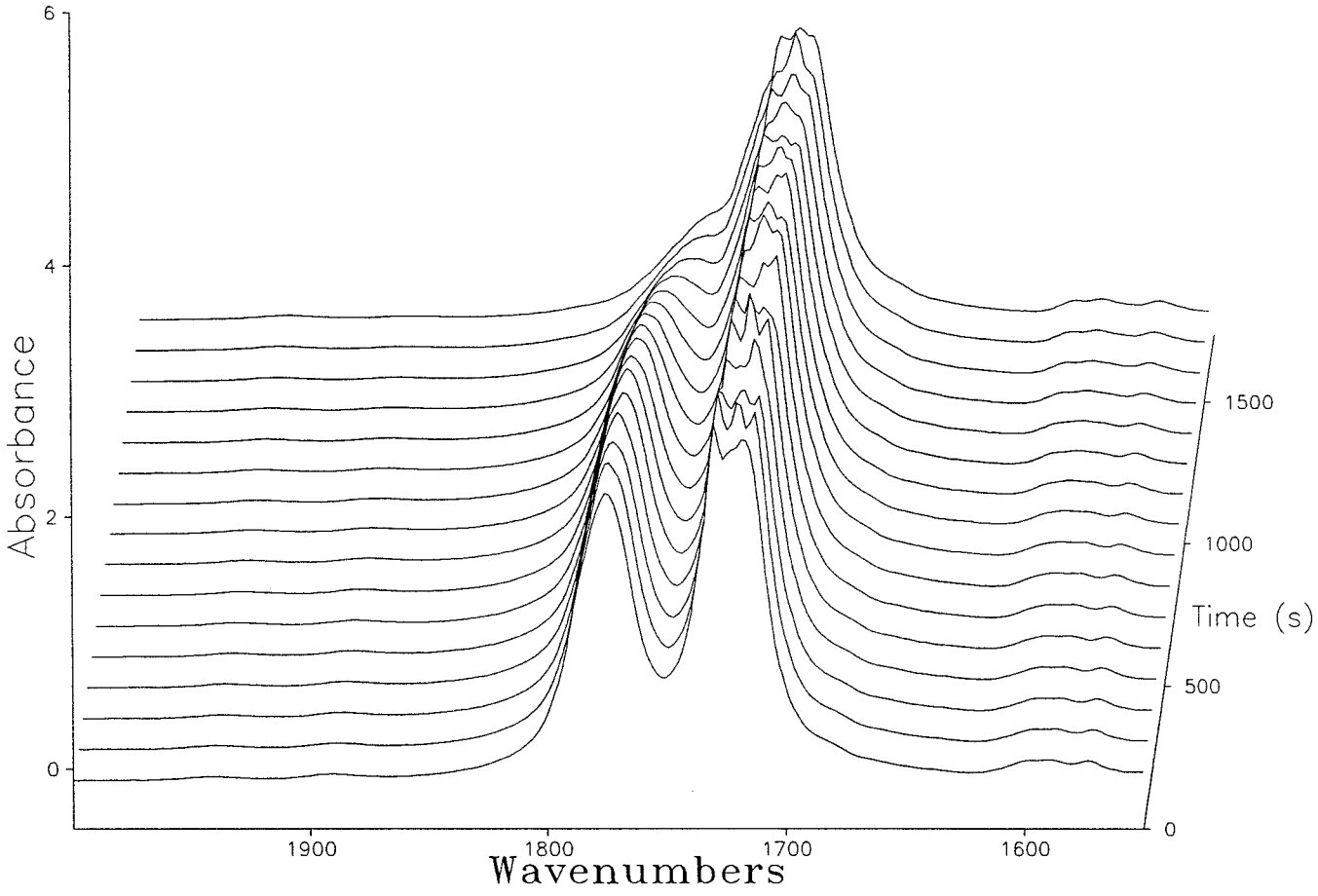

Figure 9

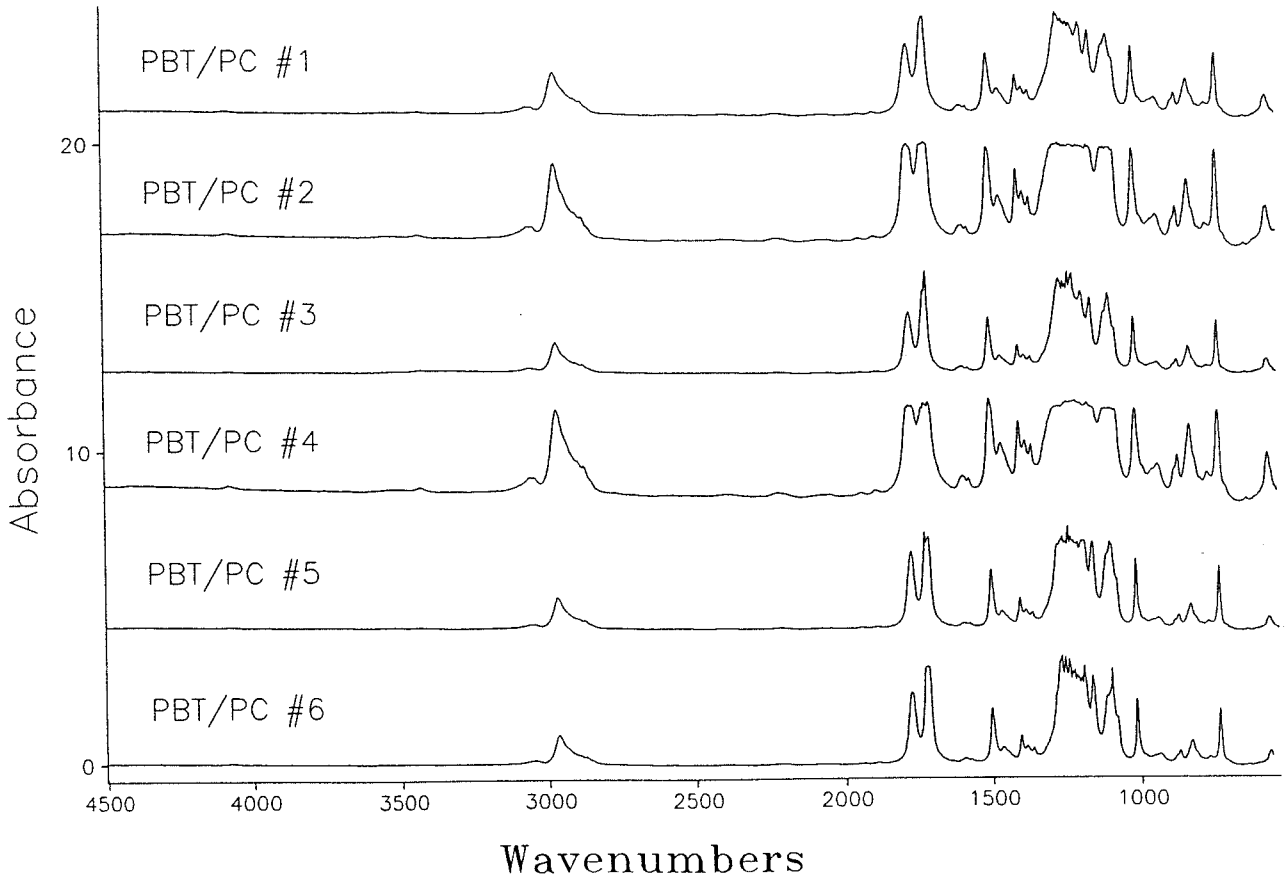

Figure 10

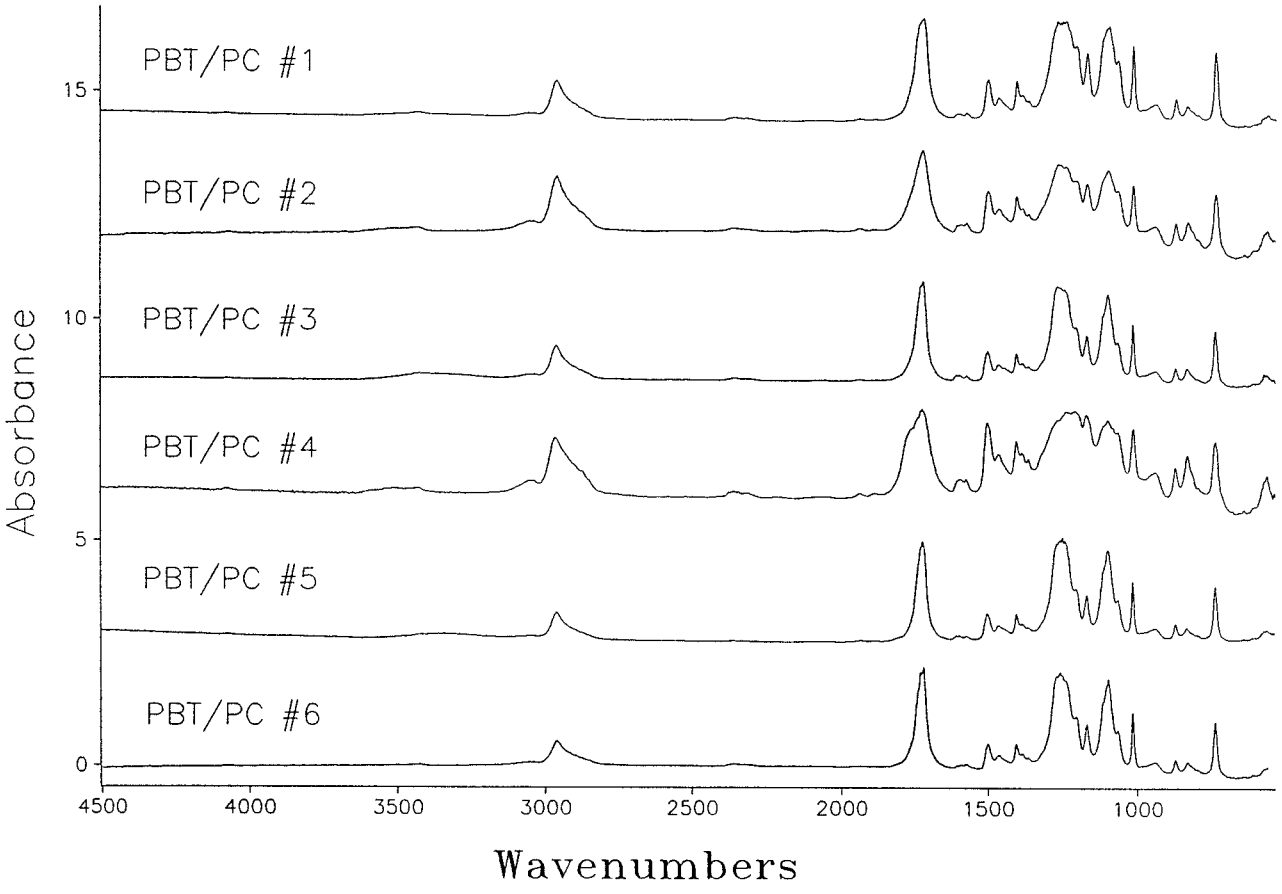

Figure 11

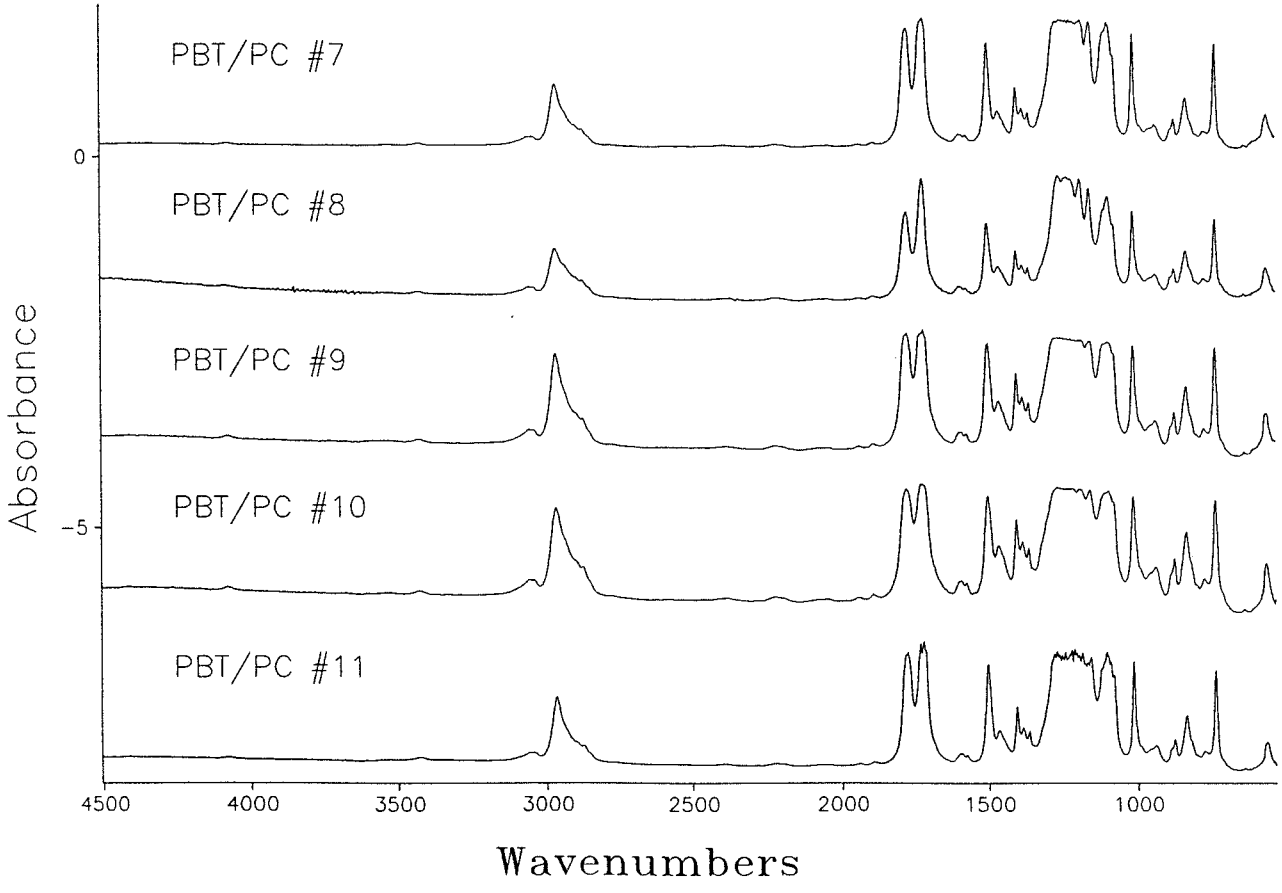

Figure 12

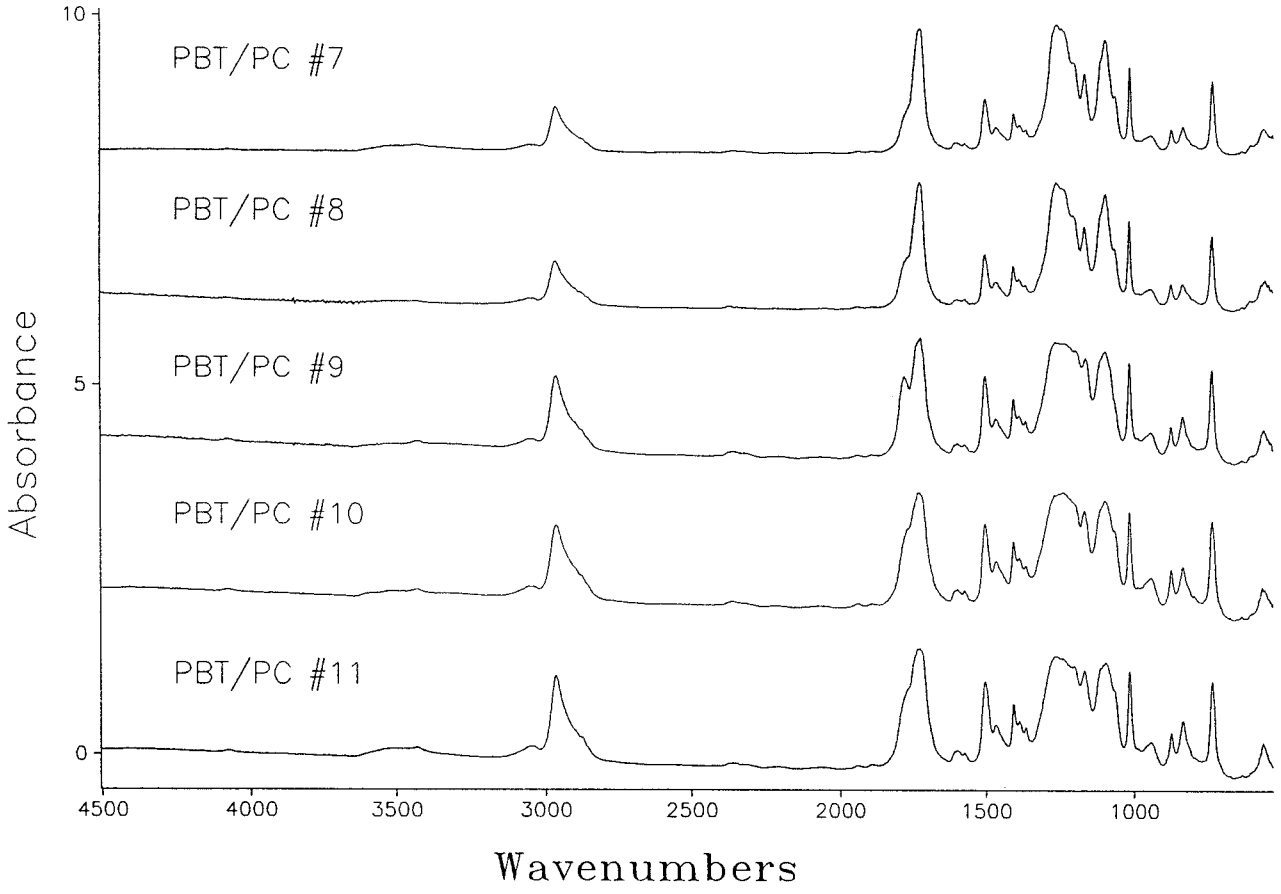

Figure 13

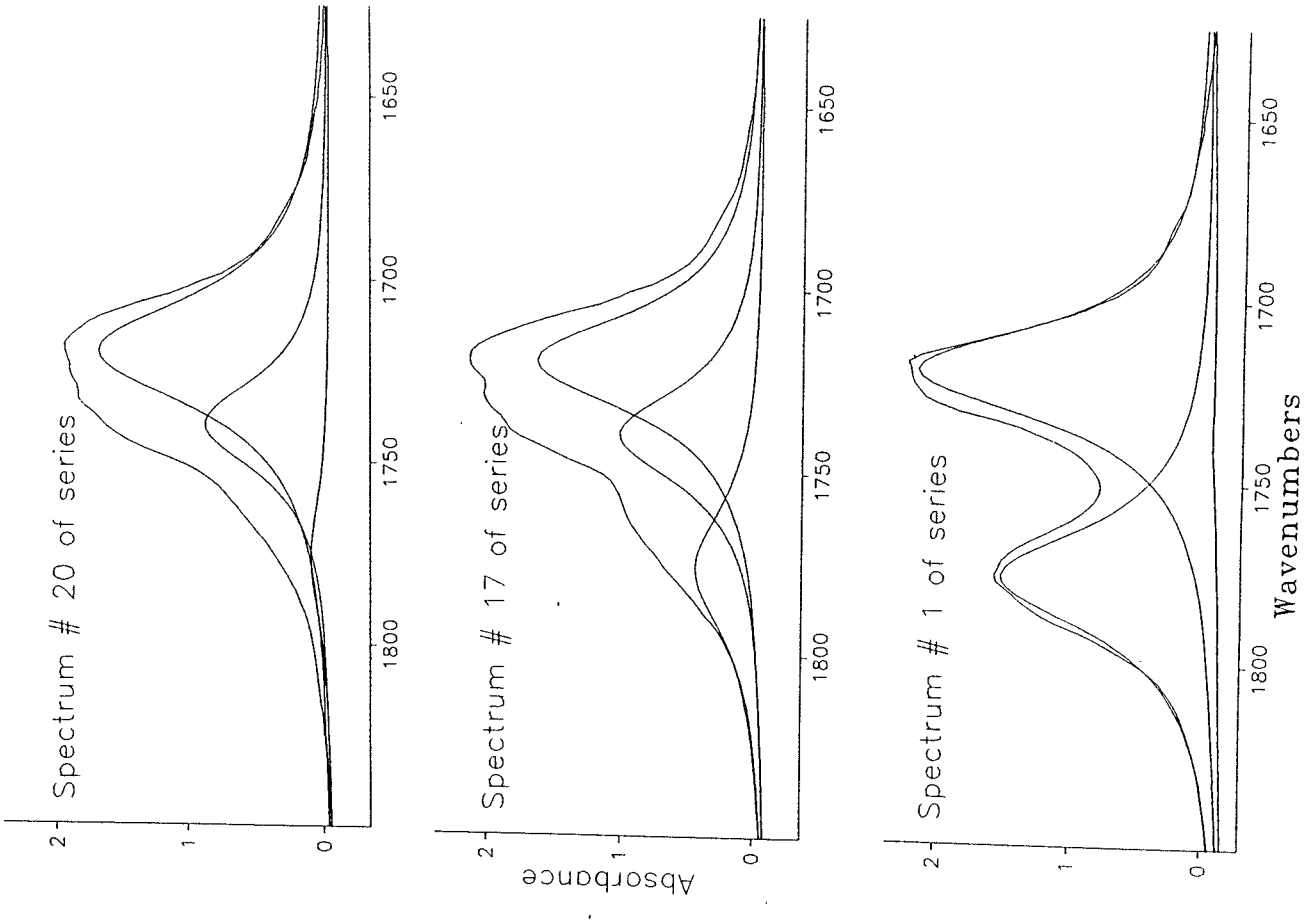

Figure 14

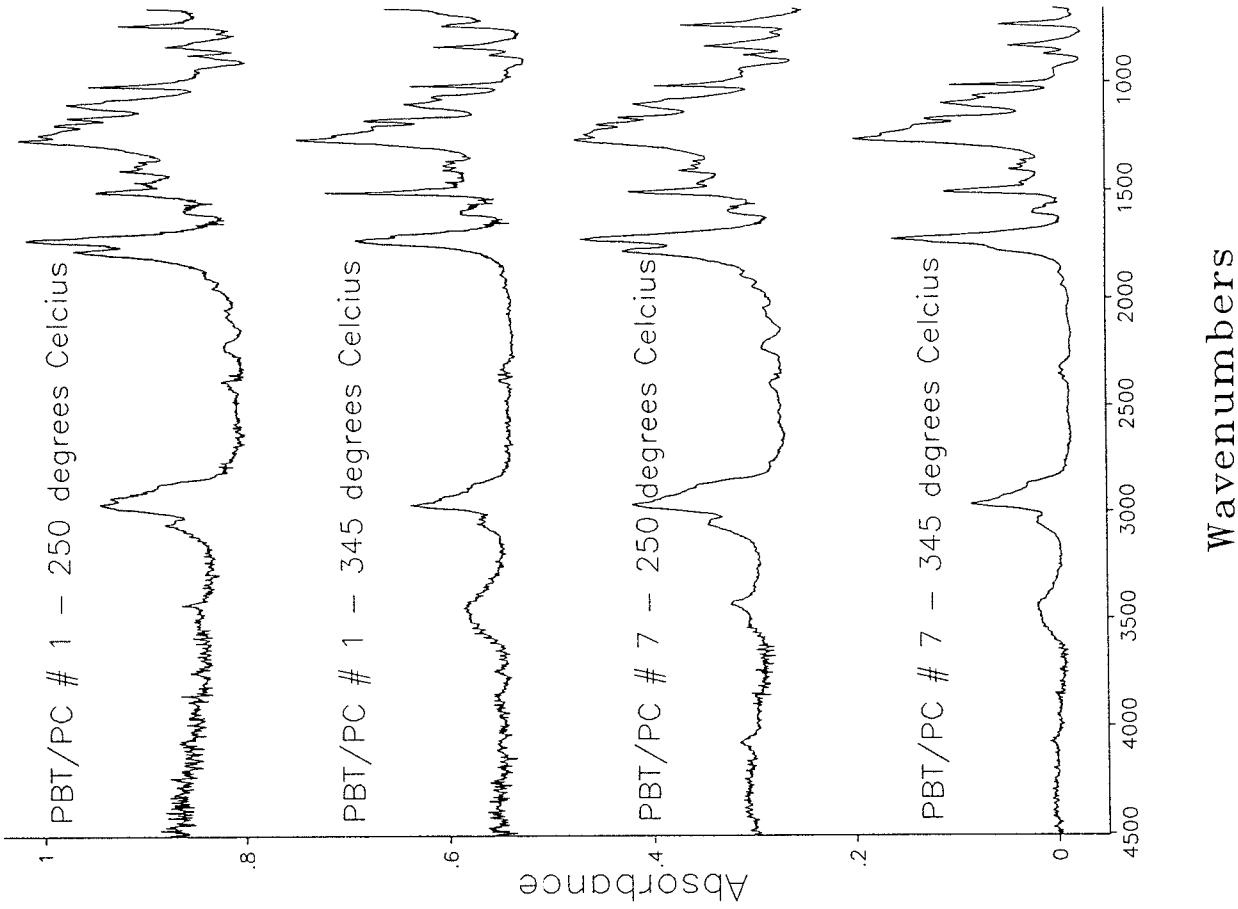
PBT/PC # 1 – 250 degrees Celcius
PBT/PC # 1 – 345 degrees Celcius
PBT/PC # 7 – 250 degrees Celcius
PBT/PC # 7 – 345 degrees Celcius
Absorbance
1
.8
.6
.4
.2
0
4500
4000
3500
3000
2500
2000
1500
1000
Wavenumbers